SMRP 210

THE DOWNBURST

MICROBURST AND MACROBURST

T. Theodore Fujita

Professor of Meteorology

The University of Chicago

Report of Projects NIMROD and JAWS

The Downburst

Printed in the United States of America

Published by Satellite and Mesometeorology Research Project (SMRP)
Department of the Geophysical Sciences
The University of Chicago

SMRP Research Paper Number 210

Library of Congress Catalog Card Number 85-50115

National Technical Information Service PB-148880

To obtain copies of this book, send a check payable to
The University of Chicago

To: Office of T. Theodore Fujita
5734 Ellis Avenue
Chicago, Illinois 60637
U.S.A.

Cost: $8 per copy for pick up at the above address
plus $3 per copy to US and Canada for handling and postage
plus $5 per copy to other countries (surface mail)
plus $12 to Europe and $17 to Asia (Airmail)

PREFACE

The fact that the energy of violent storms is concentrated inside the small section of the parent clouds has made the distinction among the scales of storms and their parent clouds more explicit during the past ten years. According to the author's planetary scale, most storms such as tornadoes, microbursts, etc., are misoscale (40 m to 4 km) phenomena, while their parent clouds are mesoscale (4 km to 400 km) disturbances. The misoscale (read as my-so-scale) downburst was not identified positively until the author called the storm "microburst" and blamed its low-altitude wind shear as being the important factor in jet aircraft accidents/incidents during takeoffs and landings.

Of the numerous post-storm aerial photographs, those taken at Beckley, West Virginia on 3 April 1974, the day of the Superoutbreak tornadoes, inspired the author with the courage to investigate the Eastern 66 accident. The author's investigation, initiated by Captain Homer Mouden (currently with Flight Safety Foundation), led to the identification of the microburst wind shear at John F. Kennedy International Airport, New York City.

The concept of the Northern Illinois Meteorological Research on Downburst (NIMROD), with the author and Prof. Ramesh Srivastava of the University of Chicago (U of C) as co-principal investigators, was examined and improved by Dr. Cliff Murino (current President of UCAR), Dr. Bob Serafin (current Director of ATD/NCAR), and Dr. Ron Taylor (NSF). When the National Center for Atmospheric Research (NCAR), sponsored by the National Science Foundation (NSF), approved the instrumentation and the field operation of NIMROD, the author's dream of detecting microbursts by Doppler radar came true. The experiment in 1978 was very successful. Painstaking analyses were made by Drs. Roger Wakimoto (current faculty of UCLA) and Greg Forbes (current faculty of Penn. State University), confirming that a Doppler radar, when operated with a specific measurement in mind, is capable of detecting microburst winds if there is no significant blockage or ground clutter.

A quantum jump in the study of microburst wind shear aimed toward aeronautical applications was made by the Joint Airport Weather Studies (JAWS) Project, with co-principal investigators the author (U of C), Dr. John McCarthy (NCAR), and Mr. Jim Wilson (NCAR). The JAWS Project, 1982, could not have been successfully completed without the devoted guidance and assistance of Dr. Wilmot Hess (Director of NCAR), Dr. Bob Serafin, and Mr. Rit Carbone (Manager of FOF/NCAR). Along with the author, the University of Chicago participants Dr. Roger Wakimoto (then research associate), and Messrs. Brian Smith and Brian Waranauskas (graduate students) wish to express their thanks to NCAR's JAWS staff members, Cathy Kessinger, Cindy Mueller, Phyllis O'Rourke, Rita Roberts, and Shelly Zucker, for their technical and secretarial assistance. During the JAWS experiment, the author shared the unforgetable experiences of flying with Prof. Al Rodi, Pilot Wayne Sands, and Mr. Bill Mahoney of the University of Wyoming, penetrating the downflow section of microbursts and taking rare pictures of violent storms from their King Air aircraft.

NCAR played an important role in obtaining the data used in this book. With a very high degree of success, both radars and PAMs were maintained and operated by a group of 28 scientists and technicians who worked on continuous alert for unpredictable microbursts. At one point during NIMROD, three Doppler radars were operated continuously for 24 hours and 45 minutes until everyone had red eyes. Without the efforts of these dedicated individuals, the data collection could not have been done with such outstanding success. Most of the Doppler imagery was photographed on 35-mm slides during operation, while selected situations were played back late at night and on off-days. NCAR's Research Data Support System (RDSS) contributed effectively in displaying and photographing the small features of misoscale phenomena in both RHI and PPI modes.

The staff members of the Satellite and Mesometeorology Research Project (1961 to the present) also played a major role in completing this publication. The author wishes to extend his thanks to Mr. Jaime Tecson, supervisory meteorologist, for his project management, manuscript review and typing; Mr. Duane Stiegler, co-editor of NOAA's Storm Data, for collecting the nation-wide microburst data and photographs; Mr. Jim Partacz for photographing and preparing the color maps and diagrams used in this book; and to the graduate students for their hard work and dedicated efforts in helping to perform the storm analyses presented in Chapter Six.

The author would like to express his appreciation to the many individuals who have helped him in preparing the manuscript of this book. Special thanks must be given to Dr. Fernando Caracena (NOAA/ERL) for his collaboration on aircraft accident/incident investigations; Mr. Greg Salotollo (NTSB) for supplying aircraft accident/incident data; Dr. Joe Golden (NWS Headquarters) for exchanging ideas and photographs of microbursts; Drs. Ron Taylor and Giorgio Tesi (NSF), Dr. Jim Dodge (NASA), Mr. Lin Whitney, Jr. (NESDIS), Messrs. Bob Kornasiewicz (NRC), Bob Abbey (former NRC), and Captains Homer Mouden, Arnie Reiner (PAA), and Tsuneo Ueda (JAL) for their assistance, suggestions, and guidance in obtaining microburst data from the two major experiments and also from throughout the United States and around the world. The up-to-date data on the operational test of the Memphis, Tennessee Network was supplied by Dr. Jim Evans and Ms. Marilyn Wolfson (MIT Lincoln Lab) and Messrs. Donald Johnson and Don Turnbull (FAA). Some art work and drafting were contributed by Mrs. Akiko Sugano. Finally, special appreciation is due to my wife, Susie Fujita, for her patience during unnumbered years and months and hidden efforts in assisting with the typing of the manuscript.

The research which led to the publication of this book was sponsored by the National Science Foundation, (NSF), National Aeronautics and Space Administration (NASA), The National Environmental Satellite, Data, and Information Service (NESDIS), Federal Aviation Administration (FAA), and the Nuclear Regulatory Commission (NRC). A special grant for publishing this book in full color was awarded by the National Science Foundation. Grant Number NSF ATM-7921260.

February 7, 1985

Tetsuya Theodore Fujita
The University of Chicago

TABLE OF CONTENTS

Chapter One

History of Downburst Identification

It was just about 10 years ago, during an aerial survey of the damage left behind by the superoutbreak of 148 tornadoes on 3-4 April 1974, when the author found a strange pattern of tree damage (Fig. 1.1). Unlike the swirling patterns of fallen trees, commonly seen from the air in the wake of tornadoes, hundreds of trees were blown down outward in a starburst pattern. Trees near the starburst center were flattened or uprooted, spattered by a brownish topsoil.

Fig. 1.1 A starburst pattern of tree damage near Beckley, West Virginia. This picture was taken by the author while surveying the paths of superoutbreak tornadoes on 3-4 April 1974. The damage suggests that an intense downburst could induce tornado-like damage.

Although the violent winds which caused the starburst damage no longer existed when the overflight was made, it is natural to visualize a jet of downdraft which hard-landed at the center of the starburst. One could easily simulate a starburst by pointing the nozzle of a garden hose downward so that a jet of water hits the surface to generate a starburst outflow. By varying the slant angle of the nozzle, a perfect starburst will turn into a fan-shaped outburst.

The superoutbreak tornadoes left behind a total of 2598 miles (4180 km) of damage paths, killing 315 persons and injuring 5484 others. However, not all of the damage paths were caused by tornadoes. There were a large number of starburst damage patterns inside and outside the tornado paths. At that time, local residents could confirm only the tornado damage. Because roofs can be blown off and trees can be twisted or uprooted easily by strong starburst winds, at least 15 percent of the path lengths were caused by outburst winds, rather than tornado winds.

While investigating the Eastern 66 accident on 24 June 1975 at John F. Kennedy Airport, New York City, the author hypothesized, on the basis of his starburst airflows, that the aircraft attempted to penetrate starburst winds similar to, but weaker than, those found and photographed over one year earlier. After an exhaustive analysis of the FDR (Flight Data Recorder) data and eyewitness accounts, the author called this windsystem the "DOWNBURST". The winds were strong enough to blow down a jet aircraft, but were too small to be detected by ground-based anemometers in time for warning approaching aircraft.

Unfortunately, the author's concept of the downburst, a strong downdraft which induces an outburst of damaging winds on or near the ground, was regarded controversial. Most meteorologists at that time believed that a downdraft, no matter how strong it may be inside or beneath the cloud, should weaken to an insignificant speed long before reaching the surface. That is to say, an aircraft on or near the ground would not be affected by the downflow-induced, outflow winds.

In an attempt to clarify the nature of the controversy late in the 1970s, the author and his co-investigators at the University of Chicago used low-flying Cessna aircraft for taking close-up photographs of damage patterns left behind by major or minor windstorms in the midwestern United States. Numerous photographs taken during a number of fact-finding missions overwhelmingly supported the concept of a near-ground airflow characterized by a concentrated downflow which patiently descends almost to the ground without attempting to spread out prematurely.

Both aerial and ground photographs taken at the dead center of a downburst show the change in the airflow direction, from vertical to horizontal, upon hitting the ground surface or a ground object. For example, cornstalks near the dead center of a downburst were either cut or broken by strong straight-line winds outbursting from a single spot in the cornfield (Fig. 1.2). Another example shows a strong horizontal airflow induced by a slanted

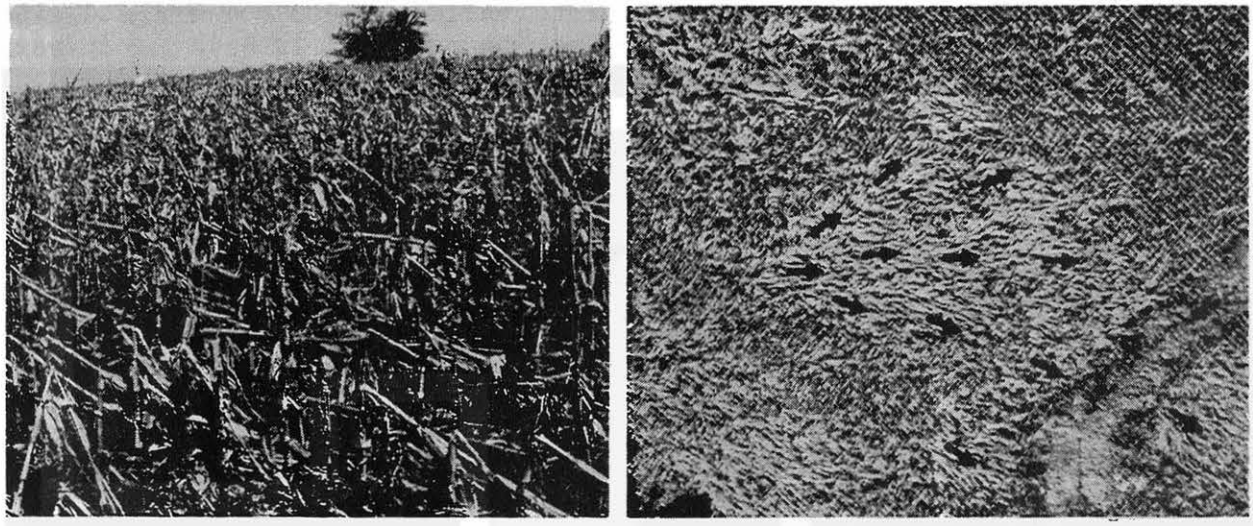

Fig. 1.2 Aerial and ground photographs of a cornfield at the dead center of a microburst in Indiana on 30 September 1977. Photo by Fujita

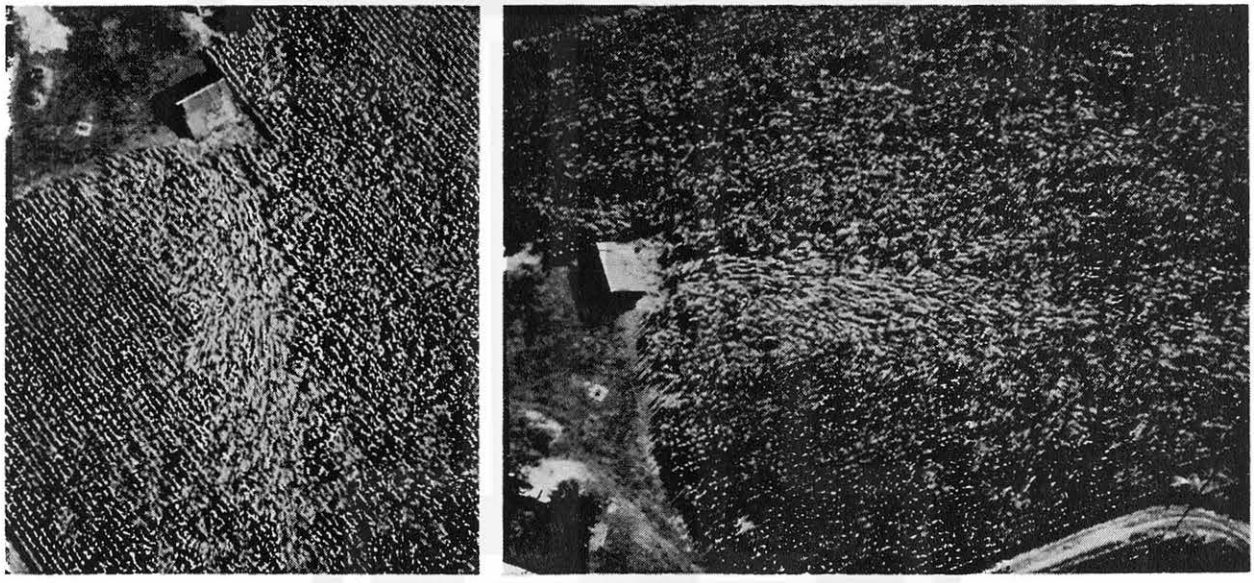

Fig. 1.3 A strong jet of horizontal airflow induced by a slanted roof at an Indiana farm on 30 September 1977. A portion of the tin roof was peeled off and carried away into the cornfield. Photo by Fujita

roof as the downflow was deflected into a cornfield. Normally, a ground object acts as an obstacle to horizontal winds, resulting in a band of weak airflow extending downwind from the object. It is difficult to explain the existence of a strong horizontal jet-like current without assuming that a downward current was deflected by the slanted roof (Fig. 1.3).

The first field program on downburst, called NIMROD (Northern Illinois Meteorological Research On Downburst), was conducted in 1978 by the University of Chicago, with principal investigators Fujita and Srivastava. The project network, located in the western suburbs of Chicago, Illinois, was designed to depict the structure of downbursts in general by using three Doppler radars and 27 PAM (Portable Automated Mesonet) stations.

During the 42 operation days of the NIMROD network, both Doppler radars and PAM depicted a large number of downbursts. Some were small, while others were very large in horizontal scale. In order to distinguish relatively small downbursts from their larger counterparts, the author subclassified the downburst into "MACROBURST" and "MICROBURST", according to the horizontal extent of the damaging winds.

The second experiment in 1982, called JAWS (Joint Airport Weather Studies) was conducted jointly by the University of Chicago and the National Center for Atmospheric Research, with principal investigators Fujita, McCarthy, and Wilson. The JAWS Network, located in the northern suburbs of Denver, Colorado was designed to depict microbursts, rather than macrobursts, because a number of microburst-related accidents and incidents kept occurring in various parts of the world. In fact, the PAA 759 accident occurred during JAWS field program in a microburst at New Orleans airport.

Table 1.1 A comparison of NIMROD (1978) and JAWS (1982) Networks and the statistics of microbursts detected by PAM stations operated 24 hours a day.

Projects	N I M R O D	J A W S
Periods	19 May - 1 July (42 days)	15 May - 9 August (86 days)
Doppler Triangles	56 x 57 x 60 km	15 x 18 x 28 km
Doppler Radars	CHILL CP-3 CP-4	CP-2 CP-3 CP-4
PAM Stations	27	27
Total microbursts	50	186
Dry microbursts	18 (36%)	155 (83%)
Wet microbursts	32 (64%)	31 (17%)

The comparison of NIMROD and JAWS Projects in Table 1.1 show that the area of the NIMROD network was much larger than that of the JAWS network. The former was designed to depict both macrobursts and microbursts, while the objective of the latter was to depict only microbursts. Of the 50 microbursts detected in the NIMROD network, 64% were accompanied by measurable rain (0.01" or more) while the other 36% had no measurable rain on the ground. Based on these statistics, microbursts were subdivided into "dry microbursts" and "wet microbursts" depending on the rainfall measured on the ground during a microburst.

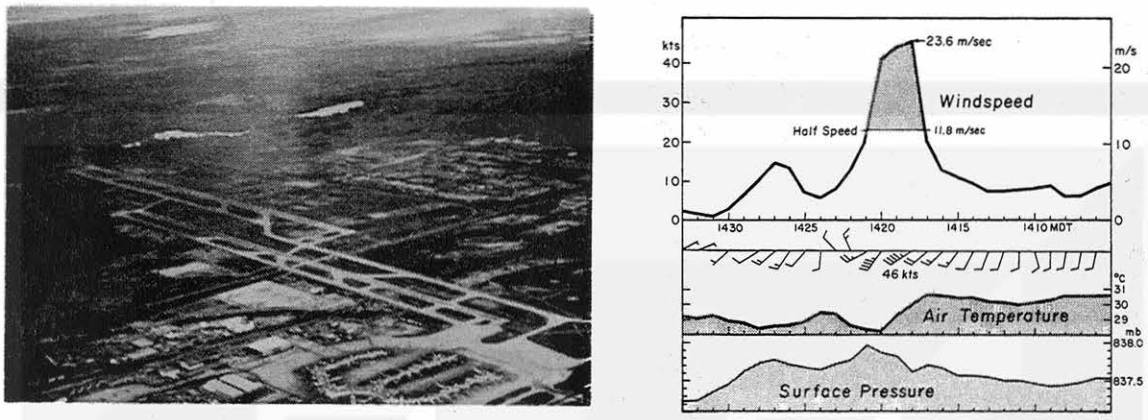

Fig. 1.4 Innocent-looking virga above Runway 35R of Stapleton Airport at Denver, Colorado on 14 July 1982 (left photo). This virga induced a microburst with a peak wind lasting only 3 minutes. Temperature dropped 2.5° C and pressure rose 0.3 - 0.4 mb (right diagram). Photo by Fujita

It is important to note that 83% of JAWS microbursts were dry, occurring mostly beneath innocuous virga. An example of a dry microburst photographed over Stapleton Airport during JAWS is no more than an innocent-looking virga. Nonetheless, PAM station 21, located near Runway 35R beneath the virga, recorded 23.6 m/sec (46 kts) peak wind (Fig. 1.4). On the other hand, 64% of the NIMROD microbursts were wet, accompanied often by blinding rain. Although no pictures of wet microbursts during NIMROD were available, a photo sequence of a wet microburst to the east of Wichita, Kansas shows a remarkable difference between the appearance of wet and dry microbursts (Fig. 1.5).

Damaging microburst winds in the United States occur predominantly during the spring and summer months. Most microbursts have been confirmed through aerial and ground surveys, one to several days after their occurrences. Cornfields with numerous cornstalks, acting like low-accuracy, high-density anemometers, are the best type of fields on which streamlines of damaging winds are preserved. A close-up photograph taken from 500' to 1000' above the ground depicts a pattern of flattened cornstalks which remain flattened until they are cut by farmers (Fig. 1.6).

Bundles of hay and other loose objects are excellent tracers of damaging microburst winds. An aerial photograph taken in Oklahoma reveals a definite flow pattern of microburst winds which are straight and divergent (Fig. 1.7).

From time to time, while surveying storm damage, we receive complaints that residents were hit by a damaging tornado without warning. Aerial surveys often reveal that a microburst rather than a tornado caused the tornado-like damage.

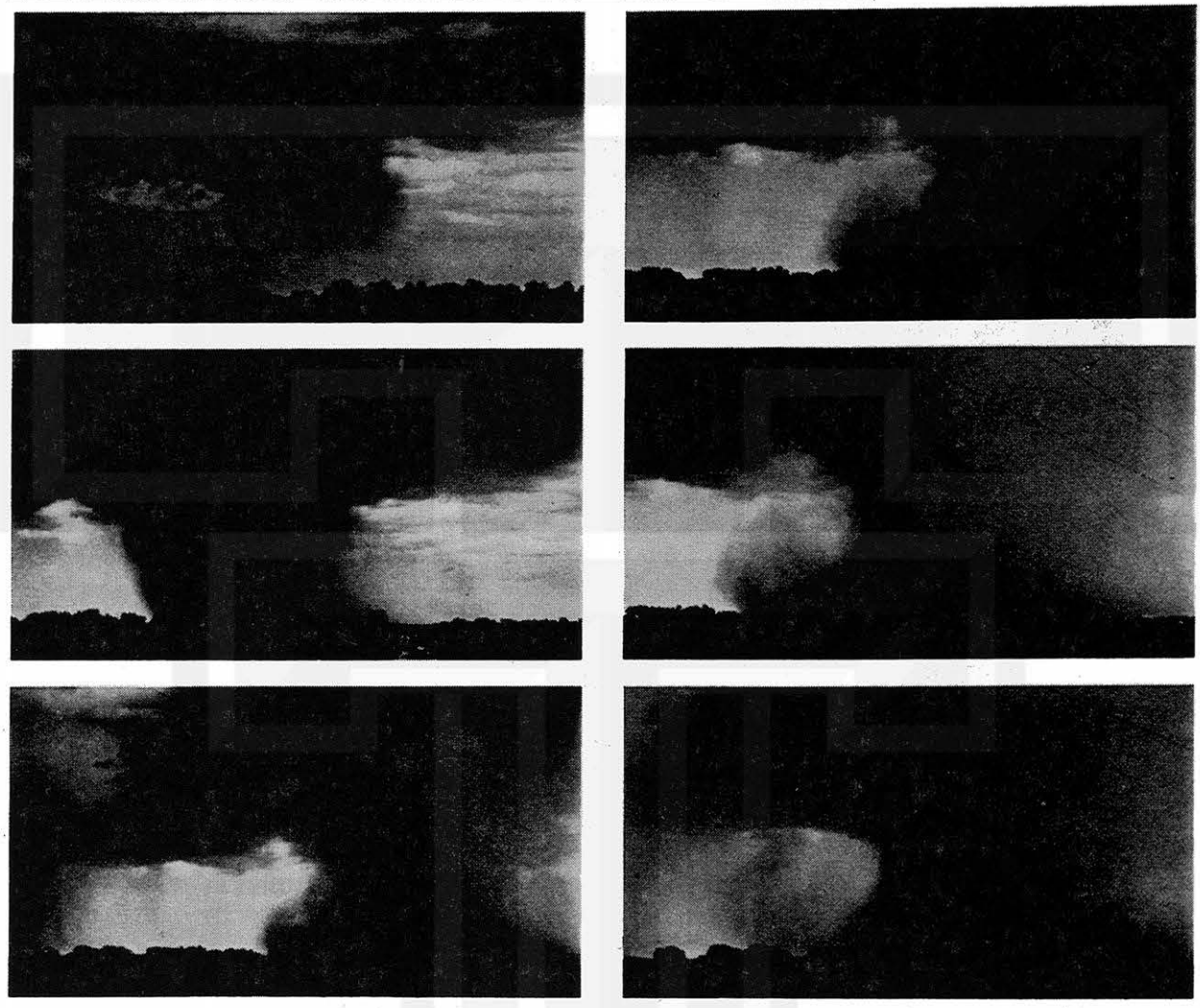

Fig. 1.5 A sequence of photos of a wet microburst on 1 July 1978 to the west of Wichita, Kansas which were taken at 10 to 60 seconds intervals, looking south. A curling motion showing a vortex with a horizontal axis is visible near the left (west) edge of the outburst flow. Copyrighted photos by Mike Smith

With the exception of the NIMROD and JAWS operations, Doppler radars located in various parts of the country rarely have detected microburst winds operationally. This is because microbursts are small and short lived. Furthermore, their maximum winds are very close to the ground where radar echoes are contaminated severely by ground clutter.

To meet an urgent requirement for safe operations of jet aircraft in and around major airports, the FAA (Federal Aviation Administration) has been developing a pulsed Doppler radar capable of detecting microbursts automatically within 20 to 40 seconds after each volume scan, updating

every one to two minutes. Until such a Doppler radar becomes available, an efficient detection of a microburst by present-day Doppler radar will not be feasible.

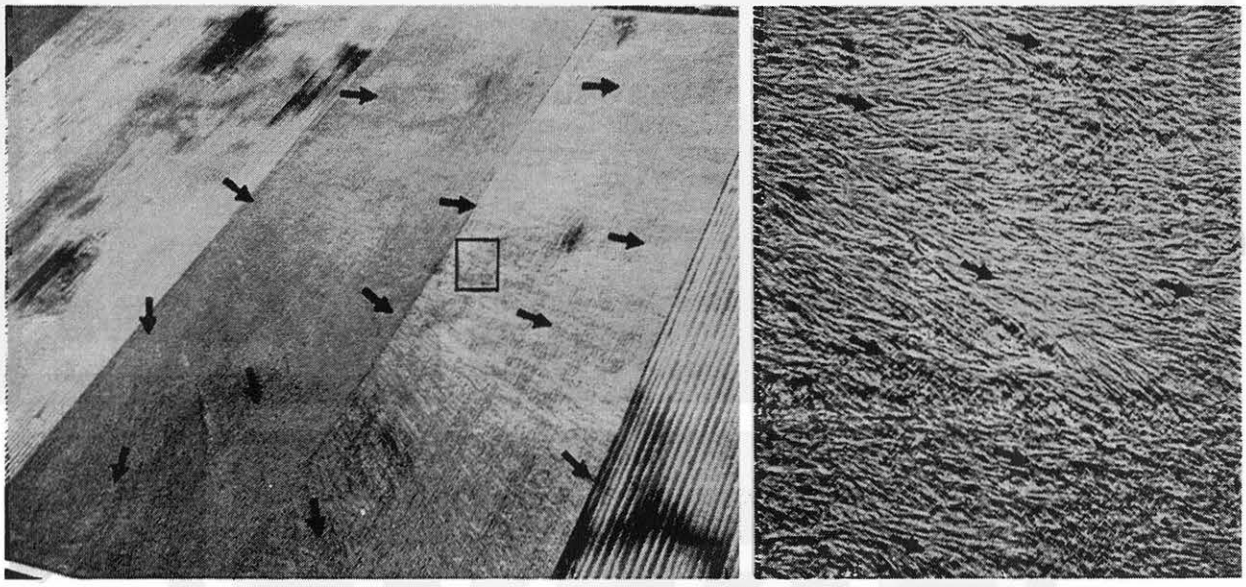

Fig. 1.6 A cornfield near Danville, Illinois flattened by a microburst on 30 September 1977. A close-up picture (right photo) shows an enlargement of the small boxed area in the left picture. Photos by Fujita

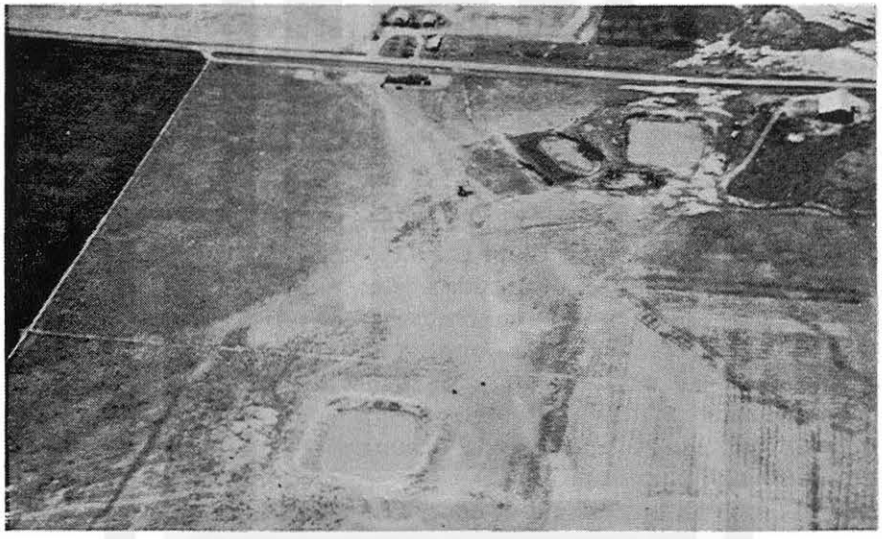

Fig. 1.7 A pattern of straight-line winds in a microburst in Oklahoma on 10 April 1979. Scratch-like lines extending from lower left to upper right are cattle and tire tracks unrelated to the winds. Photo by Fujita

Chapter Two

Observations of Macrobursts and Microbursts

A downburst is a strong downdraft which induces an outburst of damaging winds on or near the ground. Damaging winds, either straight or curved, are highly divergent. The sizes of downbursts vary from less than one kilometer to tens of kilometers. Downbursts are subdivided into macrobursts and microbursts according to their horizontal scale of damaging winds.

MACROBURST: A large downburst with its outburst winds extending in excess of 4 km (2.5 miles) in horizontal dimension. An intense macroburst often causes widespread, tornado-like damage. Damaging winds, lasting 5 to 30 minutes, could be as high as 60 m/sec (134 mph).

MICROBURST: A small downburst with its outburst, damaging winds extending only 4 km (2.5 miles) or less. In spite of its small horizontal scale, an intense microburst could induce damaging winds as high as 75 m/sec (168 mph).

2.1 Planetary Scale

The planetary scale proposed by Fujita in 1981 consists of five categories arranged in the order of the vowels, A - E - I - O - U. The length scale which separates each scale cascades down by 1/100 per scale. As shown in Table 2.1, a mesoscale disturbance covers the area of one to several states, while the misoscale disturbance has a horizontal dimension comparable or smaller than the size of a major airport. In other words, a macroburst could affect several states, whereas the birth and death of a microburst could take place inside a major airport without being noticed by those who stay outside the airport. A very small microburst could cause serious difficulties on one runway while other runways are untouched.

In the context of the planetary scale, a macroburst is a mesoscale downburst and a microburst is a misoscale downburst. By virtue of its small size and its short life of less than 10 minutes, a microburst often escapes detection by non-Doppler radars or ground-based anemometers. Consequently, an aircraft at low altitude could encounter a microburst

unexpectedly. A similar encounter could be experienced by cars and trucks on highways or by boats and ships on rivers, bays, and oceans.

Table 2.1 Fujita's (1981) planetary scale which cascades down from 40,000 km, the circumference of the earth to 4 mm, the size of a pea.

Dimension	40,000-400km	400 - 4km	4km - 40m	40m - 40cm	40cm - 4mm
Scale Read as	MASOscale (ma-so)	MESOscale (me-so)	MISOscale (my-so)	MOSOscale (mo-so)	MUSOscale (myu-so)
Downburst		MACROBURST	MICROBURST		
Cyclone	Hurricane	Mesocyclone	Tornado	Dustdevil	Turbulent Eddy

2.2 Appearance of Macrobursts

Because of its large horizontal scale, a macroburst is characterized by a pile of cold air created by a succession of downdrafts soft-landing beneath the parent raincloud. Since a dome of cold air is heavier than the warm air surrounding it, the atmospheric pressure inside the dome is higher than its environment. The pressure gradient force, pointing outward from the dome area, pushes the cold air outward inducing gusty winds behind the leading edge of the cold air outflow. The gust front denotes the leading edge of gusty winds which push the dome boundary away from the subcloud region (Fig. 2.1).

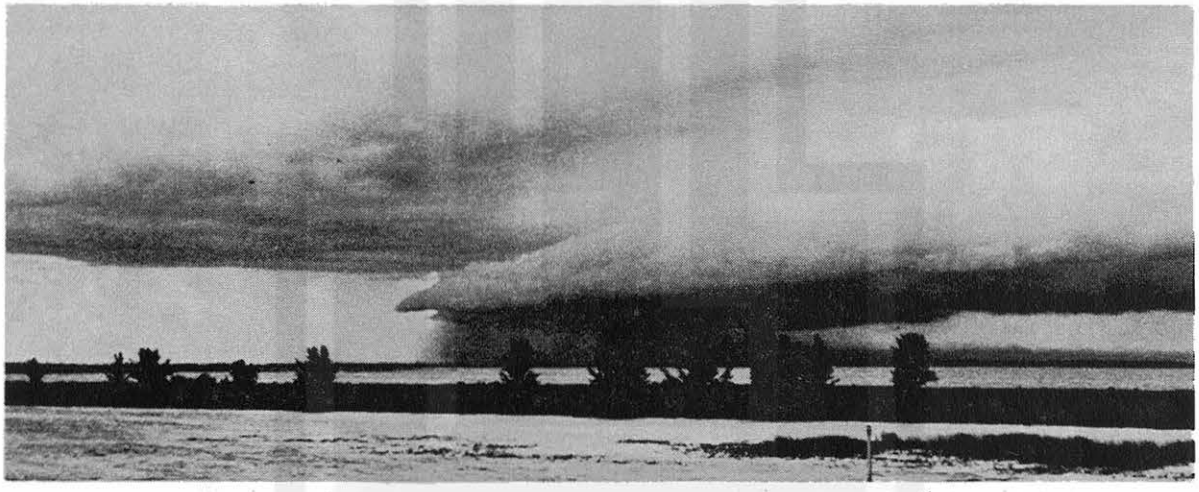

Fig. 2.1 A view of the leading edge of a macroburst on 12 August 1975 near Lake Okeechobee, Florida. The leading edge is characterized by a roll cloud, dust clouds, and a front of gusty winds (gust front). Photo by Ron Holle

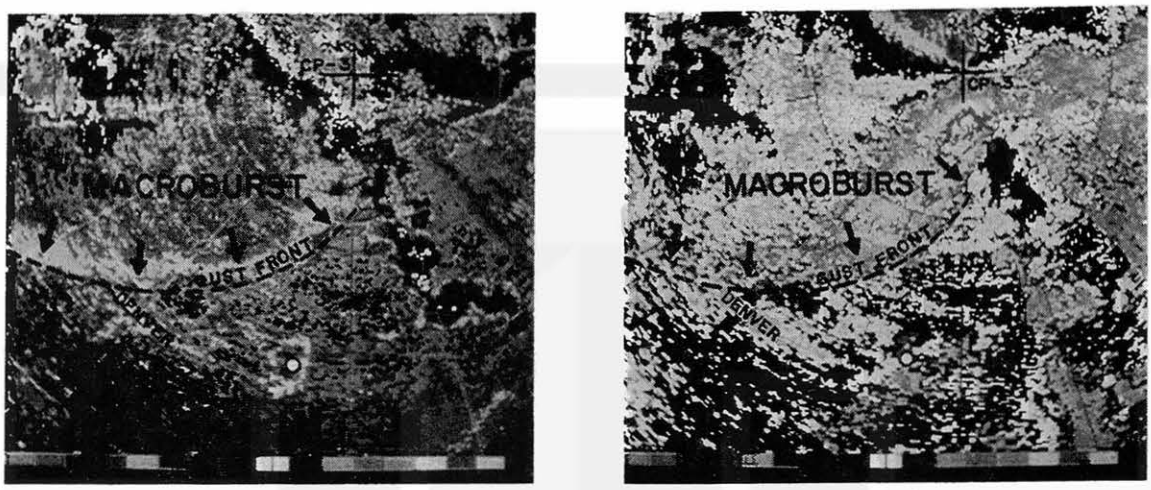

Fig. 2.2 A gust front (dashed black line) and a microburst (red and white circle) depicted by the CP-3 Doppler radar at 1440:15 MDT 14 July 1982. Reflectivity (left) and velocity (right) photos reveal the difference in the horizontal dimensions of macroburst and microburst.

A macroburst detected by a Doppler radar is characterized by an arc-shaped gust front on the reflectivity display and an extensive positive or negative velocity field behind the gust front. Figure 2.2 shows an example of both velocity and reflectivity fields of a macroburst located to the north of

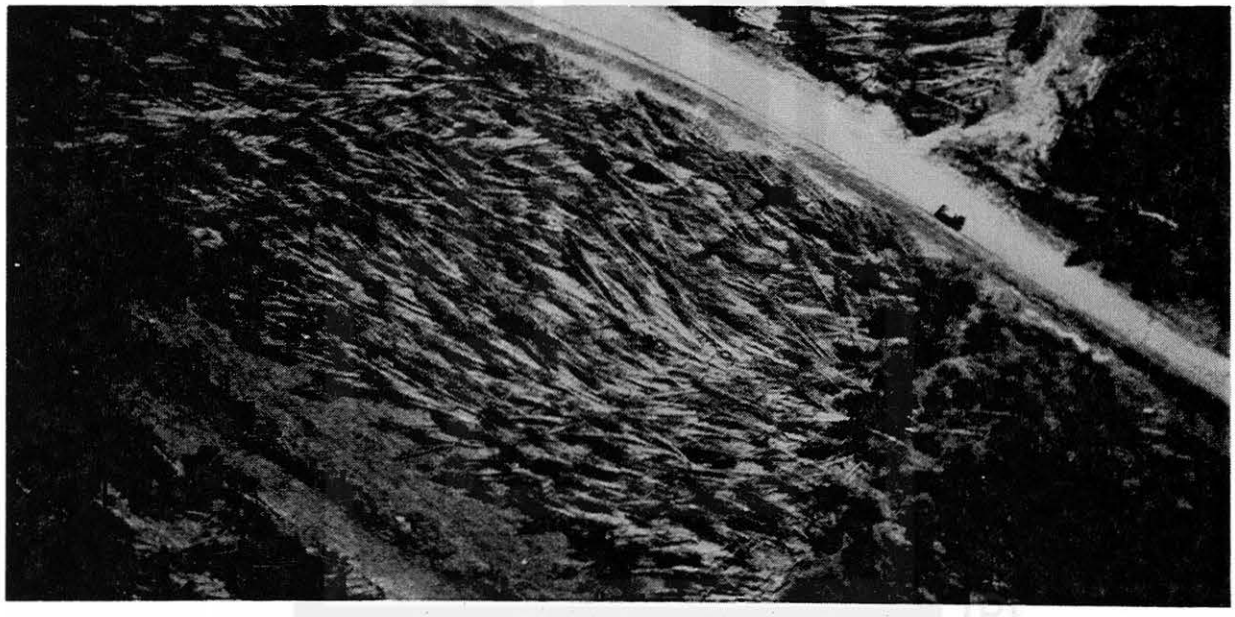

Fig. 2.3 Hundreds of trees in Sawyer County blown down by the northern Wisconsin macrobursts on 4 July 1977. Photo by Fujita

Denver. The gust front was made visible by a band of weak reflectivity echoes, up to 10 dBZ. A jump in the Doppler velocity is shown along the gust front.

A sequence of large and strong macrobursts was experienced in northern Wisconsin on the 4th of July, 1977. It was reported that several counties were hit by high winds. The tree and property damage was described as that done by an oversized tornado. Extensive aerial photography and subsequent mapping by the author revealed no evidence of a tornado. Instead, there were 25 macrobursts inside the damage path, 17 miles (27 km) wide and 166 miles (267 km) long. The maximum windspeed inside the damage area of the northern Wisconsin macrobursts was estimated to be F2 on the Fujita Tornado Scale or 113 - 157 mph (50 - 70 m/sec). Trees were blown down like matchsticks (Fig. 2.3). Some outbuildings and barns were unroofed or leveled by the macroburst winds (Fig. 2.4).

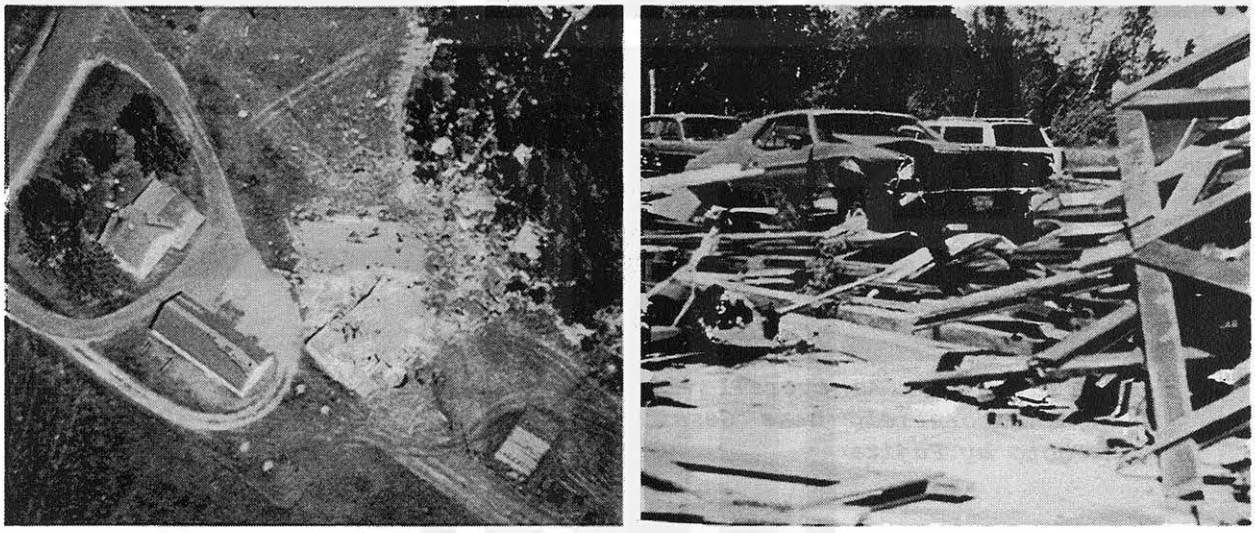

Fig. 2.4 A barn near Phillips, Wisconsin blown apart by the 4 July 1977 macroburst storm. Immediately after the storm, local residents reported that they were hit by tornadoes. Photo by Fujita

2.3 Appearance of Microbursts

Meteorologists with considerable experience in aerial photography from low-flying aircraft are able to control their flight level and aircraft attitude in order to take pictures of wind effects left behind by a damaging microburst.

An aerial photograph of a cornfield (Fig. 2.5) was taken from 6,000 ft (1.8 km) AGL, looking 40° to 50° away from the sun. By selecting a proper sun angle, one is able to increase the reflectance of damaged corncrops

Fig. 2.5 An overall view of a microburst that descended on a cornfield near Gessie, Indiana on 30 September 1977. Photo by Fujita

so that they appear light gray in aerial pictures. These damage streaks, accentuated by the black arrows, show convincingly that microburst winds which diverged from the touchdown spot blew along streamlines with cyclonic curvature (toward the aircraft) and anticyclonic curvature (away from the aircraft). Apparently, the microburst downflow hit the ground at a slanted angle while moving from right to left in the picture.

A small but very strong microburst often causes a starburst-shaped tree damage. If we assume a 25 m/sec (56 mph) outburst wind along a circle of 100 m (330 ft) radius from the microburst center, the mean divergence inside the circle is as large as 0.5 per second. In order to induce such a large divergence at the near-ground level, the downflow speed will have to be 5 m/sec (16 fps) at 10 m (33 ft) AGL and 10 m/sec (33 fps) at 20 m (66 ft) AGL. In other words, the downward current at the starburst center is very strong even at the tree-top level (Fig. 2.6).

In contrast to the very strong outburst winds inside a microburst, its

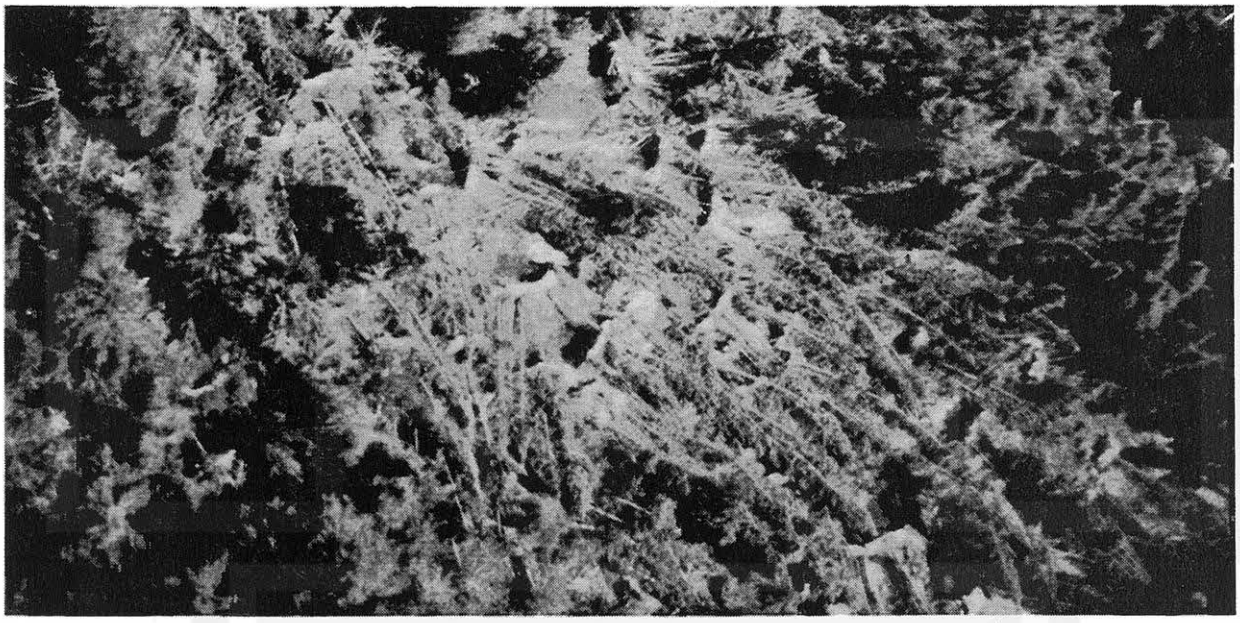

Fig. 2.6 An intense microburst embedded inside one of the northern Wisconsin macrobursts on 4 July 1977. This picture implies that a downflow descended almost to the tree-top height before spreading. Photo by Fujita

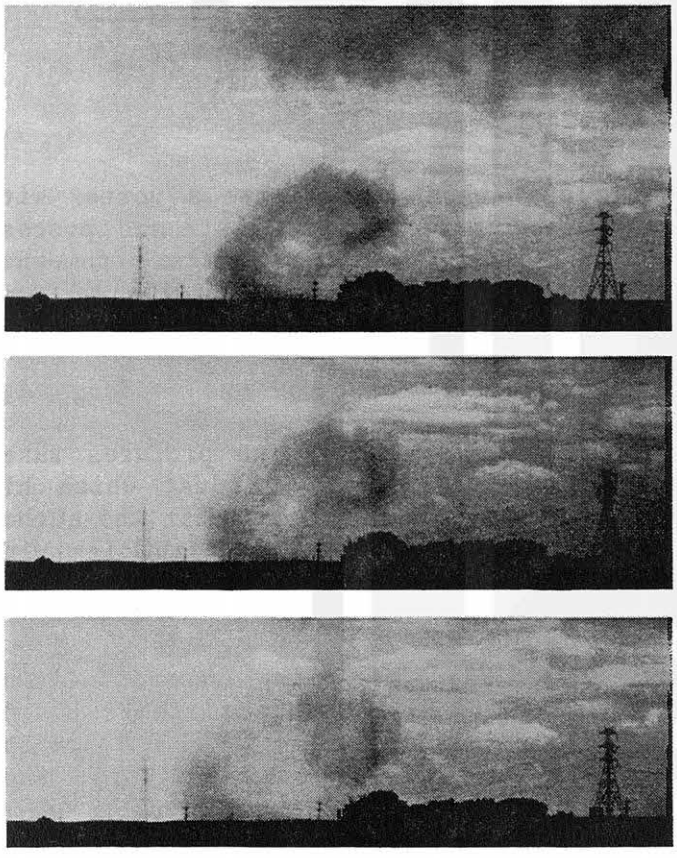

Fig. 2.7 A sequence of telephoto pictures showing the curling features of the dust clouds behind the leading edge of a microburst outflow. Pictures were taken looking south from the CP-3 site on 15 July 1982 during the JAWS field operation. Photos by Brian Waranauskas

boundary propagates outward rather slowly. Photographic evidence of the microburst winds made visible by flying dust often shows a vortex with a horizontal axis. When the horizontal vortex encircles the downflow center, forming a vortex ring, the outbursting winds beneath the vortex ring are accelerated continuously as the ring expands and stretches (Figs. 2.7 and 2.8).

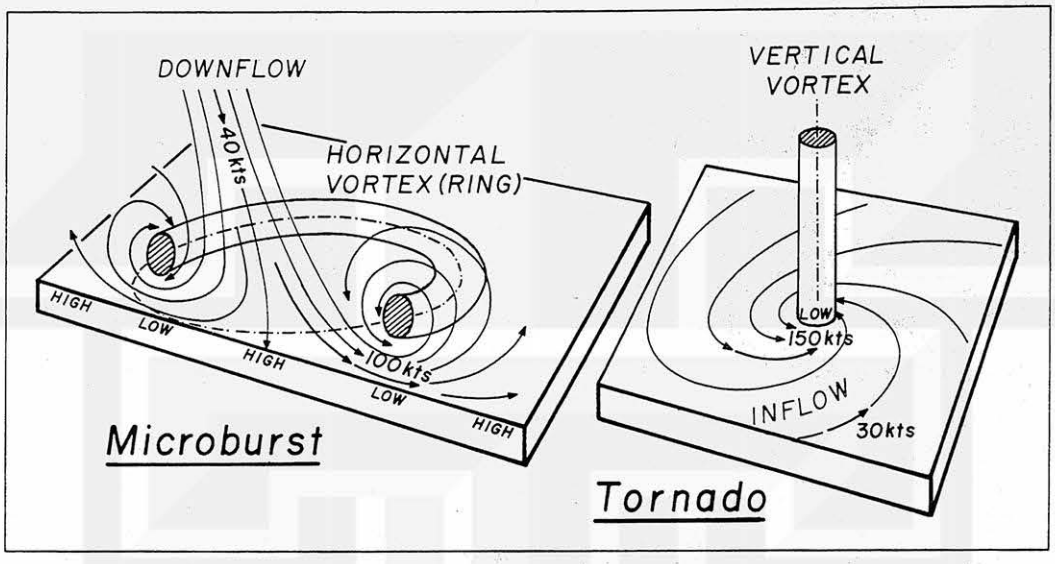

Fig. 2.8 Simplified models of a vertical vortex in a tornado and a horizontal vortex in a microburst.

Figure 2.9 shows a cloud of blowing dust which turns into a vortex with a horizontal axis. Three pictures on the left depict a strange process in which a horizontal vortex redevelops into a vertical vortex, somewhat like a giant dustdevil or a dusty tornado topped by an umbrella of thin dust.

It is rather exciting to watch an approaching cloud on the leading edge of an oncoming microburst. At 1344 MDT on 08 July 1982, a JAWS PAM station at the CP-3 site recorded an 18 m/sec (40 mph) wind. Two pictures taken at 1343:30 and 1344:25 MDT depict an advancing cloud of dust which hit the PAM station shown in the picture. When the cloud of dust hit the author at the CP-3 site, visibility dropped to zero with a single-peak high wind lasting from one to two minutes. It was the dustiest dust ever experienced by the author (Fig. 2.10).

Doppler radar is a powerful tool used for measuring and displaying microburst winds. The microburst in Fig. 2.10 was scanned in the PPI mode at three elevation angles approximately 4 minutes before the CP-3 PAM station recorded the peak wind. The PPI photos, with 2-km range markers, show a 13 m/sec approaching velocity at 0.0° elevation angle, and a 15 m/sec approaching velocity at 2.4° and 4.8° elevation angles (Fig. 2.11).

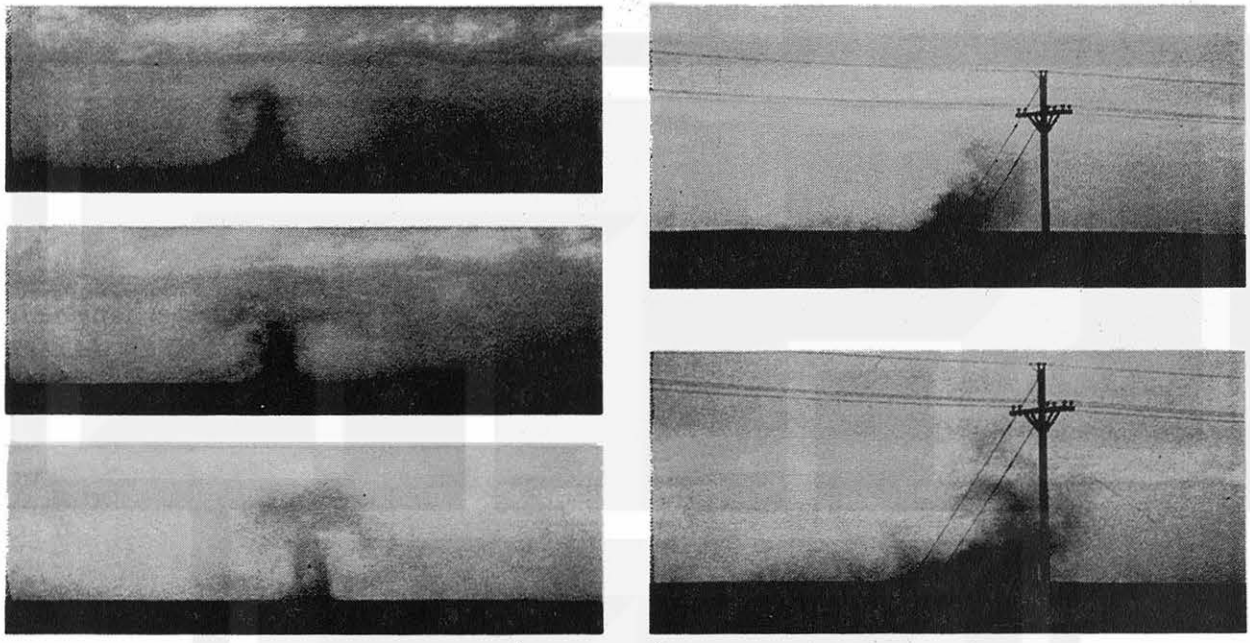

Fig. 2.9 Various features of microburst-induced dust clouds beneath a decaying anvil cloud on 18 July 1982 during the JAWS Project. Left photos: Looking NNE at 1744:35 (top), 1745:45, and 1745:55 MDT. Right photos: Looking ENE at 1758:30 (top) and 1758:55 MDT. Photos by Joe Golden

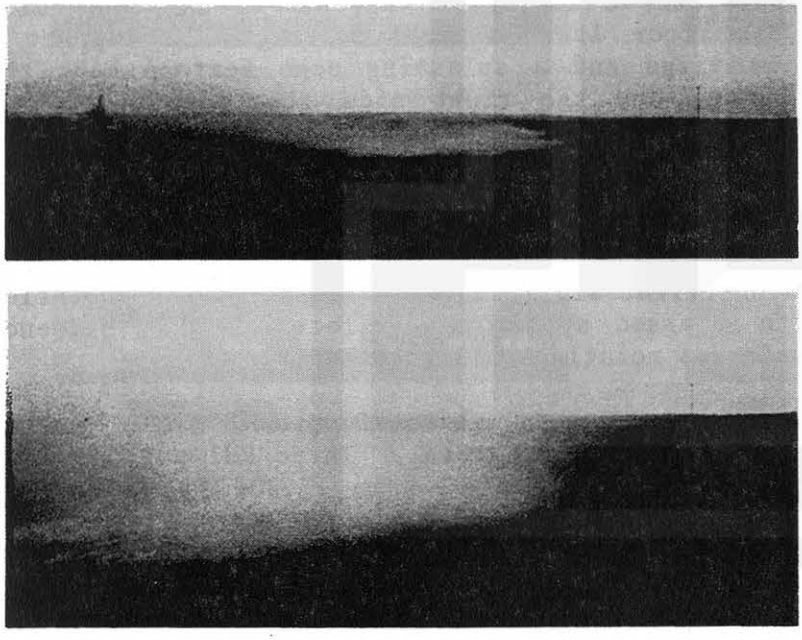

Fig. 2.10 Dust clouds on 8 July 1982 approaching the CP-3 Doppler radar site. The upper picture was taken at 1343:30 MDT, looking west, shortly before the PAM station in the picture recorded an 18 m/sec (40 mph) peak wind. The lower picture was taken a few seconds before the dust cloud hit the CP-3 site. Photo by Fujita at the CP-3 site looking west.

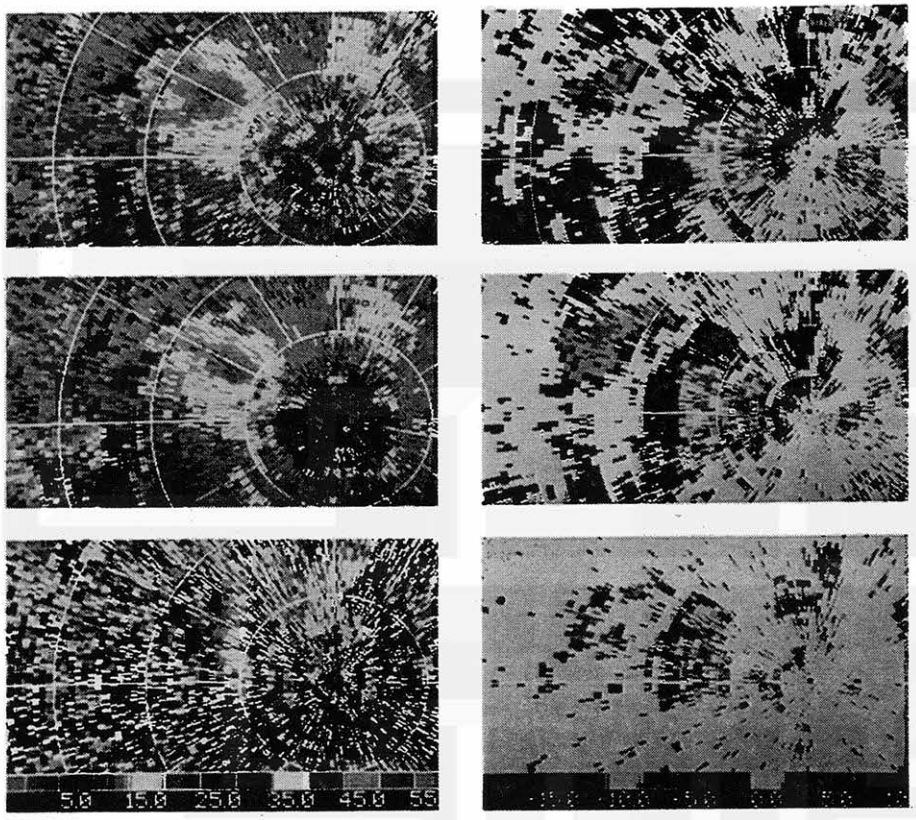

Fig. 2.11 Reflectivity (left) and velocity (right) images of the 8 July 1982 microburst in Fig. 2.10 obtained by the CP-3 Doppler radar. Top: 4.8° elevation angle at 1340:12 MDT. Middle: 2.4° elevation angle at 1339:48 MDT. Bottom: 0.0° elevation angle at 1339:23 MDT. The entire life of this microburst was observed and photographed from the CP-3 site.

The RHI scan of microbursts by Doppler radar is a very effective means of determining their vertical structure. On 12 June 1984, when a virga was passing over Stapleton Airport, a series of RHI cuts of the descending virga was made by CP-3. The four left pictures in Fig. 2.12 depict a vertical shaft of descending virga and a splashing echo feature near the ground. Doppler velocity images on the right side show an approaching velocity on the radar side of the splash and a receding velocity on the other side, indicating the existence of an outflow near the ground. The color distribution reverses at high level where the upper inflow is located. The velocity color at the middle level, the level of non-divergence, should be white, i.e., zero velocity, if the downflow was not rotating. In this case, however, the color on the right side (largest azimuth) of the downflow shaft is green with a 2 to 4 m/sec approaching velocity. This evidence proves that the downflow shaft was rotating anticyclonically.

Another important fact about microbursts revealed by RHI scans is the acceleration of the downflow at the melting level. Three RHI cuts in Fig. 2.13 show the existence of a bright band at 2.4 km (7,900 ft) above the ground. This bright band, located at 3 to 5 km range of the radar, is at the height where the velocity color changes from green (-3 m/sec) to purple (-12 m/sec) with a 9 m/sec increase in downward speed during the melting process of the ice particles. The downflow from this bright band has not reached the surface yet.

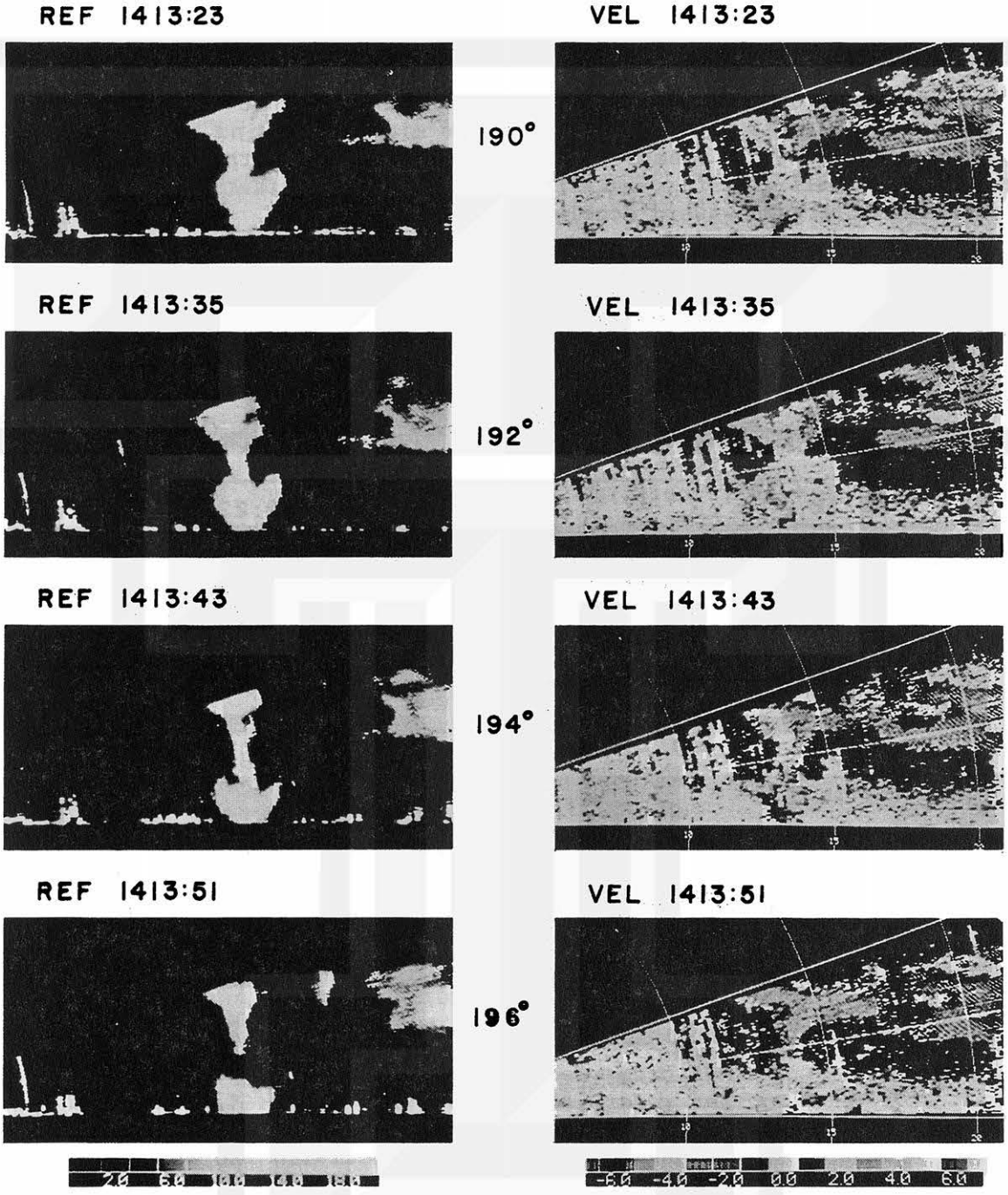

Fig. 2.12 RHI cross sections of a microburst over Stapleton Airport at Denver, Colorado on 12 June 1982. In producing these photos, the CP-3 radar scanned along the 190°, 192°, 194°, and 196° azimuths.

The other bright band, 7 to 8 km from the radar, is accompanied by a diverging flow at the surface, showing that the downflow was in the microburst stage. There is a strong approaching flow extending from near the cloud-top to the bright band, which is likely to be a current which compensates the mass which was lost in the microburst wind that had descended to the ground. This example strongly suggests that the 80 cal/g of heat required to melt falling ice crystals is an important energy source for initiating a large downward acceleration.

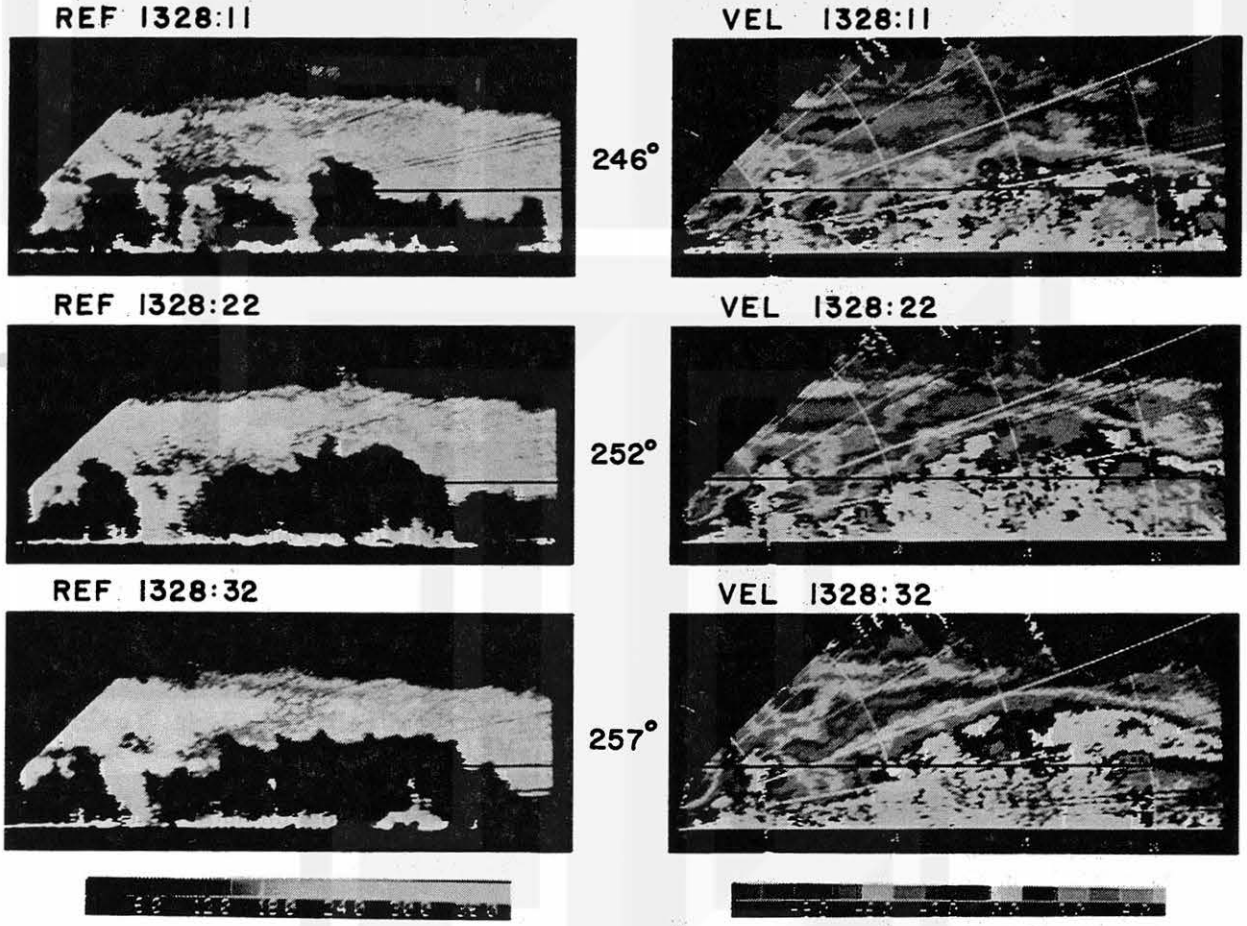

Fig. 2.13 RHI cross sections of a microburst depicted by the CP-3 Doppler radar, scanning toward the 246°, 251°, and 256° azimuths at 1328:11, 1328:22, and 1328:32 MDT respectively. The bright band in the reflectivity photos (left) was located at 3.4 km (11,000 ft) AGL. The height of the bright band in the velocity photos are shown with horizontal black lines.

Chapter Three

Microburst-related Aircraft Accidents

The flow of air which affects aircraft operations are grossly divided into "turbulence" and "wind shear". An aircraft in turbulent flow exhibits irregular and random motions while, more or less, maintaining its intended flight path. Wind shear, with or without turbulence, alters the lift force acting on an aircraft, resulting in a significant sinking or rising motion.

In meteorology, wind shear is the local variation of wind velocity in a given direction. The three components of wind shear can be described by expressing the wind velocity W by

$$W = iu + jv + kw \tag{3.1}$$

where i, j, k are unit vectors pointing toward the x, y, z directions and u, v, w are the x, y, z components of the wind vector.

Wind shear, in aviation, is the time variation of wind velocity along the path of a given aircraft, which can be written as

$$\frac{\Delta W}{\Delta t} = G\frac{\partial W}{\partial L} + \frac{\partial W}{\partial t} \tag{3.2}$$

where L is the distance measured along the flight path. The second term on the right side of this equation denotes the local variation of the winds caused by the formation or the development of a wind system penetrated by an aircraft. That is to say, the second term may not exist prior to the penetration. Whereas, the first term denotes the change of the winds as an aircraft flies into an existing wind-shear system.

Noting that the flight path is included in the x-z plane in Fig. 3.1, we define the shear of the three component winds u, v, w by

$$-\frac{\Delta u}{\Delta t} = \text{Headwind shear, + headwind ; - tailwind} \tag{3.3}$$

$$\frac{\Delta v}{\Delta t} = \text{Crosswind shear, + from right ; - from left} \tag{3.4}$$

$$\frac{\Delta w}{\Delta t} = \text{Vertical wind shear, + upward ; - downward} \tag{3.5}$$

3.1 Effects of Wind Shear upon Lift Force

An aircraft with true airspeed A, flying inside a three-dimensional wind W, moves with the ground-relative velocity G. The lift force acting on the aircraft is perpendicular to vector A, and the drag force points opposite to vector A. Using the symbols in Fig. 3.1, the lift force can be expressed by

$$F = \frac{1}{2} \rho A^2 C_L S \tag{3.6}$$

where ρ is the density of air, C_L the lift coefficient, and S the cross-sectional area of the lift force acting on the aircraft. Since β is small and both θ and G do not vary with time as fast as the winds do, we are able to approximate the ground speed and the angle of attack as

$$G \cong A + u \quad \text{or} \quad 0 = \frac{\Delta A}{\Delta u} + 1 \tag{3.7}$$

$$\alpha = \theta - \gamma + \frac{w}{G} \quad \text{or} \quad \frac{\partial \alpha}{\partial w} = 0 - 0 + \frac{1}{G}. \tag{3.8}$$

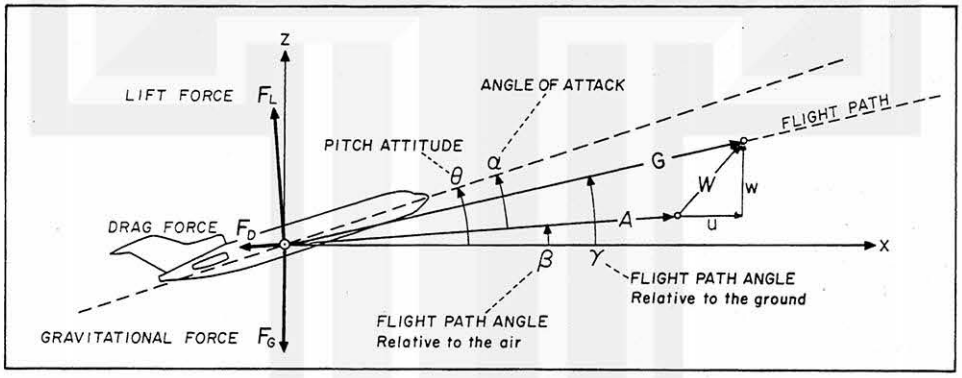

Fig. 3.1 Definition of the quantities used in this chapter. F_L -- lift force, F_G -- gravitational force, F_D -- drag force, α -- angle of attack, β -- flight path angle relative to the air, γ -- flight path angle relative to the ground, θ -- pitch attitude, W -- wind vector, u, v, w -- x, y, z components of wind vector, A -- true airspeed, and G -- ground speed.

The increment of the lift force due to the variation of u and w is computed by differentiating Eq. (3.6) as

$$\Delta F_L = \frac{1}{2} \rho C_L A^2 S \left(\frac{2}{A} \frac{\partial A}{\partial u} \Delta u + \frac{1}{C_L} \frac{\partial C_L}{\partial \alpha} \frac{\partial \alpha}{\partial w} \Delta w \right) \tag{3.9}$$

Using Eqs. (3.7) and (3.8), we simplify Eq. (3.9) into

$$\frac{\Delta F_L}{F_L} = -\frac{2}{A} \Delta u + \frac{k}{G} \Delta w \tag{3.10}$$

where $$k = \frac{1}{C_L}\frac{\partial C_L}{\partial \alpha}\ (radians) = \frac{180}{\pi C_L}\frac{\partial C_L}{\partial \alpha}\ (degrees) \qquad (3.11)$$

is determined by the characteristics of the lift coefficient during a wind-shear penetration. This equation states that the loss of lift is not only caused by the loss of airspeed but also by the loss of angle of attack which, in turn, reduces the lift coefficient.

A representative curve of a lift coefficient for swept-wing aircraft during a flap-down takeoff configuration is shown in Fig. 3.2. Values in Table 3.1, computed from the figure, reveal that the loss of lift due to a tailwind is constant, irrespective of the angle of attack at which an aircraft flies. On the other hand, the loss of lift increases appreciably with decreasing angle of attack. Eq. 3.10 suggests that the lowering of the pitch angle, selected for gaining airspeed in a tailwind/downflow wind shear, could result in a loss of lift and a subsequent heavy sink.

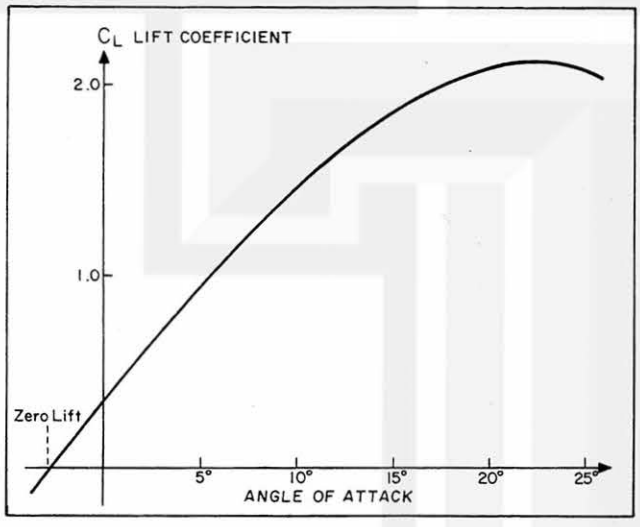

Fig. 3.2 Lift coefficient of swept-wing aircraft with a 15° flap setting and gear-up configuration. The angle of attack is fuselage-relative. The wind-relative angle of attack is approximately 2° larger than the fuselage-relative angle of attack.

Table 3.1 Fractional(%) loss of lift force due to a one knot increase of the tailwind or one knot increase of the downflow. For simplification, A = G = 150 kts was assumed.

Angle of attack	0°	5°	10°	15°	20°
Loss of lift by tailwind	1.3	1.3	1.3	1.3	1.3 % per knot
Loss of lift by downflow	13.2	4.5	2.5	1.3	0.5 % per knot

3.2 Microburst-related Accident Cases

Some aircraft accidents that occurred at low altitudes during convective activity were regarded as pilot error without blaming the weather systems as major contributing factors.

A comprehensive report on wind shear entitled "Low Altitude Wind Shear and its Hazard to Aviation" by the National Academy of Sciences in 1983 lists 27 wind-shear related accidents/incidents in the United States between 1964 and 1982. Ten weather conditions related to these accidents/incidents were selected from the list and tabulated in Fig. 3.3. This figure shows that the 21 cases (78%) were associated with showers with or without thunder, revealing that low-altitude wind shear is induced by ordinary showers as well as thundershowers.

Since June 1975, following the author's investigation of the Eastern 66 accident at JFK Airport, seven wind-shear related accidents were caused by microbursts (red squares in Fig. 3.3). There were three (3) outflow-related cases between 23 July 1973 and 30 January 1974. All of these outflows occurred with rain, suggesting that these outflows could have been microbursts. Two pressure-rise cases in 1964 and 1973 are likely to have been attributable to gust fronts or macrobursts.

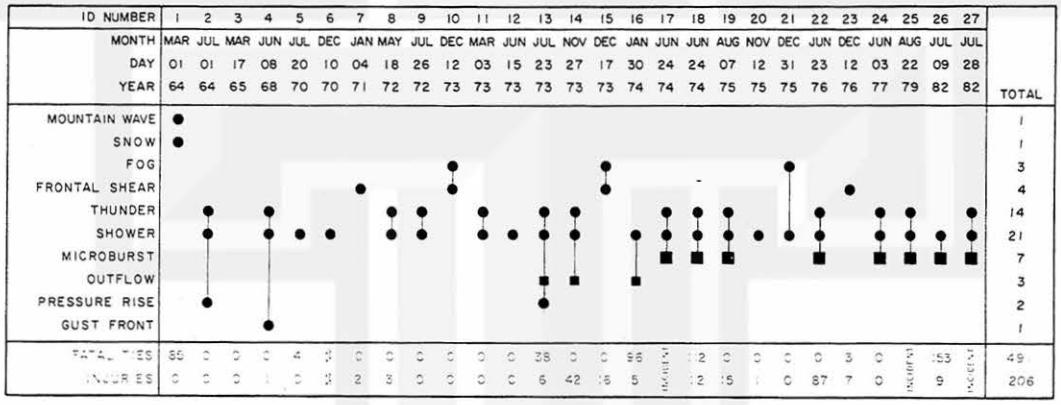

Fig. 3.3 Probable causes of the 27 aircraft accidents/incidents between 1 March 1964 and 28 July 1982. From "Low Altitude Wind Shear and its Hazards to Aviation", National Academy of Sciences (1983)

The locations of microburst-related accidents/incidents known to the author is presented in Fig. 3.4. The high concentration of accidents/incidents in the United States does not necessarily mean that microbursts occur frequently in this part of the world, but is the result of frequent landings and takeoffs, as well as the method of the accident investigation based on established knowledge of microburst wind shear.

Infrequent and spotty accident cases are seen in the tropics, on islands, along the coast, and inside the continent. One accident was reported at Bathurst, Australia in the southern hemisphere. Not until knowledge of microburst-related wind shear becomes known widely to international aviation communities, will microburst-induced wind shear be recognized as an important cause of world-wide accidents/incidents during the takeoff and landing operation.

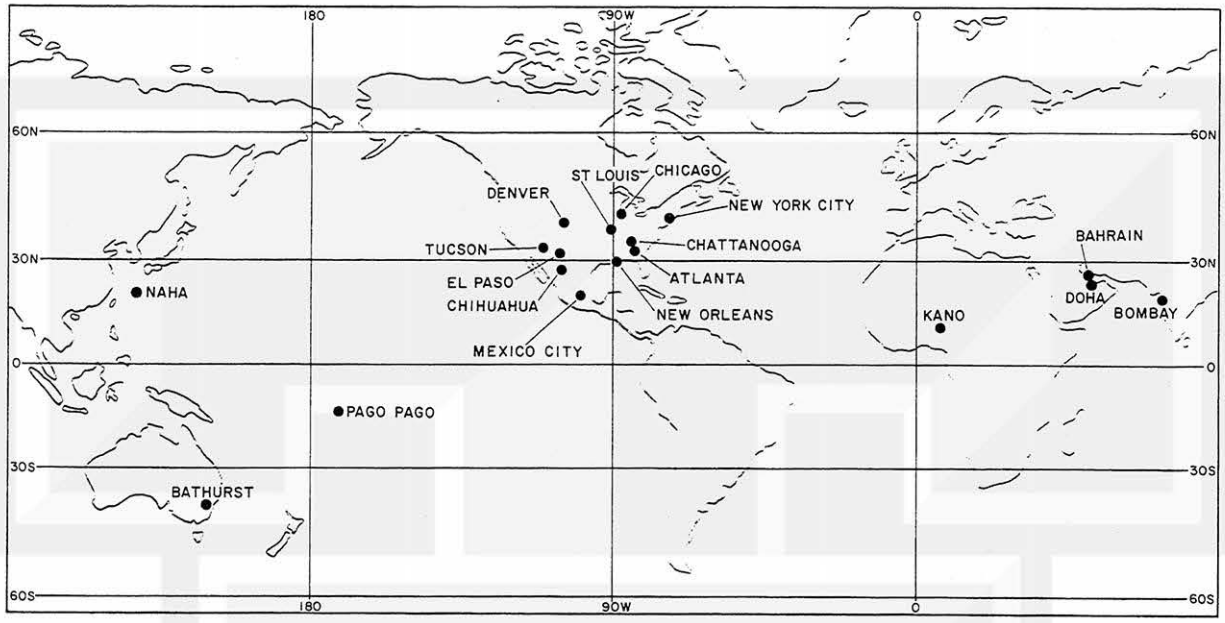

Fig. 3.4 Locations of microburst-related aircraft accidents/incidents around the world. Based on both confirmed and unconfirmed reports available to the author as of December 1984.

3.3 Accidents during Takeoff

When an aircraft encounters a microburst shortly after liftoff, its climb rate decreases as it flies into the downflow section. Then, a weakening of the downflow speed signals the beginning of the tailwind, resulting in a decrease in the indicated airspeed (IAS).

As shown in Table 3.1, a loss of lift occurs during a penetration through a downflow that reduces the angle of attack. The loss of lift due to the downflow becomes extremely large at a small angle of attack. Unless an aircraft maintains a high pitch attitude, it could sink fast before entering into the tailwind section of the microburst. Unfortunately, an aircraft cannot fly out of a microburst without penetrating the tailwind section encircling the downflow section of the storm. The loss of lift due to the tailwind is very serious, because a loss of one knot airspeed results in a 1.3% loss of the lift force.

The combined ill effects of the downflow and the tailwind in a microburst reduces both altitude and airspeed. If a microburst intensity is below the penetrable threshold, one could fly through the winds with a high pitch attitude until the IAS drops to the stickshaker airspeed. In case a microburst is so intense that it cannot be penetrated, no aircraft should fly into the winds. An early detection and warning of such a microburst is absolutely necessary.

Strong Wind Shear at Low Altitude

The altitude of the maximum tailwind is very close to the ground when a microburst is young, say 30 to 60 seconds after its touchdown. In 2 to 10 minutes, the depth of the outflow increases as the outburst winds weaken to an insignificant level.

The stage of a microburst which endangers an aircraft during takeoff operation lasts one to three minutes after the formation of the starburst airflow near the ground. The top picture of Fig. 3.5 shows this dangerous stage characterized by a near-ground outburst winds. The height of these winds is often confined to within 30 m (100 ft) above the ground. This is probably why an accident/incident aircraft keeps on sinking dangerously from 30 to 45 m (100 to 150 ft) above the runway.

The pattern of dust clouds in the lower picture, taken only 57 seconds later, reveals weakened outburst winds (Fig. 3.5). A microburst at this stage can be penetrated safely with a high pitch attitude at full takeoff power.

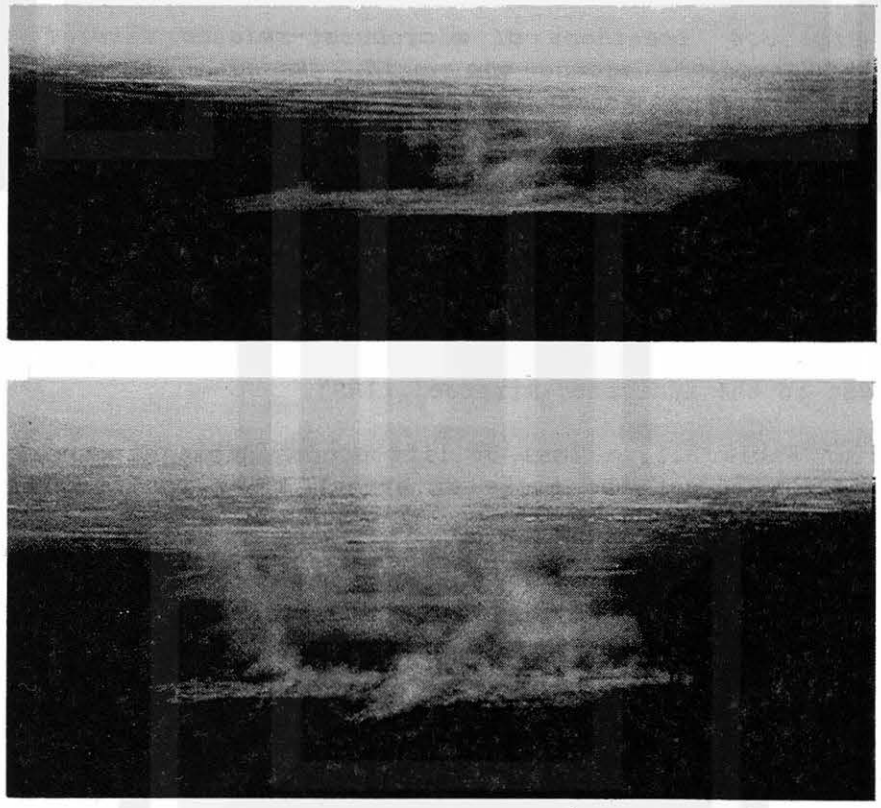

Fig. 3.5 Dust clouds in a microburst on 14 July 1982 to the northeast of Denver, Colorado. Dust in the upper photo, taken at 1546:04 MDT, was blown by a near-ground jet of outburst winds. The lower photo taken at 1547:01, 57 seconds later, indicates that the microburst weakened significantly.

The foregoing evidence of the evolution of a microburst is a warning signal to a pilot that an aircraft could encounter a strong wind shear a very short time after a preceding aircraft, departing from the same runway, reported no wind shear.

BOAC 252/773 Accident at Kano, Nigeria

The earliest microburst-related accident known to the author occurred at Kano, Nigeria on 24 June 1956. A report of that accident was mailed to the author on 25 October 1977, 21 years after the accident. It is amazing to find that BOAC identified a small-scale outflow cell located in front of the departure end of the runway that was used by the accident aircraft. From the author's definition in Chapter 2, the type of wind shear related to this accident was a microburst, 3 km (1.9 miles) in horizontal dimension (Fig. 3.6).

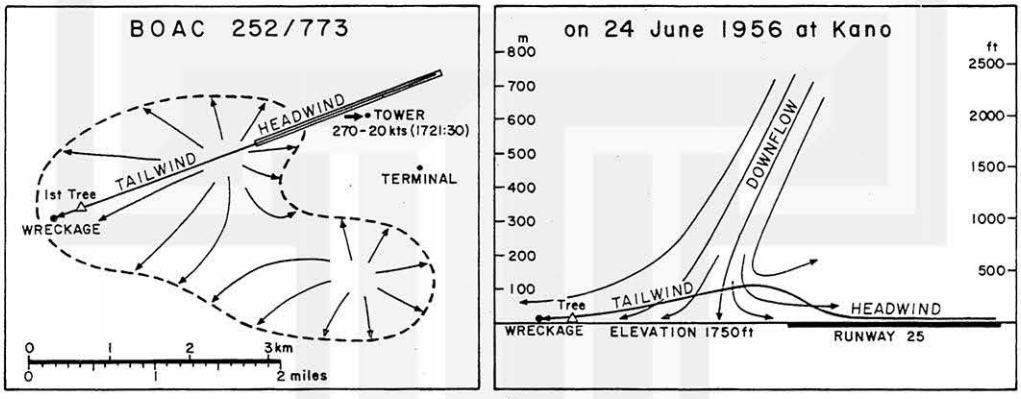

Fig. 3.6 Vertical and horizontal views of BOAC 252/773 microburst at Kano, Nigeria. Wind patterns at 1821 LST were reconstructed. From Ministry of Transport and Civil Aviation, Her Majesty's Stationary Office, London, U.K.

According to the accident report, the BOAC Argonaut, a four-engine propeller aircraft, lifted off Runway 25 at 1821:30 LST in heavy rain. Kano tower observed a surface wind of 270° at 20 kts and 1,500 yds (1.4 km) visibility during the takeoff run. After the aircraft became airborne, the visibility decreased due to heavy rain, necessitating a flight on instruments.

When the aircraft passed over the departure end of the runway at about 100 ft (30 m), its IAS was 125 kts with a maximum fluctuation of 5 kts. At that point the aircraft was climbing at 300 ft/min (1.5 m/sec) and "Flaps Up" was called. Thereafter, the IAS decreased to 103 kts and the aircraft began losing its altitude very rapidly. When it reached level flight, its altitude was only 15 - 20 ft (4 - 6 m) above the ground. The pilot then attempted to climb and the aircraft began responding to the controls.

At this point the aircraft hit the first tree and then crashed. Fire broke out before it came to rest. Of the 45 persons on board the aircraft, 32 were killed, 11 were injured, and 2 others escaped injury.

Continental 426 Accident at Denver, Colorado

This accident occurred at 1611 MDT on 07 August 1975 when Continental 426 attempted a climbout from Runway 35L. The weather situation was rather typical in the Denver area in summer with numerous scattered showers which were small and weak. Nonetheless, the accident aircraft flew into a strong wind shear which brought the aircraft down to the ground near the departure end of the runway. Upon hitting the ground, the aircraft skidded until it stopped at East 56th Avenue along the northern boundary of the airport. Of the 134 persons aboard the aircraft, 15 persons were injured while others escaped injury.

According to an analysis of three weather-related aircraft accidents during the years 1975-76 by Fujita and Caracena, two other aircraft lifted off from the same runway several minutes before Continental 426.

1605:36 MDT Liftoff -- Braniff 67 (B-727)
1608:03 MDT Liftoff -- Frontier 509 (CV-580)
1611:02 MDT Liftoff -- Continental 426 (B-727)

Braniff 67 waited at the end of Runway 36L until a dust cloud, crossing the runway from east to west, cleared up. After brake release, the aircraft accelerated normally. Then all of a sudden, it did not respond to any inputs for 2 to 3 seconds when it crossed a weak shear line. The pilot commented that "In 30 years of airline flying, I have never felt anything quite like it". Everything returned to normal again, and the aircraft lifted off. At 30 - 90 m (100 - 300 ft) altitude, it encountered a downflow and a tailwind, losing 10 - 15 kts (5 - 7 m/sec) IAS.

Frontier 509 also experienced a downflow and a tailwind at 200 ft (60 m) as the previous aircraft had. However, the IAS loss was 25 kts (13 m/sec), much larger than that encountered by Braniff 67. The aircraft reduced its pitch attitude to gain airspeed while flying horizontally for about 20 seconds. Thereafter, the climbout was normal.

Continental 426 took off with the maximum takeoff thrust. It entered rain shortly before the liftoff. After a normal liftoff, the aircraft climbed with a 14° pitch attitude. Then all of a sudden, it lost 42 kts (22 m/sec) IAS in less than 10 seconds. The captain lowered the pitch attitude to about 10°, but the aircraft continued to descend to the ground (Fig. 3.7).

The maximum divergence at the surface inside the Continental 426 microburst was estimated to be 150 - 250 per hour (0.04 - 0.07 per second). If we

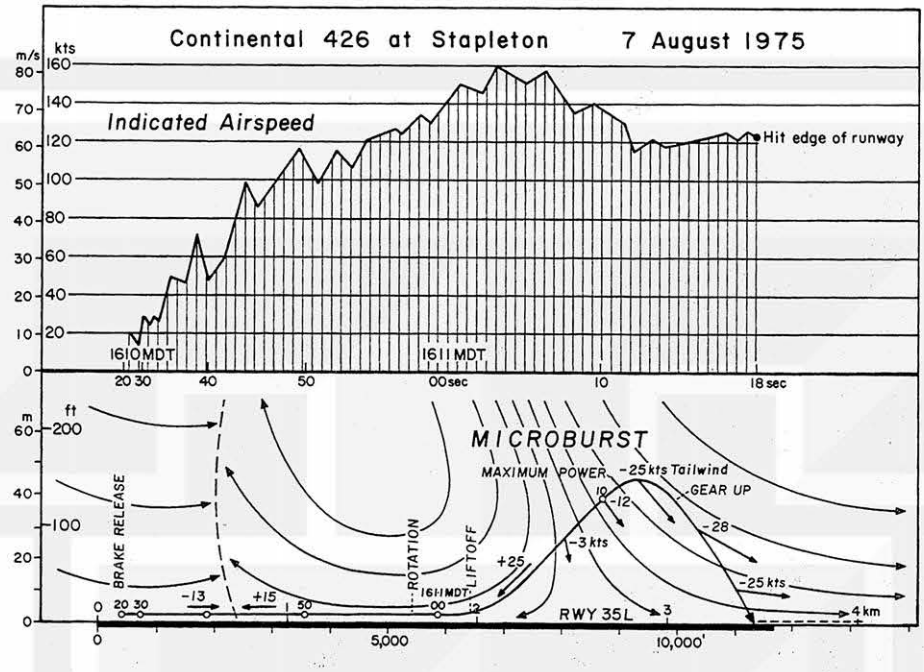

Fig. 3.7 Flight path and indicated airspeed of Continental 426 at Stapleton Airport, Denver, Colorado on 7 August 1975.

assume that this magnitude of divergence extended up to an estimated maximum altitude of 150 ft (45 m) AGL, the downflow speeds at various AGL heights were

2 - 4 fps (1 - 2 kts) at 50 ft (15 m)
4 - 7 fps (2 - 4 kts) at 100 ft (30 m)
6 - 11 fps (3 - 6 kts) at 150 ft (45 m)

Table 3.1 indicates that the loss of lift at a 10° pitch attitude is 2.5% per knot. This will result in a maximum of 15% loss of lift at 150 ft (45 m) due to the encountered downflow. The 42 kts (20 m/sec) loss of IAS was very serious in this case, because it could induce the loss of lift as much as 55%.

How can we make a decision, prior to takeoff, whether or not to fly into such a severe wind shear? Obviously, the use of radar may hold the key to such a decision. Radar photographs taken by the National Weather Service, Limon radar (10 cm) show a number of small echoes scattered all over the Denver area. The first echo of the Continental 426 microburst cloud was photographed at 1606 MDT, five minutes before the accident. The echo reached the maximum size and intensity at 1612, one minute after the accident. Thereafter, the echo split into two parts and weakened. This evidence presents a difficult problem of identifying microburst echoes by non-Doppler radars (Fig. 3.8).

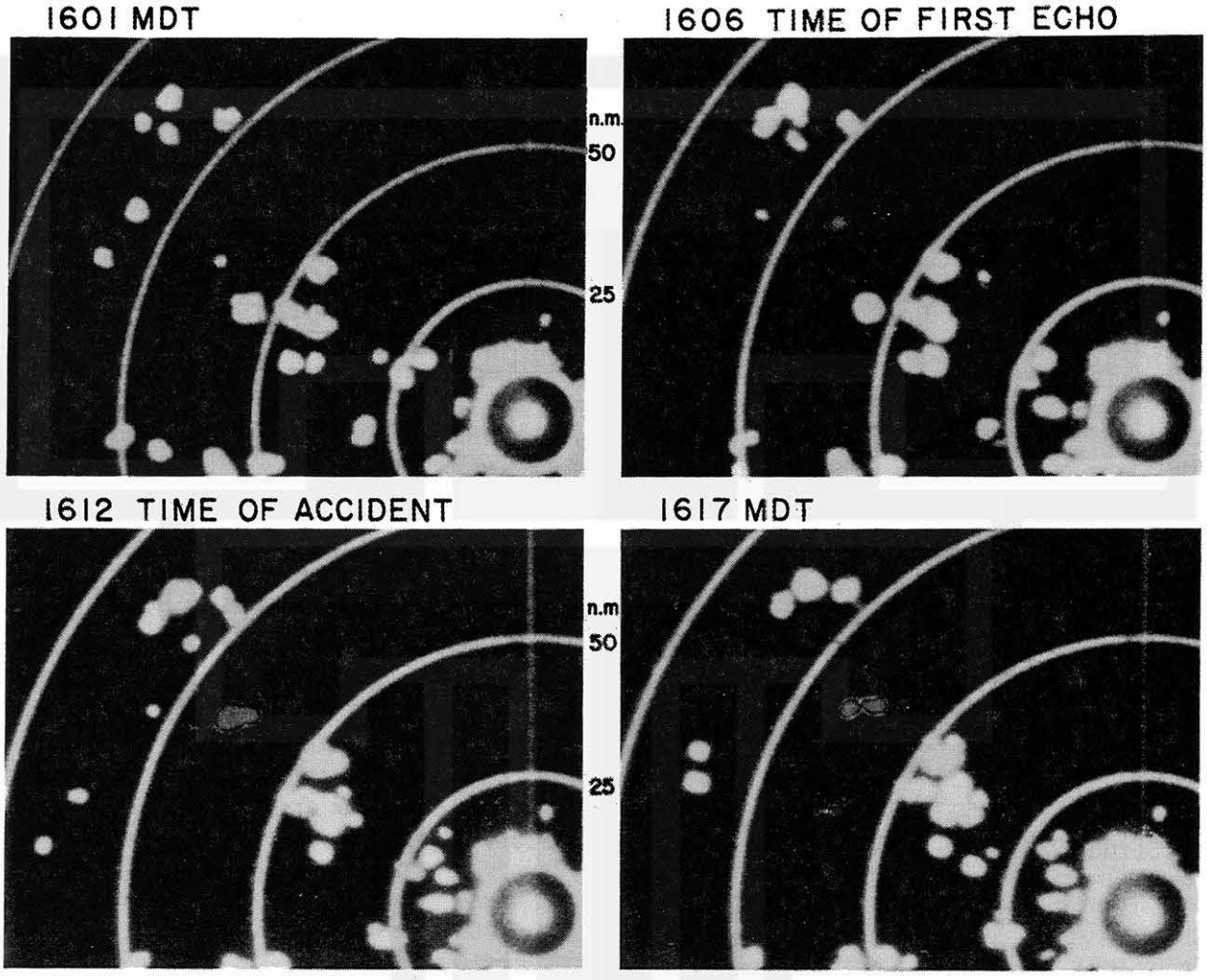

Fig. 3.8 Four radar pictures taken by the National Weather Service radar at Limon, Colorado on 7 August 1975. The echo which induced the Continental 426 microburst is tinted red. The accident time was 1611:18 MDT.

Pan American 759 Accident at New Orleans, Louisiana

This accident occurred at 1605 CDT on 09 July 1982 at New Orleans International Airport, Kenner, Louisiana during climbout in a heavy shower. No thunder was reported from the shower area. The accident aircraft released its brake at 1607:56; rotated at 1608:33; and lifted off at 1608:39 in a 14 kts (7 m/sec) headwind. "Gear Up" was called at 1608:42 after confirming a positive climb. A few seconds later at 1608:44, the pilot commented "Come on back. You are sinking, Don". After reaching the highest flight

altitude at 1608:51, the aircraft kept sinking until 1609:00, when it hit a huckleberry tree at 52 ft (16 m) AGL. Thereafter, the aircraft first climbed slightly, but then lost altitude due to the damage during the tree impact. The aircraft hit the ground at 1609:06 and burned. 152 persons were killed and 9 were injured. Of those killed, eight persons were on the ground in the residential area (Figs. 3.9, 3.10, and 3.11).

Fig. 3.9 The flight path of PAA 759 superimposed upon an aerial photograph of the New Orleans International Airport at Kenner, Louisiana. VR denotes the point of rotation and L/O, that of liftoff. A red circle indicates the point of the first tree contact. Photo by Fujita, one year after the accident.

Fig. 3.10 A telephoto view of the residential area to the east of the airport. The black line denotes the flight path. After ground contact between Fairway and Hudson Avenues, the aircraft skidded along the dashed line. Several empty lots are where houses had stood before the accident. Photo by Fujita, one year after the accident.

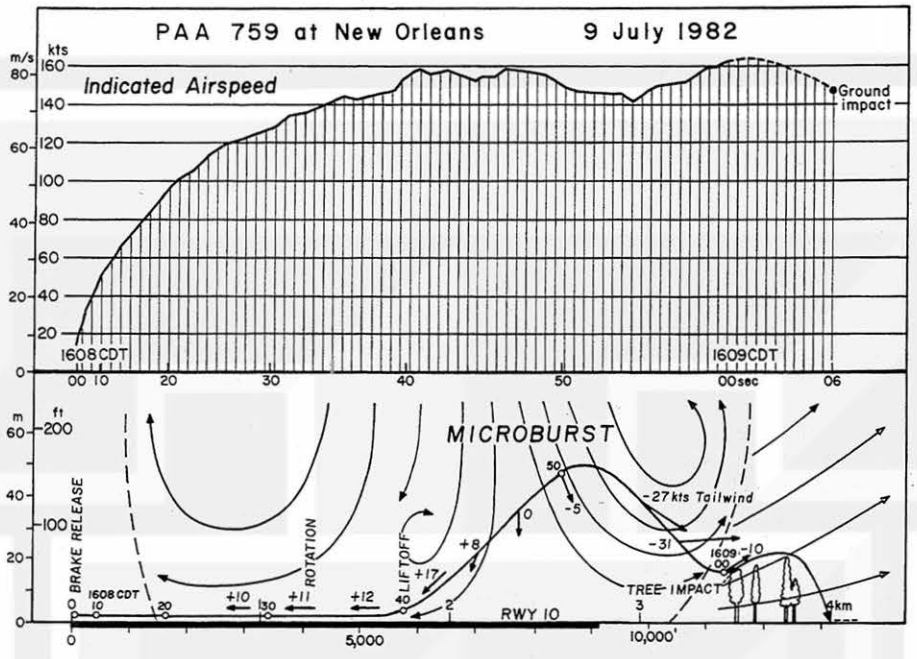

Fig. 3.11 Flight path and indicated airspeed of PAA 759 at the New Orleans Airport on 9 July 1982. According to the author's reconstruction, the aircraft reached 163 ft (50 m) AGL. Thereafter, it descended to 52 ft (16 m), contacting a tree on the east side of Williams Blvd.

Under the assumption that the accident aircraft accelerated on the runway and then lifted off at a constant 15° flap setting and a full-power thrust, the following input parameters were assigned at one-second intervals.

u -- tailwind component of the environmental winds
v -- crosswind component of the environmental winds
w -- vertical components of the environmental winds
θ -- pitch attitude of the aircraft

If the air is calm, an assignment of a normal pitch attitude after rotation will result in a climbout characterized by a gradual increase in aircraft altitude along with an increase in the distance travelled.

An input of a specific wind-shear condition, expressed by a combination of u, v, w, and a pitch attitude will generate a set of output values which are expected to be considerably different from those of a normal climbout. It is necessary, therefore, to keep changing the input data until the output values become as close as possible to the factual data, such as measured time and distance, FDR readout data, eyewitness accounts, etc. The output parameters obtained at one-second intervals through 0.1 second time-step integrations are

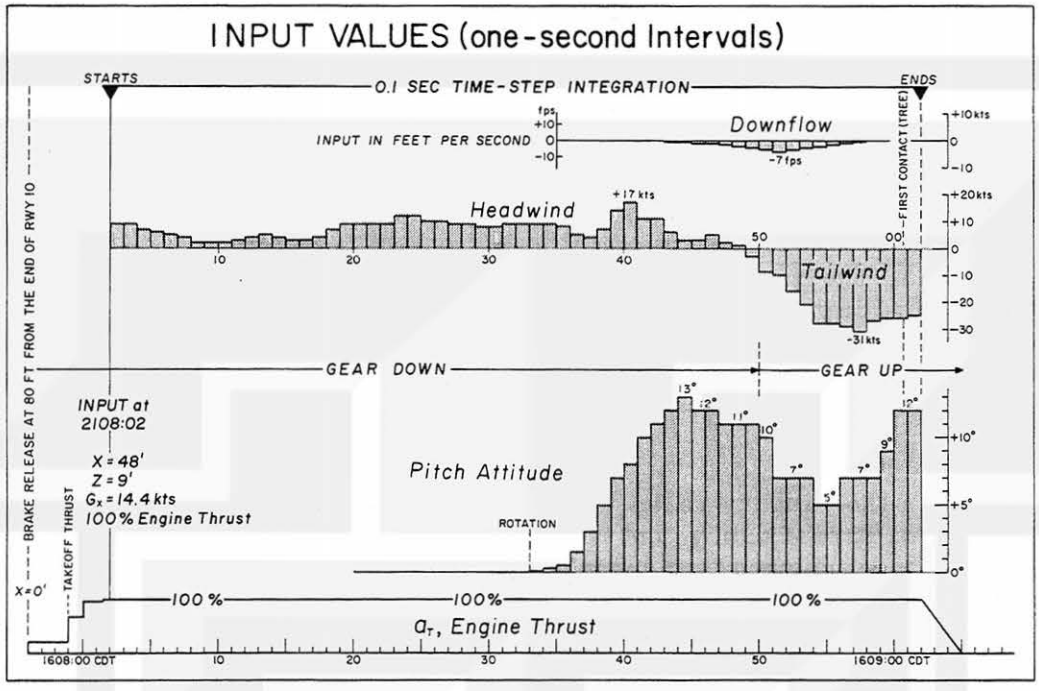

***Fig. 3.12** Input values given as a function of time at one-second intervals. They were changed at each iterative step.*

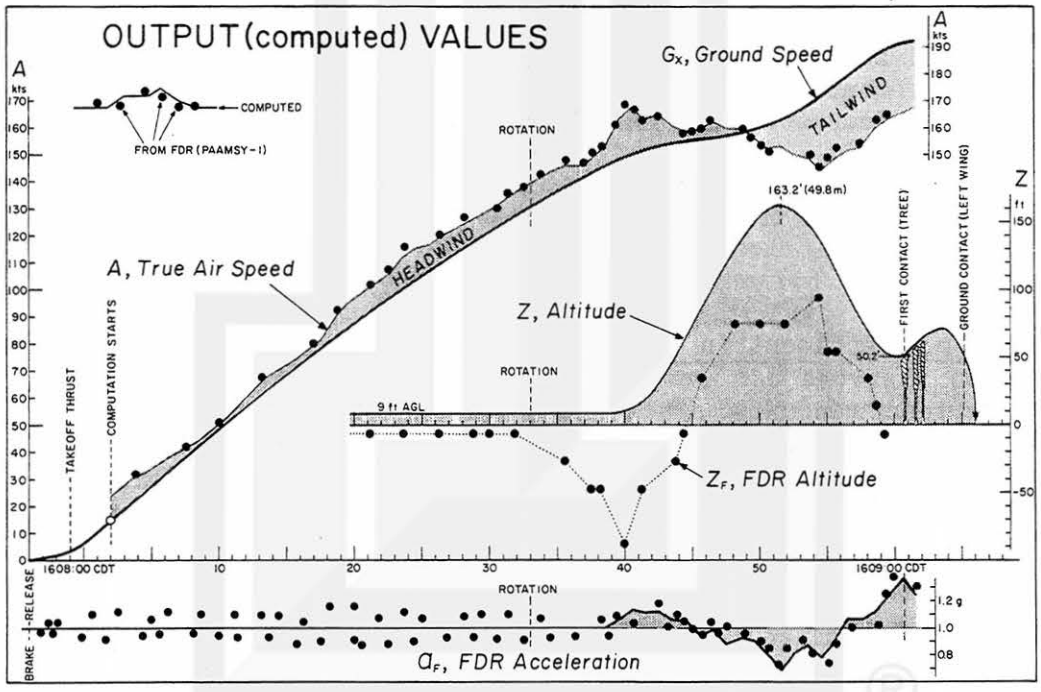

***Fig. 3.13** Output values obtained after the 27 iterative computations. Computed values are shown with lines and FDR data in dots.*

X --- distance measured along the runway centerline
Y --- cross runway distance
Z --- aircraft altitude above the runway
a_F -- vertical acceleration of aircraft
IAS - indicated airspeed of aircraft

Of these, X and Y were measured by the survey team and Z, a_F, and IAS were tabulated in the document PAAMSY-1.

As expected, the first output was far from that experienced by the accident aircraft. By improving the input, after each iterative computation, the output became closer and closer to the factual data. Finally, the output from the 27th iterative computation accurately reconstructed the flight of PAA 759 from its brake release to its first tree contact (Figs. 3.12 and 3.13).

Obviously, the input values of u, v, w cannot be chosen arbitrarily. They have to satisfy not only the equation of continuity, but also the airflow of a wind-shear inducing weather system which is, in this case, a "microburst". Throughout the 27 iterative computations, the following eight (8) constraints were checked and were satisfied:

1. Equation of continuity and microburst wind shear
2. Time between brake release and the tree contact, 64 seconds
3. Distance from brake release to the tree contact, 11,525 ft
4. Cross-runway distance of the tree contact, 172 ft
5. Impact height of the tree contact, 52 ft
6. Estimated climb rate at the tree contact, 430 feet per minute
7. Computed IAS and FDR IAS should match
8. Computed acceleration and FDR acceleration should match.

Computations revealed that these constraints narrowed down the possible input values which reconstructed the flight parameters of the accident aircraft.

Continental 63 Accident in Tucson, Arizona

This accident occurred at 1358:40 MDT on 3 June 1977. The aircraft, a B-727, released its brake on Runway 21 at 1357:34 in a 20 to 30 kts (10 to 15 m/sec) headwind. There were numerous cumulonimbus clouds all around the airport, and a gust front swept across the airport a few minutes earlier, recording a 49 kts (25 m/sec) peak gust from the southwest. As the aircraft accelerated on the runway, the headwind behind the gust front weakened.

The aircraft rolled into a microburst at 1358:20 MDT, experiencing a 20 kts (10 m/sec) loss of airspeed for a couple of seconds. It rotated at 1958:28 in an estimated 10 kts (5 m/sec) tailwind. After liftoff, the airspeed did not increase as it should, because the tailwind kept increasing. The aircraft failed to gain altitude and was unable to clear the power

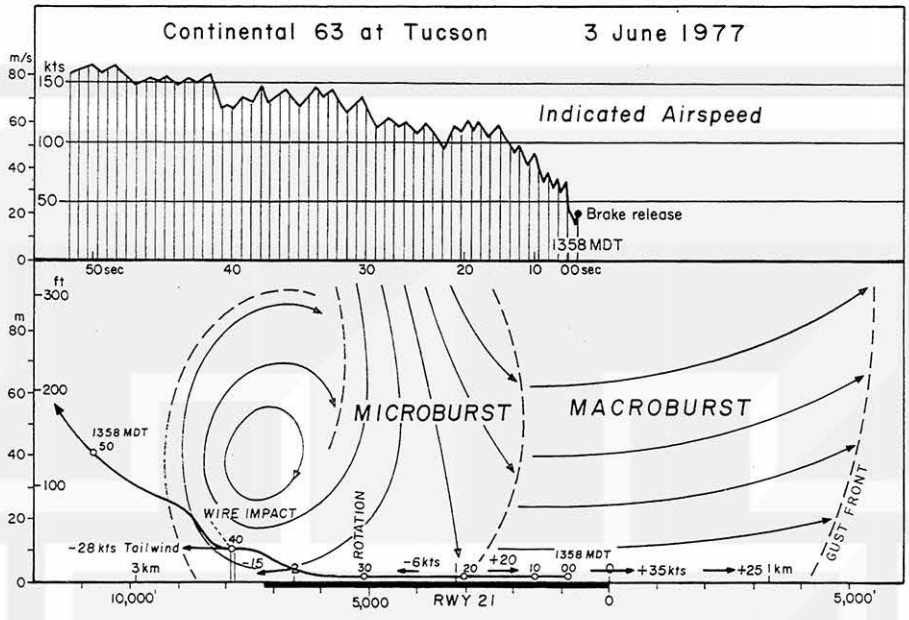

Fig. 3.14 The flight path of Continental 63 at Tucson, Arizona at 1358 MDT on 3 June 1977. The aircraft hit the power lines on both sides of the Nogales Highway.

lines along the Nogales Highway which runs north-south along the western boundary of the airport.

An eyewitness in a car, southbound on Nogales Highway, noticed that the aircraft flew over the highway less than 200 ft (60 m) in front of the car. Both left and right landing gears hit the power lines on the airport side of the highway first. Then the fuselage hit and severed power lines on the other side of the highway and knocked down a power pole, causing the power lines on both sides of the highway to come down to the ground for approximately 1/8 mile (200 m) in either direction. Thereafter, the aircraft gained altitude.

In the context of microburst-induced wind shear, the aircraft encountered a 28 kts(14 m/sec) tailwind while flying beneath a horizontal roll vortex (Fig. 3.14). Apparently, the southwestern boundary of the microburst was just to the southwest of the point of the wire impact, allowing the aircraft to climb out safely, a few seconds after the impact. Thereafter, the aircraft returned to the airport. Nobody was injured.

3.4 Accidents during the Final Approach

An accident during the final approach occurs when an aircraft attempts to land through a strong microburst located on the glide slope near the approach end of the runway. In nearly all cases, an aircraft first experi-

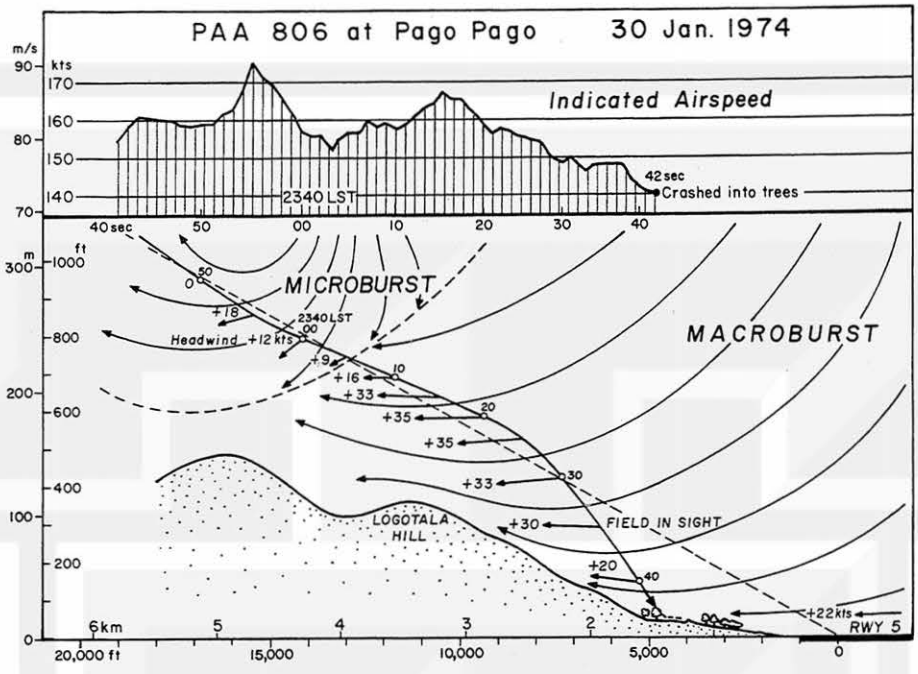

Fig. 3.15 The flight path of Pan American 806 which crash landed in a tropical forest at 2340:42 LST during an approach to Runway 5 at Pago Pago Airport, American Samoa.

ences a headwind increase while approaching a shower or virga. As a result, the aircraft gains altitude. When the pilot brings the aircraft altitude down to the glide slope, a downflow and a tailwind are waiting in front of the aircraft. Unless full power is applied early enough to regain the altitude, the aircraft could keep on sinking to the ground.

Pan American 806 Accident at Pago Pago, American Samoa

This accident occurred just about 10 minutes before midnight of 30 January 1974 during an approach to Runway 5. The aircraft crashed into trees, 3,865 ft (1,178 m) short of the runway. Of the 101 persons aboard the aircraft, 96 persons were killed and only 5 survived.

While descending to 900 ft (270 m) above the runway level, the IAS increased from 158 to 175 kts in 5 seconds, followed by a sharp drop of 23 kts in less than 10 seconds. This quick change in IAS suggests that the aircraft flew through a midair microburst in its descending stage. Thereafter, the aircraft gained IAS gradually, reaching 167 kts at 2340:16 LST. After that time, the IAS kept decreasing continuously until the aircraft crashed into a tropical forest at 2342:00 LST. The final IAS was 140 kts (Fig. 3.5).

At the Pago Pago Airport, the surface wind at 2339 LST, 2 minutes before the accident, was 040° at 22 kts in heavy rain showers. At 2345, 4 minutes after the accident, the wind shifted slightly to 020° at 13 kts, gusting to 35 kts. Heavy rain showers were still in progress.

The accident aircraft did not encounter heavy rain, however. According to the third officer, the flight encountered rain before the crash, but not heavy rain. Other survivors also confirmed that there was little or no rain before the crash, and that lights on the ground were visible.

The author's analysis presented in Fig. 3.15 depicts a macroburst located over the airport and a midair microburst approximately 4 km (2.5 miles) to the southwest of the approach end of Runway 5. We should expect that it rains heavily at the center of a microburst and a macroburst. This means that the rain intensity at the accident site could have been rather weak. A sharp rise of IAS is expected to occur beneath the roll vortex of a microburst. The "rise" will turn into a "drop" after entering the outflow section of a microburst. Therefore, the aircraft entered the strong headwind section of a macroburst. As the aircraft descended, the headwind decreased, due in part to the blocking effect of Logotala Hill located on the downwind side of Runway 5.

Because of the complicated nature of this accident, the Airline Pilot Association petitioned the Safety Board to reconsider the probable cause. As a result of this petition, the Safety Board reopened the accident investigation. After the reinvestigation, it was concluded that the probable cause of the accident was the flight crew's late recognition and failure to correct in a timely manner an excessive descent rate.

Eastern 902 Incident and Eastern 66 Accident at JFK, New York

This incident and accident occurred on 24 June 1975 within 7 to 8 minutes of each other. Both aircraft attempted to land on Runway 22L at the John F. Kennedy International Airport at New York City, New York. The first aircraft, Eastern 902 abandoned its approach at 1558 EDT while the second aircraft, Eastern 66 hit the approach lights at 1605 EDT, about 2400 ft (730 m) short of the runway threshold. Of the 124 aboard the aircraft, 112 were killed and 12 others were injured.

In spite of the fact that these two aircaft encountered very strong wind shear, two other aircraft landed at 1600 (2 minutes after EA 902) and at 1602 (3 minutes before EA 66), experiencing only 20 to 25 kts (10 to 13 m/sec) drop of the IAS. Apparently, there was a break between the wind shears penetrated by EA 903 and EA 66. For the purpose of identifying the nature of the strange wind shear at JFK, the author obtained pilot reports of the 14 aircraft that attempted to land on Runway 22L during a 26-minute period between 1544 and 1610 EDT. A summary of these reports are:

American 678 (B-747): Encountered moderate rain at about the outer marker. There was no turbulence. Broke out into light rain at 1,000'. Encountered some wind shear on the final approach. It required considerable power to maintain the approach speed, but the pilot did not consider the wind shear to be significant enough to mention to the tower.

American 187 (B-707): Experienced smooth air all the way down to the final approach. The only indication of wind shear or downflow was after passing 500'. From that point on, the pilot added power to maintain the ILS glide slope and to keep the speed from eroding. Sighted a thunderstorm about one mile away to the right of the approach path, just short of Runway 22L. The rain from the storm was falling on the approach end of the runway.

Allegheny 858 (DC-9): Experienced a downflow at about one mile from the approach end of Runway 22L. Landed in rain.

TWA 843 (B-707): Encountered moderate rain between the outer and middle markers. The approach and landing were normal. The landing rollout was made on dry runway.

SAS 911 (B-747): Experienced heavy rain at 1000'. There was some wind shear during the early part of the approach. There was little rain on touchdown.

KLM 641 (B-747): Entered rain at about 1,200'. Light rain changed into heavy rain. The airborne inertial navigation system (INS) indicated a headwind of 15 kts. IAS dropped at 300', requiring power. INS headwind was 10 kts at 100'. Rain stopped while flying over the runway threshold. Landed with a 2° left drift. First half of the runway was wet and the other half was dry.

PAA 133 (B-707): Encountered extremely heavy rain at about 800'. At 200', the crosswind was 18 kts from right of the aircraft. Windshield wipers were operating at high speed in extremely heavy rain. No drift correction was required at touchdown in heavy rain. Rolled for about 1000' and broke out on dry runway in sunlight. While on the taxiway, the pilot saw a difficult maneuver by the Flying Tigers. Pilot commented, "Thought that the pilot must have been like a cat on a hot tin roof, trying to save his airplane".

Flying Tigers (DC-8): Encountered strong, sustained downflow from about 700' down to 200'. The pilot used an abnormal amount of power for an unusually long period of time. From 200' to touchdown, the downflow was moderate, but the crosswind from the right was very strong. It was blowing about 50 to 55 kts just off the ground. Then, all of a sudden, there was practically no wind on the ground. The pilot had to use a 10° to 15° heading to the right of the runway centerline during the instrumented landing system (ILS) approach. No drift correction was required at touchdown.

Eastern 902 (L-1011): The air was smooth and it was not raining. Everything was normal to about 400'. As the aircraft flew into an extremely heavy rain, visibility dropped to zero, and the aircraft started to sink while drifting to the right. Then the airspeed dropped from 144 to 120 kts. Applied power to pull up, and the missed approach was initiated. The aircraft kept sinking to 60' above the ground before the pilot was able to stop the descent by using considerable power while pulling the nose up to an abnormally high pitch attitude. After a go-around, the aircraft landed at Newark, New Jersey.

Finnair 105 (DC-8): Rain was heaviest between 6 and 3 miles final. The INS wind at 1500' was 230° at 30 kts. At about 2 miles final, the aircraft lost 25 kts IAS. The subsequent approach and landing were normal.

N-240 (Beech): Encountered light turbulence and moderate to heavy rain from just outside the outer marker down halfway to the middle marker. The approach continued normally until about 200'-300', where a heavy sink rate was experienced. The airspeed dropped about 20 kts. Applied power to recover from the sink, and the remainder of the approach was normal.

Eastern 66 (B-727): Flew into rain at 700'. Rain became heavy at about 500'. The aircraft began sinking at 400' and IAS dropped from 138 to 122 kts in 7 seconds. The runway was in sight at 140'. The aircraft hit the approach lights at 1605:12 EDT about 2,400' short of the approach end of the runway.

National 1004 (B-727): Followed the previous aircraft on ILS approach. Instructed to go around at 1605:30 EDT.

Delta 1072 (1-1011): Followed National 1004. The airport was closed after the accident. Flew straight toward the runway heading.

Fig. 3.16 shows a flight path vs. flight time diagram designed to present the weather events experienced by the 14 aircraft listed above. A careful examination of this diagram lead to the major findings on the nature of low-altitude wind shear which endangers aircraft during final approach.

The first finding is the limited extent of the outburst winds, with their horizontal scale significantly smaller than the "MESOSCALE", with the scale centered at 10 - 100 km. The second finding is the low altitude of the outburst winds, acting like a near-ground jet. This is what the Flying Tigers had experienced just off the ground shortly before the touchdown.

On the basis of these findings, along with the evidence of the starburst damage discussed in Chapter One, the author produced in March 1976 a conceptual model of the "downburst". The downburst is now subdivided into microburst and macroburst with their dividing dimension of 4 km. It turned out that the wind-shear inducing storms under investigation were three microbursts. Eastern 66 crashed after flying into the center of microburst No. 3; Eastern 902 flew near the western edge of the downflow section of

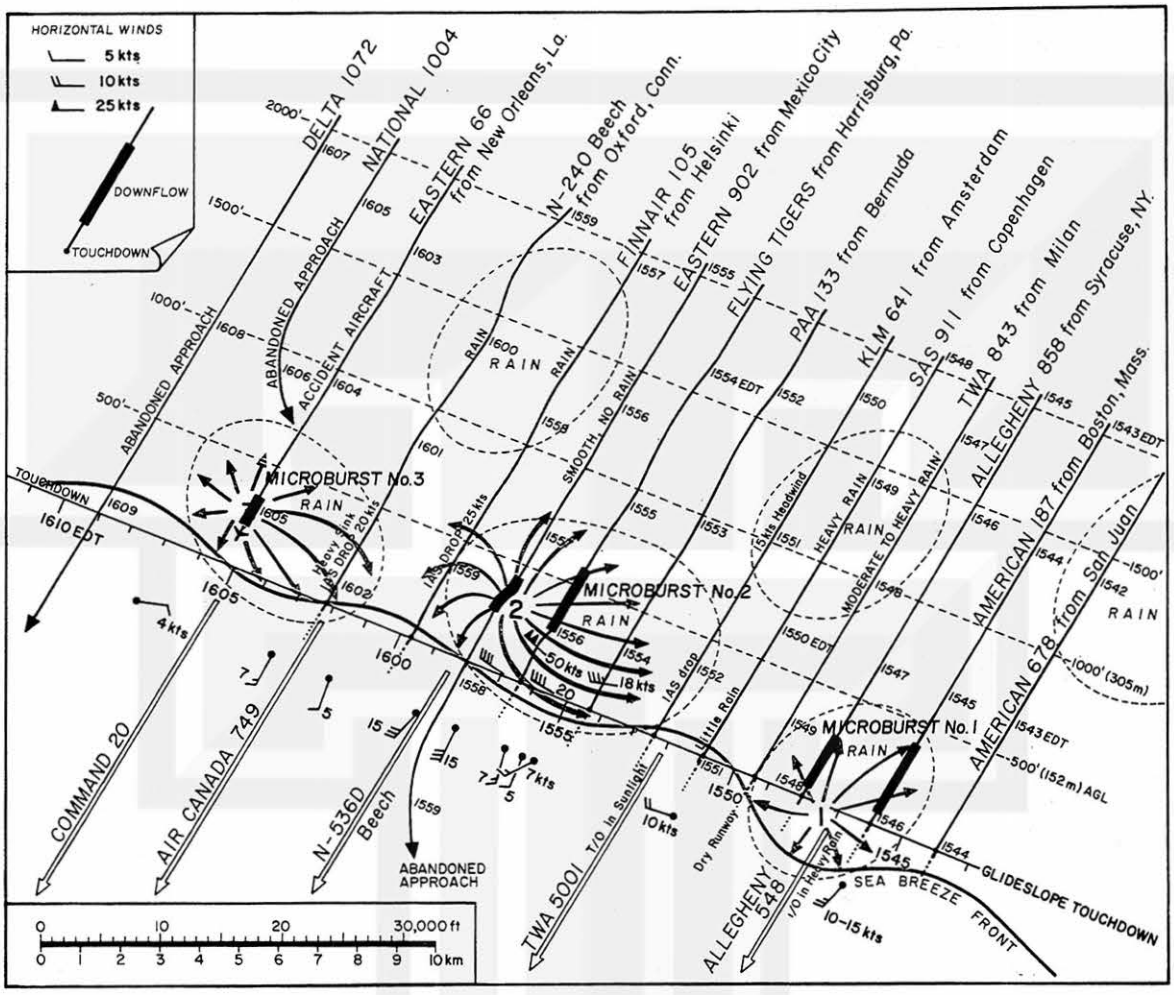

Fig. 3.16 A flight path vs. flight time diagram for presenting the weather events at JFK Airport on 24 June 1975. The approach directions are made parallel to the orientation of Runway 22L. The airport winds reported to the pilot of the 14 aircraft in this diagram were plotted at the location of the anemometer for Runway 22L. A sea-breeze front prevented the microburst winds from entering into the runway area.

microburst No. 2; the center of microburst No. 1 was at the north end of Runway 22L, without affecting both landing and takeoff operations.

Fig. 3.17 presents the chain of events experienced by Eastern 902. A "headwind increase in front of a shower" was experienced by the aircraft at about 500 ft (150 m) AGL. Then a decrease of the headwind was accompanied by an increase in the downflow speed. After penetrating the downflow center at 1557:31 EDT, the tailwind began increasing, necessitating a go-around. Full power was applied at 1557:28, but it took about 10 seconds before the aircraft began climbing. The pilot's comment "Pushed down while drifting

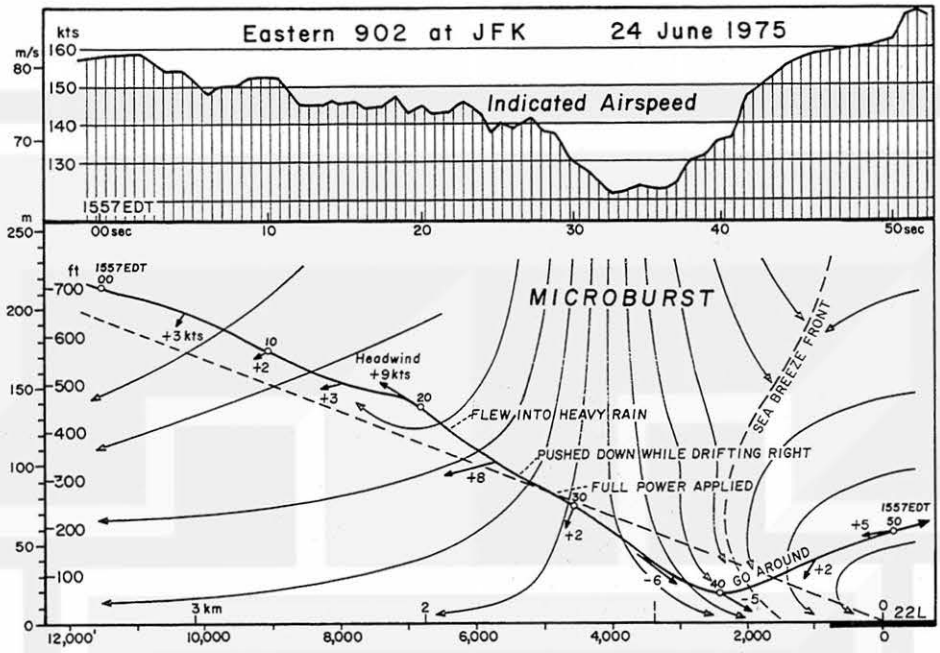

Fig. 3.17 The flight path of Eastern 902 at JFK Airport on 24 June 1975. The aircraft flew into microburst No. 2, descending to 60 ft AGL before it gained altitude. This incident occurred seven (7) minutes before the Eastern 66 accident.

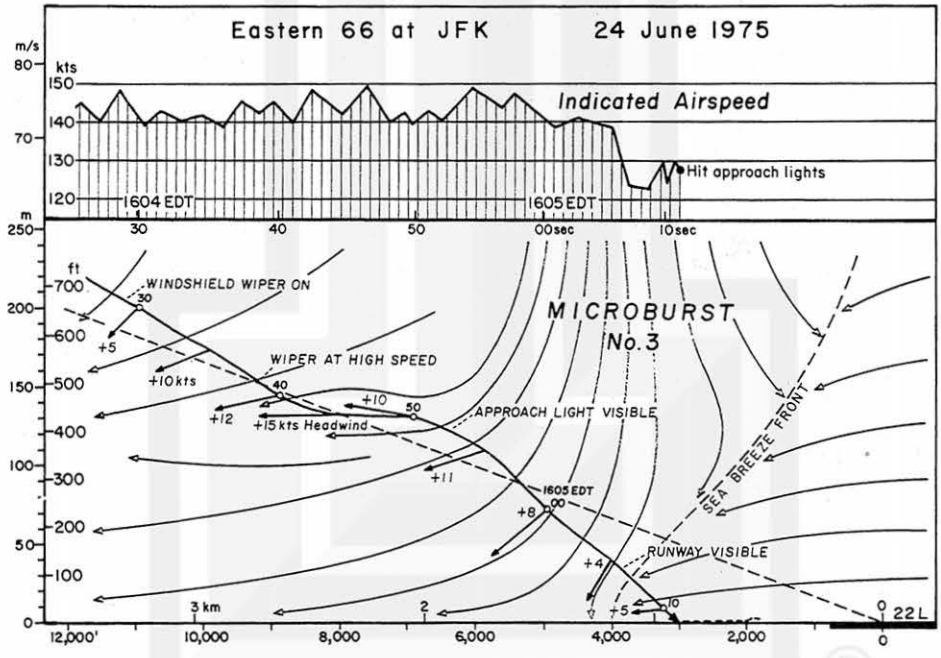

Fig. 3.18 The flight path of Eastern 66 at JFK Airport at 1605 EDT on 24 June 1975. The aircraft failed to fly out of microburst No. 3 and hit the landing lights.

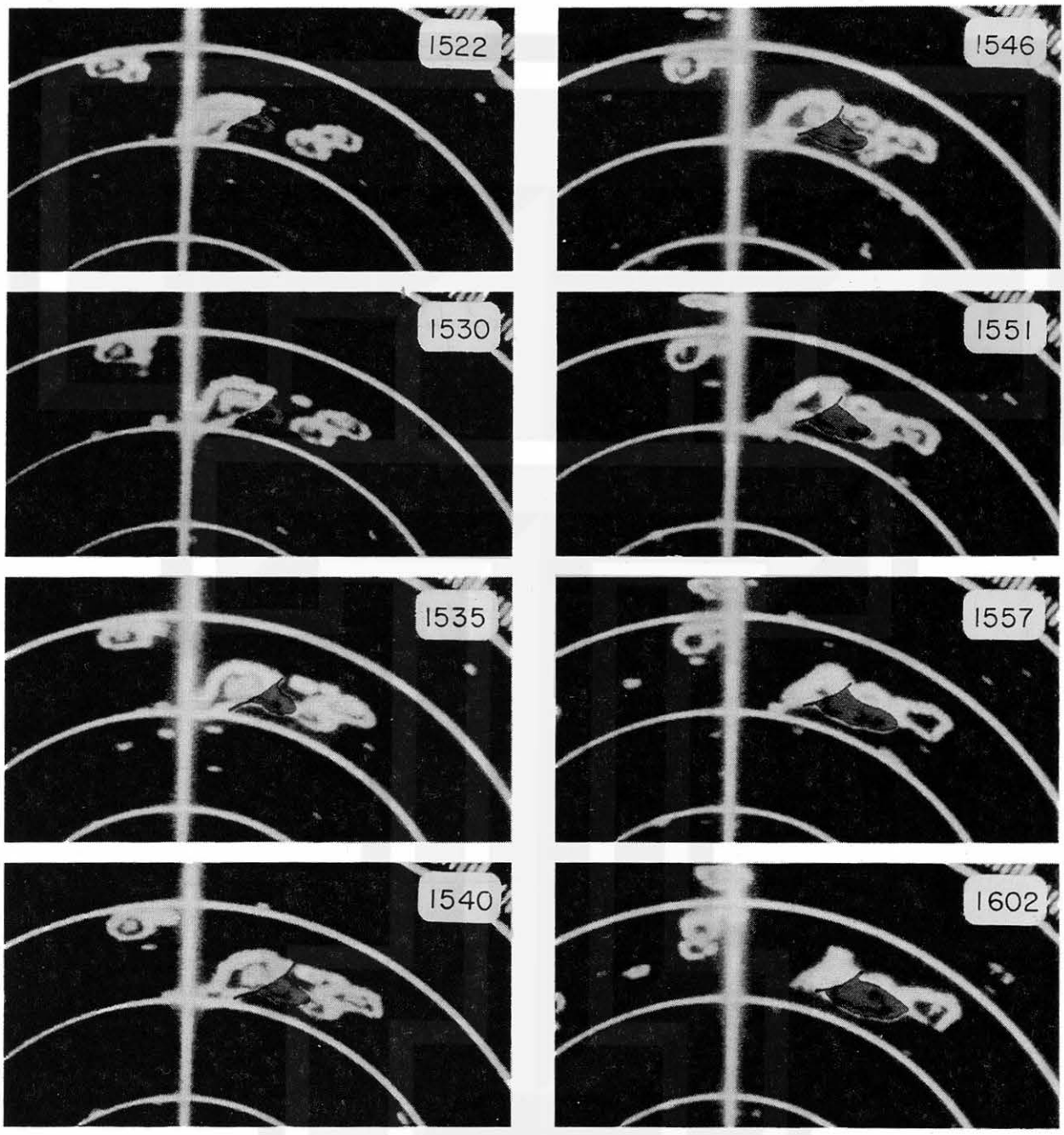

Fig. 3.19 A spearhead echo (tinted red) on 24 June 1975 that spawned three microbursts near the approach end of Runway 22L at JFK Airport. The three concentric circles in each photo are 50, 75, and 100 nautical mile range markers of the National Weather Service, Atlantic City, New Jersey radar.

right" indicates that the aircraft was on the right side of the downflow center.

Eastern 66 also experienced a "headwind increase in front of a shower", but it was a strong one. Consequently, the aircraft gained altitude appreciably. When the aircraft descended to the glide slope, the headwind decreased rapidly and the downflow intensified, resulting in a heavy sink of the aircraft. The rapid decay of the headwind, coupled with a strong downflow, did not allow the aircraft to regain altitude (Fig. 3.18).

The JFK thunderstorm photographed by the Atlantic City radar consisted of several cells. However, none of them were large and intense enough to be called a supercell. At 1522 EDT, a small pendant echo (tinted red) began extending out from a medium-sized echo (tinted blue) on the west side of the Hudson River. At 1530, the tip of the red echo reached lower Manhattan. Thereafter, the red echo pushed out rapidly toward the east-southeast, reaching JFK at 1551 EDT (Fig. 3.19).

Microburst No. 1 at 1548 was located beneath the tip of the red echo. By 1602, the red echo covered the western portion of Long Island, inducing microbursts Nos. 2 and 3 along its southern edge. It is hard to believe that a succession of three microbursts descended from such a small echo. Unlike the others, however, the red echo extended rapidly like an arrow on a bow. In his early papers, the author called this echo a "spearhead echo". However, the mechanism that develops a spearhead echo and that which spawns microbursts from a spearhead echo are not known yet.

Royal Jordanian 600 Accident at Doha, Qatar

This accident occurred at 0238 LST on 14 May 1976 at Doha Airport, Qatar when the aircraft attempted to go-around. Upon reaching 750 ft (230 m) AGL, the aircraft began losing altitude, descending to the ground and striking the left-side edge of the runway with a 10° pitch attitude. The aircraft bounced off and then slid 800 m (2,600 ft), tail first, into the fire station garage. The fuselage broke into three main sections. 45 persons were killed, 15 injured, while 4 escaped injury.

The first part of the flight from Amman to Doha was uneventful. As the aircraft approached Doha, it encountered thunderstorms. Doha airport has only one runway, oriented in a 160° - 340° direction. At 0208 LST, the pilot wanted to land towards the south. Runway 16 was requested and was cleared for a visual approach. As the aircraft began descending toward the requested runway, the wind direction changed from 90° at 17 kts to 340° at 6 kts. At that point, the pilot had not seen the runway. A missed approach was initiated and a new approach to Runway 34 was requested.

At 0235 LST when the aircraft completed the turn and the field was in sight, landing clearance was given. However, the runway wind changed again to 180° at 6 kts, which is a tailwind on Runway 34. The rain was very heavy and visibility at the tower was less than 1,000 m (0.6 mile). Before reach-

ing the decision height, a second missed approach was initiated at 0237:19 LST at about 300 ft (90 m) AGL. The pilot then requested clearance to Daran.

The aircraft began climbing at a 12° pitch attitude at 1,300 fpm (6.6 m/sec) rate of climb. During this climb, IAS kept decreasing to 140 kts. Upon reaching 750 ft (230 m) AGL, the aircraft began to descend until it struck the ground with a vertical speed of 4,200 fpm (21 m/sec). During the last 7 seconds, the IAS increased rapidly to 170 kts, while the ground proximity warning system (GPWS) gave a continuous warning 11 seconds prior to the impact.

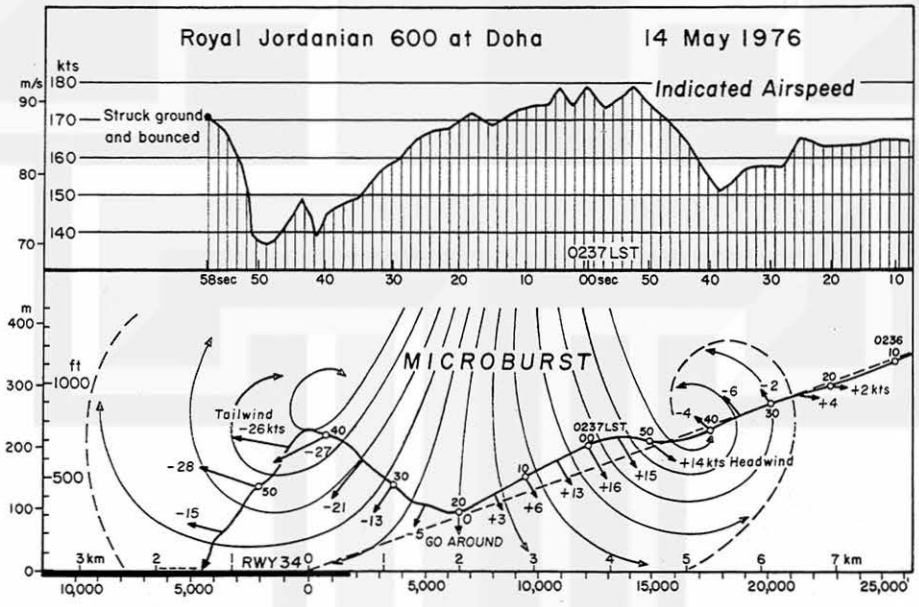

Fig. 3.20 The flight path of Royal Jordanian 600, which crash landed at Doha Airport, Qatar at 0238 LST 14 May 1976. According to the author's analysis, the aircraft flew into a strong tailwind inside the horizontal vortex of a strong microburst.

The author's analysis in Fig. 3.20 shows that the aircraft experienced a 28 kts increase of the headwind, from 151 to 179 kts. It is likely that the aircraft flew beneath a roll vortex. When the second go-around was initiated at 0237:19, the aircraft was at the dead center of the downflow, without realizing that it was penetrating the tailwind section of the microburst. As the aircraft was flying out of the microburst, the IAS was lost to the point that the aircraft could no longer maintain its altitude. After reaching its peak altitude, the aircraft kept losing altitude until ground impact at 0237:58 LST.

For the purpose of visualizing the horizontal roll of a wet microburst, the middle picture on the right side of Fig. 1.5 was enlarged. This picture shows clearly an awesome feature of a roll vortex located along the leading

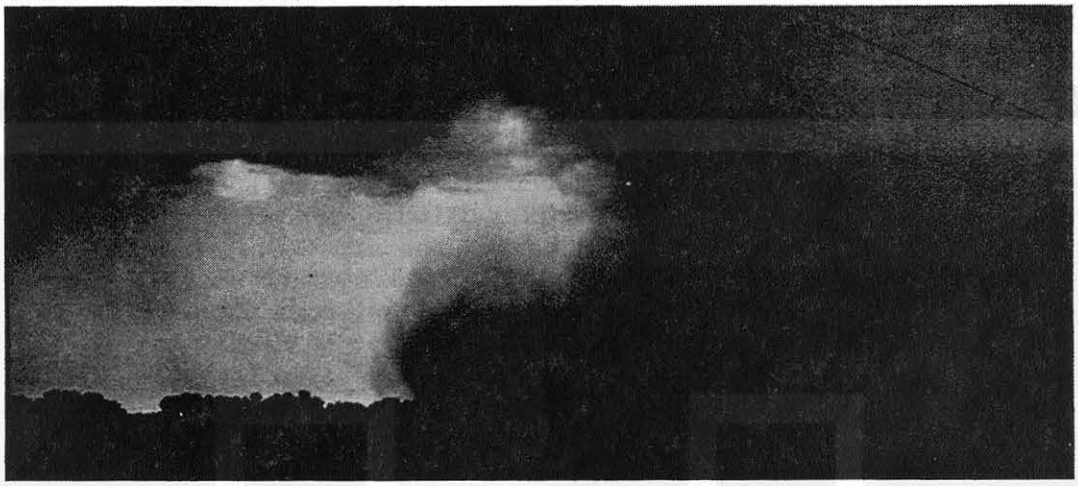

Fig. 3.21 A ground view of a horizontal vortex of the Wichita, Kansas microburst on 1 July 1978. This photo is an enlargement of one of the copyrighted photos in Fig. 1.5 taken by Mike Smith.

edge of a microburst. In this case, the vortex was made visible by the raindrops blown out of a wet microburst (Fig. 3.21).

Allegheny 121 Accident at Philadelphia, Pennsylvania

This accident occurred at 1711:48 EDT on 23 June 1976 when the aircraft attempted to land on Runway 27R at the Philadelphia Airport. The aircraft

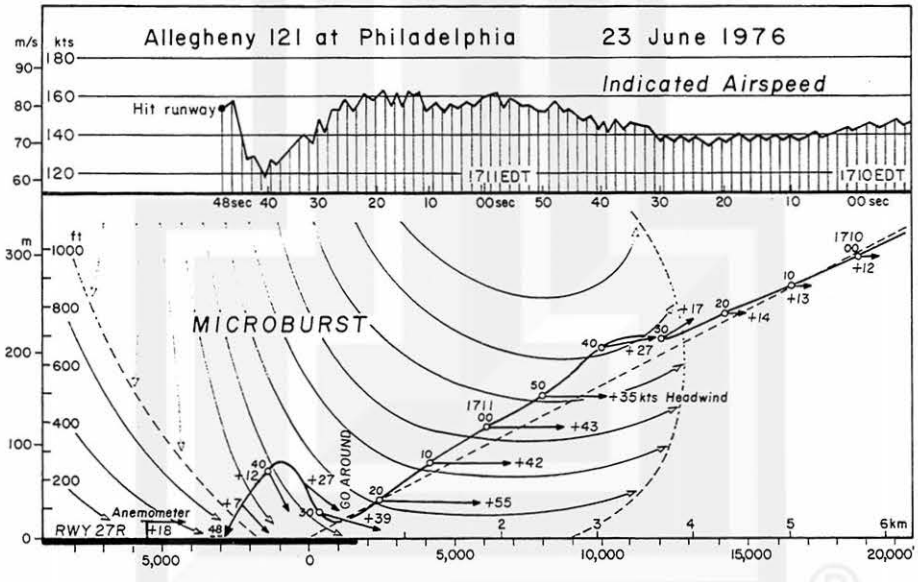

Fig. 3.22 The flight path of Allegheny 121 which impacted the ground at Philadelphia Airport at 1700:48 EDT on 23 June 1976.

experienced the usual "headwind increase in front of a shower" at 1710:30. The aircraft gained altitude above the glide slope, but it was brought down to the nominal height within the next 50 seconds. As the aircraft altitude decreased, the headwind kept increasing to over 50 kts. While flying at 160 kts IAS in a 50 kts headwind, the groundspeed was only 110 kts. Since it was too low to accomplish a normal landing, a go-around was initiated at 1711:28 EDT. While climbing to 250 ft (80 m) AGL, the IAS decreased to 120 kts. At this point, the aircraft began losing altitude, and the aircraft hit the ground 350 ft (100 m) to the right of the runway centerline (Fig. 3.22). Of the 106 persons on board, 86 were injured while 20 others escaped injury.

Chapter Four

NIMROD and JAWS Networks

NIMROD 1978 and JAWS 1982 were two major field experiments in the United States conducted for investigating the downburst with emphasis on the microburst. The acronyms of these projects were introduced by the National Center for Atmospheric Research (NCAR) during the organization phase of each experiment.

NIMROD, Northern Illinois Meteorological Research on Downbursts, is an appropriate term in identifying the first project in search of the downburst, a controversial wind system at that time. Nimrod, in the Bible, is the son of Cush, referred to as a mighty hunter.

JAWS, Joint Airport Weather Studies, signifies a man-eating shark and the powerful wind shear which endangers jet aircraft during landings and takeoffs at Stapleton Airport at Denver, Colorado.

4.1 NIMROD Network near Chicago, Illinois

The chronological events leading to the field experiment of the NIMROD Project progressed rapidly. Needless to say, the Eastern 66 accident at JFK on 24 June 1975 had triggered the necessity of the experiment. To meet the requests of both meteorological and aviation communities after the tragic event, the author printed in March 1976 2,000 copies of SMRP Research Paper 137, entitled "Spearhead Echo and Downburst near the Approach End of John F. Kennedy Airport Runway, New York City". A heavy demand for this paper necessitated a second printing in September 1976.

The planning of the NIMROD Project was nearly completed in January 1977, in advance of the formal publication of "Spearhead Echo and Downburst in the Crash of an Airliner" by Fujita and Byers in the Monthly Weather Review in February 1977. The funding for the field experiment, mostly from the National Science Foundation, was secured late in 1977 and the selection of both radar and PAM sites had begun early in 1978. Ted Fujita and Ramesh Srivastava of the University of Chicago served as co-principal investigators of the experiment.

A LANDSAT photograph (Fig. 4.1) from the National Aeronautics and Space Administration (NASA) was used extensively in locating the NIMROD network, because radar and PAM stations had to be located in unobstructed areas which were not too far from the O'Hare International Airport. The picture shows numerous forest preserves (brown color) all around the city of Chicago. There are, however, extensive cornfields (dark green) to the west of the urban and forested areas.

In order to produce the approximately 60-km (38 miles) base lines of the triple Doppler radars, Yorkville (YKV) was chosen as the CP-3 site and the command post. The CP-4 and CHILL radars were placed at the O'Hare Airport and at Monee, respectively. After the completion of the Doppler triangle and the PAM station network, nested in the western suburbs, the data collection began on 19 May 1978 (Fig. 4.2).

Selected photographs taken during the experiment are shown in Figs. 4.3, 4.4, and 4.5. The command post at Yorkville was located on a dike of a small artificial lake. The Doppler radar exposure was excellent, especially to the southeast through southwest. PAM data was received by the tall antenna in the picture. The data was recorded and presented in the form of both map and time plots on a real-time basis, on demand by the project researchers.

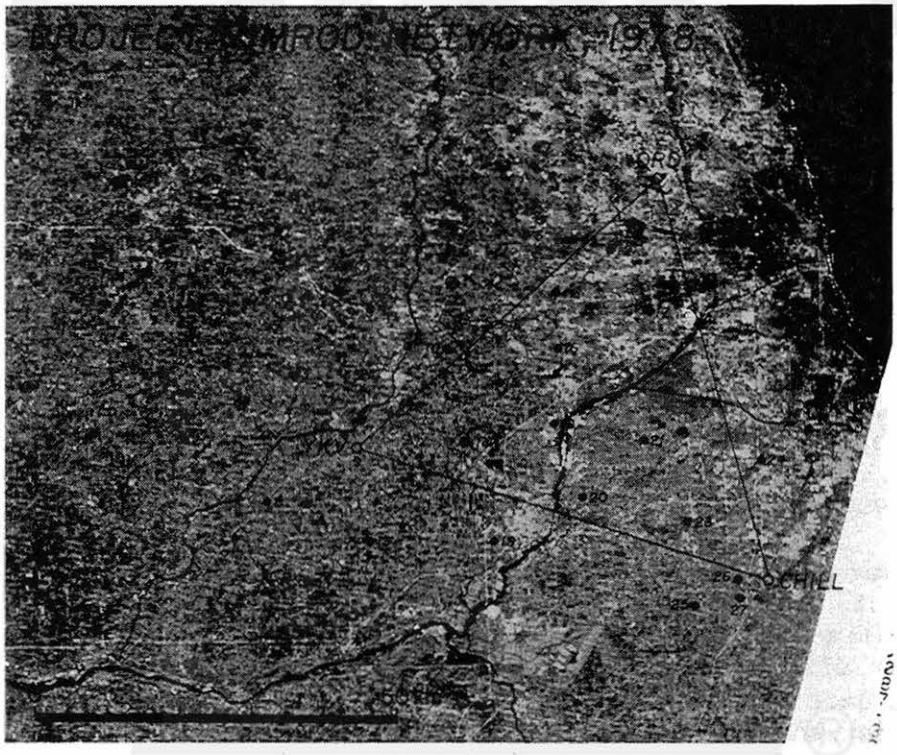

Fig. 4.1 The NIMROD Network superimposed upon a LANDSAT photograph showing Chicago and vicinity.

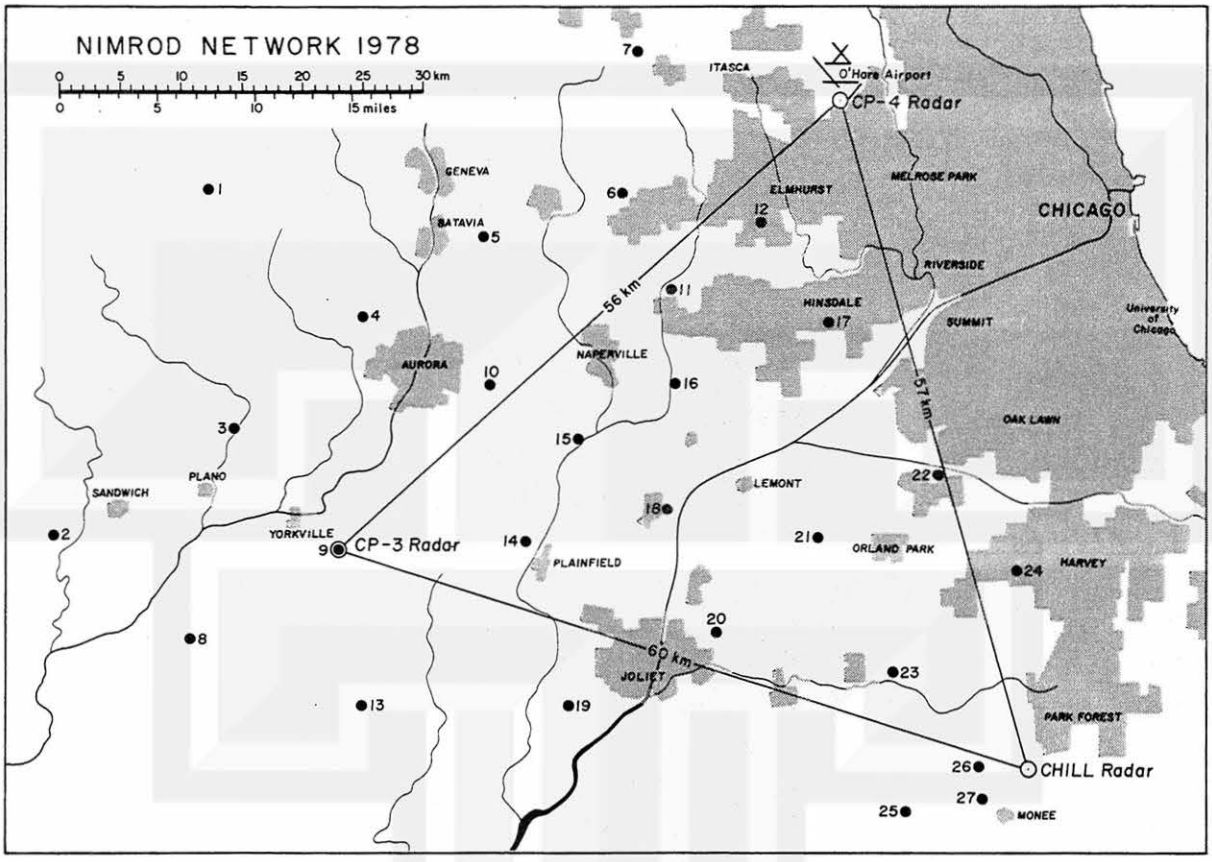

Fig. 4.2 A Doppler triangle and 27 PAM stations nested in the western suburbs of Chicago, Illinois. The network was operated for a 42-day period between 19 May and 1 July 1978.

Two GMD-Is were used for receiving rawinsonde signals. Balloons were released at one to two hour intervals or, sometimes, every 30 to 45 minutes. Due to a limited funding situation, no launch shelter was available for all-weather releases. However, eager students and staff smembers did their best in filling balloons with helium, and in releasing them during showers and high winds.

During the first quarter of the experiment, it was found that not all microbursts occur in severe thunderstorms. Some were induced by relatively weak echoes without thunder. A time section of upper-air winds and temperatures during the entire operation period reveals a poor correlation between microbursts and their meteorological environment expressed by winds aloft, temperature anomalies, etc. This subject will be discussed later, along with the parent clouds of macrobursts and microbursts (Fig. 4.6).

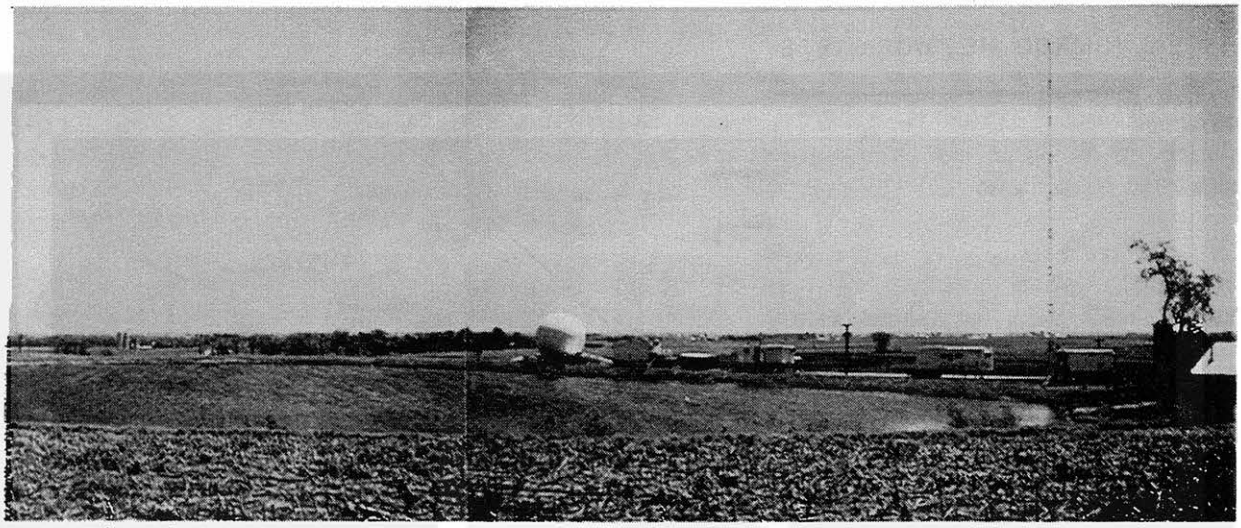

Fig. 4.3 The command post of the NIMROD Network at Yorkville.

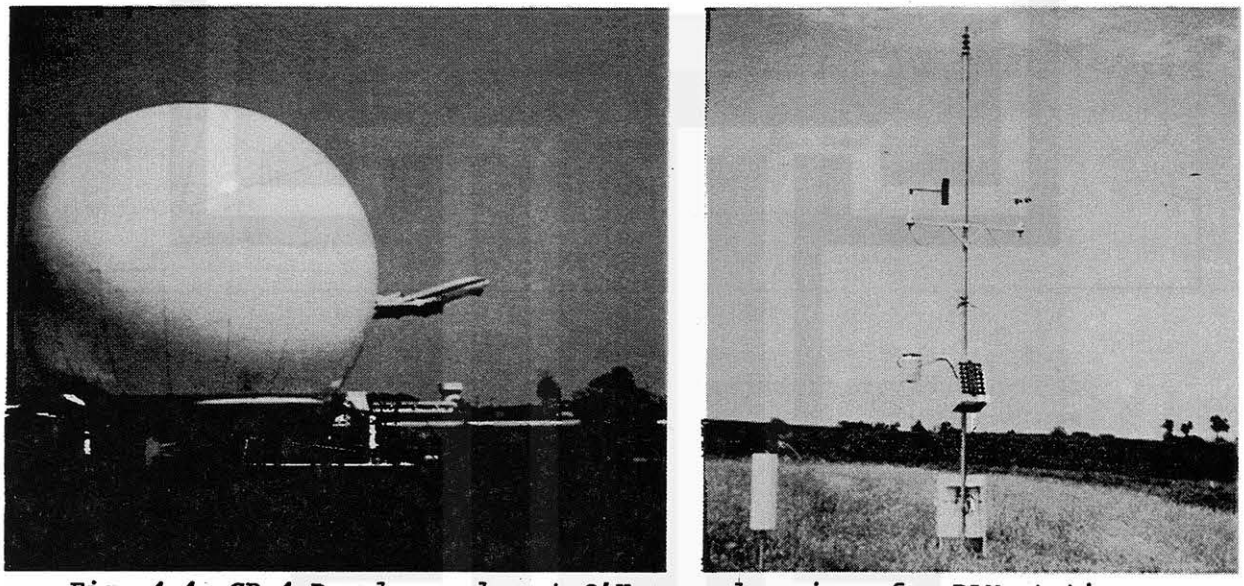

Fig. 4.4 CP-4 Doppler radar at O'Hare and a view of a PAM station.

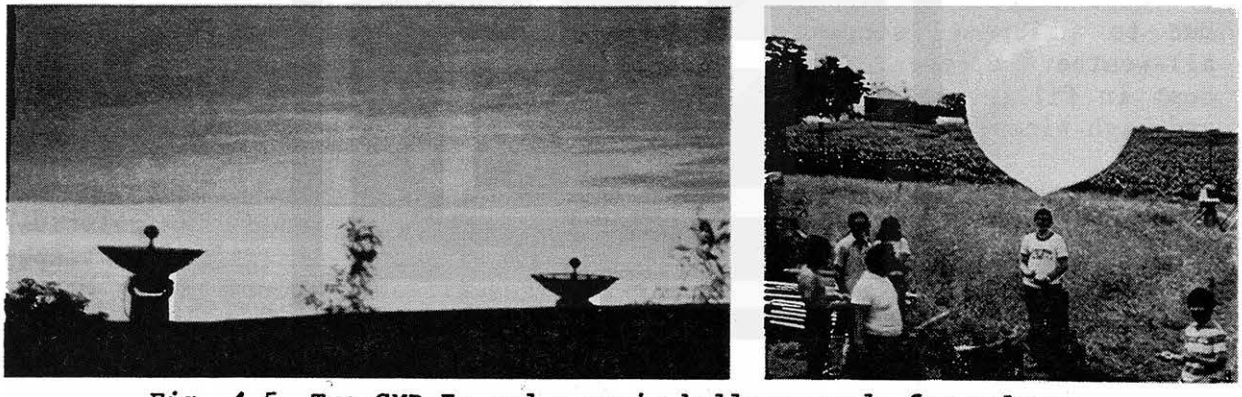

Fig. 4.5 Two GMD-Is and a rawin balloon ready for release.

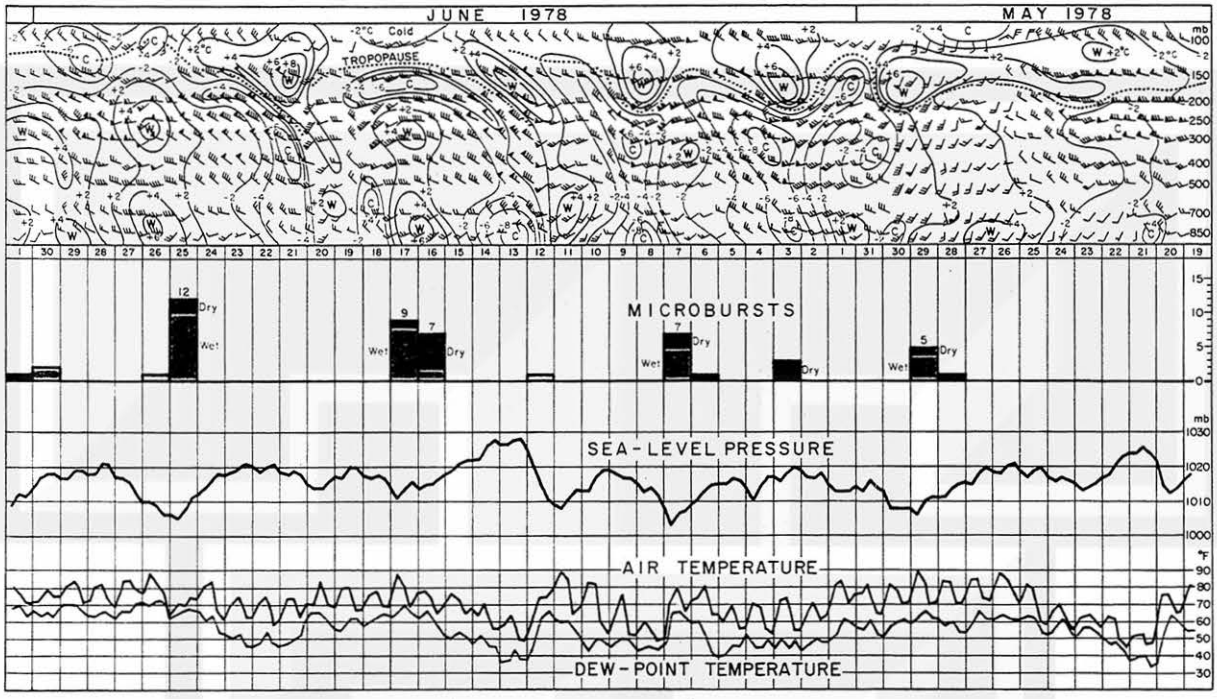

Fig. 4.6 Microburst frequencies in relation to the meteorological situation during the NIMROD experiment, 19 May through 1 July 1978.

4.2 JAWS Network near Denver, Colorado

The second fact-finding experiment of microbursts, to be conducted in the Denver area, was a brainchild of NCAR promoted by McCarthy and Wilson of the Field Observing Facility. It was hypothesized that a deep subcloud layer of dry adiabatic lapse rate over the high plains would produce a new type of microburst quite different from those detected during the NIMROD experiment.

The first planning meeting of JAWS was held at Miami Beach during the 19th Conference on Radar Meteorology, 15-18 April 1980. It was agreed upon that the next experiment should be conducted in the Denver area with Ted Fujita of the University of Chicago, John McCarthy and Jim Wilson of NCAR serving as co-principal investigators.

During the next two years following the first planning meeting, quarterly meetings on JAWS were held alternatively at NCAR and at the University of Chicago. Although the co-principal investigators at no time felt that they were financially out of the woods, the site selection of the radars and PAM stations was completed in April 1982.

As presented in Fig. 4.7, the Doppler base lines were selected to be much shorter than those adopted in the NIMROD Experiment. Meanwhile, 27

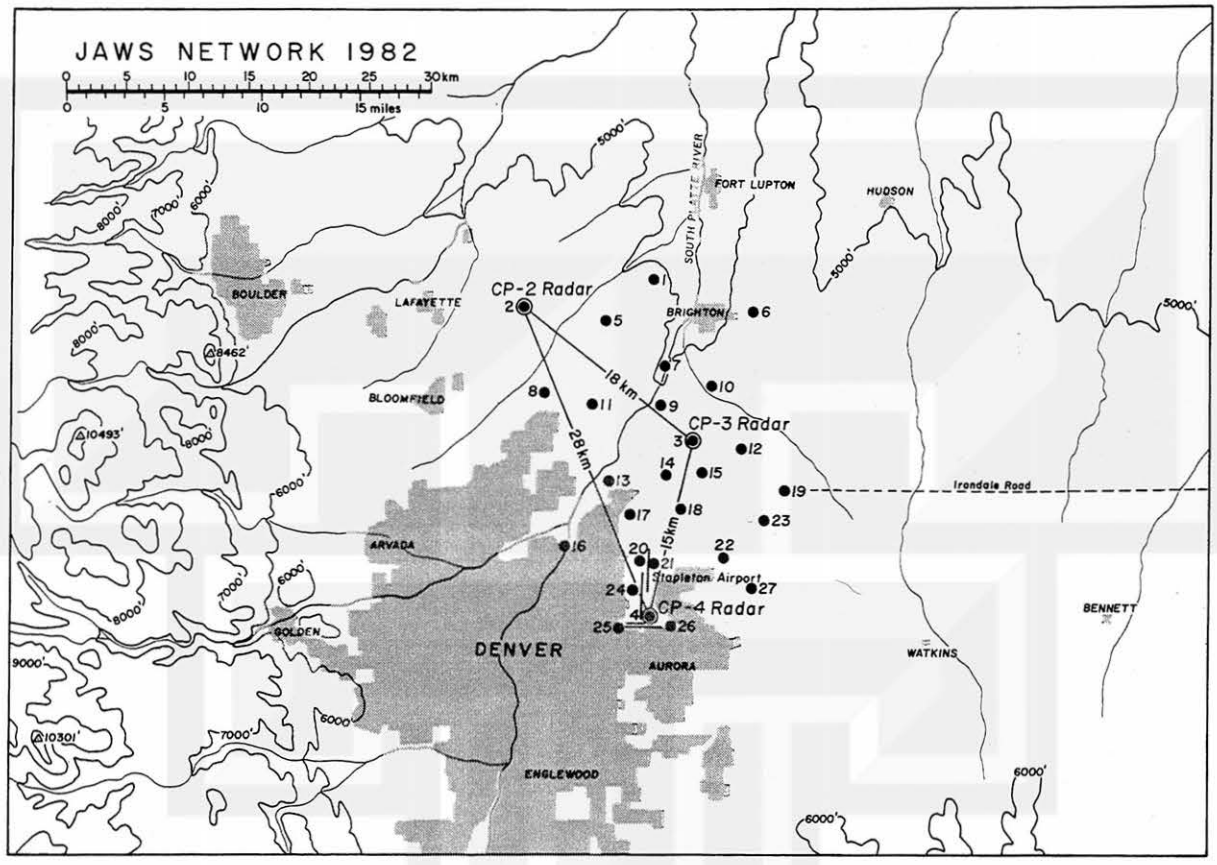

Fig. 4.7 A Doppler triangle and 27 PAM stations nested in the northern suburbs of Denver, Colorado. The network was operated for an 86-day period between 15 May and 9 August 1982.

PAM stations were brought into a much smaller area than the NIMROD case. The JAWS Network, nested in the northern suburbs of Denver, is within one hour driving distance from NCAR at Boulder, making the operation and the maintenance of the network very convenient and economical.

A collection of photographs in Figs. 4.8, 4.9, and 4.10 shows some scenes of the JAWS Experiment. We experienced frequent thunder and lightning over the network. The ending of these events was often spectacular, with a greeting by the sun shining at a low angle above the snow-covered Rockies. On one afternoon, the sky in a storm became so dark that the CP-2 radar appeared like a giant white pumpkin in a pitch dark night. CP-4 located at Stapleton Airport collected excellent data in support of the CP-2 and CP-3 radars, allowing dual and triple Doppler radar analyses.

The CP-3 site, located on an elevated terrain just to the east of the South Platte River, was the best spot for observing and taking pictures of microburst-inducing clouds. The author, along with his students, spent

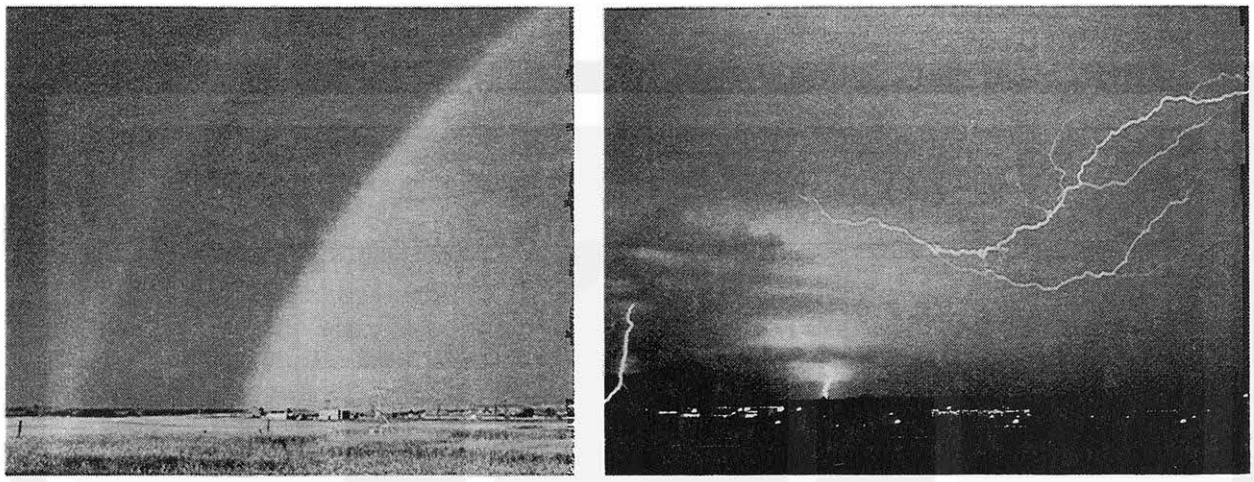

Fig. 4.8 Primary and secondary rainbows (by Roger Wakimoto) and cloud-to-cloud/cloud-to-ground lightning (by Brian Smith) during JAWS.

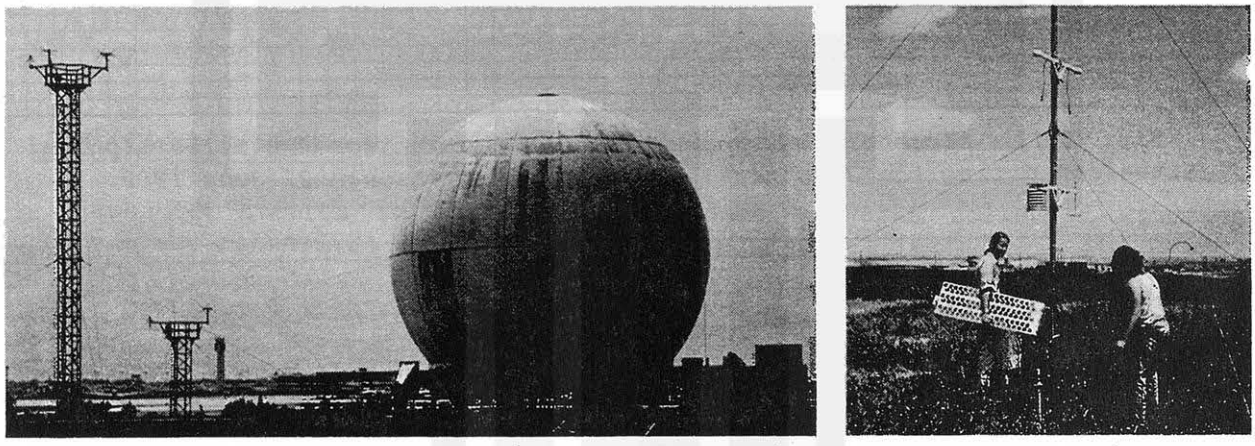

Fig. 4.9 CP-4 Doppler radar at Stapleton Airport and a PAM station under construction.

Fig. 4.10 A giant white pumpkin (JAWS CP-2) standing against a dark storm cloud and JAWS CP-3 Doppler operated without radome.

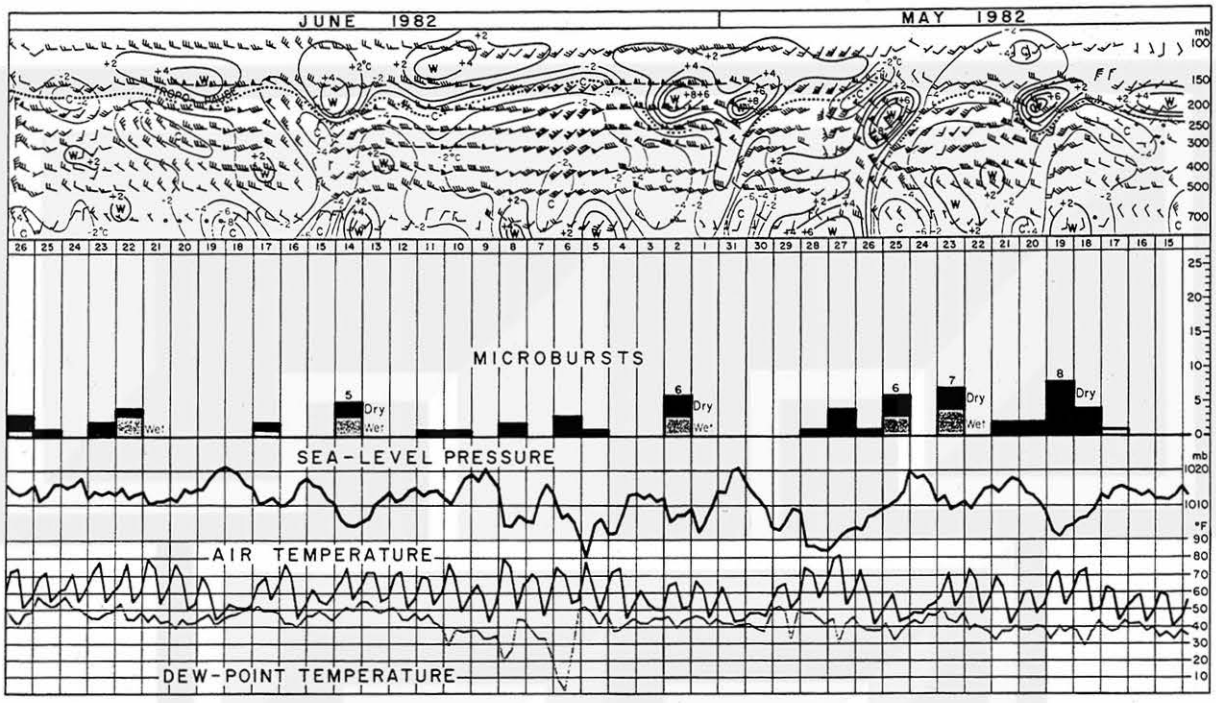

Fig. 4.11 Microburst frequencies in relation to the meteorological situation during the JAWS first period, 15 May through 27 June 1982.

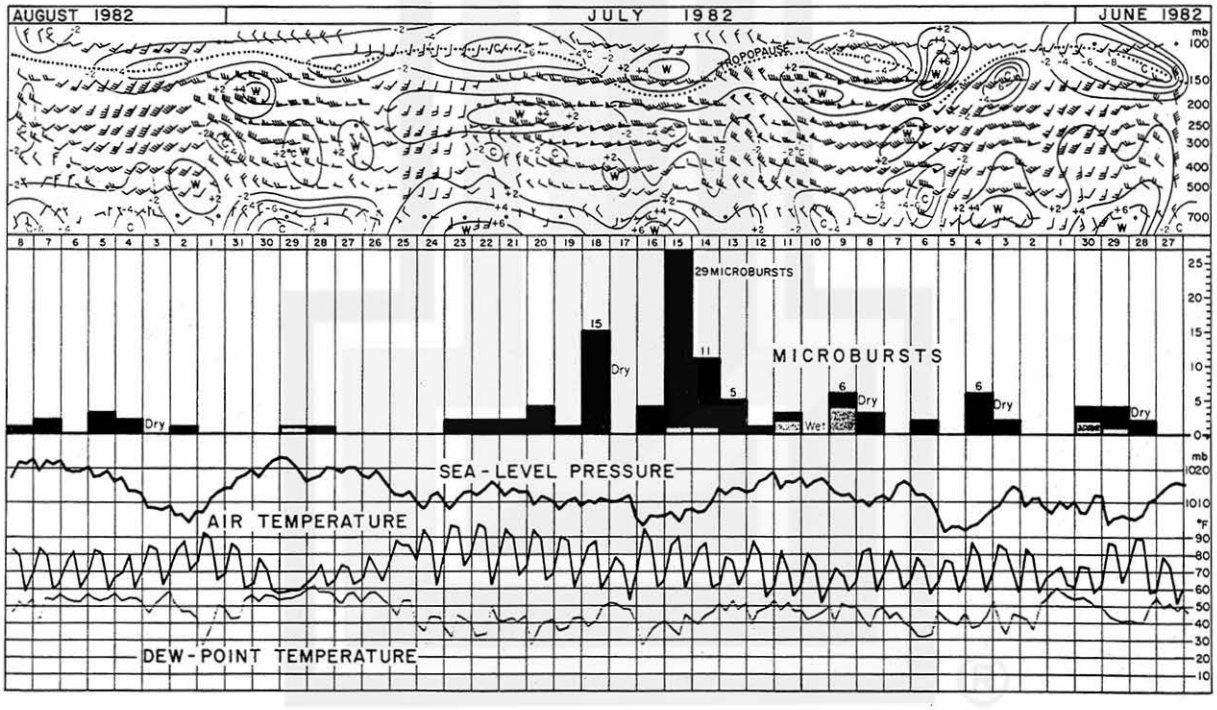

Fig. 4.12 Microburst frequencies in relation to the meteorological situation during the JAWS second period, 27 June through 8 August 1982.

considerable time identifying suspicious clouds and initiating Doppler radar scans in RHI and PPI modes. On 12 June 1982, a rotating cloud base was spotted visually. Thereafter, the entire life cycle of a tornado that spawned from the cloud base was photographed and scanned by three Doppler radars.

The Pan American 759 accident at New Orleans on 9 July 1982 occurred in the midst of the JAWS experiment. The cause of the accident was quickly attributed to a microburst on the east side of the airport. As a result, the JAWS researchers felt equally that the microburst phenomena should be understood as quickly as possible for the sake of aircraft safety. Meanwhile, additional funding for JAWS became available, thus accelerating the observational effort used in solving the mystery of the microburst.

Prediction of microbursts based on upper-air and surface observations does not seem to be promising at this time. Against expectation, microburst occurrences are poorly correlated to the winds aloft and to the temperature anomalies presented in Figs. 4.11 and 4.12. The main reason for this discouraging relationship is that microbursts in the Denver area are spawned by large cumulonimbus clouds as well as relatively small cumulus clouds. These cumulus clouds develop under non-severe storms environment.

4.3 Identification of Microbursts by Computer

Each PAM station in the NIMROD and JAWS networks collected windspeeds once every minute, 24 hours a day. These windspeeds include

- One-min mean wind --- speed averaged over the past one minute
- One-min maximum wind --- maximum speed during the past one minute.

Of these, the maximum winds were used in identifying the microbursts which affected the PAM stations in these networks.

According to the statistics, each PAM station collected a large number of maximum winds during the periods of network operations: 61,766 maximum winds from NIMROD and 123,956 maximum winds from JAWS. The total maximum winds from the 27 stations in both networks were 5,014,494. The only efficient way to sort the microburst winds out of this data is to single out all possible wind characteristics by means of a microburst identification algorithm.

As shown in Fig. 4.13, a microburst is characterized by a mound-shaped wind profile with a peak, center wind $\dot{W}$. In order to determine the magnitude of the rise and the drop of the winds in the mound, the mean windspeeds before and after the mound are computed from

$$\bar{W}_- = \frac{1}{6}\,(W_{-2} + W_{-3} + \cdots\cdots\cdots + W_{-7}) \quad \text{pre-peak mean speed} \qquad (4.1)$$

$$\bar{W}_+ = \frac{1}{6}\,(W_{+2} + W_{+3} + \cdots\cdots\cdots + W_{+7}) \quad \text{post-peak mean speed} \qquad (4.2)$$

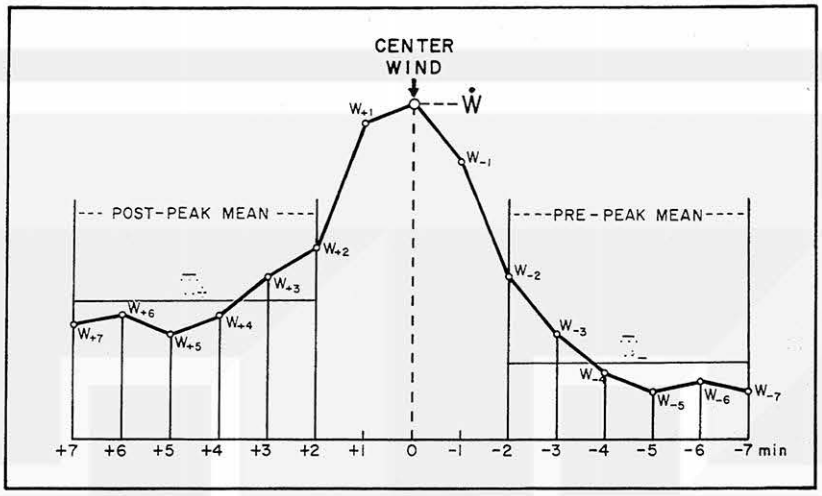

Fig. 4.13 A typical variation of microburst winds characterized by a mound-shaped high wind. Two windspeeds, one minute before and after the center wind, were not used in computing both pre-peak and post-peak windspeeds.

without using the speeds, one minute before and after the center wind. If we include the winds only one minute away from the center wind, it could result in an unusual increase in the mean speeds, because the mound-shaped wind in a microburst lasts 2 to 5 minutes.

The first-guess algorithm in identifying microbursts consists of a group of six conditions which must be satisfied simultaneously.

Condition 1 Center wind should be faster than 10 m/sec

Condition 2 Center wind should be at least 5 m/sec faster than $\overline{W}_+$

Condition 3 Center wind should be at least 5 m/sec faster than $\overline{W}_-$

Condition 4 Center wind should be 1.25 $\overline{W}_+$ or faster

Condition 5 Center wind should be 1.25 $\overline{W}_-$ or faster

Condition 6 $\overline{W}_+$ should not exceed 1.5 $\overline{W}_-$

Condition 1 specifies that the center wind must be faster than 10 m/sec (19.4 kts) in order to be called a microburst. Conditions 2 and 3 state that the mound-shaped profile must be elevated at least 5 m/sec (10 kts) above the level of the pre- and the post-peak mean windspeed. Conditions 4 and 5 will reject a small mound superimposed upon the sustained high winds. Finally, Condition 6 will exclude the gust front which is characterized by an exponential decay of the gusty winds behind a front.

The first-guess algorithm was applied to each one of the 5 million winds to obtain 143 first-guess microbursts in NIMROD and 436 first microbursts in JAWS.

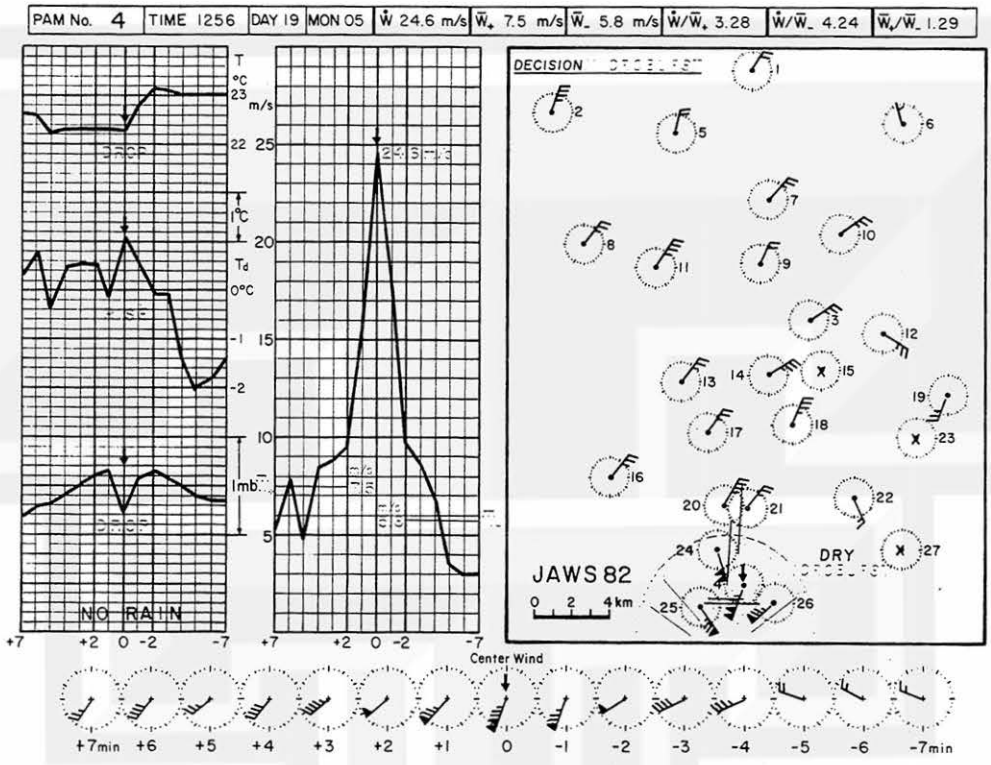

Fig. 4.14 The misoanalysis chart in making final decision of a "yes" or a "no" microburst. This example shows a "yes" microburst at Station 6 at 1256 MDT 19 May 1982. A strong outflow from the south of Stapleton Airport is firm evidence of a microburst.

However, a detailed examination of individual PAM data, along with the known cases of microbursts, indicated that the number of these first-guess microbursts is excessive. Some may not be real microbursts. They could be just high peak winds. It was also found that a further tightening of the six conditions could eliminate true microburst cases.

To overcome this difficulty, the variation of winds in every first-guess microburst was plotted on a misoanalysis chart. The final decision of a "yes" or a "no" was made ultimately by meteorologists who performed the misoanalysis (Fig. 4.14). Finally, 50 microbursts in NIMROD and 186 microbursts in JAWS were identified and tabulated in Tables 4.1 and 4.2.

Table 4.1 List of 50 microbursts detected by the 27 PAM stations of the NIMROD Network in the western suburbs of Chicago, Illinois. PAM stations were operated 24 hours a day between 1103 CDT 19 May 1978 through 0729 CDT 1 July 1978. The total operation period was 42 days 21 hours 26 minutes.

Number	Time (CDT)	Day	Month	Year	PAM	Peak (m/s)	Direction (deg)	Duration (min)	Rain (inch)	ΔT (°C)	ΔT_d (°C)	ΔP (mb)
1	1841	28	May	1978	13	13.4	220	2.1	--	-1.7	+3.8	+0.1
2	2003	29	May	1978	20	17.8	160	4.8	--	-1.8	+1.4	0.0
3	2100	29	May	1978	27	14.8	200	5.5	0.02	-0.9	-0.4	+0.1
4	2148	29	May	1978	9	21.2	220	5.7	0.08	-2.4	-3.5	+0.6
5	2223	29	May	1978	10	13.8	200	3.4	0.18	+3.1	-1.9	+0.2
6	2223	29	May	1978	12	18.0	130	2.1	0.25	-2.6	+1.3	+1.2
7	1237	3	Jun	1978	26	11.5	240	3.1	--	+0.2	-0.2	+3.1
8	1307	3	Jun	1978	25	12.4	180	1.7	--	-1.3	-0.4	-0.1
9	1404	3	Jun	1978	3	15.5	260	4.0	--	-3.0	+3.9	+0.6
10	1408	6	Jun	1978	13	11.0	310	2.6	--	-0.1	0.0	0.0
11	1749	7	Jun	1978	6	10.1	220	3.5	--	-3.4	-0.4	+0.2
12	1845	7	Jun	1978	7	19.2	300	2.1	0.11	-1.5	+0.4	+0.3
13	1905	7	Jun	1978	5	10.6	300	2.4	0.07	-2.2	+0.5	+0.3
14	1905	7	Jun	1978	9	19.1	210	4.4	0.03	-3.9	+1.2	+0.2
15	1948	7	Jun	1978	12	21.8	250	1.5	0.01	-0.1	-0.4	+1.3
16	1955	7	Jun	1978	18	20.5	290	6.4	--	-2.6	-2.8	+1.0
17	2016	7	Jun	1978	27	14.9	250	2.6	0.11	-2.5	+0.7	+0.7
18	1328	12	Jun	1978	26	13.8	320	2.0	--	-2.6	+5.8	+0.2
19	1016	16	Jun	1978	1	13.8	130	2.7	0.33	-1.1	-1.3	-1.2
20	1017	16	Jun	1978	4	27.3	010	2.7	0.24	+1.6	+0.9	+0.5
21	1022	16	Jun	1978	16	22.0	330	2.9	--	+1.2	-0.2	+1.2
22	1043	16	Jun	1978	24	20.0	330	3.0	--	+1.7	-1.2	+1.3
23	1047	16	Jun	1978	23	21.0	360	1.9	--	+2.8	-1.1	+0.4
24	1055	16	Jun	1978	26	25.3	340	2.2	--	+2.0	-1.3	+0.4
25	1312	16	Jun	1978	12	14.5	190	3.2	--	0.0	-0.1	0.0
26	0340	17	Jun	1978	1	10.6	180	2.1	0.02	-0.5	+0.4	-0.9
27	0516	17	Jun	1978	21	13.4	350	4.7	--	-1.8	+0.7	+0.6
28	0522	17	Jun	1978	20	13.2	300	2.5	0.05	-3.2	+2.1	+0.3
29	0530	17	Jun	1978	23	14.0	330	4.3	0.03	-2.2	+1.2	+1.3
30	2118	17	Jun	1978	5	14.2	270	4.2	0.24	+1.1	-1.5	+0.3
31	2222	17	Jun	1978	22	16.6	250	2.6	0.10	-1.2	+0.2	+1.4
32	2302	17	Jun	1978	7	26.8	250	3.9	0.26	-0.6	-1.4	-0.7
33	2323	17	Jun	1978	27	17.9	260	2.7	0.01	-0.8	-0.2	+0.7
34	2354	17	Jun	1978	3	14.1	240	4.2	0.01	+0.3	-0.5	+0.5
35	1045	25	Jun	1978	6	13.0	010	3.6	0.01	-0.4	-0.9	-0.1
36	1134	25	Jun	1978	8	25.9	010	3.3	0.69	+0.9	-0.5	-0.5
37	1154	25	Jun	1978	9	31.3	140	3.9	0.11	-0.1	-0.3	-0.6
38	1334	25	Jun	1978	27	15.0	130	2.7	0.41	-0.6	-0.3	-0.7
39	1438	25	Jun	1978	2	23.9	330	4.2	0.72	-1.4	-1.1	+4.0
40	1450	25	Jun	1978	8	24.1	330	3.3	0.33	-1.7	-1.4	+3.1
41	1502	25	Jun	1978	19	14.4	350	5.3	0.10	+0.4	+0.5	+1.7
42	1642	25	Jun	1978	9	20.0	130	3.9	--	?	-3.7	-2.0
43	1704	25	Jun	1978	3	19.9	190	2.7	0.42	+0.9	-1.1	-3.7
44	1708	25	Jun	1978	8	16.3	360	3.6	0.31	?	?	+2.4
45	1720	25	Jun	1978	9	16.4	190	3.9	--	+3.6	-1.4	-2.9
46	1725	25	Jun	1978	13	24.1	010	2.2	1.01	+1.4	+1.2	-1.1
47	0747	26	Jun	1978	24	15.5	290	7.0	0.05	+0.4	-0.5	+0.3
48	0736	30	Jun	1978	27	11.1	300	4.9	0.05	+1.1	-1.4	+0.8
49	0831	30	Jun	1978	18	12.1	340	3.9	0.10	-0.9	-0.4	+1.1
50	0629	1	Jul	1978	7	14.4	340	4.1	--	-0.4	-0.6	+1.2

Table 4.2 List of 186 microbursts detected by the 27 PAM stations of the JAWS Network in the northern suburbs of Denver, Colorado. PAM stations were operated 24 hours a day between 0801 MDT 15 May 1982 and 0957 9 August 1982. The total operation period was 86 days 1 hour 56 minutes.

Number	Time (MDT)	Day	Month	Year	PAM	Peak (m/s)	Direction (deg)	Duration (min)	Rain (inch)	ΔT (°C)	ΔT_d (°C)	ΔP (mb)
1	2054	17	May	1982	24	14.9	310	2.5	0.01	-0.2	-2.7	+0.3
2	1839	18	May	1982	11	16.3	310	2.7	--	+1.6	-3.1	+0.2
3	1853	18	May	1982	10	17.3	320	3.0	--	+1.3	-3.9	+0.3
4	1855	18	May	1982	25	10.9	060	4.3	--	+1.2	+2.3	-0.3
5	1909	18	May	1982	22	18.2	150	2.4	--	+1.3	-3.7	-0.6
6	1242	19	May	1982	19	16.1	060	2.9	--	+0.4	-3.9	-0.6
7	1256	19	May	1982	4	24.6	200	2.3	--	-0.8	+2.3	+0.4
8	1308	19	May	1982	14	12.7	360	2.6	--	+1.0	-5.7	+0.3
9	1311	19	May	1982	3	13.6	060	2.9	--	+1.5	-7.7	+0.5
10	1408	19	May	1982	1	23.2	180	2.4	--	-1.6	-3.9	+0.5
11	1442	19	May	1982	27	19.1	170	3.6	--	-0.7	-0.7	0.0
12	1636	19	May	1982	18	15.7	280	2.4	--	+0.4	-2.3	+0.1
13	1727	19	May	1982	17	20.6	320	3.3	--	-0.1	-3.6	+0.4
14	0851	20	May	1982	26	10.5	130	1.2	--	+0.5	+0.2	0.0
15	1302	20	May	1982	12	13.1	050	1.6	--	+0.6	+0.6	0.0
16	1223	21	May	1982	16	12.6	350	2.4	--	+0.9	-0.7	+0.2
17	1555	21	May	1982	26	12.1	340	1.7	--	+1.6	+0.5	0.0
18	1234	23	May	1982	24	13.0	090	1.6	--	+0.8	+1.1	0.0
19	1329	23	May	1982	9	10.7	060	1.9	--	+0.4	-0.2	0.0
20	1425	23	May	1982	9	18.7	340	3.7	0.07	-2.6	-3.8	0.0
21	1435	23	May	1982	3	15.1	310	4.4	0.05	-1.1	-2.2	+0.4
22	1450	23	May	1982	20	18.4	080	2.5	0.05	-1.6	-5.3	+0.3
23	1502	23	May	1982	24	15.3	070	1.6	0.05	+1.6	+1.4	0.0
24	1709	23	May	1982	11	15.2	050	5.0	--	-1.5	+0.5	+0.2
25	1705	25	May	1982	10	11.4	030	1.6	0.01	-1.0	-2.5	-0.2
26	2152	25	May	1982	7	14.0	240	1.2	0.01	+0.9	-2.1	-0.4
27	2156	25	May	1982	9	15.4	240	2.7	--	+1.4	-3.5	-0.3
28	2159	25	May	1982	12	15.7	280	3.9	--	+0.2	+1.1	0.0
29	2212	25	May	1982	18	16.0	180	3.5	0.01	+2.8	-5.1	-0.6
30	2225	25	May	1982	21	12.6	150	2.6	--	+0.9	-2.4	+0.2
31	0854	26	May	1982	26	12.0	150	1.7	--	-0.6	-0.3	0.0
32	1305	27	May	1982	21	12.3	140	3.3	--	-0.9	-0.8	0.0
33	1425	27	May	1982	14	13.9	290	2.4	--	+0.4	-2.3	?
34	1441	27	May	1982	5	23.5	190	2.1	--	-2.0	-1.2	+0.2
35	1457	27	May	1982	1	22.2	290	3.1	--	-2.3	+3.1	+0.4
36	1551	28	May	1982	18	12.7	230	1.7	--	+1.3	+0.8	0.0
37	1517	2	Jun	1982	10	10.1	330	1.6	--	+0.5	+0.7	0.0
38	1908	2	Jun	1982	14	23.0	320	3.2	0.01	+0.4	-0.9	+0.2
39	1912	2	Jun	1982	15	22.4	320	4.0	--	0.0	-0.4	?
40	1914	2	Jun	1982	6	13.1	250	1.8	0.02	-0.3	+0.2	+1.5
41	1914	2	Jun	1982	18	26.3	340	4.2	--	+0.3	-0.9	+2.3
42	1915	2	Jun	1982	7	13.9	050	5.1	0.35	-0.8	+0.4	?
43	0235	5	Jun	1982	26	12.1	320	1.7	--	+1.7	-1.0	+0.2
44	1159	6	Jun	1982	24	12.0	280	3.4	--	-1.0	-2.3	+0.1
45	1336	6	Jun	1982	21	14.0	260	1.5	--	-0.9	-4.8	+0.1
46	1957	6	Jun	1982	14	11.9	020	2.4	--	-0.1	-2.0	+0.2
47	1522	8	Jun	1982	1	12.9	090	1.8	--	+0.5	+0.3	0.0
48	1654	8	Jun	1982	13	10.3	010	2.2	--	-0.7	+0.1	0.0
49	1734	10	Jun	1982	24	14.0	350	1.8	--	-0.2	-2.0	+0.2
50	1528	11	Jun	1982	15	14.1	080	2.9	--	+0.6	-0.9	0.0

Table 4.2 Continued

Number	Time (MDT)	Day	Month	Year	PAM	Peak (m/s)	Direction (deg)	Duration (min)	Rain (inch)	ΔT (°C)	ΔT_d (°C)	ΔP (mb)
51	1306	14	Jun	1982	21	21.2	310	3.8	0.16	-5.9	-0.9	+1.6
52	1315	14	Jun	1982	11	19.7	290	4.7	--	-2.6	-4.0	+2.0
53	1325	14	Jun	1982	27	19.2	330	3.1	0.29	?	-8.1	?
54	1340	14	Jun	1982	18	17.1	300	3.0	--	+3.5	-0.4	0.0
55	1344	14	Jun	1982	12	13.8	010	4.3	0.34	+3.5	+0.7	0.0
56	1430	17	Jun	1982	16	10.5	330	2.0	0.26	-3.1	+1.1	+0.3
57	1724	17	Jun	1982	15	13.9	020	2.6	--	-1.8	-0.7	+0.3
58	1245	22	Jun	1982	6	10.7	090	1.3	--	+0.1	+0.3	0.0
59	1623	22	Jun	1982	20	12.8	210	2.6	0.07	+0.8	-0.6	+0.2
60	1629	22	Jun	1982	3	14.0	170	2.2	0.06	+1.1	-2.5	0.0
61	1810	22	Jun	1982	22	14.0	280	2.1	0.01	+0.6	-0.8	+0.2
62	1614	23	Jun	1982	3	13.3	270	5.1	--	-3.1	-0.7	+0.2
63	1811	23	Jun	1982	1	12.8	340	4.1	--	+0.5	-1.4	+0.2
64	1855	25	Jun	1982	22	17.6	250	1.6	--	-1.0	+0.5	+0.2
65	1257	26	Jun	1982	5	16.1	320	4.0	--	-2.8	+2.2	+0.4
66	1312	26	Jun	1982	17	18.6	360	3.7	0.08	-4.6	+3.9	+0.4
67	1420	26	Jun	1982	1	13.0	030	2.4	--	-0.9	+2.6	+0.1
68	1421	28	Jun	1982	11	11.3	020	2.2	--	+0.6	+1.9	0.0
69	1442	28	Jun	1982	5	13.4	110	1.6	--	+0.8	+1.7	0.0
70	1943	29	Jun	1982	16	19.6	180	2.7	--	+0.5	?	?
71	2006	29	Jun	1982	23	13.7	180	2.9	0.05	-7.0	-6.6	+0.7
72	2026	29	Jun	1982	4	12.7	310	3.0	--	+0.1	-1.3	+0.3
73	2201	29	Jun	1982	21	15.1	170	3.7	--	+0.4	-1.0	+0.2
74	1809	30	Jun	1982	4	16.7	180	2.5	--	-0.2	-0.9	+1.0
75	1812	30	Jun	1982	27	17.6	280	6.0	--	-1.4	-0.7	+0.3
76	1831	30	Jun	1982	23	29.1	260	2.8	0.10	+1.0	+0.8	+0.2
77	1846	30	Jun	1982	10	20.6	170	4.0	0.17	-0.3	-1.4	+0.4
78	1459	3	Jul	1982	19	12.1	040	2.8	--	+0.8	+1.7	+0.1
79	1533	3	Jul	1982	27	11.7	140	3.2	--	0.0	-0.6	0.0
80	1729	4	Jul	1982	8	14.2	270	3.0	--	+1.3	-0.3	0.0
81	1736	4	Jul	1982	1	24.4	280	2.5	--	+0.9	-7.1	+0.3
82	1811	4	Jul	1982	17	15.5	290	2.6	--	+0.9	-5.1	+0.3
83	1824	4	Jul	1982	27	12.1	250	1.2	--	-0.1	-2.3	0.0
84	1840	4	Jul	1982	13	20.7	180	2.3	--	-0.4	+0.3	0.0
85	1845	4	Jul	1982	14	12.9	270	4.0	--	+0.9	-3.0	+0.1
86	1230	6	Jul	1982	15	10.7	280	2.9	--	-0.6	-0.8	0.0
87	1300	6	Jul	1982	24	13.0	330	2.6	--	?	?	0.0
88	1327	8	Jul	1982	13	16.4	220	2.1	--	-2.0	+1.4	+0.9
89	1328	8	Jul	1982	16	18.4	280	3.7	--	-1.2	+1.1	+0.2
90	1344	8	Jul	1982	3	18.4	280	3.0	--	0.0	-0.5	0.0
91	1425	9	Jul	1982	9	15.9	280	2.4	--	-2.3	-4.8	+0.4
92	1429	9	Jul	1982	3	17.0	310	4.2	0.04	-2.0	-3.8	0.0
93	1431	9	Jul	1982	13	15.7	270	3.6	--	+2.1	-4.5	-0.3
94	1432	9	Jul	1982	10	16.3	270	3.0	0.09	-3.3	-4.2	+0.5
95	1439	9	Jul	1982	6	11.3	230	6.0	0.03	-3.7	-0.6	+0.1
96	1442	9	Jul	1982	21	14.2	240	4.2	0.18	-2.9	-2.3	+0.2
97	1858	11	Jul	1982	8	13.8	290	4.2	--	-2.1	-2.2	+0.8
98	1907	11	Jul	1982	13	10.8	050	1.5	0.05	+0.5	-1.7	+0.1
99	1915	11	Jul	1982	25	15.3	050	2.2	0.02	-1.1	-1.3	+0.1
100	1440	12	Jul	1982	14	10.8	030	1.8	--	-0.4	-1.6	0.0

Table 4.2 Continued

Number	Time (MDT)	Day	Month	Year	PAM	Peak (m/s)	Direction (deg)	Duration (min)	Rain (inch)	ΔT (°C)	ΔT_d (°C)	ΔP (mb)
101	0141	13	Jul	1982	5	11.4	290	1.8	--	+3.2	-1.2	0.0
102	1501	13	Jul	1982	2	18.1	210	2.0	--	+1.8	-5.3	-0.1
103	1547	13	Jul	1982	3	11.2	190	3.0	--	+0.9	-2.1	0.0
104	1547	13	Jul	1982	25	13.2	260	3.5	--	-0.3	-0.3	+0.1
105	1605	13	Jul	1982	12	14.4	210	4.0	--	-0.2	+0.9	0.0
106	1344	14	Jul	1982	25	12.4	210	1.7	--	+0.1	-6.0	-0.2
107	1409	14	Jul	1982	16	18.9	240	2.6	--	-0.5	-4.5	-0.3
108	1412	14	Jul	1982	26	14.7	100	2.3	--	-0.4	-0.4	0.0
109	1418	14	Jul	1982	17	14.3	240	2.1	--	+0.1	-2.9	+0.1
110	1419	14	Jul	1982	21	22.9	220	3.1	--	-0.8	-0.9	+0.4
111	1435	14	Jul	1982	27	28.3	250	3.2	--	-0.9	+1.1	+0.4
112	1447	14	Jul	1982	27	12.0	080	2.7	--	+0.7	-0.5	0.0
113	1512	14	Jul	1982	10	16.7	360	2.6	0.03	+1.4	-2.0	+0.1
114	1518	14	Jul	1982	15	18.9	030	6.2	--	-0.6	-0.3	-0.1
115	1648	14	Jul	1982	1	18.4	330	2.1	--	+2.0	-9.1	-0.2
116	1756	14	Jul	1982	22	17.1	010	2.2	--	+2.3	-5.7	-0.3
117	1357	15	Jul	1982	4	26.6	310	8.0	--	-2.1	+0.2	0.0
118	1359	15	Jul	1982	21	32.6	190	7.5	--	-1.5	+1.4	0.0
119	1416	15	Jul	1982	27	14.9	300	4.0	--	+0.6	+0.3	+0.1
120	1423	15	Jul	1982	5	12.9	270	1.8	--	-0.9	-0.2	+0.1
121	1423	15	Jul	1982	16	15.9	180	2.5	--	-0.1	-1.2	+0.3
122	1432	15	Jul	1982	27	21.3	200	4.5	--	-0.5	+1.8	-0.2
123	1446	15	Jul	1982	4	10.8	060	2.2	--	-0.3	-2.9	+0.1
124	1454	15	Jul	1982	3	11.9	200	1.9	--	0.0	+1.2	0.0
125	1513	15	Jul	1982	4	29.0	300	3.1	--	-0.5	+0.8	+1.0
126	1514	15	Jul	1982	15	14.0	270	2.8	--	-0.2	+0.2	+0.1
127	1515	15	Jul	1982	16	17.7	190	5.6	--	-1.4	+1.2	0.0
128	1523	15	Jul	1982	21	21.3	250	5.2	--	-0.9	+1.2	+0.3
129	1533	15	Jul	1982	27	24.8	320	7.3	--	-2.0	+2.2	+2.0
130	1534	15	Jul	1982	7	13.5	210	6.0	--	-0.8	-0.5	+0.2
131	1534	15	Jul	1982	13	15.3	190	3.0	--	-0.3	+1.0	+0.1
132	1537	15	Jul	1982	22	14.4	240	3.5	--	+0.3	-0.6	+0.2
133	1540	15	Jul	1982	15	26.6	250	2.9	--	-0.2	-0.6	-0.3
134	1541	15	Jul	1982	6	14.4	210	3.1	--	-0.6	-1.2	+0.1
135	1543	15	Jul	1982	3	19.4	190	5.2	--	-0.4	+2.3	0.0
136	1544	15	Jul	1982	23	22.7	200	3.1	--	-0.2	+0.6	+0.8
137	1544	15	Jul	1982	27	17.8	250	2.9	--	0.0	0.0	0.0
138	1548	15	Jul	1982	12	29.5	310	2.7	0.01	-0.4	+0.2	+1.0
139	1606	15	Jul	1982	15	16.1	190	4.9	--	-0.7	-0.1	0.0
140	1613	15	Jul	1982	16	16.6	130	2.6	--	+0.5	-1.4	+0.4
141	1639	15	Jul	1982	23	15.1	180	2.2	--	+0.6	-1.1	0.0
142	1643	15	Jul	1982	8	16.6	260	6.4	--	+0.3	-0.1	0.0
143	1649	15	Jul	1982	19	19.1	180	3.0	--	-0.1	0.0	0.0
144	1650	15	Jul	1982	3	13.4	210	2.8	--	-0.1	-0.2	+0.2
145	1700	15	Jul	1982	27	21.3	200	4.2	--	+0.8	-0.9	0.0
146	1150	16	Jul	1982	14	16.4	320	1.5	--	+0.5	+1.3	0.0
147	1255	16	Jul	1982	18	12.8	240	2.3	--	-1.1	-1.0	0.0
148	1501	16	Jul	1982	20	11.4	020	1.2	--	-0.4	-2.3	0.0
149	1615	16	Jul	1982	27	22.0	280	2.0	--	-0.3	-0.2	+0.2
150	1039	18	Jul	1982	14	16.0	200	1.0	--	-0.4	-0.7	+0.1

Table 4.2 Continued

Number	Time (MDT)	Day	Month	Year	PAM	Peak (m/s)	Direction (deg)	Duration (min)	Rain (inch)	ΔT (°C)	ΔT_d (°C)	ΔP (mb)
151	1152	18	Jul	1982	5	11.1	150	1.2	--	-0.6	-0.2	0.0
152	1326	18	Jul	1982	20	14.2	310	1.5	--	+0.9	+1.0	0.0
153	1701	18	Jul	1982	13	22.2	300	2.7	--	-1.4	-0.2	+0.6
154	1708	18	Jul	1982	18	24.7	210	4.0	--	-1.4	+1.0	-0.1
155	1724	18	Jul	1982	13	16.1	270	3.7	--	+0.7	-1.1	+0.2
156	1725	18	Jul	1982	21	20.1	360	1.9	--	-0.1	+0.2	0.0
157	1730	18	Jul	1982	18	23.0	170	3.0	--	-1.8	+1.9	+1.1
158	1731	18	Jul	1982	10	20.0	210	3.2	--	-0.6	+1.1	+0.1
159	1732	18	Jul	1982	17	29.6	010	1.7	--	-1.9	+2.1	+0.8
160	1737	18	Jul	1982	9	12.4	160	3.6	--	+0.7	-1.4	+0.1
161	1743	18	Jul	1982	6	13.8	190	4.7	--	+0.4	-0.9	0.0
162	1753	18	Jul	1982	10	12.8	060	2.7	--	-0.2	+0.1	0.0
163	1757	18	Jul	1982	24	14.2	290	2.0	--	0.0	0.0	+0.1
164	1803	18	Jul	1982	18	11.7	150	2.2	--	+0.6	-1.1	0.0
165	1418	19	Jul	1982	22	10.8	070	1.2	--	-0.5	+0.5	+0.1
166	1211	20	Jul	1982	22	12.2	310	1.0	--	+1.1	+0.8	0.0
167	1504	20	Jul	1982	15	13.3	020	1.3	--	-0.6	-0.3	0.0
168	1549	20	Jul	1982	22	11.1	090	2.2	--	-0.9	+1.4	0.0
169	1842	20	Jul	1982	27	16.1	150	2.0	--	+0.1	+0.4	+0.1
170	1451	21	Jul	1982	6	10.9	300	1.6	--	+1.1	-0.2	0.0
171	1452	21	Jul	1982	23	12.9	330	1.9	--	+0.7	-0.4	0.0
172	1230	22	Jul	1982	4	10.7	160	3.2	--	+0.1	0.0	0.0
173	1533	22	Jul	1982	4	14.4	160	1.9	--	+1.1	+0.7	0.0
174	1316	23	Jul	1982	4	10.1	160	1.3	--	-0.6	-0.8	0.0
175	1320	23	Jul	1982	18	10.5	030	2.1	--	-1.6	-0.3	-0.1
176	1157	28	Jul	1982	25	11.4	030	1.3	--	+0.3	-0.2	0.0
177	1243	29	Jul	1982	2	21.0	350	2.5	0.01	+0.1	+0.4	0.0
178	1316	2	Aug	1982	8	11.4	010	1.8	--	0.0	+0.6	+0.1
179	1202	4	Aug	1982	5	13.4	130	1.3	--	+1.3	-0.6	0.0
180	1501	4	Aug	1982	20	14.1	350	3.5	--	-1.2	+1.0	+0.3
181	1840	5	Aug	1982	4	10.6	280	4.4	--	+0.7	-3.9	0.0
182	1849	5	Aug	1982	24	12.7	210	2.0	--	+0.8	-1.2	0.0
183	2047	5	Aug	1982	24	16.0	240	2.3	--	+1.2	-1.8	+0.1
184	1356	7	Aug	1982	4	12.6	310	1.4	--	-0.3	+0.4	-0.1
185	1606	7	Aug	1982	7	12.1	030	1.4	--	-0.3	-0.3	0.0
186	1454	8	Aug	1982	27	13.8	160	1.4	--	-0.3	+0.4	0.0

4.4 Meteorological Parameters of Microbursts

Most macrobursts are accompanied by a dome of high pressure induced by rain-cooled air. Along the leading edge of the front of a macroburst, a pressure surge or jump takes place accompanied by gusty winds and a temperature drop.

In microbursts, however, a strong downflow descends very close to the ground before spreading. The downflow air warms up dry-adiabatically, all the way to the ground, unless embedded raindrops evaporate fast enough to maintain a moist-adiabatic descent. However, this is very unlikely

in a strong microburst. The air temperature in microbursts can be either warmer or colder than their environment. The surface pressure in a microburst can also be higher or lower than the environmental pressure, because the outburst winds lose their pressure head while being accelerated outward from the microburst center. Thus, the changes in the meteorological parameters in microbursts are very complicated (Table 4.3).

Table 4.3 Expected changes in the meteorological parameters in macrobursts and in microbursts.

	MACROBURSTS	MICROBURSTS
Air temperature	decrease	increase or decrease
Dew-point temperature	increase or decrease	increase or decrease
Relative humidity	rise	rise or dip
Surface pressure	rise or jump	rise or fall

Direction of Peak Winds

The peak winds induced by microbursts may come from any direction. Statistics show, however, that it is less likely to experience peak winds from the easterly direction. Fig. 4.15 presents statistical distributions of the NIMROD and JAWS microbursts which are subdivided into dry (red) and wet (blue) microbursts.

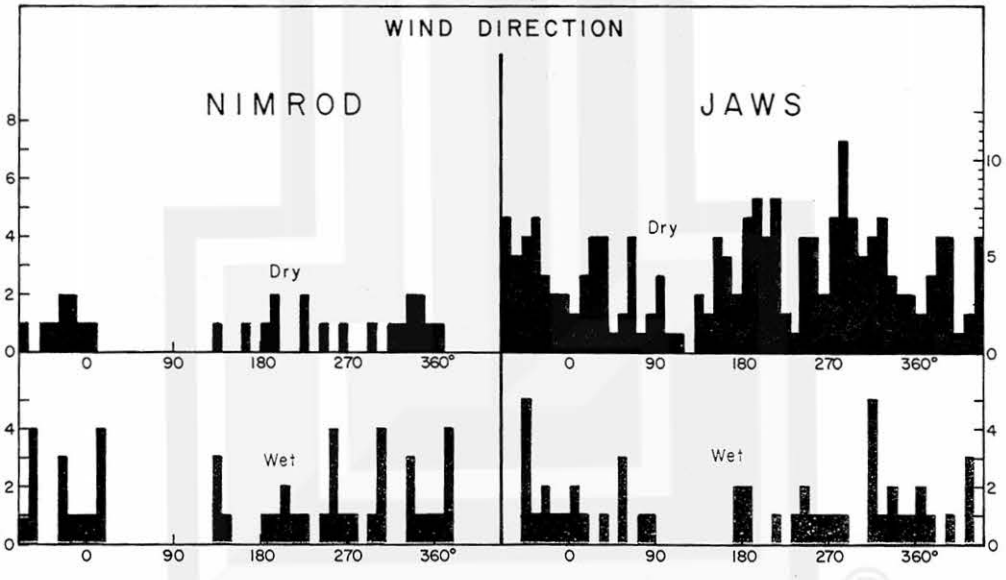

Fig. 4.15 Frequency distribution of the directions of peak winds induced by the NIMROD and JAWS microbursts. Wind directions were measured by 27 PAM stations in each network.

The direction of peak winds in the NIMROD Network is predominantly from 135° (southeast) through 360° (north). Practically no peak winds came from between 20° (north-northeast) and 120° (east-southeast). The peak winds in the JAWS Network show a sinusoidal distribution with their maximum frequency at 290° (west-northwest). Despite a small number of wet microbursts in JAWS, there is no basic difference in the directional frequencies of dry and wet microbursts.

Because of the fact that microbursts descend from the traveling parent clouds, we expect that the direction of the peak winds coincides with the motion of the parent clouds. In other words, a parent cloud, traveling from west to east, is likely to induce the maximum microburst wind coming from the west. This subject can be studied by plotting the direction of winds aloft as a function of the direction of microburst winds.

Fig. 4.16 shows two scatter diagrams relating the direction of the 500 and 700 mb winds to that of NIMROD and JAWS microburst winds. In both cases, the scatter of data points is very large, but their distribution centers can be located at 260° winds aloft and 260° peak winds (NIMROD) and 270° winds aloft and 270° peak winds (JAWS). If we assume that microburst-inducing clouds move with the 700-500 mb winds, we may expect that the direction of peak winds will coincide with that of the 700-500 mb winds. However, Fig. 4.16 shows otherwise.

One of the reasons for the large scatter in data points is the location of PAM stations relative to microburst centers. When a microburst center passes to the south of a PAM station, for example, PAM will measure a peak wind from the southerly direction. This means that the direction of the starburst winds in a microburst varies widely depending upon the relative location of microburst center and PAM station.

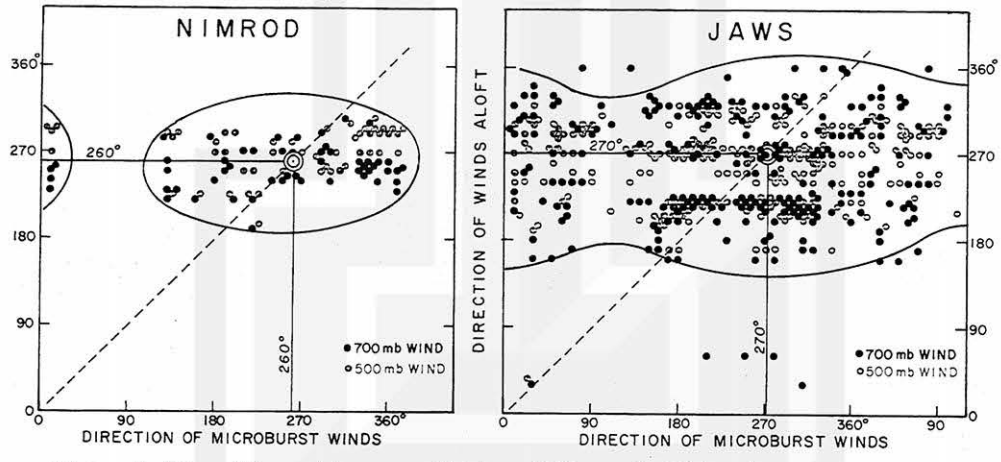

Fig. 4.16 Directions of the 500 and 700 mb winds plotted as a function of the directions of the peak microburst winds. If the directions of winds aloft coincide with those of microburst winds, all data points should be on the 45° line in each diagram.

Another reason for the large scatter is the horizontal gradient of the surface pressure field in which microburst winds spread out. Quite often, the pressure field of an earlier macroburst or a microburst at the location of a descending microburst affects the pattern of the outburst winds on or near the ground.

Peak Windspeed of Microbursts

Frequencies of microburst winds presented in Fig. 4.17 reveal that the probability of experiencing a specific windspeed reaches a peak within a windspeed range of 12 to 14 m/sec (27 to 31 mph). As the windspeed increases, the frequency decreases exponentially, reaching practically zero at 33 m/sec (74 mph). The maximum windspeed measured in the NIMROD experiment was 31.3 m/sec (70 mph) and that in JAWS was 32.6 m/sec (73 mph). The trend of the exponential decrease is almost identical in both experiments as well as in dry and wet microbursts.

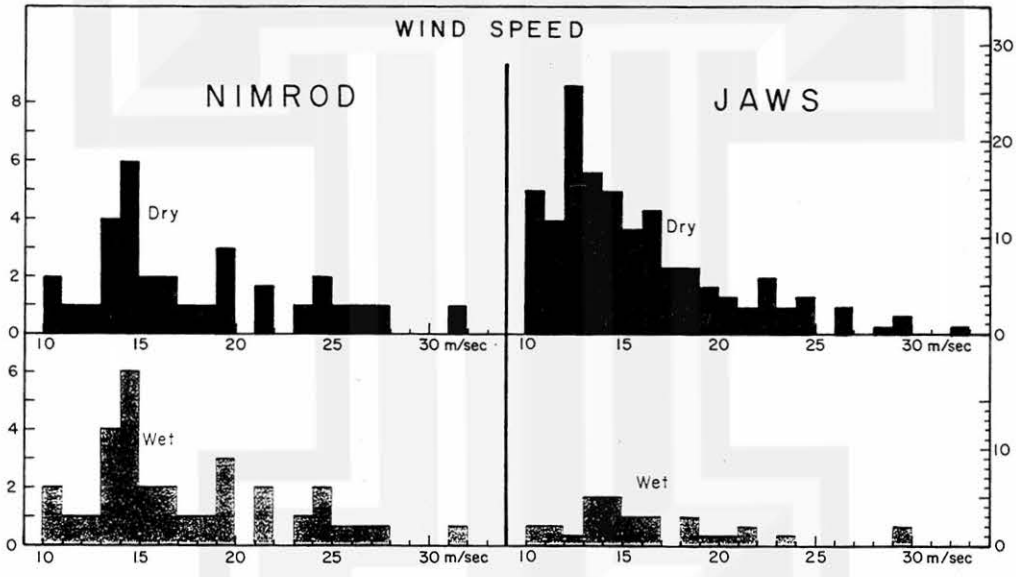

Fig. 4.17 Frequencies of the NIMROD and JAWS microbursts plotted as a function of their peak windspeeds measured by the 27 PAM stations in each network.

As expected, these results indicate that the lower the occurrence probability, the higher the windspeed. In assessing the occurrence probability of microburst winds, the frequencies in Fig. 4.17 were converted into the probability per PAM station per year. On the probability vs. windspeed diagram in Fig. 4.18, both NIMROD and JAWS data points can be approximated by two straight lines.

Extrapolations of these lines permit us to estimate the extreme windspeeds expected to occur with very low probabilities. These statistical results indicate that microburst frequencies per PAM station per year are high in JAWS, and that the peak windspeeds are low in JAWS compared with NIMROD.

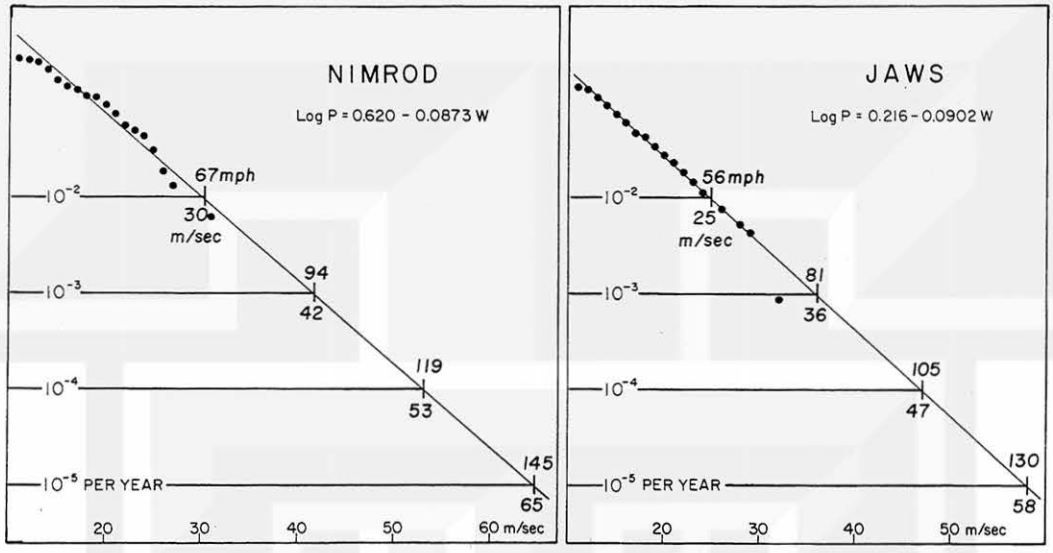

Fig. 4.18 Two straight lines expressing the maximum windspeeds in the NIMROD and JAWS microbursts. W in m/sec

Duration of Half-speed Winds

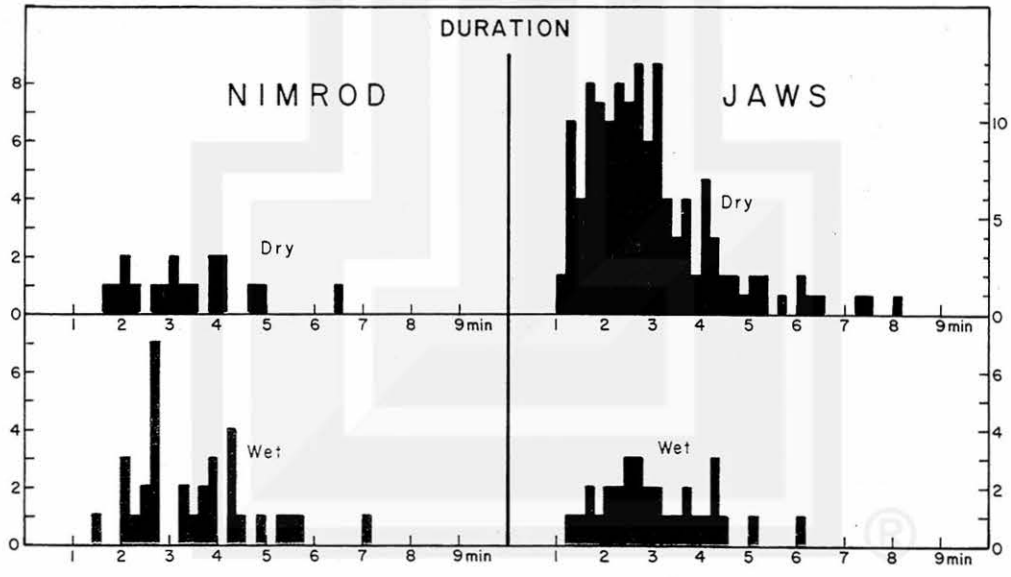

Fig. 4.19 Frequencies of the NIMROD and JAWS microbursts plotted as a function of the half-speed period.

The average duration of microburst winds, defined as the period of one-half of the peak windspeed (half-speed period) varies between one and eight minutes. The pattern of the frequency distributions of NIMROD and JAWS dry and wet microbursts appears to be identical. The average duration of the half-speed period is approximately three minutes (Fig. 4.19).

Air Temperature and Dew-point Temperature

One might expect that the surface temperature in microbursts would be colder than the environment. Against expectation, statistical results in Fig. 4.20 reveal that approximately 40% of the NIMROD and JAWS microbursts, either wet or dry, are warmer than their environment.

The reason for expecting a cold microburst is the cooling of the downflow due to evaporation or sublimation of the hydrometeors falling inside the descending current. However, these particles do not always evaporate fast enough to keep the downflow cool and saturated. A warm downflow is able to descend to the ground by virtue of its downward momentum.

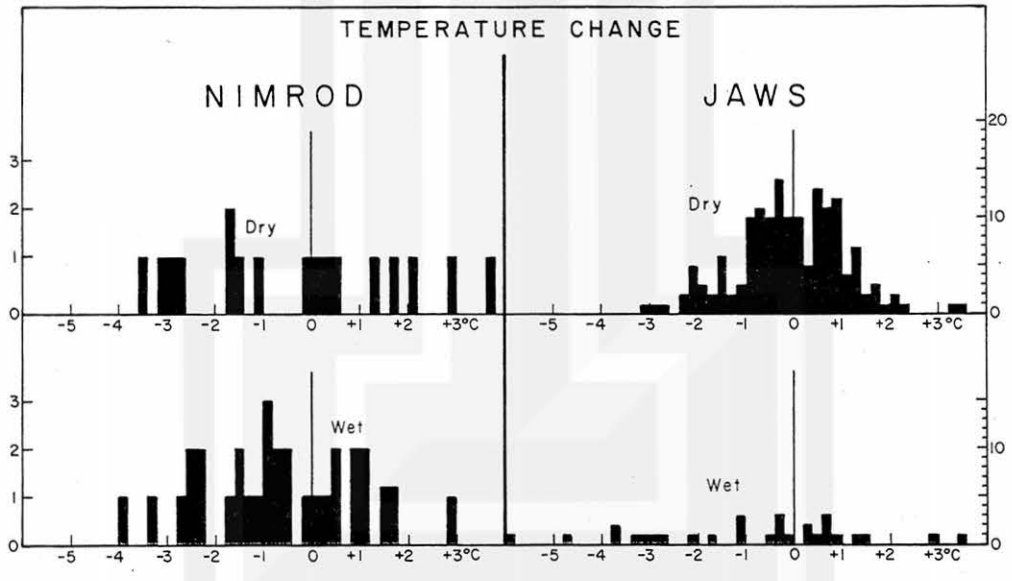

Fig. 4.20 Difference in temperature within microbursts and their environment. A positive temperature denotes that the microburst is warmer than its environment.

Dew-point temperature in microbursts is either higher or lower than their environment. One might expect that the dew-point temperature in a precipitation-cooled downflow would be relatively high. However, the statistical results in Fig. 4.21 reveal that it is either higher or lower. The lower dew-point temperature is likely to be caused by the dry air which entrains into the downflow during its fast descent to the ground.

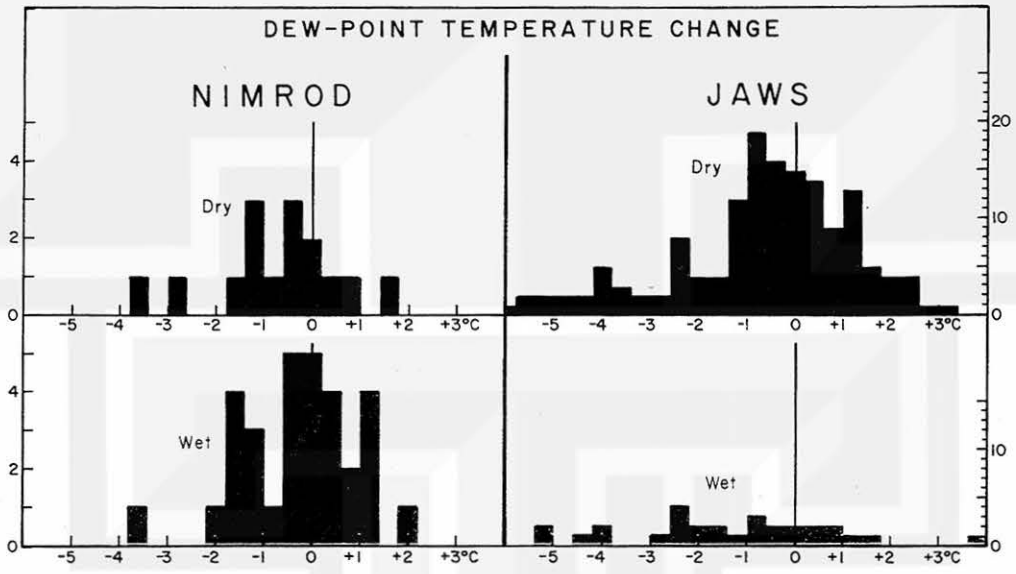

Fig. 4.21 Dew-point temperature difference between microbursts and their environment. The positive value denotes that the dew-point temperature in microbursts is higher than their environment.

Surface Pressure in Microbursts

Inside a microburst, we expect to measure high surface pressure which is caused by a strong downflow impinging upon the surface. Statistical distributions of pressure changes at the time of peak windspeeds show, however, that the pressure does not always increase during high winds. On the average, the surface pressure increases only several tenths of a millibar. In individual cases, it could increase or decrease by as much as 2 to 3 mb (Fig. 4.22).

The main reason for the strange pressure change is the conversion of total pressure into velocity pressure. At the dead center of a microburst, the surface pressure is high and the air is calm. The high total pressure at the microburst center accelerates the air outward. The atmospheric pressure decreases as the outflow speed increases, reaching a minimum at the location of the maximum windspeed. If we assume a frictionless outflow, Bernoulli's theorem can be applied for computing the pressure change as a function of the windspeed (Fig. 4.23).

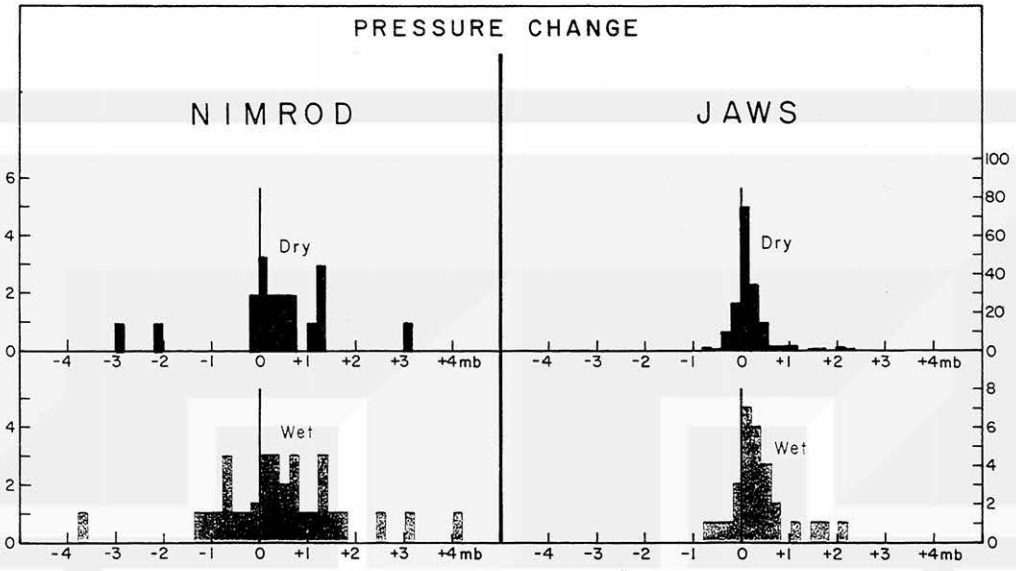

Fig 4.22 Surface pressure inside the NIMROD and JAWS microbursts. A positive pressure change denotes that the pressure at the peak wind time is higher than the environmental pressure.

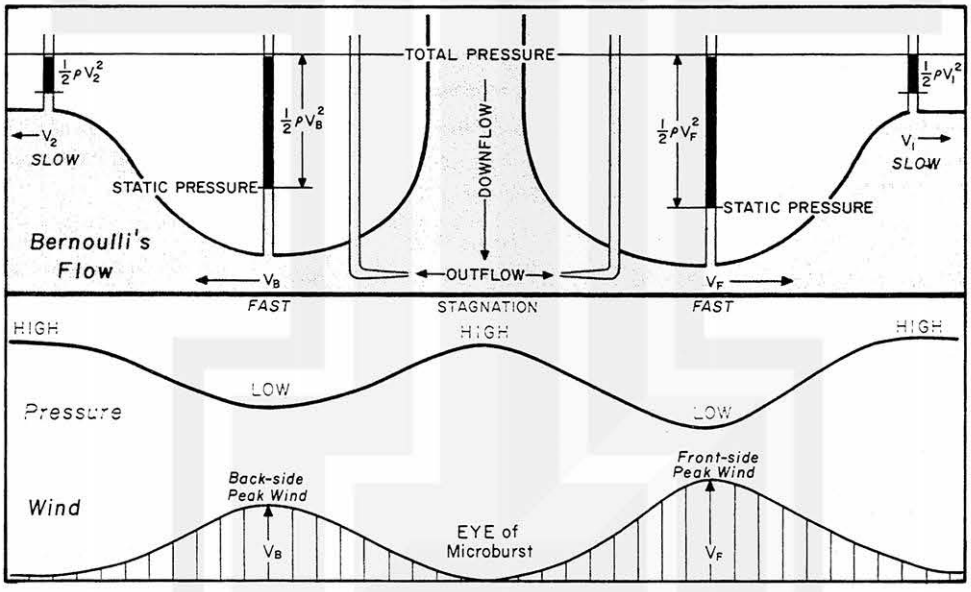

Fig. 4.23 Bernoulli's theorem indicating that the total pressure, a sum of the static pressure (blue) and the velocity pressure or the dynamic pressure (red), remains constant during a frictionless outflow from the center of a microburst. Pressure sensors, such as the ones used in PAM stations, measure the static pressure.

Schematic profiles of the surface pressure across a microburst vary widely, depending upon the location relative to the microburst center. The pressure field is characterized by high pressure at the microburst center which is encircled by a ring of low pressure (low pressure ring). The low pressure ring is surrounded by a high pressure ring located just inside the outer boundary of a microburst (Fig. 4.24).

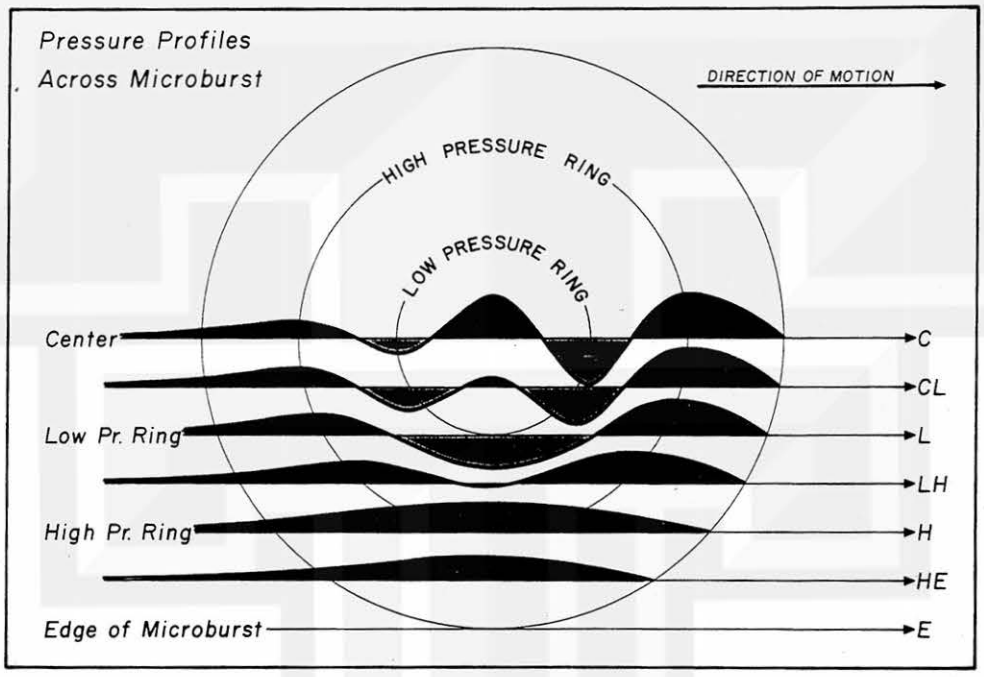

Fig. 4.24 Pressure profiles across various portions of a microburst. C--the center, CL--between the center and the low pressure ring, L--low pressure ring, etc.

4.5 Diurnal and Spatial Variations of Microbursts

Because the parent clouds of microbursts are convective clouds, their diurnal variations are closely related to the time of convective activity in specific regions.

Dry microbursts in the NIMROD Network occurred between 5 a.m. and 9 p.m. CDT with the peak occurrence at 10-11 a.m. Frequencies of wet microbursts increased progressively from 3 a.m. to midnight, reaching a peak between 5 p.m. and midnight (Fig. 4.25).

Dry microbursts in the JAWS Network showed two distinct occurrence peaks at 2-4 p.m. and 5-6 p.m. Wet microbursts occurred with a distinct peak at 2-3 p.m. and a secondary peak at 7-8 p.m. The earlier peak coincides with the time of small convective clouds, while the later peak denotes the time of large thunderstorms late in the afternoon to early evening hours.

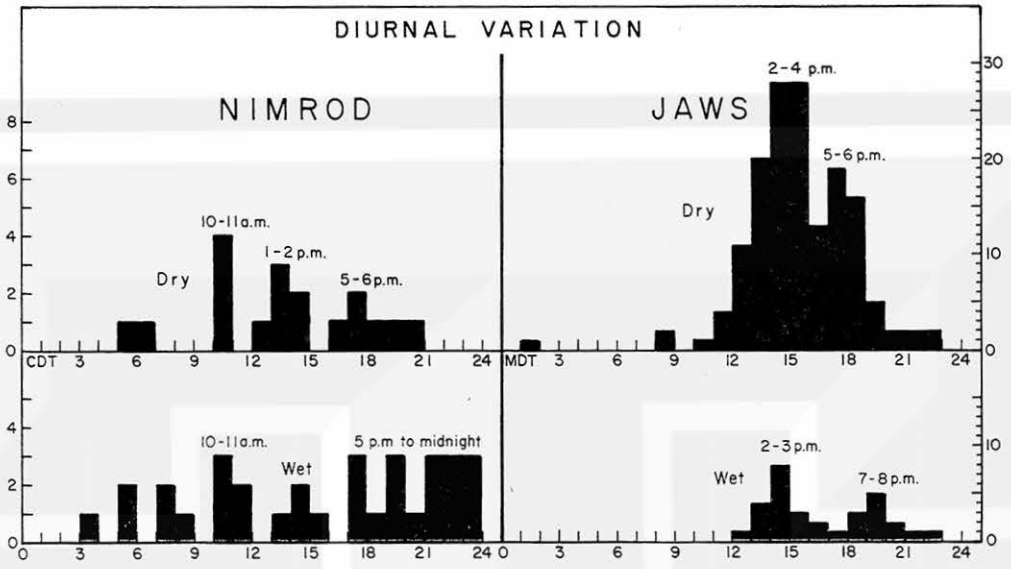

Fig. 4.25 Diurnal variations of the NIMROD and JAWS microbursts. It should be noted that the occurrence peaks of dry and wet microbursts are quite different.

The spatial distribution of microbursts in NIMROD shows zero frequency on the northwest side of the Doppler triangle. The maximum occurrences of five at the CP-3 site and near the CHILL site can be prorated to ten in 86 days, the period of the JAWS operation. The JAWS microbursts occurred frequently along the base line connecting the CP-3 with the CP-4 Doppler radars. In fact, Stapleton Airport was hit by strong microbursts frequently. For some reason, the CP-2 site was relatively free from microbursts, showing only two occurrences in 86 days.

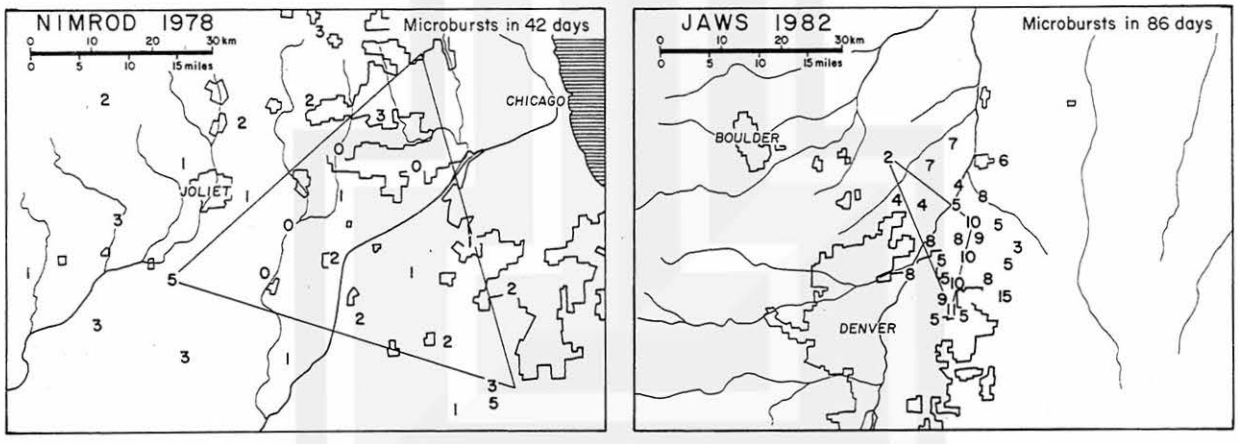

Fig. 4.26 Spatial distribution of microburst frequencies at each PAM station in the NIMROD and JAWS Networks. The maximum frequency in NIMROD is five and in JAWS is fifteen. Multiply by a factor of 2 to prorate NIMROD frequencies into JAWS frequencies.

Chapter Five

Types of Microbursts and Parent Clouds

Not all microbursts are alike; some are accompanied by heavy rain, while others form beneath small virga. The first major classification of microbursts is based on the precipitation received on the ground during a specific storm. Likewise, the temperature change can be used in distinguishing warm microbursts from cold microbursts. They can also be classified according to their appearance, movement, etc.

The parent clouds which induce microbursts are not always thunderstorms. Quite often, isolated rainshowers spawn relatively strong microbursts which endanger aircraft operations at low altitude. Presented in this chapter is a proposed classification of parent clouds known to the author as of January 1985.

5.1 Classification of Microbursts

Wet and Dry Microbursts

Prior to the NIMROD and JAWS experiments, the author assumed that most microbursts occur in heavy rain. This presumption turned out to be incorrect. As shown in Table 1.1, 36% of the NIMROD microbursts and 83% of the JAWS microbursts were not accompanied by rain on the ground. These statistics show evidence that the raindrops in microbursts in dry regions often evaporate completely before reaching the ground. Once it gains sufficient downward momentum, a downflow without rain could reach the ground to induce a microburst.

In the wet region of the United States, such as Louisiana, Florida, etc., practically all microbursts are accompanied by heavy rain. Both Pan American 759 at New Orleans and Allegheny 121 at Philadelphia encountered blinding rain during their microburst penetrations.

In general, the high cloud base in the dry region provides the falling raindrops with sufficient time and distance for their dissipation before reaching the ground. Furthermore, the low relative humidity in the subcloud layers accelerates evaporation processes (Fig. 5.1).

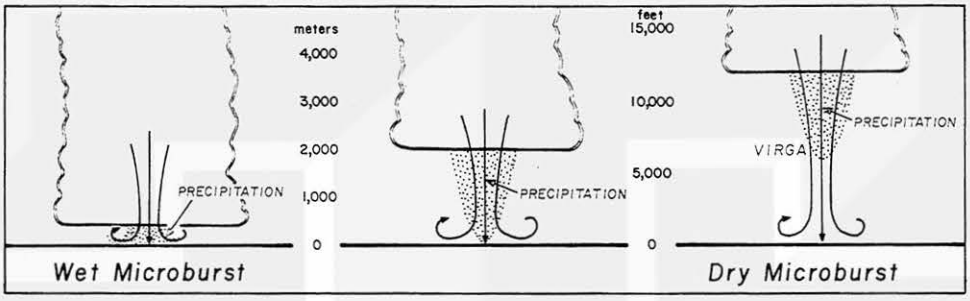

Fig. 5.1 Schematic views of wet and dry microbursts. Wet microbursts are expected to occur in the wet regions of the world, while dry microbursts are commonly seen in the dry regions with high bases of convective clouds.

Stationary and Traveling Microbursts

If a stationary microburst spreads inside an undisturbed environment, a perfect starburst outflow with an annular ring of high winds will be observed. In reality, however, the traveling motion of a microburst distorts the airflow from circular to elliptical shape. The front-side wind intensifies while the back-side wind weakens, resulting in a crescent-shaped area of high winds (Fig. 5.2).

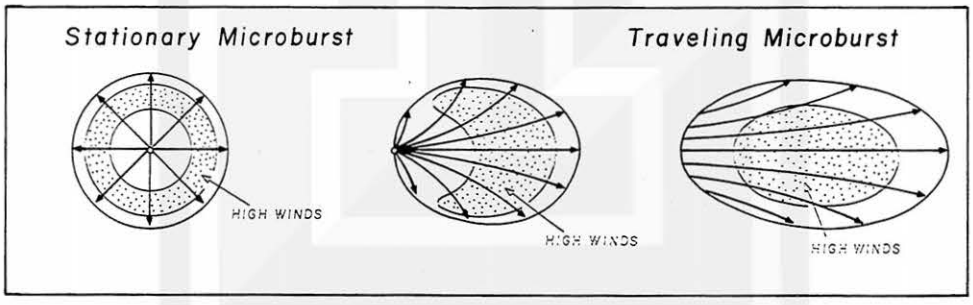

Fig. 5.2 The variation of airflow inside microbursts with different traveling speeds. A stationary microburst shows a starburst airflow with an annular ring of high winds.

A fast-moving microburst is characterized by the surface winds with straight or mostly parallel streamlines. These types of winds are often called "straight-line winds". An aerial survey and a detailed mapping of damage vectors will be able to identify the wind effects of a fast-traveling microburst.

Radial and Twisting Microbursts

Radial streamlines are seen if microburst winds are irrotational. However, when a microburst descends inside a strong mesoscale cyclone (mesocyclone), its airflow at the surface is characterized by a cyclonically curved (twisting) streamlines. This type of microburst has been confirmed during aerial surveys of tornadoes spawned by supercell thunderstorms (Fig. 5.3).

Frequently, damage maps of tornadoes reveal a widening of the paths prior to their ends. When the end of a tornado's path becomes 2 to 3 miles (3 to 5 km) wide, the flow pattern becomes very similar to that of a twisting microburst. At the present time, we have no data to determine if a tornado turns into a microburst before its dissipation.

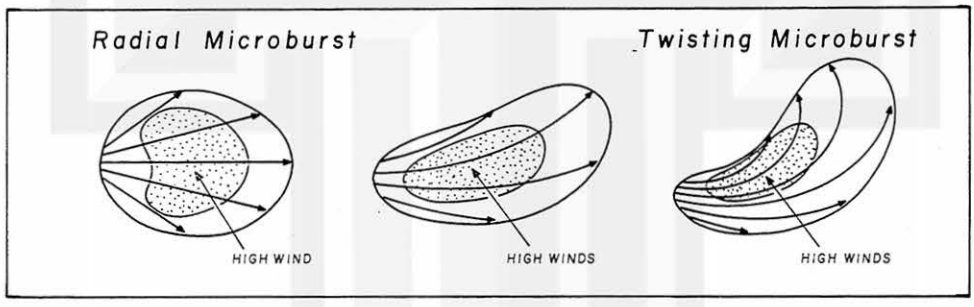

Fig. 5.3 A radial microburst characterized by the straight-line outflow and a twisting microburst with curved streamlines. Twisting microbursts often occur in mesocyclones.

Midair and Surface Microbursts

No microbursts form on or near the ground. Instead, they descend from the bases of convective clouds. A microburst with its characteristic winds located above anemometer heights is called a "midair microburst". A midair microburst may remain aloft until it dissipates, or it may keep descending to the ground.

A microburst after its touchdown is called a "surface microburst". When a surface microburst spreads out onto a large area, the downflow keeps supplying the mass until it sinks to the ground. After that, a microburst flattens and its expansion terminates.

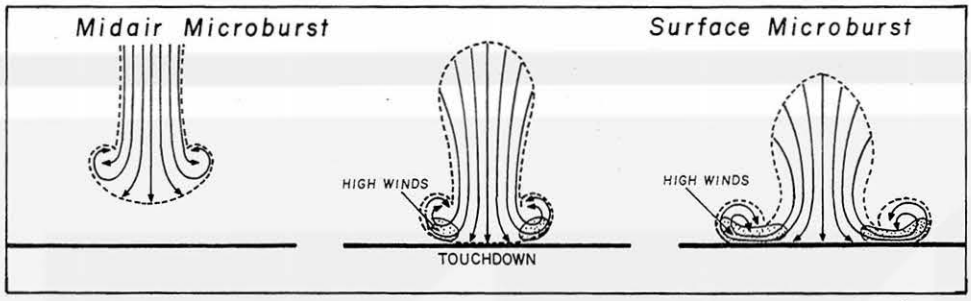

Fig. 5.4 Three stages of a descending microburst. A mid-air microburst may or may not descend to the surface. If it does, the outburst winds develop immediately after its touchdown.

Outflow and Rotor Microbursts

A microburst accompanied by a strong downflow and outflow is called an "outflow microburst". This is a common type of microbursts documented during the NIMROD and JAWS field experiments. Observational evidence shows that a slow-traveling outflow microburst is often, but not always, encircled by a vortex ring (Fig. 5.5).

The ring vortex keeps stretching as a surface microburst gets older, until reaching a stretching limit. Thereafter, the vortex is cut into several pieces of roll vortices, each with a horizontal axis. Some of these vortex rolls run away from their source region, inducing bands of high winds, lasting two to three minutes.

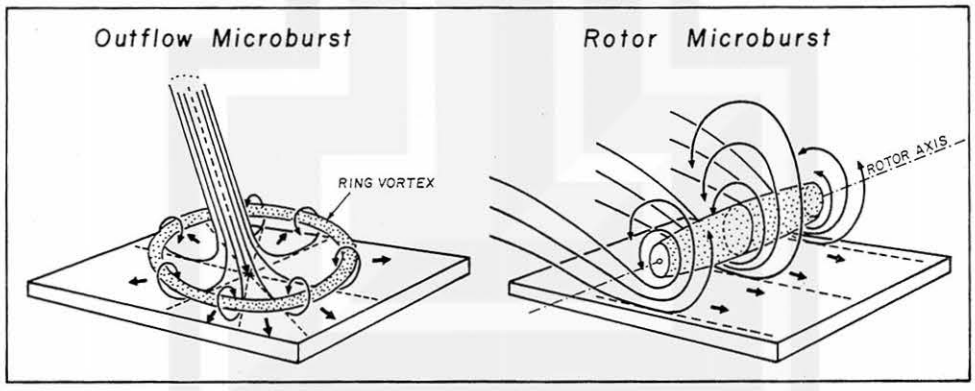

Fig. 5.5 Outflow microbursts are the most commonly observed type of microbursts. Some rotor microbursts develop inside macrobursts behind their gust fronts.

A "rotor microburst" is a runaway vortex roll which leaves behind a band of wind damage. This microburst behaves like a steam roller, or a tornado with a horizontal vortex axis, damaging structures and uprooting trees inside a narrow swath. Because of a narrow damage path which occurs with a roaring sound of a rotor microburst, it has been identified as a tornado by mistake. In 1981, Fujita and Wakimoto called a rotor microburst swath a "burst swath" (Fig. 5.6).

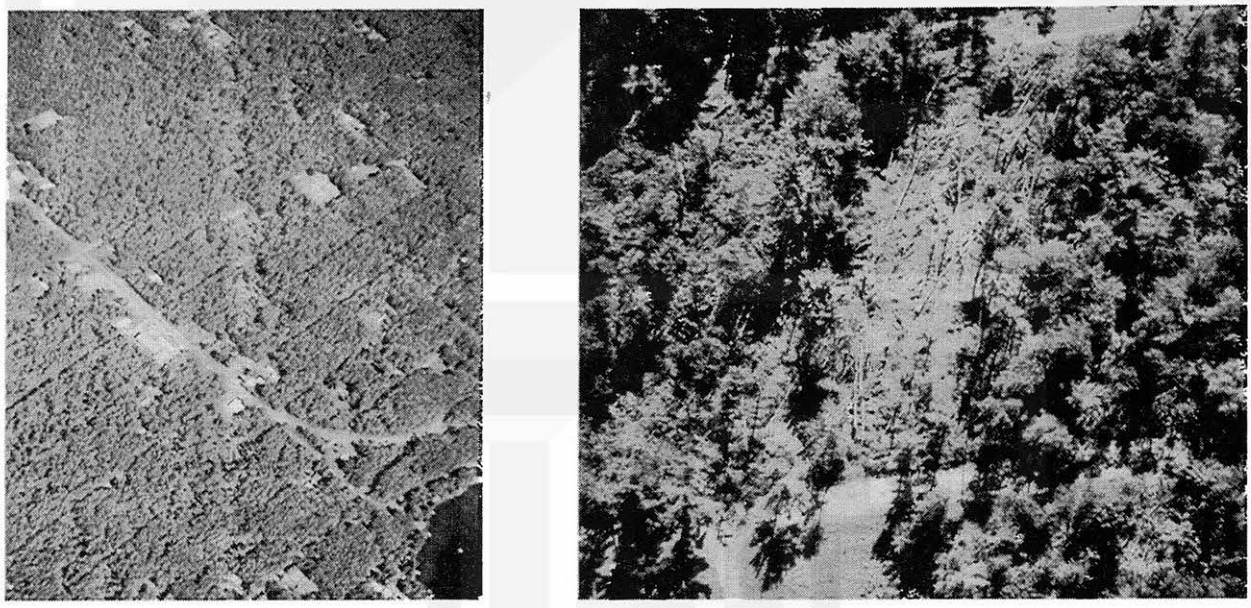

Fig. 5.6 Aerial photos of a burst swath caused by a rotor microburst at Northwood Beach, Wisconsin on 4 July 1977. Aerial photo by Fujita

Microbursts with Misocyclones

Outburst winds of outflow microbursts are mostly irrotational. This means that the streamlines of outburst winds spread out radially without rotating around the center of the outflow. However, the wind field aloft measured by the JAWS Doppler radars showed definite signs of rotation at the height of the downflow. The direction of rotation appears to be 90% cyclonic, while the other 10% rotates anticyclonically.

The misoscale cyclone in which the downflow of a microburst is embedded is called a "misocyclone" (read as my-so-cyclone). Flight level winds measured by the University of Wyoming King Air aircraft during JAWS also confirmed the existence of misocyclones around downflow regions. It is very likely that a misocyclone aloft acts as a collector of hydrometeors which funnel into a concentrated downflow (Fig. 5.7).

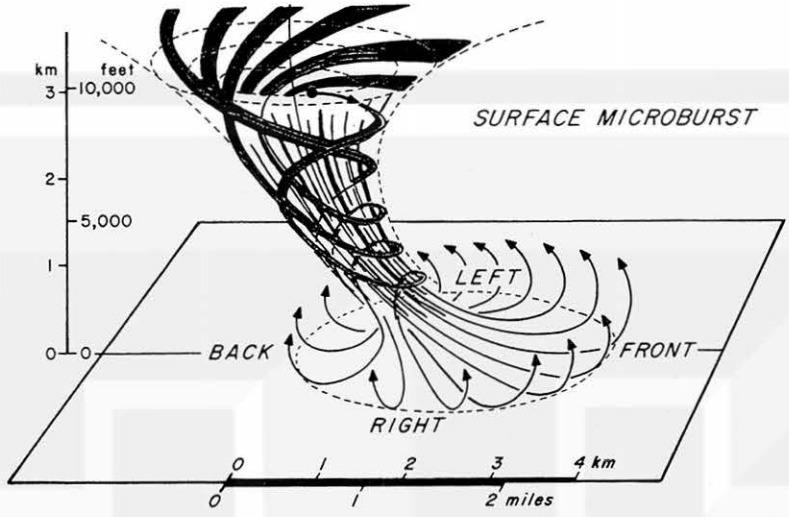

Fig. 5.7 A schematic view of a surface microburst accompanied by a misocyclone aloft. Most misocyclones, less than 4 km in diameter, rotate cyclonically while exceptional ones rotate anticyclonically.

5.2 Classification of Parent Clouds

Type "A", Anvil Cloud and Type "S", Supercell

During the JAWS experiment, we observed the formation of microbursts beneath the virga descending from anvil clouds in their post-mature stages. However, it is very unlikely that anvil clouds in wet areas induce microbursts on the ground.

Supercell thunderstorms are likely to produce strong tornadoes. Post-storm aerial surveys often reveal the existence of microburst winds in the vicinity of tornadoes, suggesting strongly that these two types of storms are somehow related. However, their dynamical relationship has not is not known.

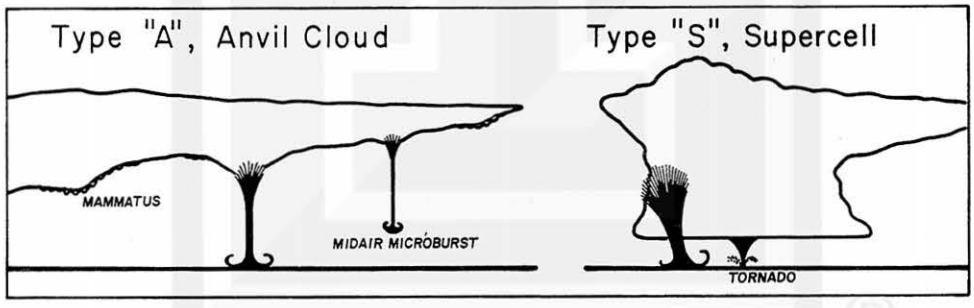

Fig. 5.8 Schematic diagrams showing the formation of microbursts beneath an anvil cloud in dry areas. Supercell thunderstorms are inducers of tornadoes and microbursts.

Type "B", Bow Echo

A bow echo is an inducer of strong macrobursts and microbursts. Usually, high winds push out from the position of an arrow attached to a bow. During the mature stage of a bow echo, both tornadoes and microbursts could occur simultaneously. During the dissipation stage of outburst winds, hydrometeors are blown outward very rapidly, drying out the echoes in the source region.

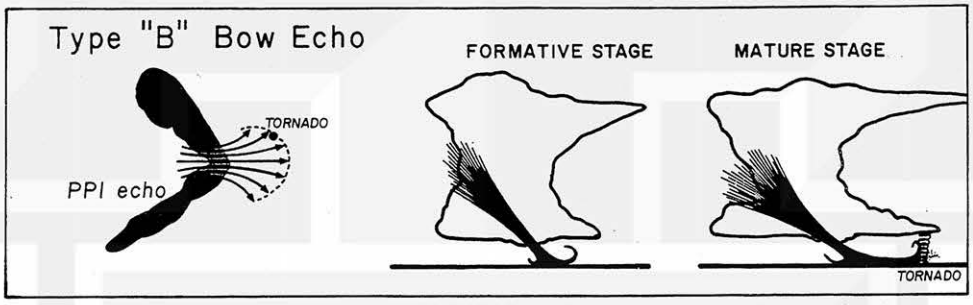

Fig. 5.9 Schematic diagram showing the shape of the bow echo and microbursts in formative and mature stages.

Type "I", Isolated Shower

Isolated showers, with or without thunder, induce microbursts. In fact, the parent clouds of the Eastern 66 and the Pan American 759 microbursts were isolated showers which were relatively small and short-lived. The main problem in issuing a timely warning is that not all isolated showers spawn microbursts. Furthermore, the intensity of radar echoes and the windspeeds of the induced microbursts are practically unrelated. This means that a pilot cannot make a decision, either to land or to go-around, on the basis of airborne radar which depicts rain, but not wind.

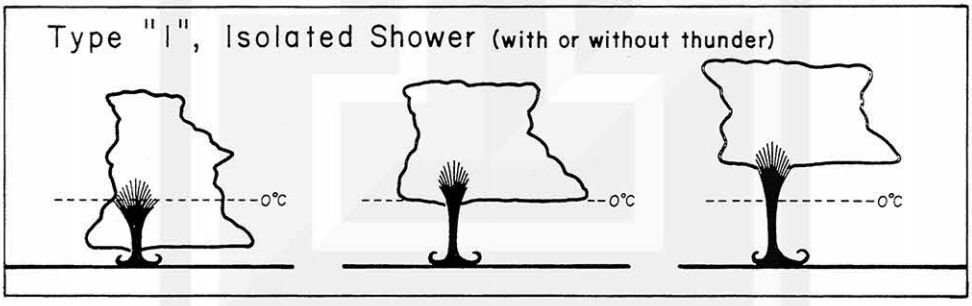

Fig. 5.10 Freezing levels of Type "I" showers, which vary from location to location and from season to season. A cloud base with 0°C or colder temperature is called "cold cloud base" and others are called "warm cloud base".

Type "C", Cumulus Cloud

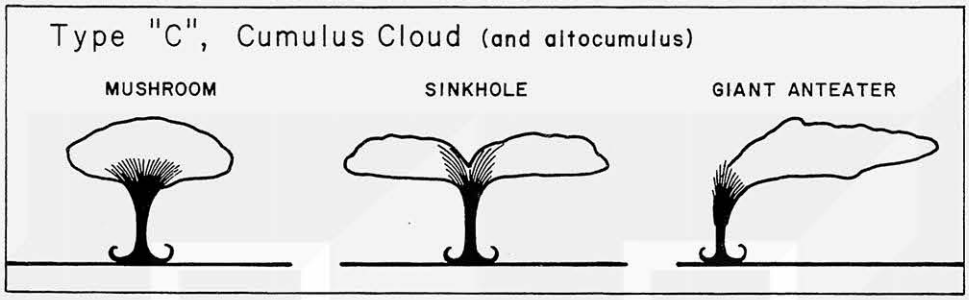

Fig. 5.11 Three subclassifications of Type "C" parent clouds. They are the mushroom cloud, sinkhole cloud, and giant anteater cloud. More clouds are expected to be added in future years.

Type "C" parent clouds are large cumulus clouds, sometimes having an appearance of altocumulus castellanus, which produce rain or snow that may or may not reach the surface. Based on the observational evidence obtained in JAWS, these clouds are subdivided into mushroom, sinkhole, and giant anteater clouds.

The "mushroom cloud" (Example: Rit Carbone Microburst on 7/14/82, page 97) is an isolated large cumulus with a microburst descending from its center. Because the echo top is much higher than the inflow height, the mound-shaped top is not affected by the downflow, maintaining the shape of a mushroom during a microburst.

The "sinkhole cloud" (Example: Flat tire microburst on 5/19/82, page 85) is a cumulus cloud with a small vertical growth. The entire cloud is embedded inside the inflow layer of an induced microburst. A sinkhole develops atop the cloud directly above the microburst downflow in mature and post-mature stages.

The "giant anteater cloud" (Example: Giant anteater microburst on 7/16/82) is a cumulus or altocumulus cloud with a glaciated top. When a downflow forms on the upwind side of the cloud, the cloud base lowers, turning into the shape of the head of a giant anteater. A microburst descends from the head section which keeps lowering until reaching the ground. When a surface microburst forms, the entire head section descends to the ground, turning into a headless giant anteater. This type of cloud can be detected only by an RHI scan, and not by a series of PPI scans.

Chapter Six

Specific Case Studies

Unlike the tornado statistics available since 1916, little is known about the frequencies of downbursts in the United States. According to the "Outstanding Storms of the Month" in NOAA's STORM DATA, however, downbursts have been reported from just about everywhere. Some examples of damaging downbursts since 1981 are: two box cars overturned in Indio, CA (8/12/81); warehouse damaged near Macon, GA (3/21/82); cars flipped over in downtown Springfield, IL (5/20/82); intense microbursts in Sioux Falls, SD (7/6/82); $2 million damage at JEFFCO Airport, CO (8/20/82); 155 homes damaged and 11 injured at Baton Rouge, LA (1/31/83); 113 mph wind recorded at Jacksonville, FL (2/2/83); 6 killed near Houston, TX (5/20/83); numerous downbursts in Wisconsin (7/3/83); school damaged in Broken Arrow, OK (10/3/83); three downbursts during the Carolina tornadoes (3/28/84); five acres of pines blown down at Southborough, MA (3/29/84); two deaths at Rowena, SD (6/11/84). Refer to STORM DATA for details.

Frequencies in Table 6.1 were computed from the average probabilities of the NIMROD and JAWS statistics in Fig. 4.18. We assume that a PAM station will detect microbursts within a 2-km radius, and that their occurrences are uniformly distributed over the contiguous United States throughout the year. This table reveals that the number of damage-causing (75 mph or stronger) microbursts in the United States is expected to be 3,510 per year, just about four times more frequent than tornadoes.

Specific case studies presented in this chapter are three from NIMROD and six from JAWS. In addition, a 149 mph microburst at Andrews AFB and one over-water accident case are discussed. Finally, a case study from the latest FAA Network at Memphis, Tennessee Airport is presented.

Table 6.1 Frequencies (per year) of microbursts expected to occur within the contiguous United States.

Windspeed	(mph)	50	75	100	125	150	175
	(m/s)	22	33	45	56	67	78
Probability	(yr^{-1})	3.4×10^{4}	3.5×10^{3}	3.7×10^{2}	3.5×10^{1}	3.6×10^{0}	3.8×10^{-1}
Frequency	(yr^{-1})	34,000	3,510	367	38	3.9	0.4

6.1 Yorkville Microburst on 29 May 1978

It was 2133 CDT on a dark night when a flash of lightning lit up a small shower cloud to the southeast of the CP-3 Doppler radar at Yorkville, Illinois. Immediately thereafter, a scan sector was established for a microburst. The first volume scan which started at 2136:04 revealed the existence of an outburst airflow with a 31 m/sec (69 mph) approaching velocity at 0.5° or 70 m (230 ft) AGL. The Doppler velocity decreased rapidly as the elevation angle increased, obtaining 26 m/sec (58 mph) at 1.5°, 24 m/sec (54 mph) at 2.5°, etc. Fig. 6.1 shows the PPI imagery depicting the microburst winds' folded orange and yellow colors.

RHI cross sections along the 208° CP-3 azimuth in Fig. 6.2 present reflectivity (left) and velocity (right) fields. The maximum front-side

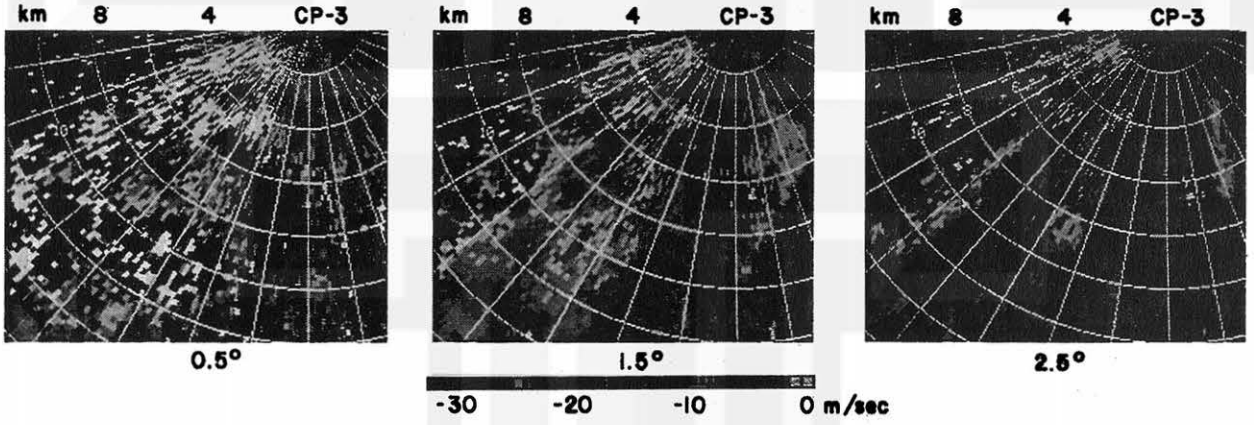

Fig. 6.1 RDSS imagery showing the velocity fields of the Yorkville microburst at three elevation-angle scans beginning at 2136:04 CDT. Due to velocity folding, the color bar for the -17 m/sec (38 mph) or stronger winds turns into warm colors.

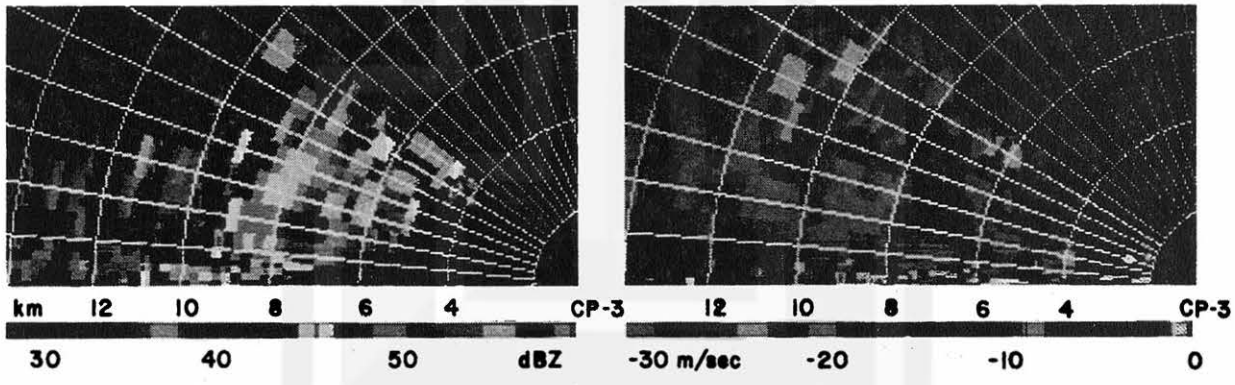

Fig. 6.2 Computer-generated RHI cross sections of the Yorkville microburst and its parent cloud, moving left to right in the figure. The shallow outburst winds beneath the parent echo are made visible by folded colors. RDSS photos by Brian Smith.

wind, 8.5 km (5.3 miles) from the radar, is located beneath a 56 dBZ core at 2.6 km (8,500 ft) AGL. The 35 dBZ echo top was only 6 km (19,500 ft) and the echo diameter was 5 km (3 miles). It was a small shower which was not recognized until after seeing the first lightning.

Vertical cross sections of horizontal and vertical windspeeds in Fig. 6.3 show that the maximum windspeed is located less than 100 m (330 ft) above the ground. Another cross section made six minutes later depicts the maximum windspeed at about 30 m (100 ft) above the ground (Fig. 6.4).

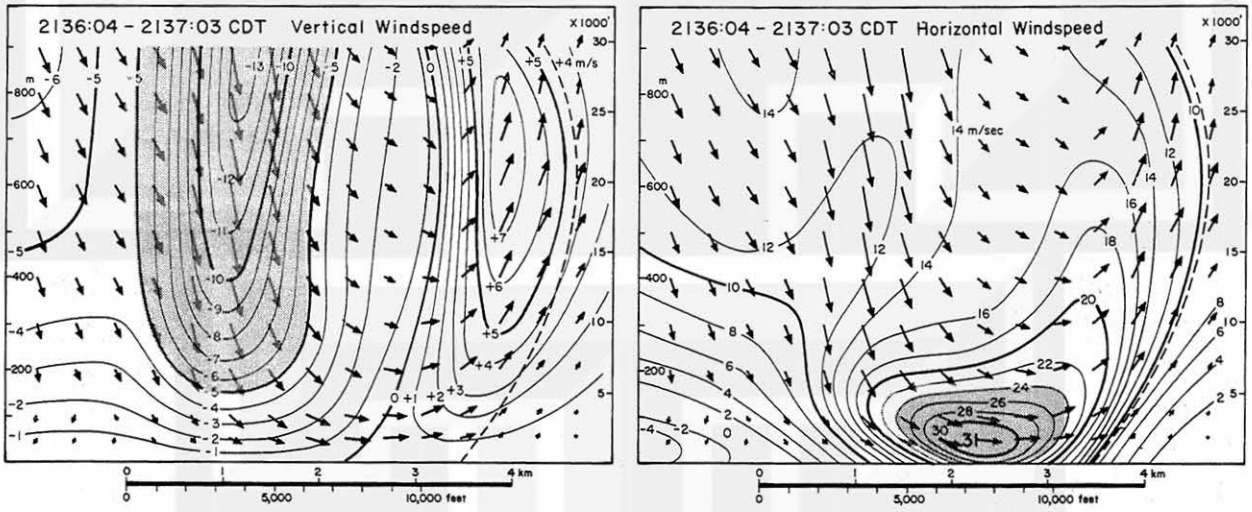

Fig. 6.3 Vertical cross section of the microburst at 2136 CDT when its maximum wind was detected 8 km (5 miles) south-southwest of CP-3.

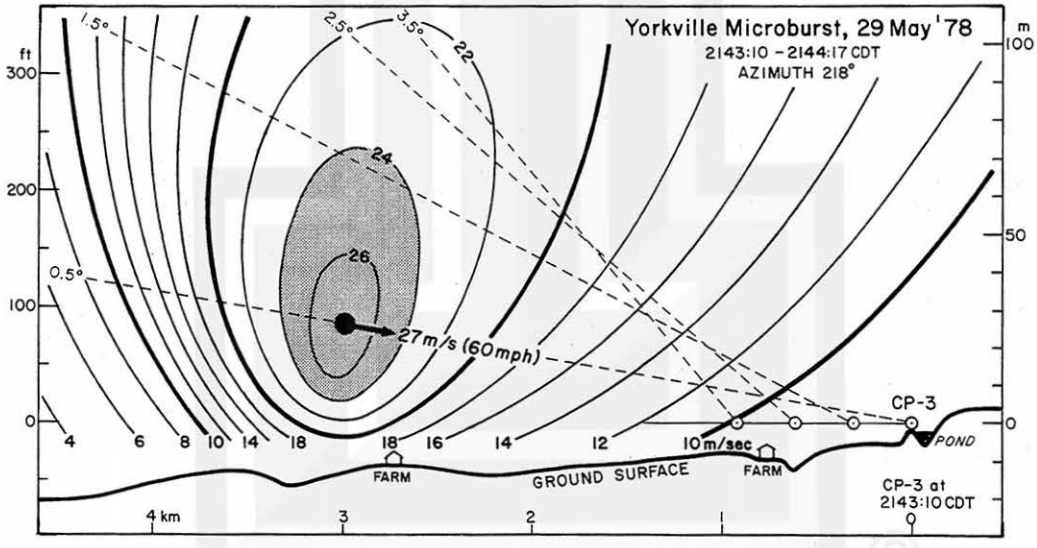

Fig. 6.4 Vertical cross section of the microburst at 2143 CDT when the maximum wind was approaching 3 km (2 miles) southwest of CP-3 at Yorkville.

During the NIMROD experiment, rawinsonde ascents were made at Yorkville every one to three hours and tracked by two GMD-Is. Most balloons were tracked during their ascent as well as their descent after bursting at about 20 km (65,000 ft) MSL.

Soundings on 29 May 1978 were made mostly at one-hour intervals. Despite careful analysis of the serial ascents, no detectable variation of meteorological parameters related to the microburst-producing shower was found. The tropopause, located at 12 km (39,000 ft), showed practically no variations except that the old tropopause was replaced by a new one about one hour before the microburst. Tropospheric temperature, with shallow inversion layers embedded, did not change much. It is likely that a small microburst-inducing shower, such as this one, cannot be predicted by a serial ascent at one location at one hour intervals (Fig. 6.5).

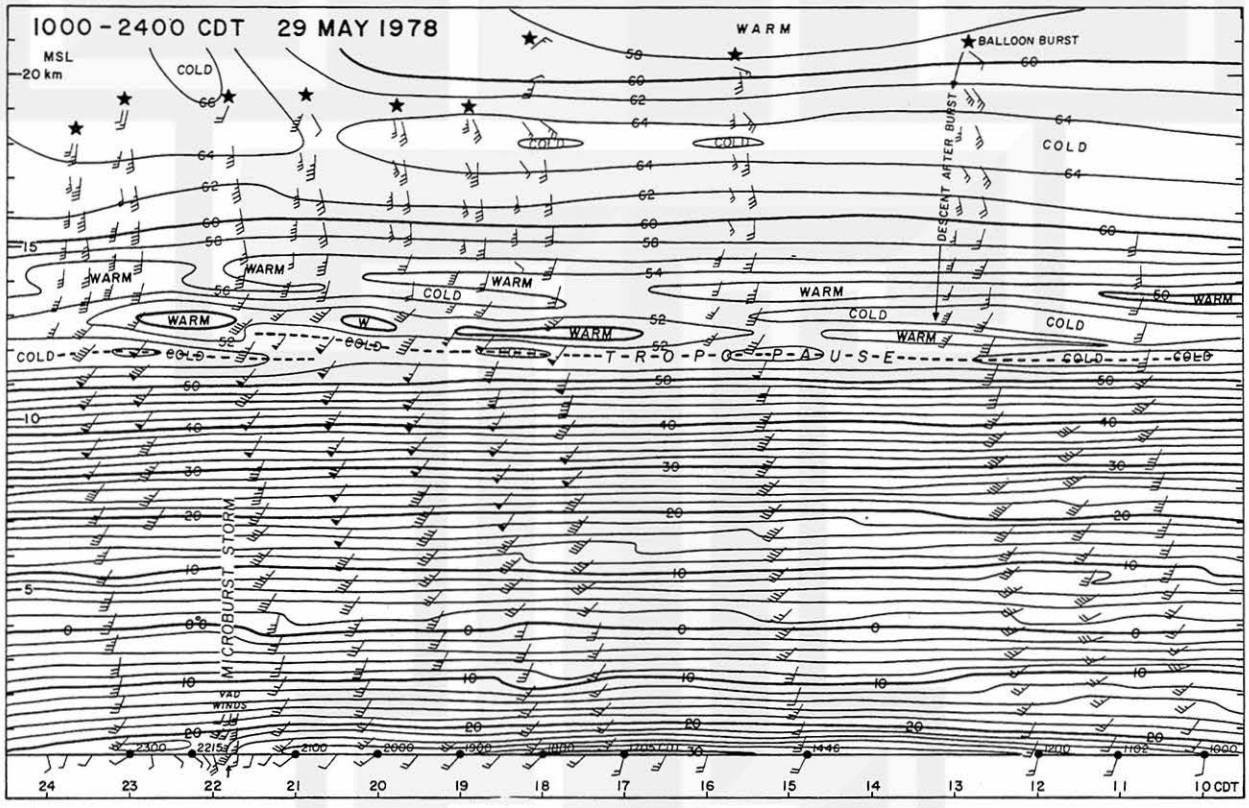

Fig. 6.5 The temperature and winds aloft on the day of the Yorkville microburst. 11 balloons were released.

6.2 O'Hare Microburst on 7 June 1978

This microburst induced a 19.2 m/sec (43 mph) peak wind measured by PAM 7 located 17 km (11 miles) to the west-northwest of O'Hare Airport where the CP-4 Doppler radar was located during the NIMROD experiment.

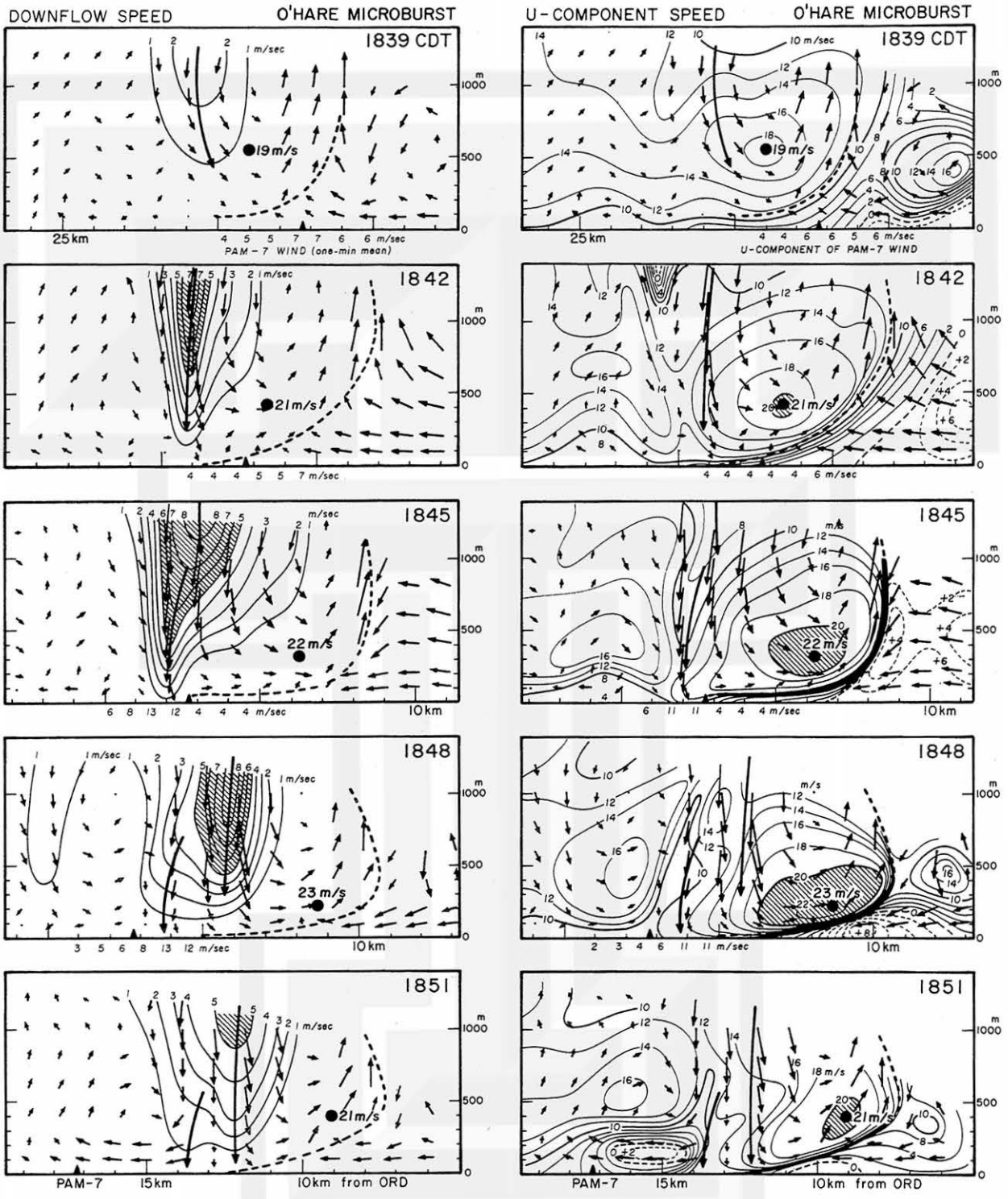

***Fig. 6.6** Vertical cross sections of the O'Hare microburst in the RHI plane of the CP-4 Doppler radar at O'Hare Airport. Isotachs of vertical (left) and horizontal (right) windspeeds are contoured for every 1 m/sec and 2 m/sec, respectively.*

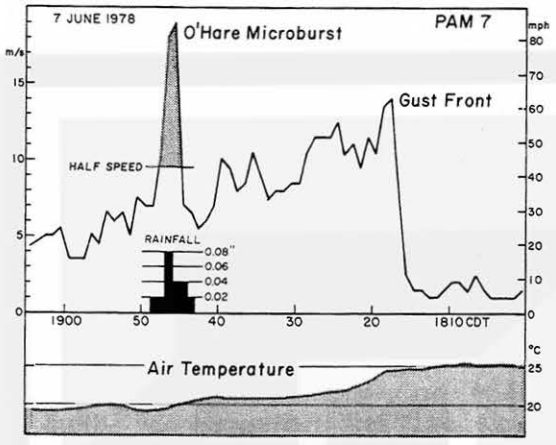

Fig. 6.7 Maximum windspeed, rainfall, and temperature measured by PAM 7 between 1800 and 1905 CDT on 7 June 1978. A gust front with a 14 m/sec (31 mph) peak wind passed over the station at 1819 CDT. Thereafter, the temperature dropped from 25 to 20 °C. It was a wet microburst accompanied by a total rainfall of 0.22" (5.6 mm) which fell in a six-minute period. The maximum rainfall rate was 4.8 in/hr (120 mm/hr).

Fig. 6.7 shows a series of RHI cross sections on the 284° azimuth of CP-4, which is the direction of PAM 7. These cross sections were constructed from PPI scans at 0.5°, 1.5°, 2.5°, etc. elevation angles.

A weak downflow at 1839 CDT intensified in the next three minutes, inducing a 21 m/sec (41 kts) outflow at 400 m (1,300 ft) above the PAM station. The 284° component (U-component) of PAM 7 wind was only 4 m/sec (8 kts), indicating that a midair microburst was passing over the station. AT 1845, the tip of the downflow hit the ground, producing a 13 m/sec (25 kts) U-component wind while a 22 m/sec (43kts) wind stayed aloft. The strongest outflow of 23 m/sec (45 kts) was pushing toward O'Hare Airport at 1848, while the near-ground wind was +8 m/sec (16 kts) blowing in the opposite direction. The shear of the horizontal wind along the vertical (vertical wind shear) was 15.1 m/sec/100 m (9 kts/100 ft). This shear was so large that an aircraft landing through it could have encountered serious difficulties.

The O'Hare microburst winds superimposed upon the gust front winds in Fig. 6.7 indicate the difference between these two types of wind systems. First of all, we should understand the nature of these winds, and then realize that a ground-based anemometer does not always detect a serious wind shear just above the ground. A very strong shear was 100 m (300 ft) above the ground in this case, but no aircraft was involved.

6.3 Bow-echo Microburst on 25 June 1978

It has been known that a line echo with a wave pattern is an inducer of high winds on or near the ground. Further examination indicated that a bow-shaped section of the wave pattern is where the high winds push out of the echo. In 1978, the author called this type of echo the "bow echo".

On 25 June 1978, the elevation-angle drive motor of the CP-3 Doppler radar failed. Taking advantage of the azimuth-angle motor which was functioning, a continuous PPI scan at 3.0° elevation angle was performed. Fortunately, the handicapped scan recorded a spectacular development of a bow echo which induced downburst winds and two tornadoes (Figs. 6.8 and 6.9).

First, a line echo at 1249:08 CDT induced a pocket of receding (+) winds when the echo began bulging out toward the southeast. At 1301:56, a weak echo "trench" appeared along the center axis of the pushing winds. At 1310 CDT, a tornado formed at the leading edge of the high winds followed by a 31 m/sec (69 mph) flow from the northwest.

Fig. 6.10 presents isotachs of Doppler velocities measured by CP-3 at 3.0° elevation angle. A four-minute-old tornado is located on the leading edge. A gate-by-gate examination of Doppler velocities revealed that the CP-3 computer was not able to assign velocities to gates that are located where the velocity gradient were extremely large. The gate without a velocity assignment due to a wide-spread Doppler spectra was identified as the "black hole" and is plotted by a black circle.

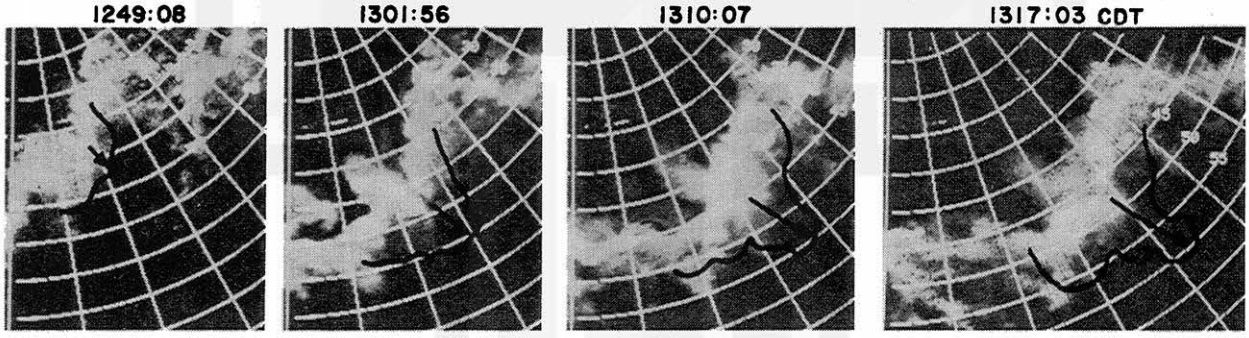

Fig. 6.8 Formation and development of a bow echo in the southeastern sector of CP-3 Doppler radar. Range markers are 5 km and azimuths are 10° intervals. Note a weak echo "trench" at 1301:56 CDT.

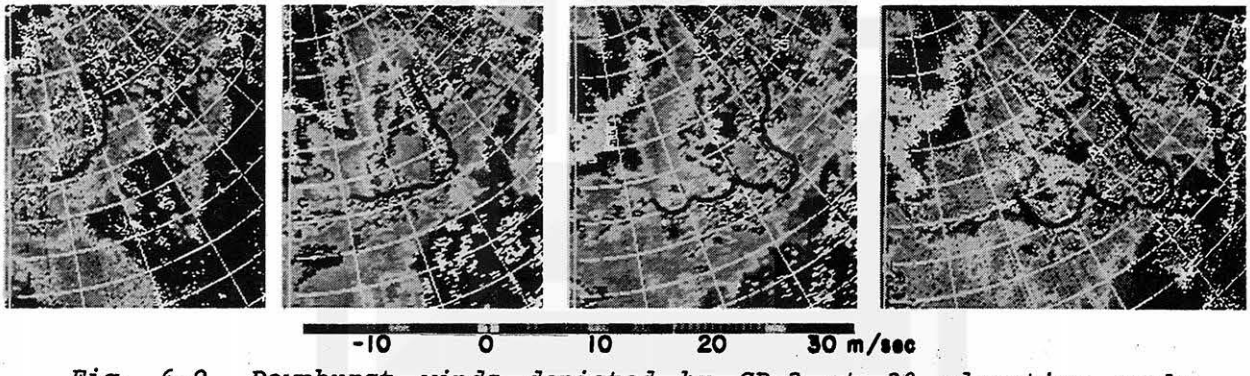

Fig. 6.9 Downburst winds depicted by CP-3 at 3° elevation angle. Receding velocities are color coded as shown by a color bar with folded velocities above 17 m/sec (38 mph). The maximum velocity increased from 20 m/sec (45 mph) to 32 m/sec (72 mph) in 28 minutes.

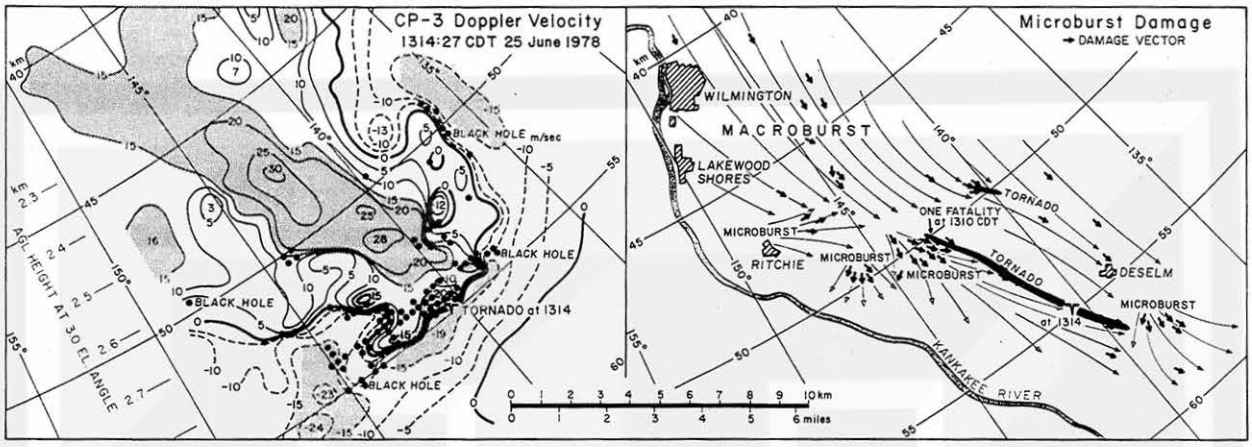

Fig. 6.10 CP-3 Doppler velocity (left) and microburst damage (right) surveyed after the storm. Four microbursts and two tornadoes were embedded inside an overall macroburst. Aerial survey by Greg Forbes

6.4 Flat Tire Microburst on 19 May 1982

Shortly before reaching CP-3, the author had a flat tire. While changing the tire, a number of tumbling weeds began crossing the road. A dry microburst was passing directly over the car, moving toward the radar. As soon as he reached the radar, the author took cloud pictures (Fig. 6.11) while standing by the radar as it obtained RHI cross sections (Fig. 6.12) of the parent cloud which was a sinkhole cloud. Meanwhile, PAM 3 at the CP-3 site recorded the pressure and winds through the center of the microburst (Fig. 6.13).

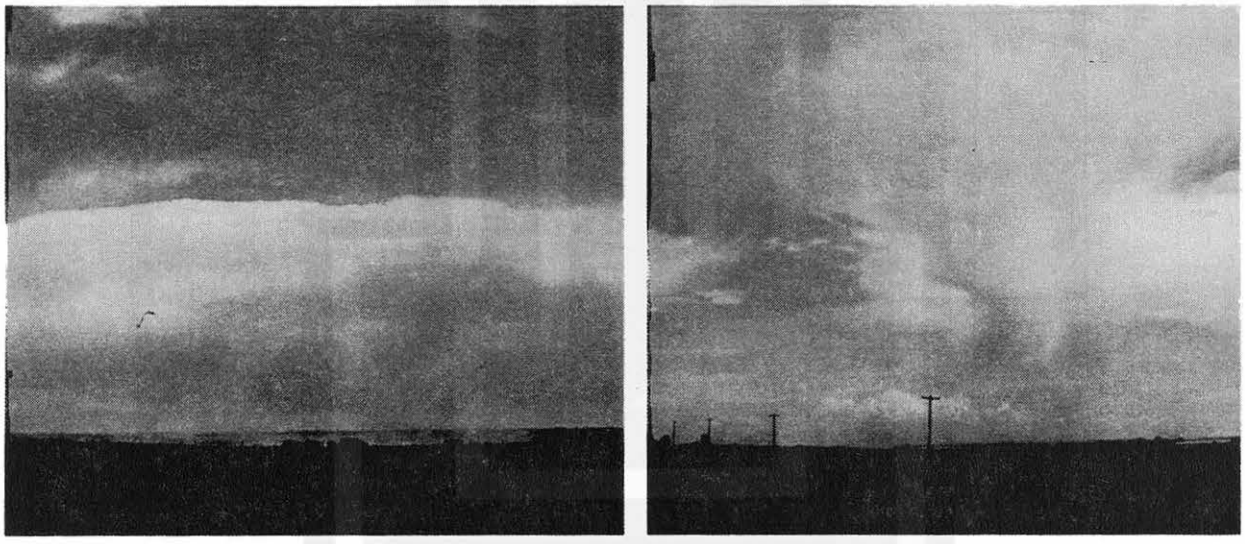

Fig. 6.11 The downflow section of the flat tire microburst at the 20° azimuth, characterized by low-hanging virga (right) with dust clouds and dust devils generated along the microburst front (left). Photos by Fujita at 1320 MDT

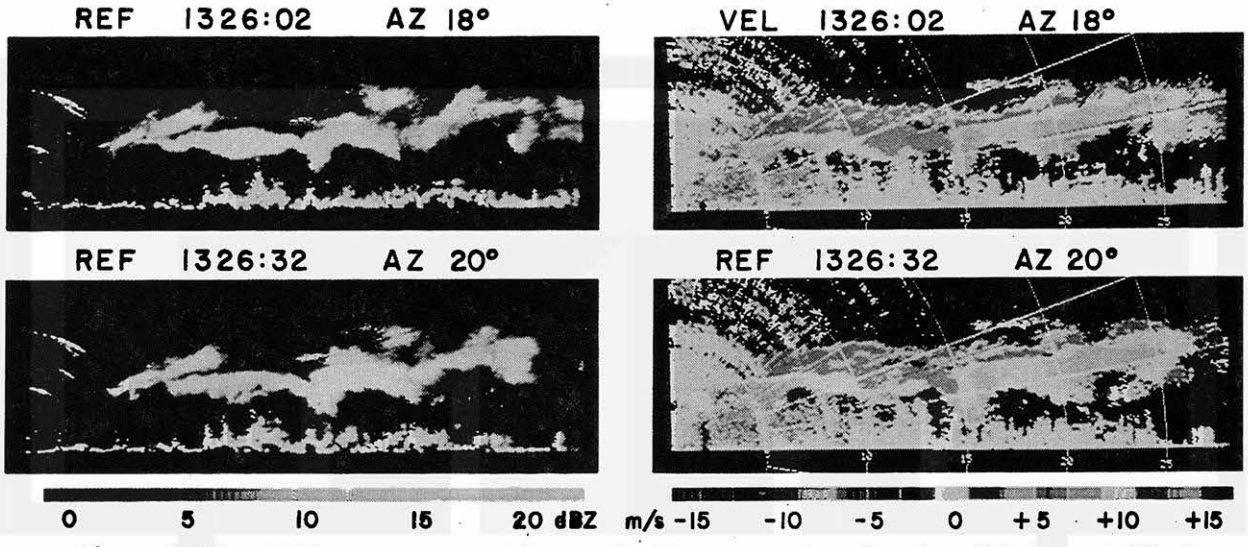

Fig. 6.12 RHI cross section of the parent cloud with a sinkhole located 15 km (10 miles) to the north-northeast of CP-3. Reflectivity (left) and velocity (right) imagery are shown.

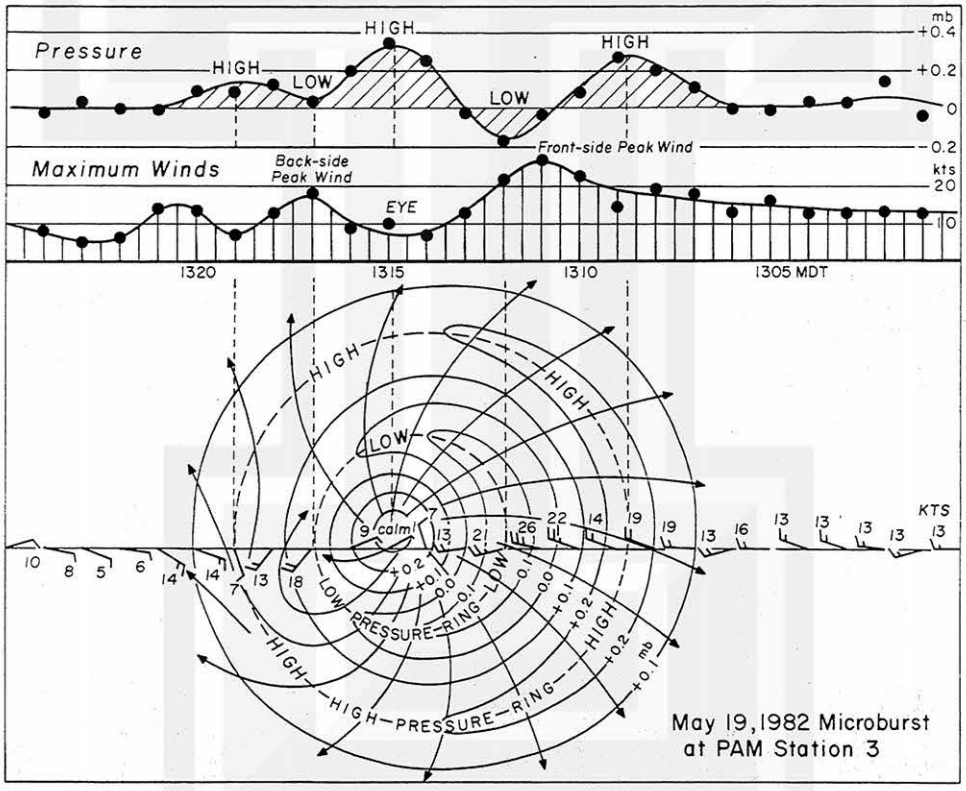

Fig. 6.13 Change in pressure and winds across the center of the flat tire microburst. This microburst may not have been noticed had the author's car not gotten a flat tire at the right place and at the right time.

6.5 Rotor Microburst on 30 June 1982

This microburst, with its peak windspeed of 29.1 m/sec (65 mph), was characterized by a temperature increase and a pressure drop during the microburst winds (Fig. 6.14). The CP-2/CP-4 dual Doppler winds indicate that the microburst was embedded inside a macroburst. However, the maximum Doppler wind was 21 m/sec (47 mph) which was significantly less than the PAM 23 peak windspeed, because a low blocking hill in front of CP-2 prevented the radar from measuring the near-ground winds (Fig. 6.15). On the other hand, CP-3/CP-4 dual Doppler winds revealed the existence of 27 m/sec (60 mph) Doppler winds just to the south of PAM 23, suggesting that both radars did measure the near-ground winds (Fig. 6.16).

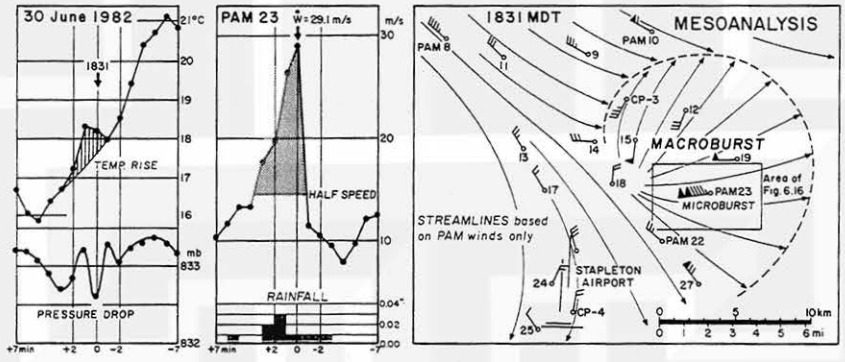

Fig. 6.14 Meteorological parameters of the PAM 23 microburst and a mesoanalysis (mesoscale analysis) of PAM winds showing a macroburst in which a microburst is embedded.

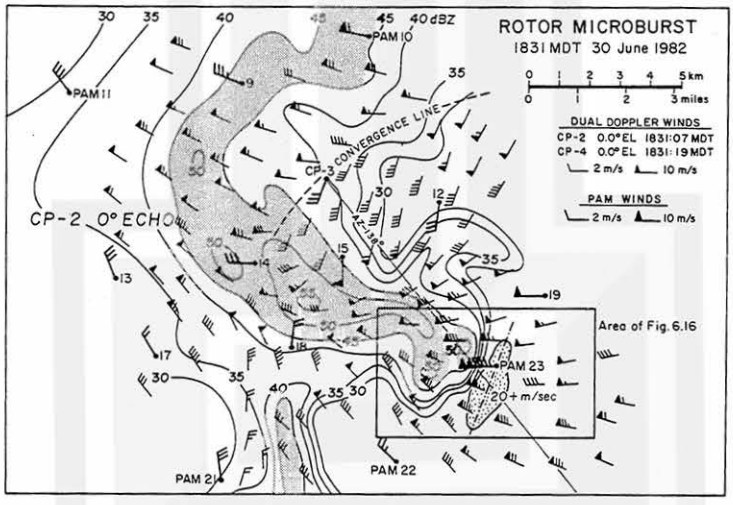

Fig. 6.15 Near-ground airflow of the macro- and microbursts as depicted by the CP-2/CP-4 dual Doppler winds. Due to a blocking hill, CP-2 at 0.0° elevation angle did not detect the near-ground winds over the microburst area. Analysis by Brian Waranauskas

A vertical cross section along the 138° azimuth of CP-3 shows the feature of the rotor microburst located just ahead of a 50+ dBZ echo. Precipitation particles from the echo region were blown forward by microburst winds, forming a precipitation roll, similar to the one found by Wakimoto in 1982 in his study of NIMROD gust fronts. It is seen that wind directions reverse, from positive to negative, at 800 m (2,600 ft) above the ground (Fig. 6.17).

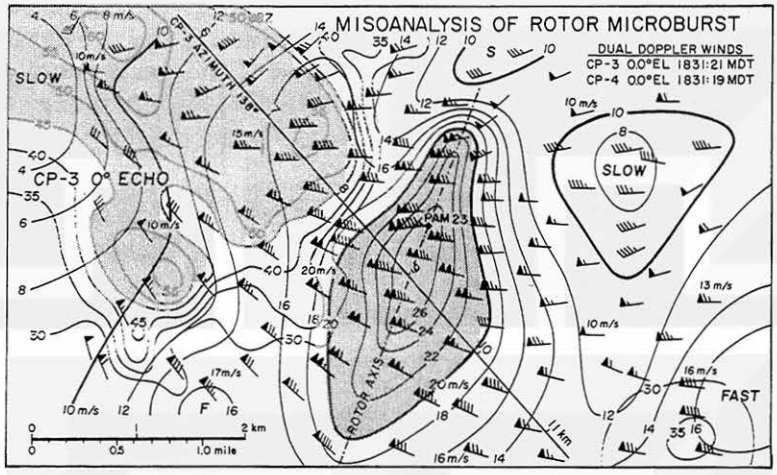

Fig. 6.16 A misoanalysis (misoscale analysis) of the PAM 23 microburst made possible by the CP-3/CP-4 dual Doppler data. Analysis with Brian Waranauskas

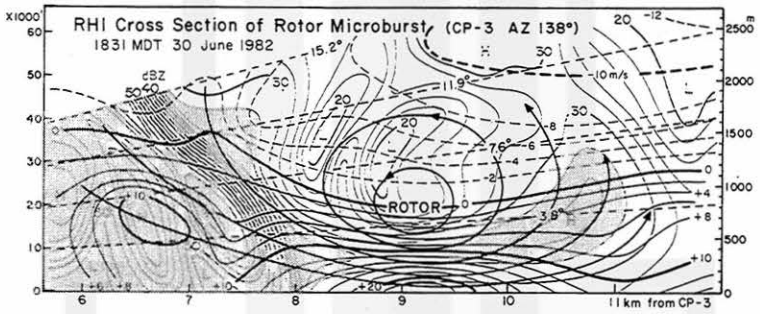

Fig. 6.17 A vertical cross section of the rotor microburst along the 138° azimuth of CP-3.

6.6 North Platte Valley Microburst on 8 July 1982

An outbreak of microbursts in the North Platte River Vally, Colorado provided us with very important evidence of a microburst family. As shown in a sequence of Doppler radar imagery in Fig. 6.18, four microbursts marched down the valley along a line extending from southwest to northeast and every one in the family was rotating cyclonically.

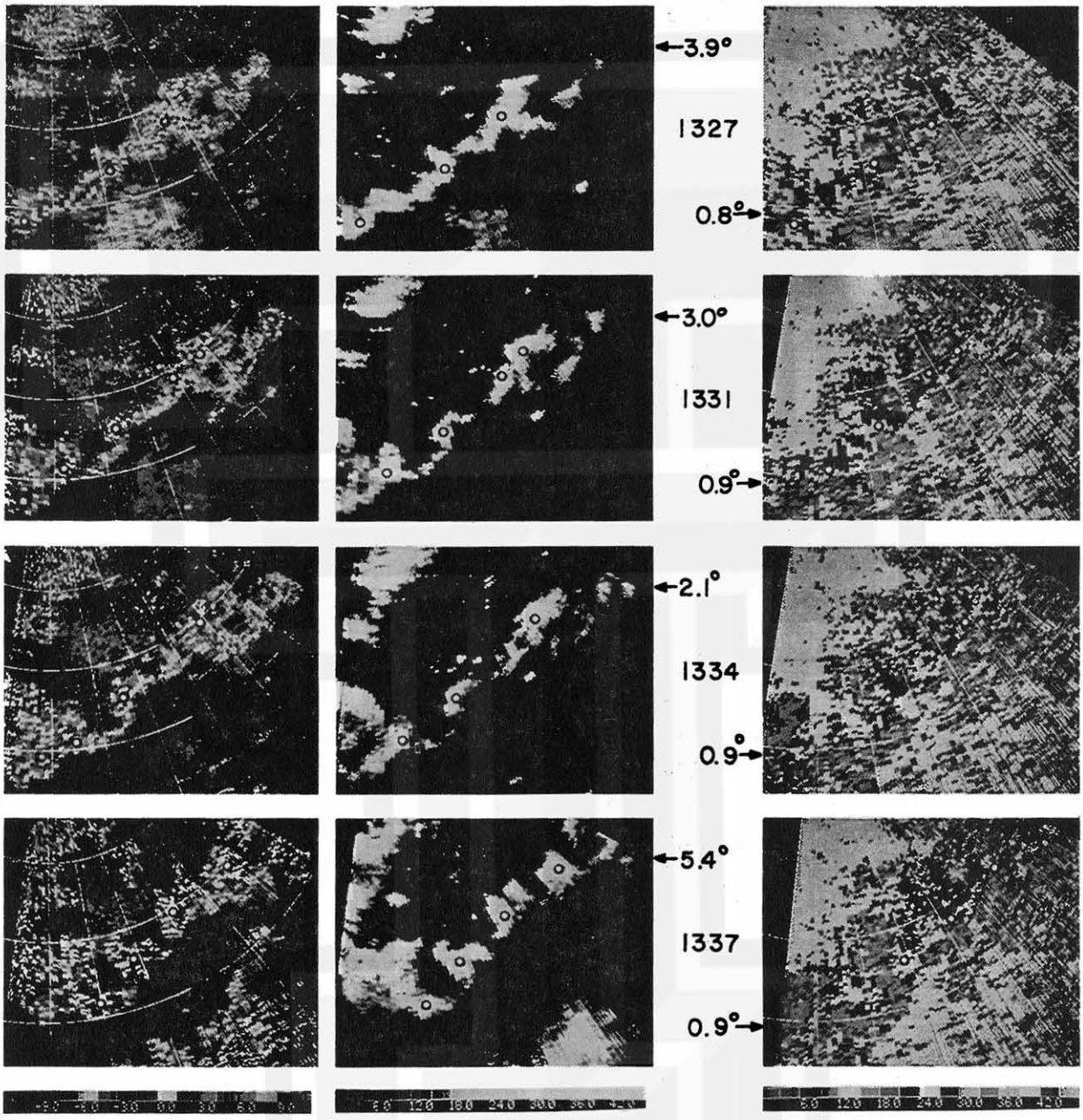

Fig. 6.18 Four microbursts in a sequence of CP-2 Doppler radar photos. Concentric circles in the imagery represent 10, 15, 20, and 25 km ranges. The color coded reflectivity fields (left) is reproduced in black and white imagery (center) in order to emphasize the rotational characteristics of microburst-inducing clouds. Velocity fields (right) are presented by the standard color scheme of NCAR's RDSS.

The microburst family in Fig. 6.18 consisted of four members as identified by Nos. 1, 2, 3, and 4. At 1326 MDT, the oldest microburst (No. 1) near the southwest corner of the picture was in its dissipating stage. Its approaching velocity (green to blue) decreased to near zero during the next ten minutes.

It should be noted that each of these microbursts went through very rapid growth and decay within less than ten minutes. The parent clouds in their formative stage were characterized by misoscale waves, somewhat like miniature polar-frontal waves. As the microbursts became older, these waves turned into misocyclones, 2 to 4 km (1.5 to 2.5 miles) in diameter.

The 1400 MDT sounding at Denver is characterized by a dry-adiabatic layer extending to 3.7 km (12,100 ft) AGL. The cloud layer, as inferred by the near-saturation dew-point temperature, is located 5.3 to 5.9 km (17,400 to 19,300 ft) MSL. The location of the microburst family relative to the high peaks of the Rockies suggests that a shear flow in the wake of the 14,264 ft Mt. Evans could extend to the North Platte River Valley. The orientation of the misoscale waves coincides with the winds aloft at the cloud height. Although the cloud base is located 3,100 ft (900 m) above the top of Mt. Evans, the inflow winds in the wake of the mountain could transport shear vorticity upward, contributing to the formation of a street of misocyclones.

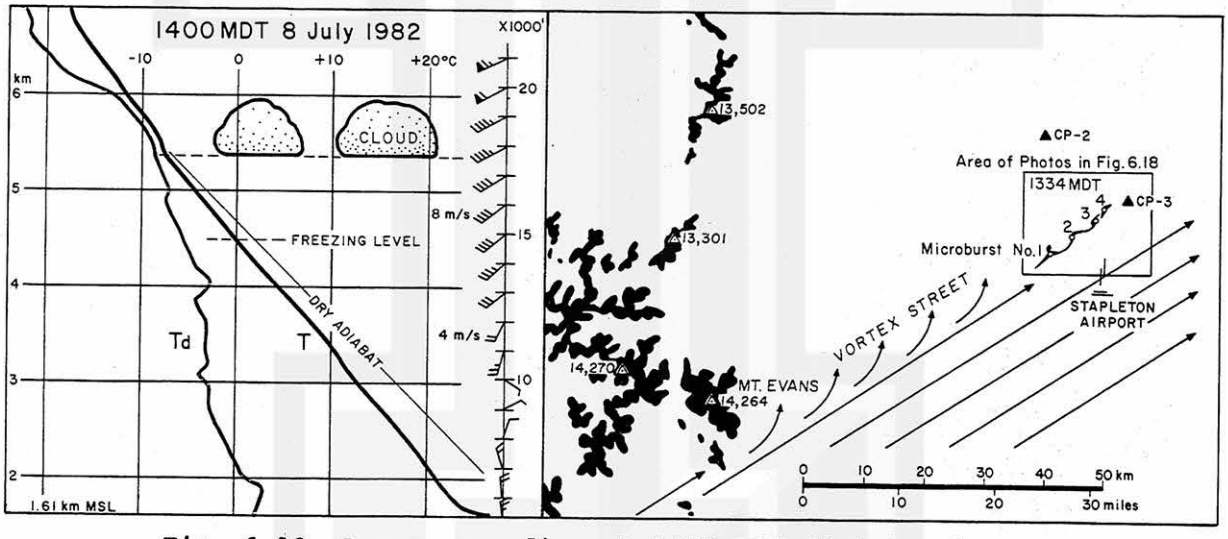

Fig. 6.19 Denver sounding at 1400 MDT (left) and an anticipated formation of a vortex street in the wake of Mt. Evans.

6.7 Bow echo Microburst on 14 July 1982

This microburst touched down 28 km (18 miles) west-southwest of CP-3 at 1643:15 MDT, reaching its peak intensity approximately five minutes later. The microburst winds came out of the tip of a bow echo. Fig. 6.20 presents both PPI and RHI sections of the bow echo.

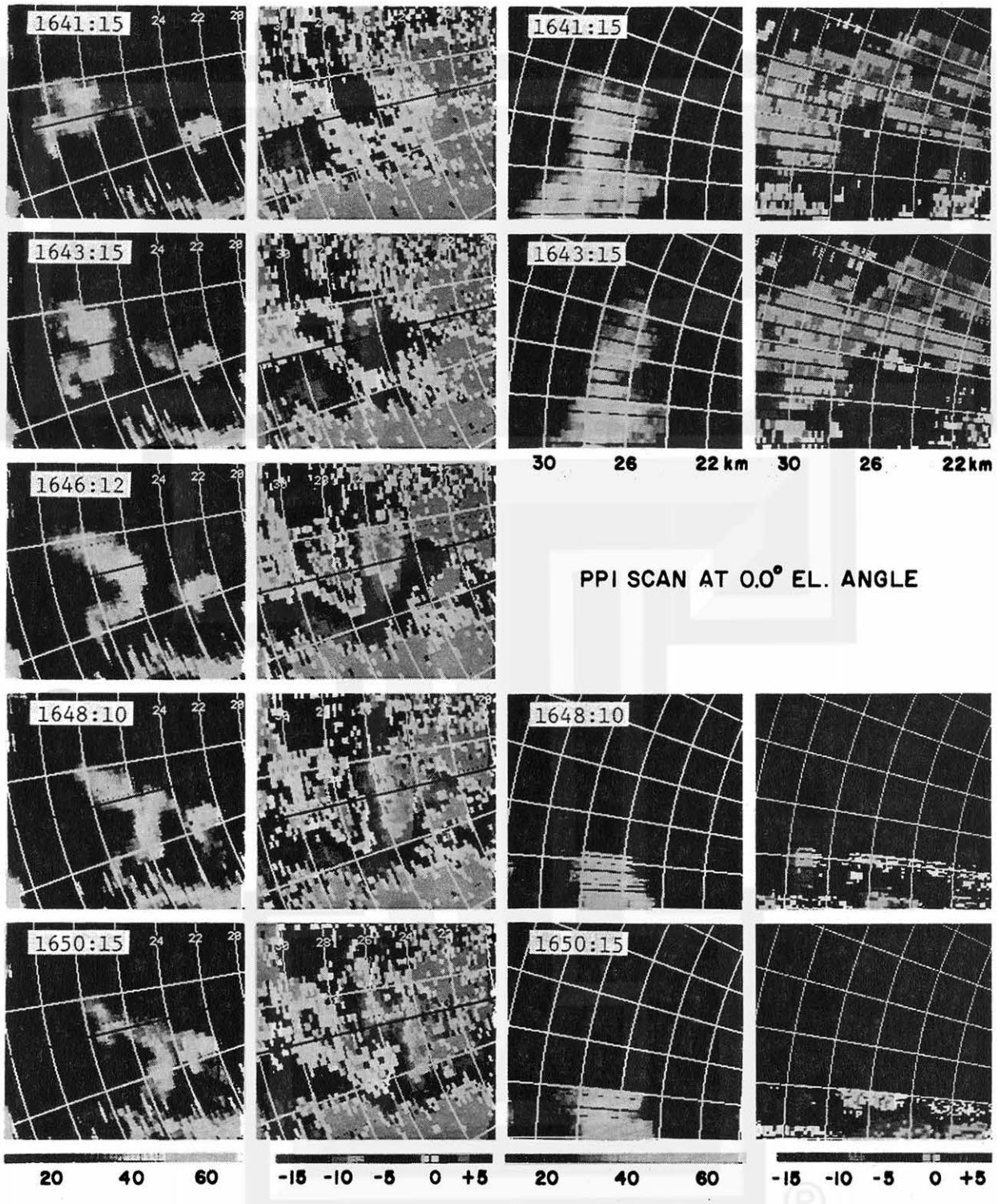

Fig. 6.20 PPI (left) and RHI (right) imagery of a bow echo and its induced microburst on 14 July 1982. RHI cross sections were generated by Brian Smith by using NCAR's RDSS.

In order to determine echo-relative velocities as a function of time, mean Doppler velocities averaged over the entire area of the 40 dBZ or stronger echo inside the 256° RHI plane were computed and subtracted from ground-relative Doppler velocities. The result in Fig. 6.21 shows clearly that the microburst winds (echo-relative) spread out uniformly toward and away from CP-3.

Vertical sections of echo-relative velocities in Fig. 6.22 reveal the existence of strong outburst winds (tinted light red) accompanied by the vortices with horizontal axes. It is seen that the 20 to 40 dBZ echoes stretch out toward CP-3, being embedded inside the outburst winds. Red full lines denote the isotachs of positive velocities and dashed lines denote those of negative velocities.

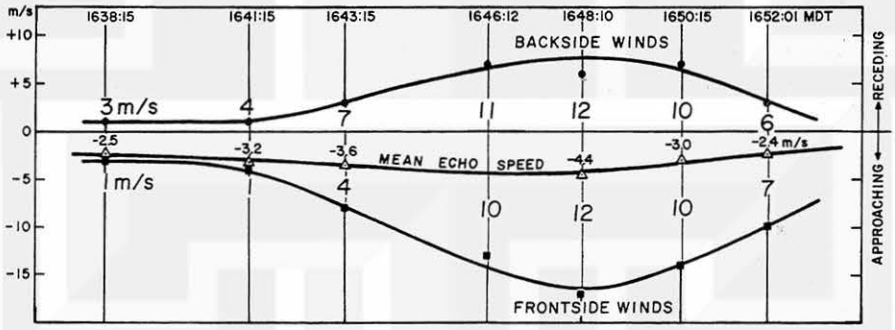

Fig. 6.21 Frontside (blue) and backside (red) winds of the bow echo-induced microburst. Velocities are echo-relative. Analysis with Brian Smith

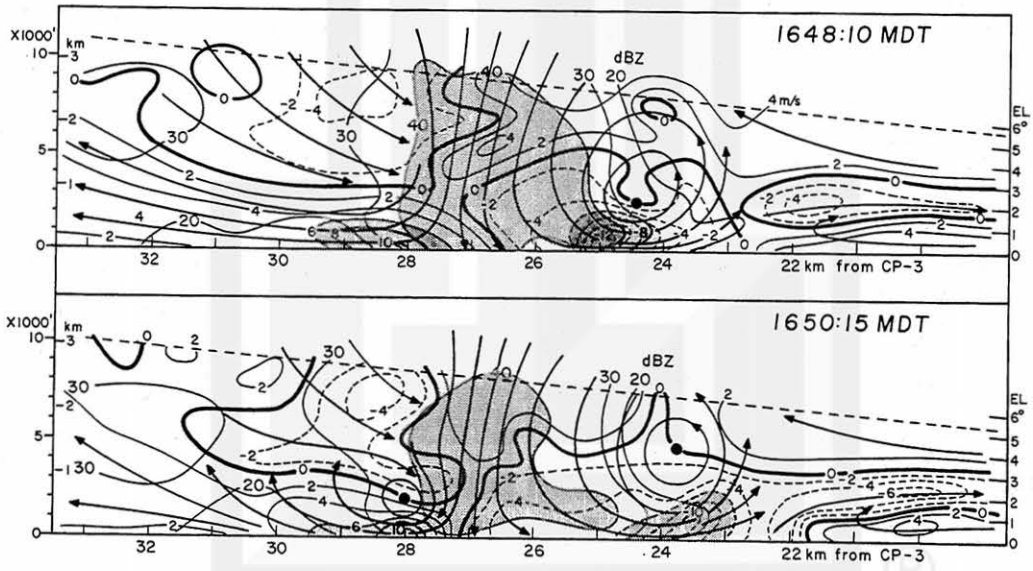

Fig. 6.22 Echo-relative Doppler velocities at 1648:10 and 1650:15. Echoes with 40 dBZ or higher reflectivity are tinted light blue. Analysis with Brian Smith

6.8 Denver Area Microbursts on 14 July 1982

On board the King Air, the author followed a misocyclone cloud for about one hour, witnessing the formation of microbursts (Fig. 6.23). The first microburst descended at Commerce City where PAM 16 recorded an 18.9 m/sec (42 mph) peak wind at 1409 MDT. The second one, which descended on Runway 35R, was already presented on Fig. 1.4. Two more microbursts will be discussed later.

It was found that these four microbursts and the bow-echo microburst in Fig. 6.20 are on a straight line extending downwind from a relatively low spot in the Rockies. Both the bow echo and misocyclone rotated cyclonically, while the Rit Carbone Microburst was accompanied by anticyclonic rotation at 5.6 km (18,400 ft) MSL. Winds aloft in Fig. 6.24 suggest the existence of a strong downslope flow extending from a low spot in the Rockies. The flow could induce a cyclonic vortex street on the left side and an anticyclonic vortex street on the other side.

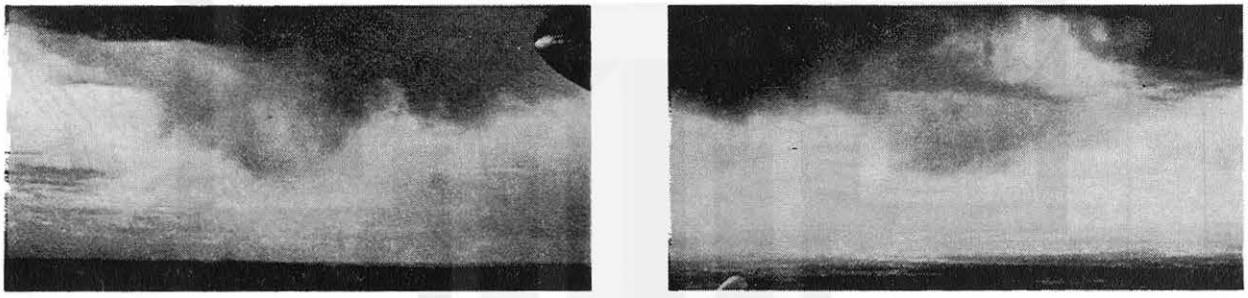

Fig. 6.23 Misocyclone cloud at 1409:16 when the Commerce City microburst was on the ground (left) and that at 1433:39 shortly before the diverging dust microburst formed (right). Photo by Fujita

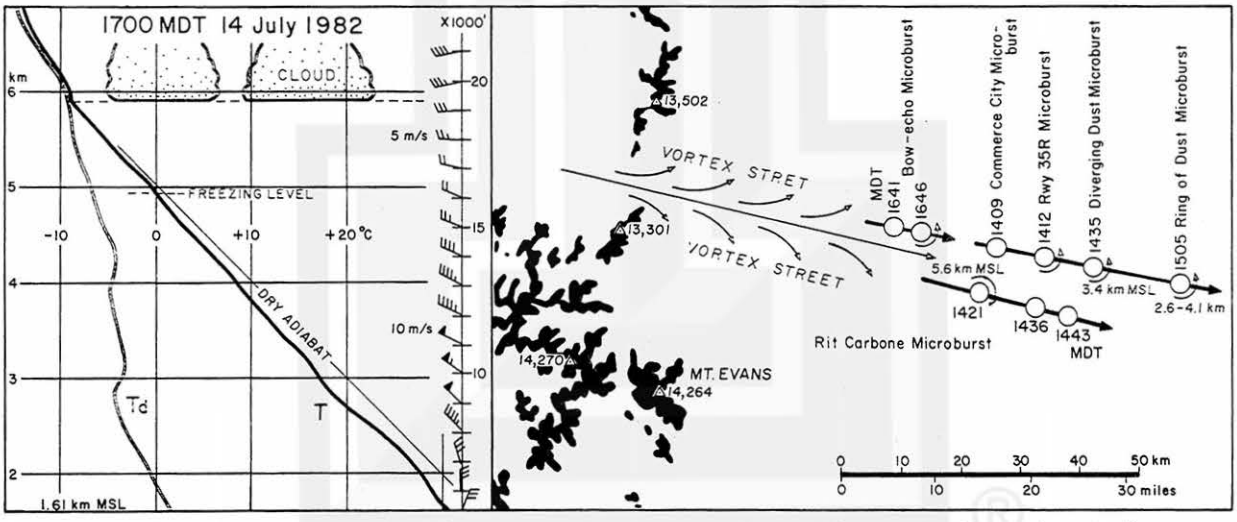

Fig. 6.24 A schematic model of the formation of the misoscale vortices which induced the Denver-area microbursts on 14 July. Analysis with Eric Peterson

Diverging Dust Microburst East of Stapleton Airport

The diverging dust microburst formed shortly after the misocyclone cloud was photographed at 1433:39 (Fig. 6.23). The isochrones of the dust front were determined by mapping the dust clouds in aerial photos taken from the King Air. There were diverging winds (miso to mesoscale) on the ground behind the dust front. CP-3/CP-4 dual Doppler winds show a misocyclone circulation at 1.8 km AGL. The wind and radar echo relationship in Fig. 6.26 indicates clearly that large echoes induce mesoscale wind systems while some small echoes are the inducers of microbursts, necessitating a Doppler radar for detecting winds.

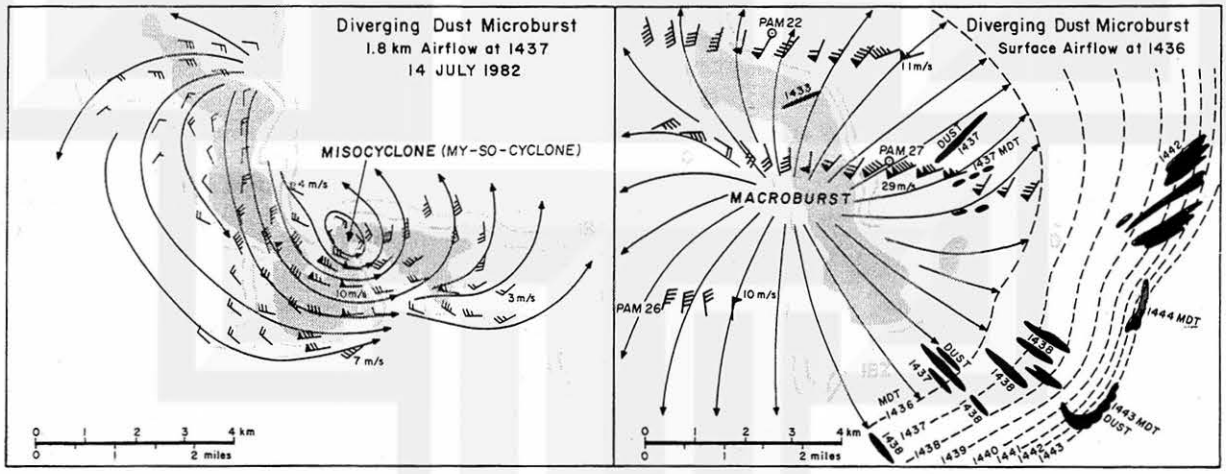

Fig. 6.25 Isochrones of dust front of the diverging dust microburst which expanded into the dimension of a macroburst. The airflow at 1.8 km (5,900 ft) AGL is dominated by a misocyclone circulation.

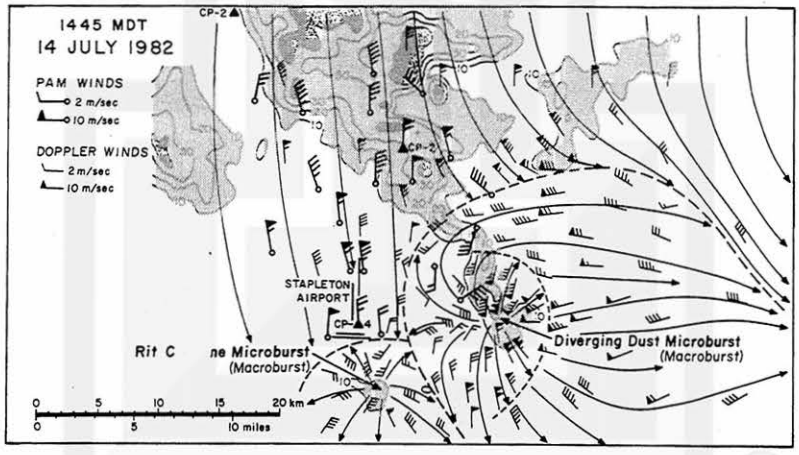

Fig. 6.26 Three outflow wind systems at 1445 MDT on 14 July 1982. It is seen that small echoes are the inducers of microbursts while large, strong echoes spawn large, mesoscale wind systems.

Ring of Dust Microburst near Watkins, Colorado

Fig. 6.27 A ring of dust generated by the outburst winds of a microburst 27 km (17 miles) east of Stapleton Airport. Photo by Fujita at 1504:53 MDT from King Air at 500 m AGL.

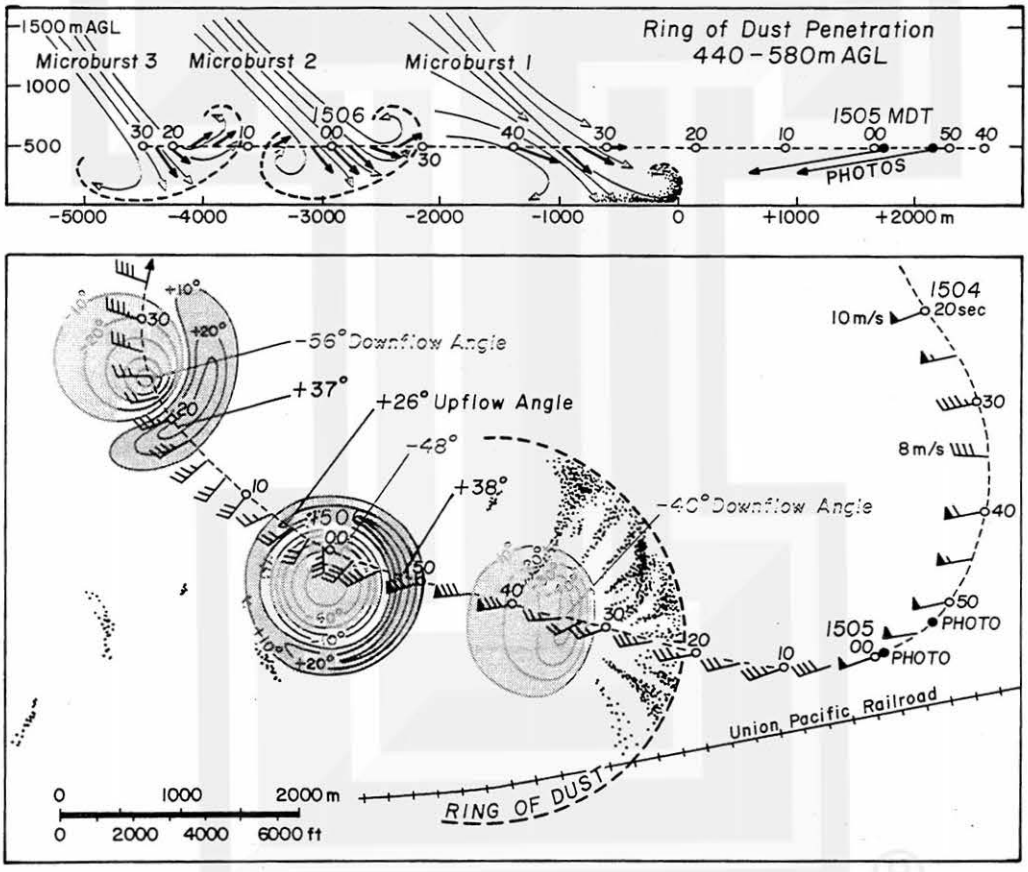

Fig. 6.28 The path of King Air in relation to three microbursts penetrated by the aircraft.

During the research flight on 14 July 1982, the author spotted a ring of dust cloud near Watkins. Immediately after taking the picture (Fig. 6.27), the author flew over the area of the outburst winds at 500 m (1,600 ft), maintaining a safe altitude above the ground (Fig. 6.28). The aircraft collected cloud particles, but there were no raindrops. The temperature fell 2° C inside the downflow of the first microburst.

The downflow angle computed by combining the horizontal and the vertical winds at aircraft positions varied significantly from -60° (downflow) to +30° (upflow). No upflow angle was measured inside microburst No. 1, a surface microburst. Two others were associated with large upflow angles (Fig. 6.29). An enlargement of the airflow of microburst No. 2 is presented in Fig. 6.30.

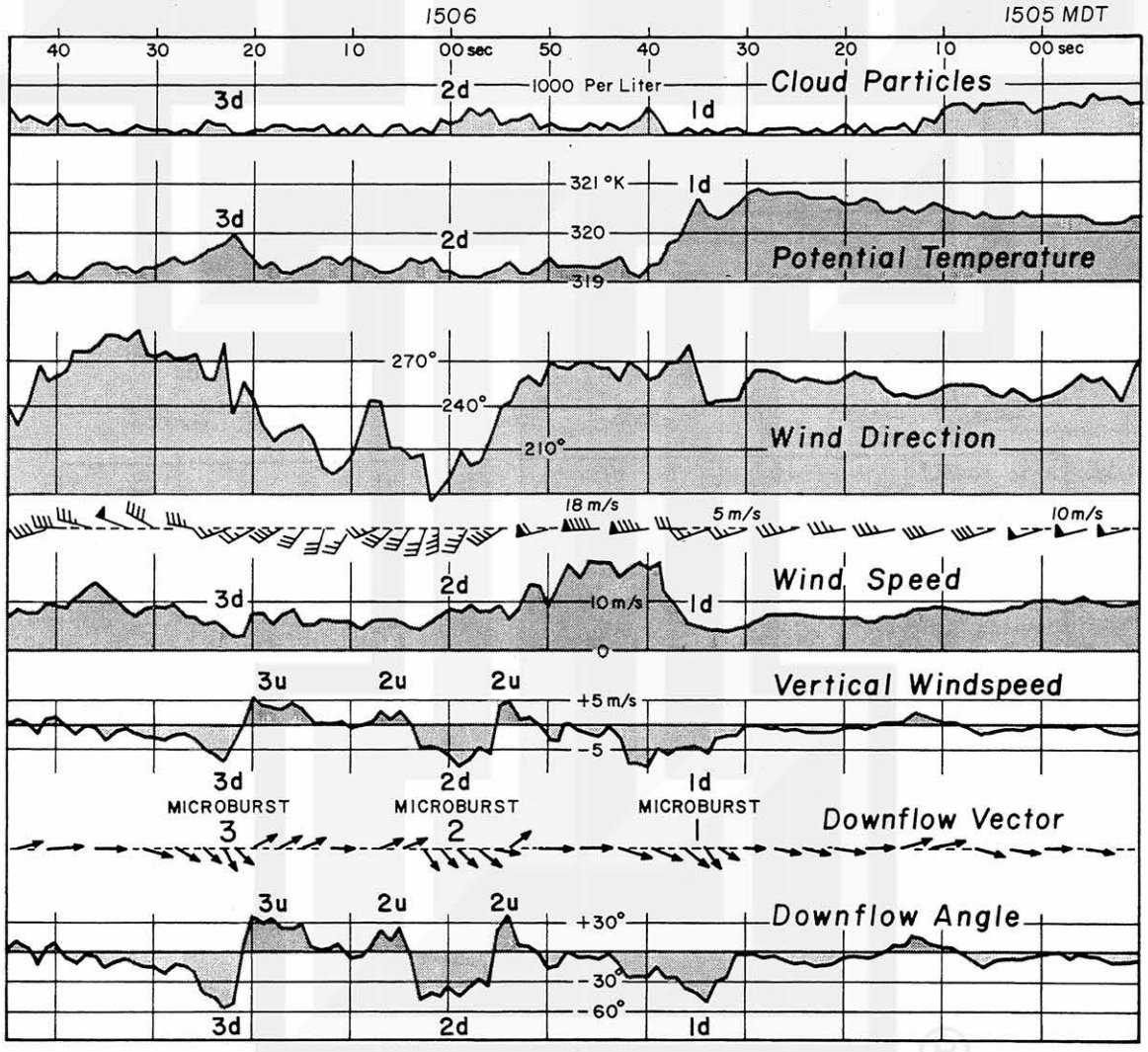

Fig. 6.29 Meteorological parameters measured at 1 sec intervals by King Air during its penetrations of three microbursts. The downflow vector denotes the wind in the vertical plane.

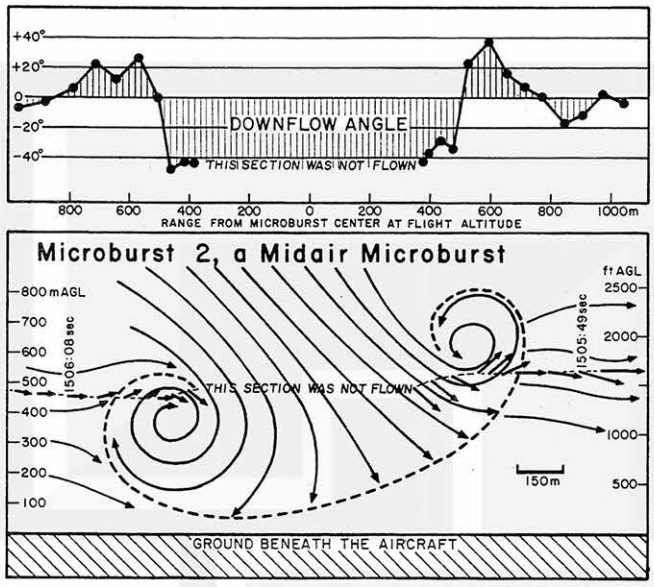

Fig. 6.30 An enlargement of the flight data between 1505:47 and 1506:10 MDT in Fig. 6.29. The aircraft did not fly through the center of the downflow, but its closest point was 400 m (1,300 ft) to the north-northeast of the center (see Fig. 6.28). The distance scale in this figure is the range from the downflow center of Microburst No. 2, a midair microburst which was not inducing dust clouds on the ground. The change in the downflow angle indicates that the aircraft penetrated near the center of roll vortices.

Rit Carbone Microburst

This microburst passed over downtown Denver at 1245 MDT and moved toward the glide slope of Runways 35L/R of Stapleton Airport. Continental 414 was cleared to land at 1440:00. A few seconds later, the aircraft began sinking in a microburst wind shear. The pilot applied full power, but the aircraft kept sinking. A go-around was executed immediately and the aircraft climbed successfully to 8,000 ft. Rit Carbone of NCAR was on board Western 364 which was following Continental 414 and experienced excitement. In recognition of his unforgettable experience, this microburst was called "Rit Carbone Microburst" (Fig. 6.31).

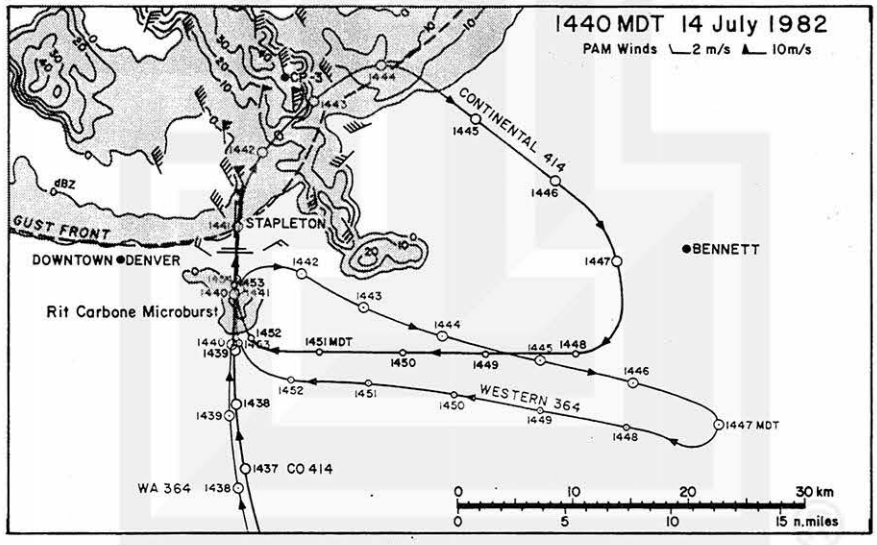

Fig. 6.31 Paths of CO 414 and WA 364 which executed a go-around while penetrating the Rit Carbone Microburst.

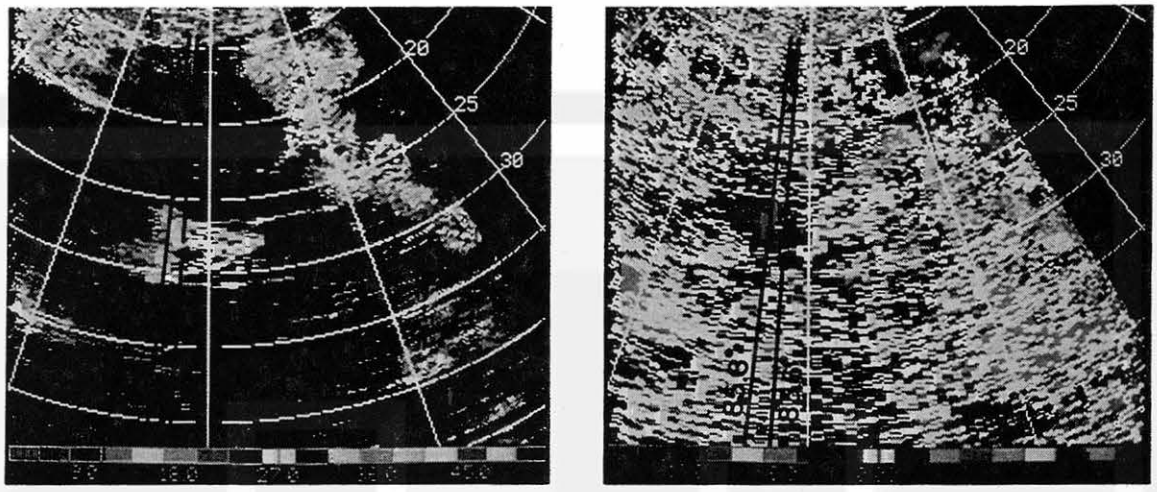

Fig. 6.32 Reflectivity (left) and velocity (right) fields of the Rit Carbone microburst at 1421:29. PPI scan by CP-3 at 1.4° elevation.

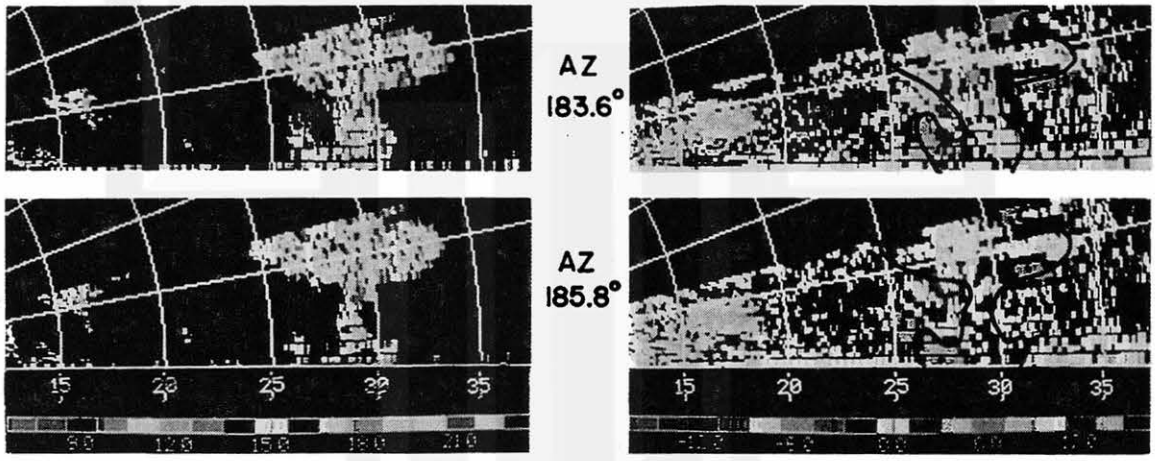

Fig. 6.33 RHI scans along two CP-3 azimuths produced by combining multiple PPI scans. NCAR's RDSS imagery by Brian Smith

Western 364 followed CO 414 by approximately one minute. It also encountered a heavy sink at 1441, necessitating a go-around. The aircraft made a sharp right turn to 080° and climbed to 8,000 ft. As shown in Table 6.2, Continental 458 experienced a 30 kts tailwind but it landed uneventfully. Both Republic 760 and Western 46 landed on schedule in a 13 to 20 knot tailwind.

The parent cloud of the Rit Carbone Microburst was a Type "C", mushroom cloud. Both reflectivity and velocity fields by CP-2 reveal that it is a small and weak echo (Fig. 6.32). Two RHI scans, reconstructed by NCAR's Research Data Support System (RDSS) show clearly the shape of the mushroom cloud characterized by a descending column and the outburst winds near the ground (Fig. 6.33).

Table 6.2 Wind shears experienced by the seven aircraft that penetrated the Rit Carbone microburst on the approach path of Runway 35 at Stapleton Airport on 14 July 1982. Time: MDT

Aircraft	Cleared to land	Landing, go-around, and comments
42 W	1437:10	Landed 35L at 1438; no wind shear reported
■ CO 414	1440:00	Go-around 1440; heavy sink; had full power on, but still sinking; climbed runway heading; landed 35R at 1454.
■ WA 364	-------	Go-around 1441; picked up heavy sink; turned right 080°; climbed and maintained 8,000'; landed 35R at 1455.
CO 458	1440:55	Landed 35L at 1442; a 20 kts tailwind at 600' and a 30 kts tailwind below that.
RC 760	1440:00	Landed 35R at 1444; sink was still there; 13 kts loss.
WA 46	1440:05	Landed 35L at 1444; confirmed plus 30, minus 20 kts shear.
ASP 434	1440:34	Landed 35L at 1445; no wind shear reported.

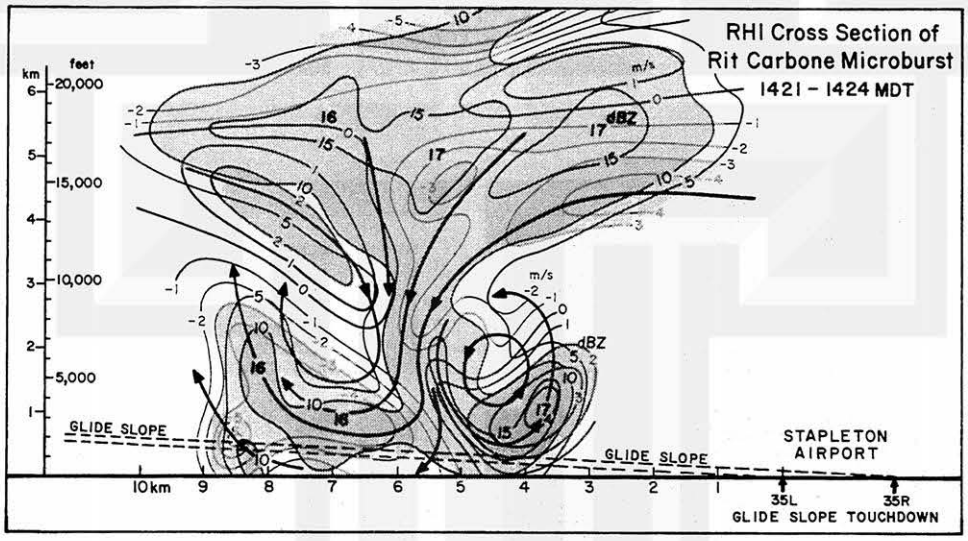

Fig. 6.34 The Rit Carbone Microburst at 1421-1424 MDT placed at its position at 1440 when CO 414 and WA 364 decided to abandon their approaches.

No volume scans to high elevation angles are available at the time of the go-around by CO 414 and WA 364. However, the microburst, volume scanned 16 to 19 minutes earlier, was placed at its position at 1440 MDT, in order to simulate the airflow in relation to the go-around aircraft. Due to a 30 km distance from CP-2 and also to the existence of a blocking hill, the radar was not able to measure near-ground velocities. Much stronger tailwinds could have existed at the glide slope height.

Fortunately, the tailwinds were located 4 km (2 n. miles) south of the runway threshold. If the tailwinds had been 2 km (1 n. mile) closer to the runway, one of the go-around aircraft would have been in serious difficulty because the glide slope height decreases to 100 m (300 ft) AGL.

6.9 Giant Anteater Clouds on 16 July 1982

The Denver area on July 16 was relatively quiet without experiencing thunderstorm activity within 50 miles of Stapleton Airport. For the purpose of studying possible downflows induced by high-base cumulus clouds, the author made a late afternoon research flight over Irondale Road to the east of CP-3 (refer to JAWS Network map in Fig. 4.7). Both CP-2 and CP-4 made PPI sector scans, while CP-3 performed RHI scans inside the same sector. Brian Smith, meanwhile, kept taking cloud pictures from the CP-3 site looking east.

Four high-base cumuli formed one after another approximately 20 km (13 miles) to the east of CP-3 and moved away toward the east. RHI pictures in Fig. 6.35 show these clouds identified by the letters, A, B, C, and D, of which A was the oldest one. Cloud A is no longer in the RHI pictures. Strangely, the upwind side of each cloud began descending 15 to 20 minutes after the formation, turning finally into the shape of a giant anteater.

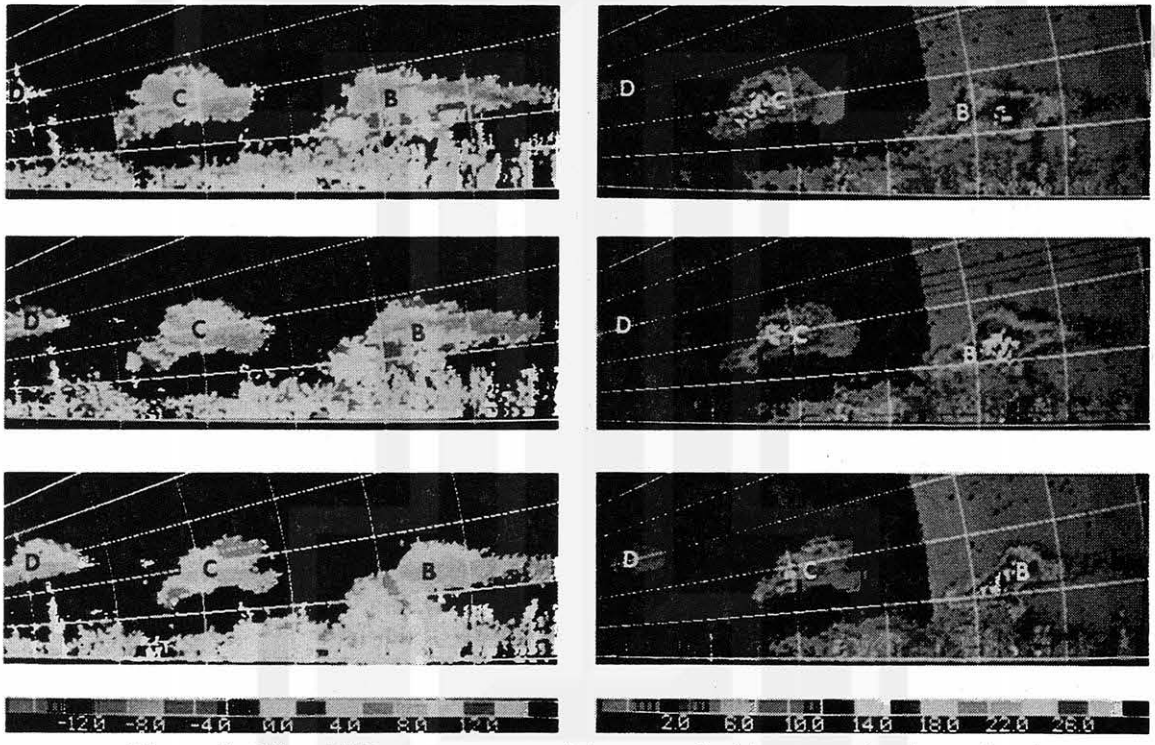

Fig. 6.35 RHI cross sections of three giant anteater clouds made by CP-3 along its 96.2° azimuth. Cloud "D" is the youngest cloud, having an appearance of altocumulus. The head section of cloud "C" was coming down when the author penetrated its downflow at 1757:30 MDT. Cloud "D" induced a surface microburst at 1807, the time of the bottom pictures.

Figure 6.36 shows pictures of clouds A - D taken by Brian Smith at the CP-3 site while looking east. The youngest cloud "D" has the appearance of an altocumulus; the top of cloud "C" is glaciated; cloud "B" has the shape of an anteater; and cloud "A" is in its dissipating stage.

The author, in the King Air, penetrated the head section of cloud "C" at the location of the red circle while flying toward the west. As the aircraft approached the cloud, a rapidly descending virga shaft appeared. The aircraft penetrated the virga just above the descending, dark shaft in the picture, measuring a 7.1 m/sec (23 fps) downward speed.

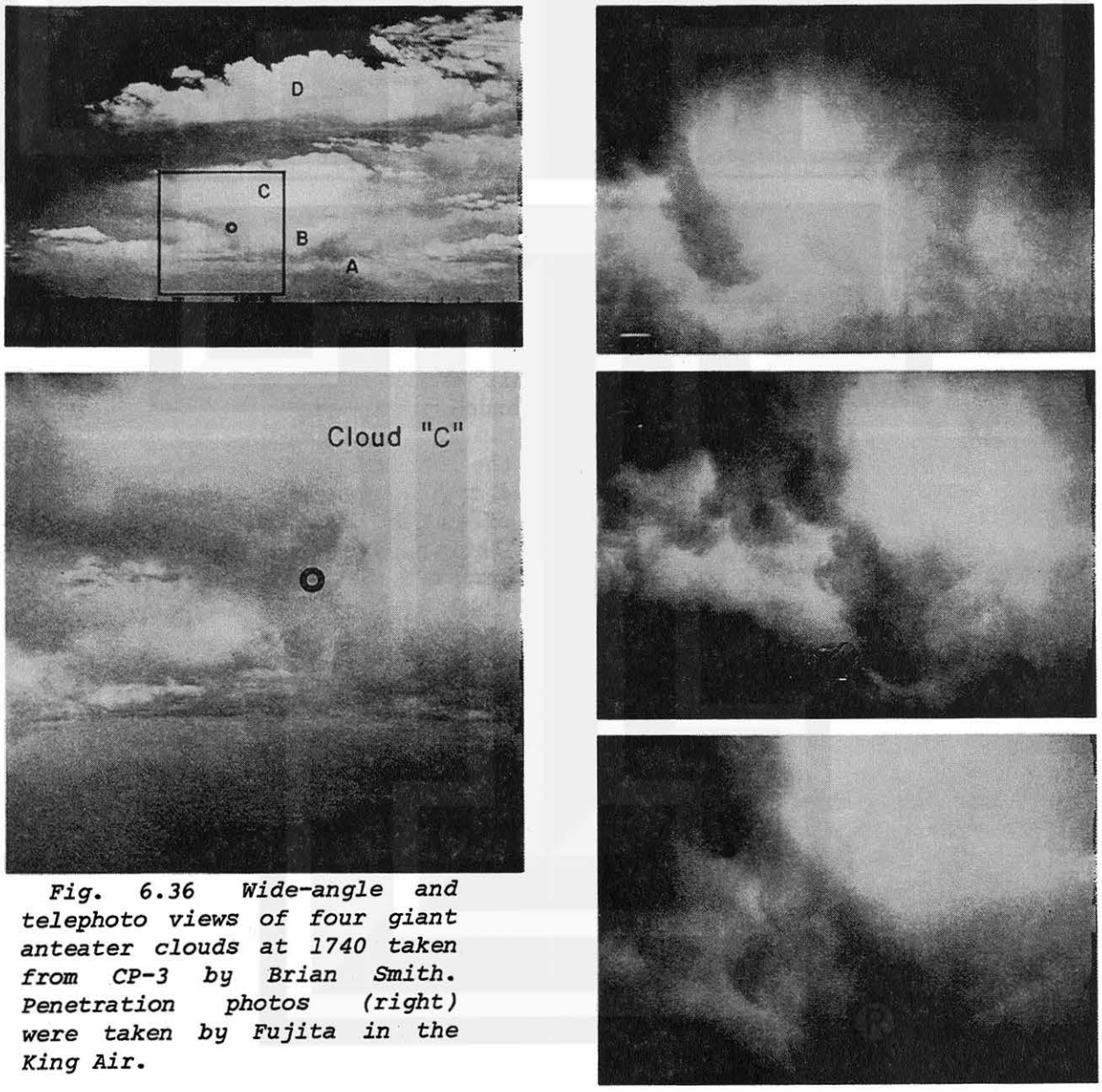

Fig. 6.36 Wide-angle and telephoto views of four giant anteater clouds at 1740 taken from CP-3 by Brian Smith. Penetration photos (right) were taken by Fujita in the King Air.

Giant anteater clouds are hard to detect by PPI scans. In this particular case study, CP-3 performed continuous RHI scans within the eastern sector. CP-2 and CP-4, meanwhile, made PPI sector scans within the same area. Figure 6.37 presents PPI photos made between 1759:23 and 1800:50 MDT. These photos do not reveal that the scanned cloud has the shape of a giant anteater. On the other hand, RHI cross sections made by CP-3, within several minutes of the PPI scans, depict the anteater shape of the cloud along its 96.2° azimuth.

The 1.0° scan in Fig. 6.37 shows a gust front moving from east to west. Due to its low-altitude airflow, the gust front weakens and disappears as the elevation angle increases. At 4.5° elevation angle, the scan plane intersects the base of anteater cloud "B". The low spots on the cloud base are seen as ring-shaped echoes which do not imply the shape of an anteater.

As the elevation angle increases, the radar beam slices the middle and upper sections of the anteater clouds without depicting the characteristic shape expected to be seen in RHI imagery.

Figure 6.38 presents the flight path superimposed upon the anteater clouds depicted by the RHI scans by CP-3. Since the flight plan is included inside the RHI plane, aircraft-measured particle concentrations and the CP-3 reflectivity field fit very well. Two particle-size distributions at the bottom of Fig. 6.38 show that the younger cloud "C" contained more particles of all sizes than the older one. This evidence implies that some large particles in cloud "B" had already descended to the ground.

The flight path superimposed upon the Doppler velocity field in Fig. 6.39 suggests that the King Air happened to penetrate a level of low Doppler velocity, caused by a swirling pattern of the airflow inside the misocyclone in which both downflows are embedded. The depths of the low-velocity winds are only 2 - 3 km (600 to 1,000 ft), implying that misoscale circulations are most significant within a relatively shallow layer.

After completing the initial westward penetration at 1756, the head of the anteater cloud "B" was penetrated repeatedly: from west to east at 1801, east to west at 1805, and finally from west to east at 1809. The maximum downflow speed of 13.9 m/sec (46 fps) was measured at 1805:00. During the final approach at 1807, an arc of dust appeared beneath the location where the anteater's head had existed. The aircraft measured a 7.8 m/sec (26 fps) downflow at 1808:46 in clear air, in the wake of the anteater's head, which turned into an arc of dust clouds 1.2 miles (2 km) long.

This case study shows the life cycle of a giant anteater cloud which first appears as an altocumulus cloud. After the cloud top glaciates, the upwind section of the cloud descends gradually, taking the shape of a giant anteater. Suddenly, thereafter, the head descends to the ground, inducing an arc of dust clouds.

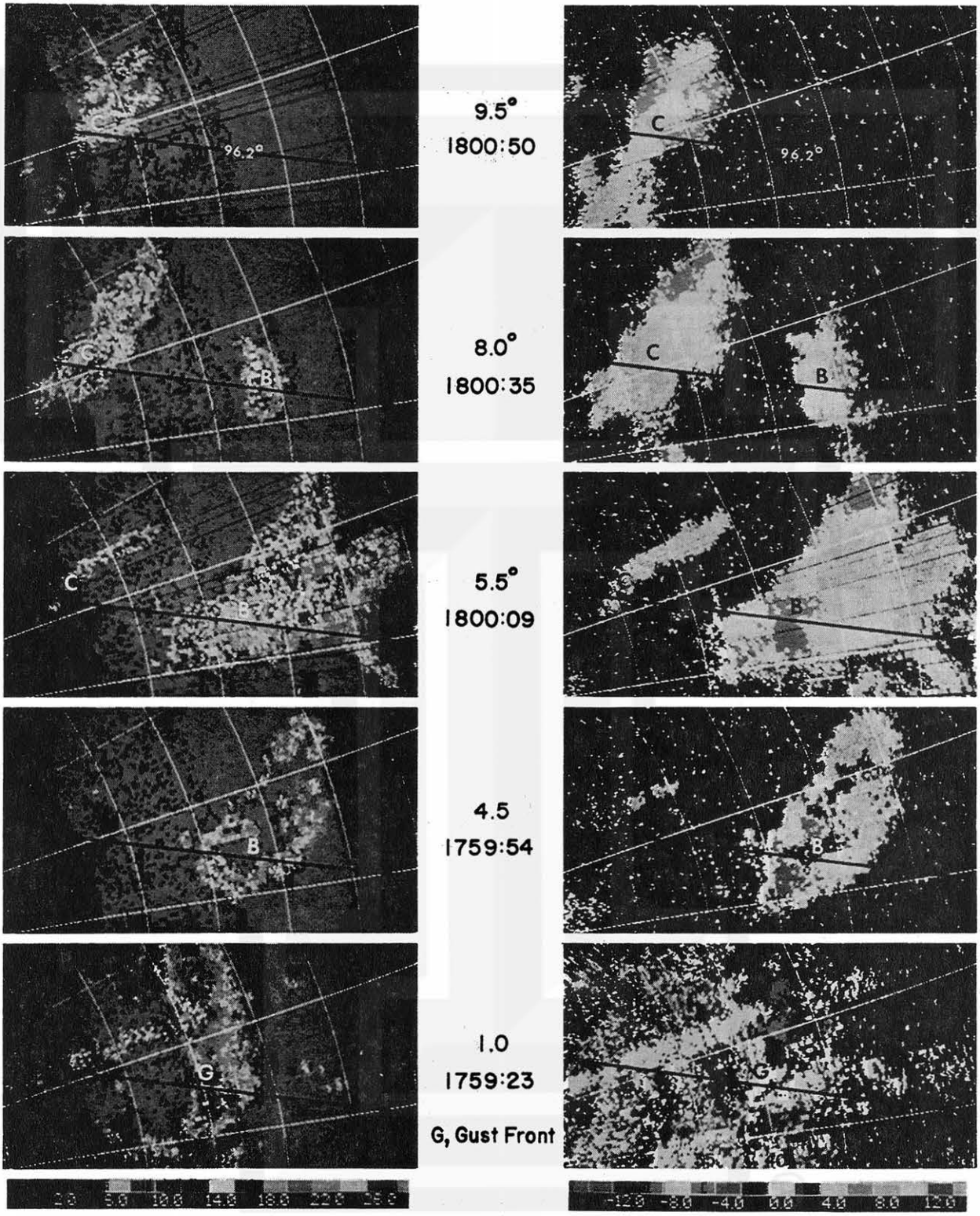

Fig. 6.37 PPI photos of reflectivity (left) and velocity (right) fields of the giant anteater clouds "B" and "C" depicted by the PPI scans of CP-4.

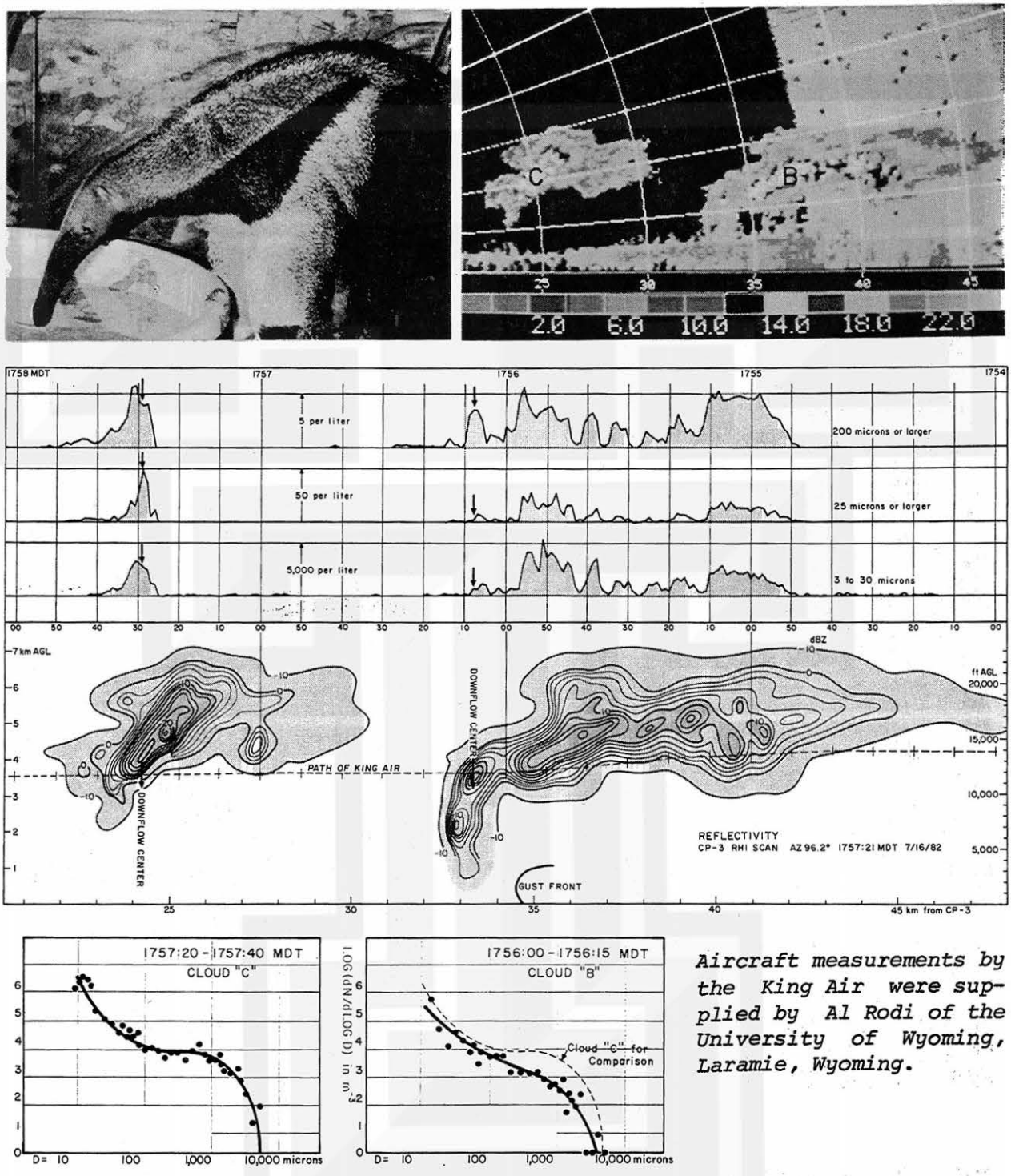

Aircraft measurements by the King Air were supplied by Al Rodi of the University of Wyoming, Laramie, Wyoming.

Fig. 6.38 Giant anteater clouds "B" and "C" penetrated by the author in the King Air. The flight path is superimposed upon the RHI reflectivity field of CP-3 as scanned at 1757:21 MDT. The shape of the mature cloud "C" is very similar to a giant anteater. Photo by Fujita at Brookfield Zoo

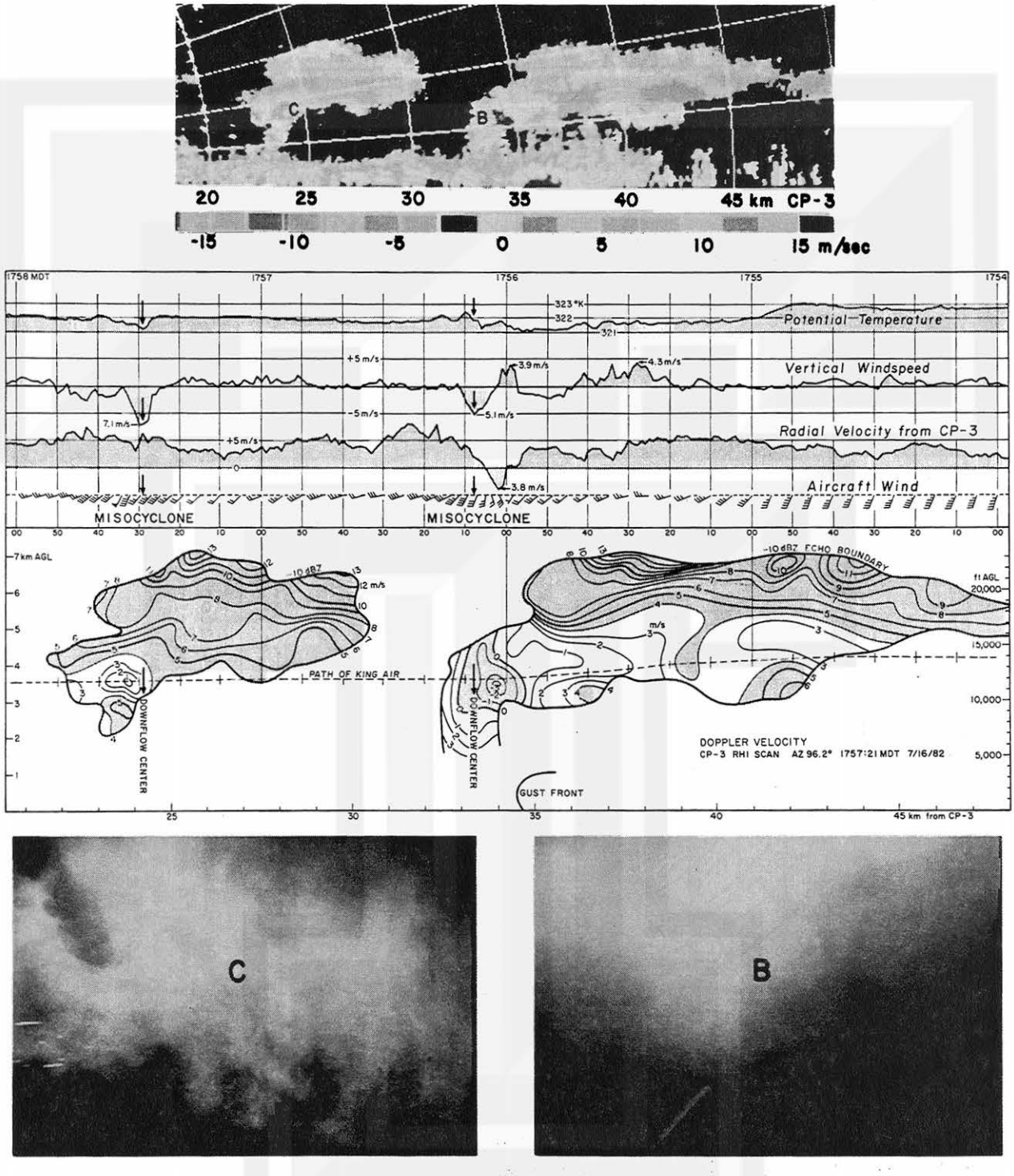

Fig. 6.39 Velocity fields of clouds "B" and "C" depicted by the RHI scans of CP-3 along the 96.2° azimuth. The bottom photos show the downflow sections of cloud "C" (left) and "B" (right). Radial velocity from CP-3 denotes the component of the aircraft wind along the CP-3 azimuth.

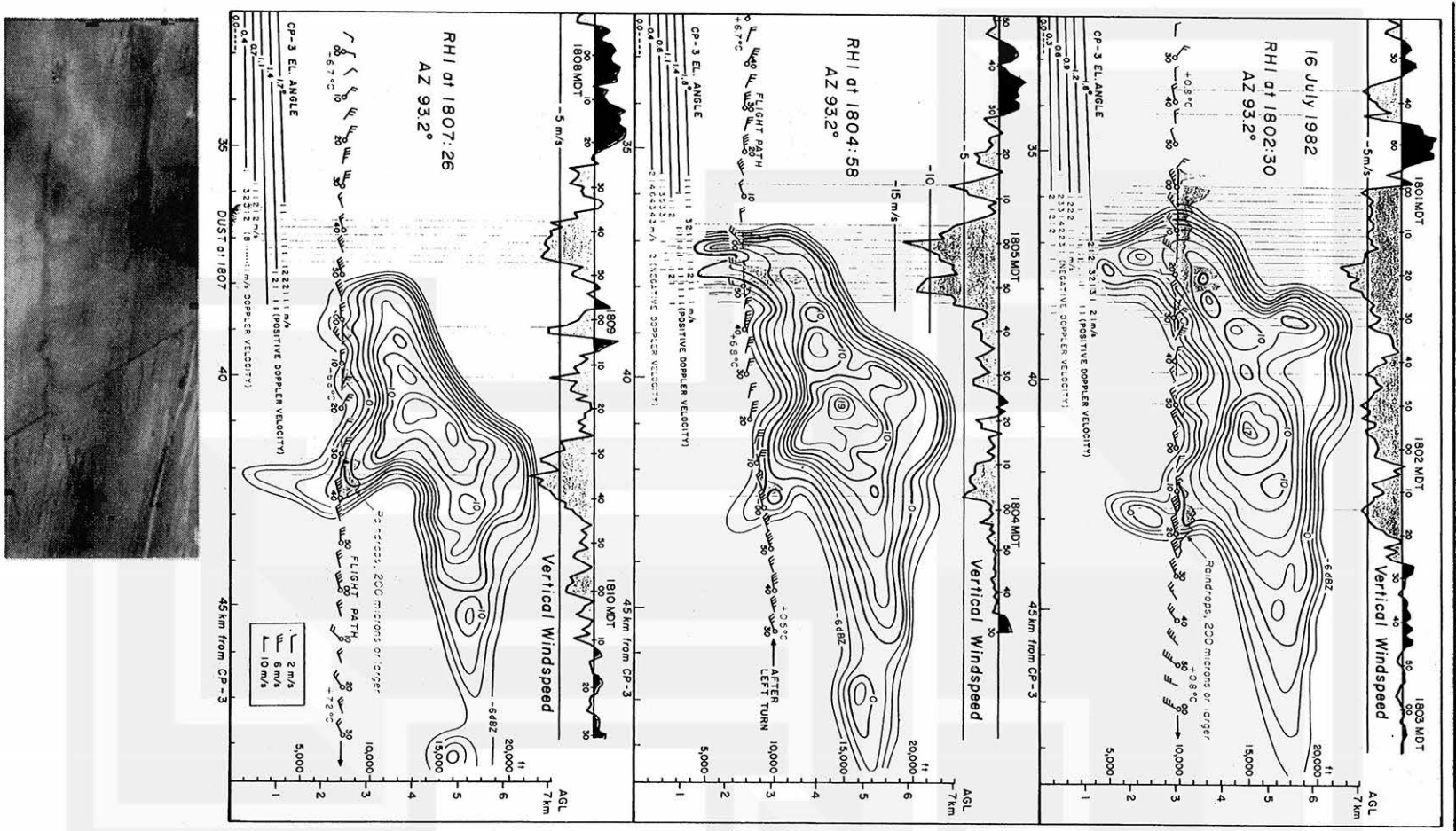

Fig. 6.40 Repeated penetrations of the anteater cloud "C" from west to east at 1801, east to west at 1805, and west to east at 1809, approximately once every four minutes. The vertical windspeed, at the top of each diagram, reveals that the anteater's head was accompanied by both downflow and a cyclonic misocyclone.

Red lines denote the reflectivity field of the RHI data of CP-3 obtained within one to two minutes of each penetration. CP-3 velocity values at low altitudes beneath the anteater's head are plotted in red (positive) and blue (negative) numbers in m/sec. Suddenly at 1807, an arc of dust formed on the ground. The anteater's head was gone. Arc of dust photo by Fujita

6.10 Andrews Air Force Base Microburst on 1 August 1983

The 120+ kt (150 mph) wind recorded at Andrews Air Force Base during the 1 August 1983 microburst was the highest microburst windspeed recorded at an airport. The GMG-20 propeller anemometer at 16 ft (4.9 m) AGL was located on the north side of the runway area (Fig. 6.41).

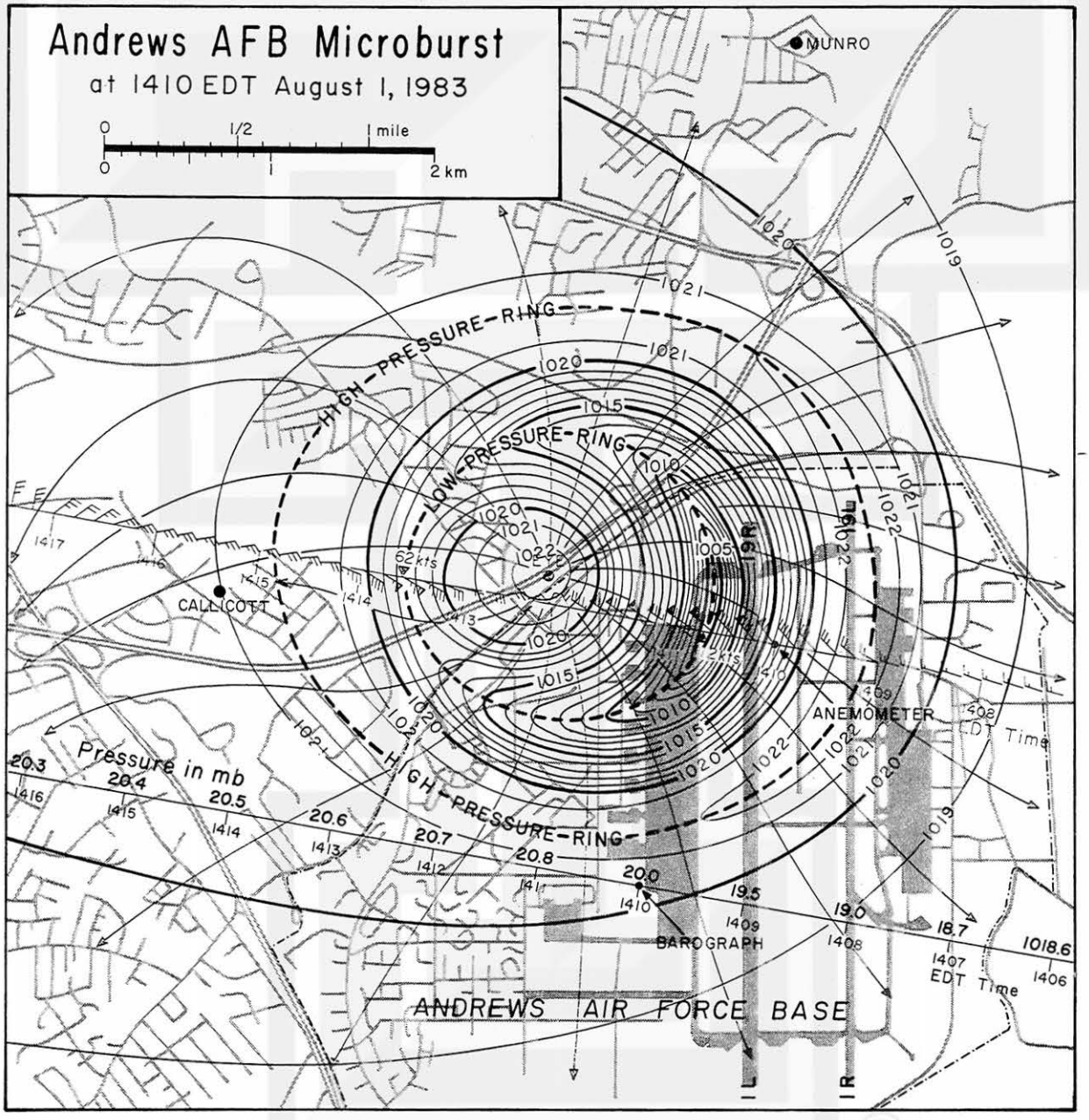

Fig. 6.41 Wind and pressure fields of the Andrews AFB microburst constructed by time-space conversions of wind and barograph traces. Tree damage occurred at Callicott, while the peak winds at Munro were 5 to 6 kts.

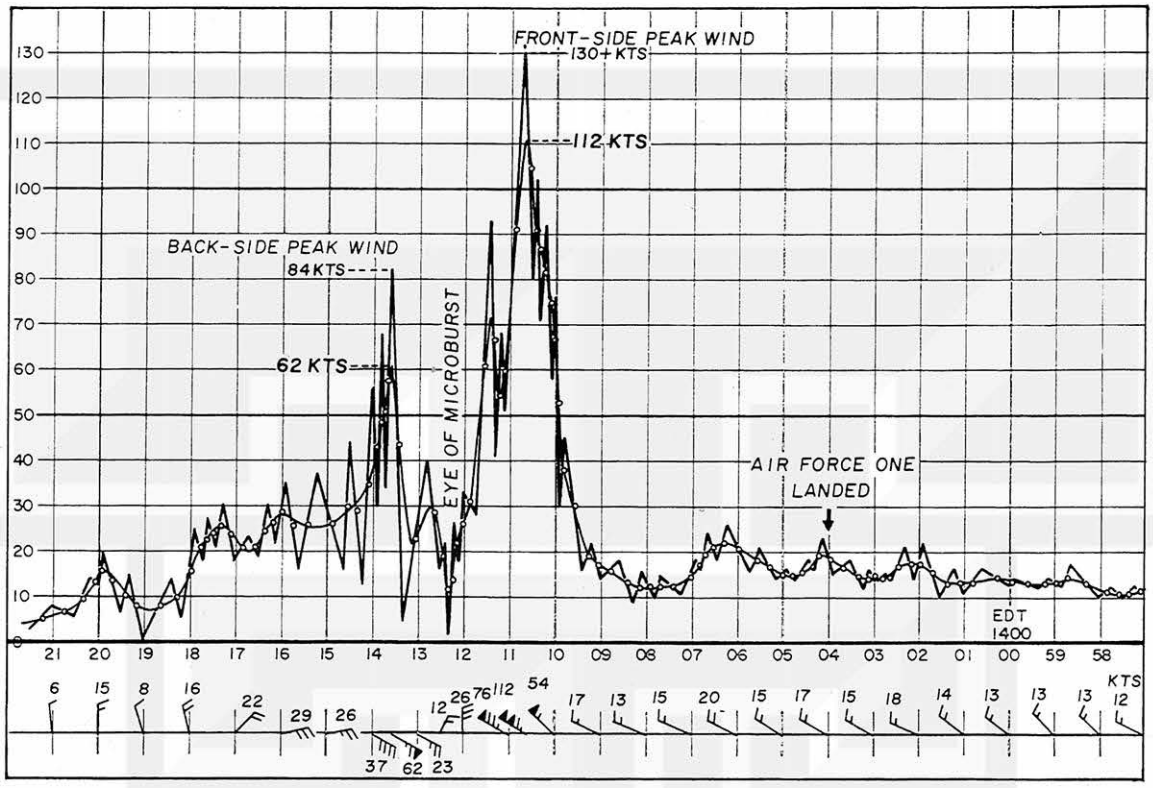

Fig. 6.42 An enlarged wind trace showing a 120+ kt peak wind (112 kts mean) on the front side and an 84 kt peak wind (62 kts mean) on the back side of the microburst. There was an eye at the center of the microburst. Winds plotted in red denote the mean values of successive lulls and gusts.

According to newspaper reports, Air Force One, with President Reagan on board, landed at 1404 EDT on the dry runway. Winds began increasing at 1409:20, reaching a peak at 1410:45. Then, the windspeed decreased very rapidly to only 2 kts (1 m/sec) when the eye of the microburst passed over the anemometer. The second peak wind at 1413:40 came from the southeast, opposite from the northwesterly direction of the first peak (Fig. 6.42).

Occurrence frequencies of microbursts in Table 6.1 indicate that the chance of experiencing a 150 mph (67 m/sec) microburst is rare. Only four (4) such microbursts per year are expected within the contiguous United States. Although such an occurrence probability is extremely low, a close call could happen to any aircraft landing at or taking off from numerous airports around the world.

6.11 Huntsville Boat Microburst on 7 July 1984

The July 1984 issue of NOAA's STORM DATA reported "Eleven people lost their lives and two people were injured when an apparent downburst from a severe thunderstorm capsized the 90 ft sternwheeler boat upon which they were passengers. Eighteen people were aboard the boat when the tragedy struck near Ditto Landing on the Tennessee River south of Huntsville. The victims were reported to have drowned after apparently being trapped in the lower cabin. The captain was reported to have been heading back to the landing and had turned the boat into the wind when the gust from the downburst struck the craft from the side. Wind gusts to 70 mph were reported at Redstone Arsenal in Huntsville at 1027 CST. Trees were flattened and mobile sheds were overturned southwest of the river in the Lacey Springs area of Morgan County".

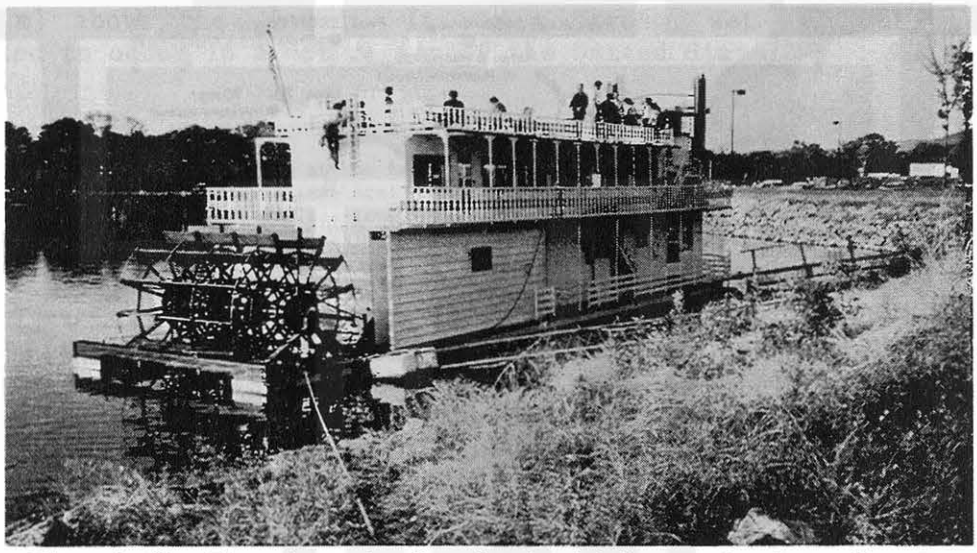

Fig. 6.43 The sternwheeler boat which capsized on the Tennessee River at 1125 CDT on 7 July 1984. Of the 18 persons on board, 11 lost their lives. From NOAA's STORM DATA, July 1984 issue. Photo by Gary McClusky

A picture of the sternwheeler boat taken before the accident is shown in Fig. 6.43. The double-decked boat is 92 ft long, 20 ft wide, and 25 ft tall. It was traveling down the river heading toward the northwest. Rain began at 1120 CDT in estimated 30 kt (15 m/sec) westerly winds. Winds became stronger and stronger in the next several minutes, reaching an estimated 60 to 70 kts (31 to 36 m/sec) blowing from 290°. The captain of the boat turned the heading to 290°, directly toward the oncoming winds. All of a sudden at 1125 CDT, the wind direction changed as much as 90 degrees. A strong wind struck the sternwheeler from the left side and the boat capsized.

Within a couple of minutes after the accident, the wind weakened to about 20 kts (10 m/sec). At 1130 CDT, five minutes after the accident, there was practically no wind; the air was calm.

There were three recording anemometers within 25 km (16 miles) of the accident site. A 44 mph (20 m/sec) peak wind was recorded at the National Weather Service at Huntsville Airport, and a 28 mph (13 m/sec) wind was recorded at the Marshall Space Flight Center. A peak wind of 70 mph (31 m/sec) was recorded at the Redstone Arsenal located 9 km (5 miles) to the northwest of the accident site (Fig. 6.44).

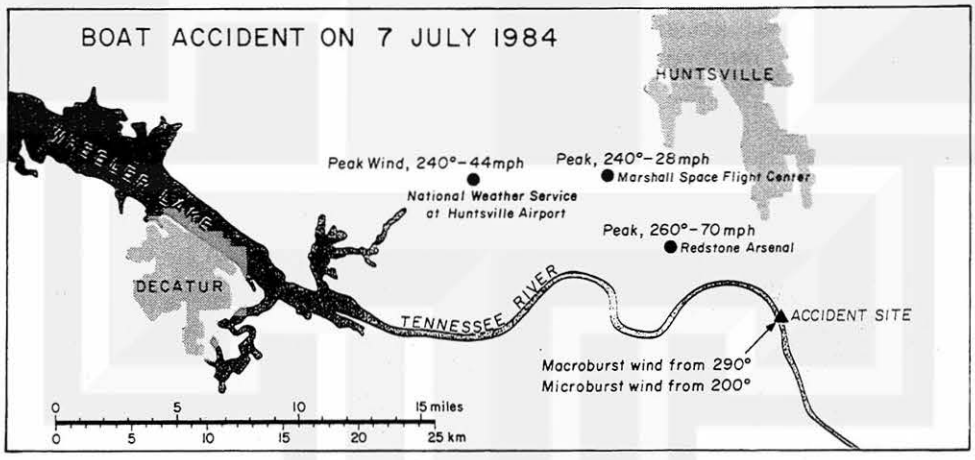

Fig. 6.44 Three anemometers located in the vicinity of the accident site. Of these, both National Weather Service and Marshall Space Flight Center anemometers were affected only by the macroburst winds. The Redstone Arsenal and the accident sites were under the influence of both macroburst and microburst winds.

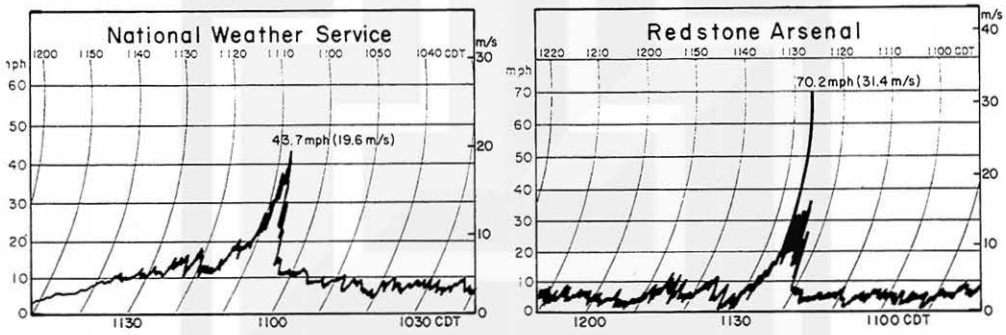

Fig. 6.45 The macroburst winds recorded at the National Weather Service (left). The Redstone Arsenal record shows a spike of microburst wind superimposed upon the macroburst winds (right).

The anemometer record from the National Weather Service shows a rapid increase of windspeed in three minutes, between 1105 and 1108 CDT. The decrease after the peak was an exponential decay in windspeed, suggesting that the peak wind occurred just behind the gust front of a macroburst, rather than a microburst. The Redstone Arsenal anemometer was affected by both macroburst and microburst winds. The macroburst winds began at 1121 CDT, reaching 36 mph (16 m/sec) in three minutes. Winds decreased exponentially, thereafter, to almost zero in 10 minutes. The microburst winds, superimposed upon the macroburst winds, lasted only less than one minute (Fig. 6.45).

Detailed observations of the weather events at the Arsenal, presented in Table 6.3, reveal that the microburst winds occurred when a thunderstorm was passing directly over the site. Lightning at 1127 was continuous, flashing in-cloud, cloud-to-cloud, and cloud-to-ground. The visibility in blinding rain was 1/8 mile (200 m) with a low cloud base located 1,000 ft (300 m) above the ground. It was a strong, wet microburst as would be expected to occur in a wet region of the United States.

Table 6.3 Weather observations at the Redstone Arsenal taken before, during, and after the microburst of 7 July 1984. Abbreviations are: S..scattered, B..broken, O..overcast, Visib..visibility, T..thunder, RW..rainshower, Press..sea-level pressure, T..air temperature, Td..dew-point temperature, Der..wind direction, Max Mean Min..maximum mean minimum windspeeds within one minute centered at the observation time, MVG..moving, DST..distant, OCNL..occasional, LTG..lightning, OVHD..overhead, CONT.. continuous, FQT..frequent, N NE E SE S..eight-point directions.

Time (CDT)	Sky and Ceiling	Visib (miles)	Weather	Press (mb)	T/Td (°F)	Dir (deg)	Max	Mean (mph)	Min	Remarks
0855	3500'S 10000'S 25000'B	7		1016.8	80/72	230		05		
0956	3500'S 10000'S 25000'B	7		1016.5	82/72	300		03		
1035	3500'S 10000'S 25000'B	7	T	1016.1	84/71	250		05		T SW-N MVG NE DST LTG
1058	3500'S 10000'B 25000'O	7	T	1015.7	86/74	190	06	05	01	T W-N MVG NE OCNL LTG
1120			T RW-	1016.5	84/70	240	07	06	06	
1121			T RW-	1016.4	84/70	250	11	10	06	
1122			T RW-	1016.4	84/70	250	26	18	11	
1123	1500'B 3000'O	2.50	T RW	1016.3	83/60	260	25	20	15	T OVHD MVG E CONT LTG
1124			T RW	1016.3	82/69	260	36	26	17	
1125	1500'Overcast	0.75	T RW+	1016.2	68/67	270	33	25	19	T OVHD MVG E CONT LTG
1126			T RW+	1016.2	67/66	260	69	34	16	
1127	1000'Overcast	0.12	T+RW+	1016.2	67/66	260	70	26	14	T OVHD MVG E CONT LTG
1128	1000'Overcast	0.75	T+RW+	1016.1	67/66	210	14	11	05	T OVHD MVG E CONT LTG
1129			T RW	1016.1	67/66	220	11	08	04	
1131	1000'B 3000'O	3	T RW-	1016.0	67/66	270	05	03	00	T N-E-SE MVG E FQT LTG
1157	1000'B 3000'O	5	T RW-	1016.8	68/67	110	06	05	03	T NW, NE-E-SE MVG E
1215	1500'B 3000'O 10000'O	7	T	1016.6	68/67	160	07	06	05	T N, E MVG E OCNL LTG

The small-scale microburst winds embedded inside the overall macroburst winds can be depicted by mapping the direction of damaging winds on a local map. Fig. 6.46 shows the vectors of damaging winds as determined by the aerial photographs taken after the storm. The airflow pattern analyzed on this map indicates the existence of three microbursts in the vicinity of the accident site. They are:

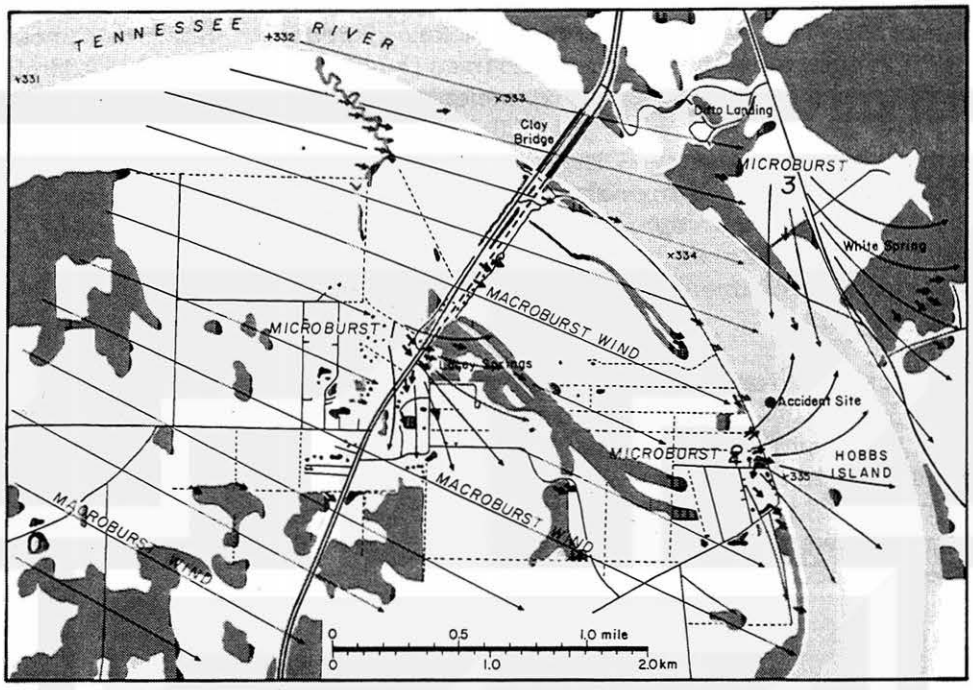

Fig. 6.46 The airflow pattern of three microbursts and one macroburst near the accident site. This map was constructed on the basis of the aerial photographs taken after the storm.

Microburst No.1 located at Lacey Springs where some trees were blown down and mobile sheds were overturned.

Microburst No.2 located to the south of the accident site. Trees in the forests directly beneath the microburst center were pushed down and their branches broken.

Microburst No.3 located at White Spring where a pattern of diverging winds was depicted through an aerial survey and subsequent mapping of damage vectors.

The damaging winds outside these microbursts were straight-line winds, suggesting that the entire area of the map was under the influence of the macroburst winds blowing from a 290° direction. If there was an anemometer inside one of these microbursts, it would have recorded the Redstone Arsenal type winds. On the other hand, an anemometer outside these microbursts would have recorded the National Weather Service type winds which are characterized by a sharp increase followed by an exponential decay in the windspeed.

Because of a small-scale (misoscale) airflow of a microburst, its outburst winds do not extend over a large area. The Redstone Arsenal microburst was probably limited to a small area inside the Arsenal. It should be treated as Microburst No.4 which was unrelated to the sternwheeler accident on the Tennessee River.

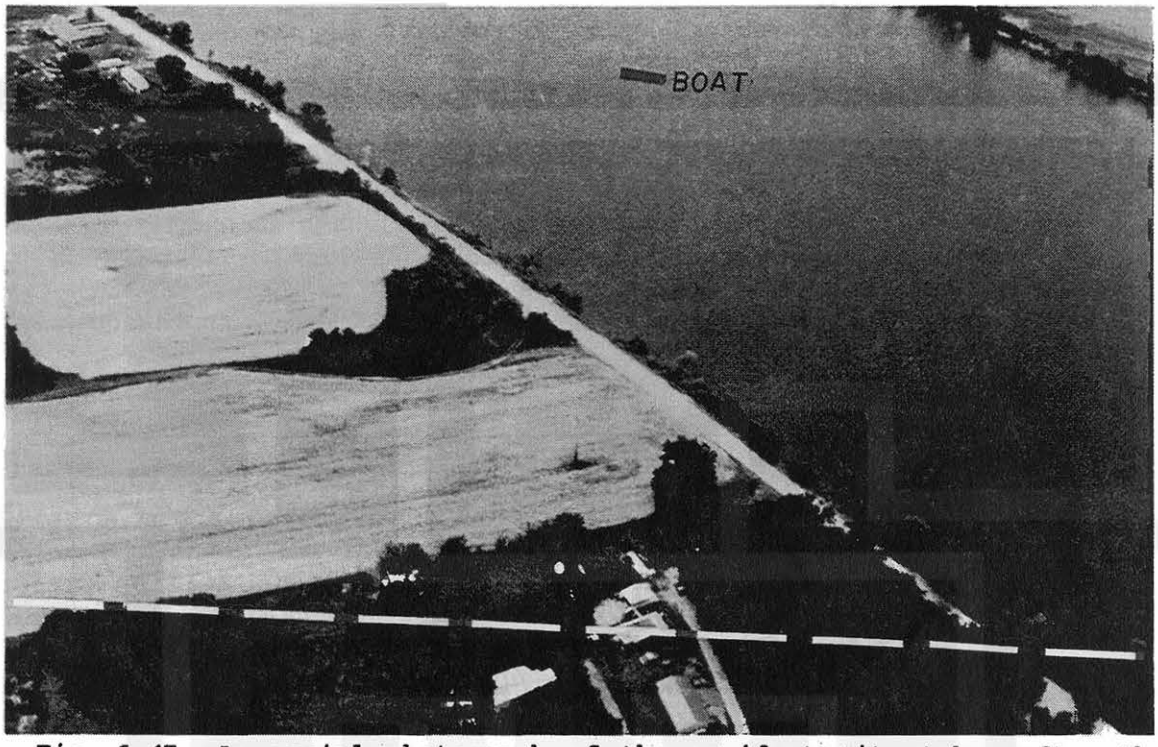

Fig. 6.47 An aerial photograph of the accident site taken after the accident looking north-northeast. The path of the microburst is shown with a red-and-white dashed line. The location of the accident boat is shown with a red bar. Photo by Fujita

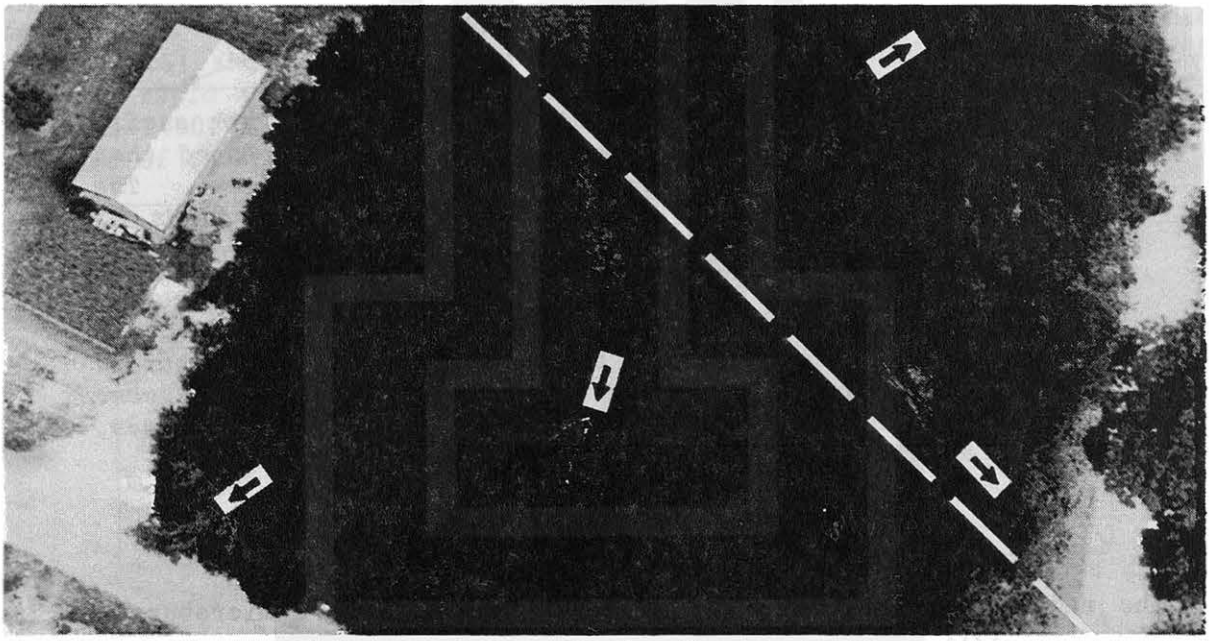

Fig. 6.48 A close-up photo of the forest looking north-northwest. Trees in the forest were pushed down and damaged by the starburst winds made visible by black arrows. Photo by Fujita

The path of the microburst center in relation to the sternwheeler boat is shown in Fig. 6.47. The microburst center passed directly over a forest between Eugene Malone's house and the river. A close-up aerial photograph of the forest shows the effect of the starburst winds which uprooted a tree and broke branches in radial directions (Fig. 6.48).

A schematic diagram of the microburst presents the descending stage when the downflow began inducing a ring vortex. The microburst touched down approximately five seconds before the accident. Thereafter, the vortex roll expanded, reaching the sternwheeler boat from a south-southwesterly direction (Fig. 6.49).

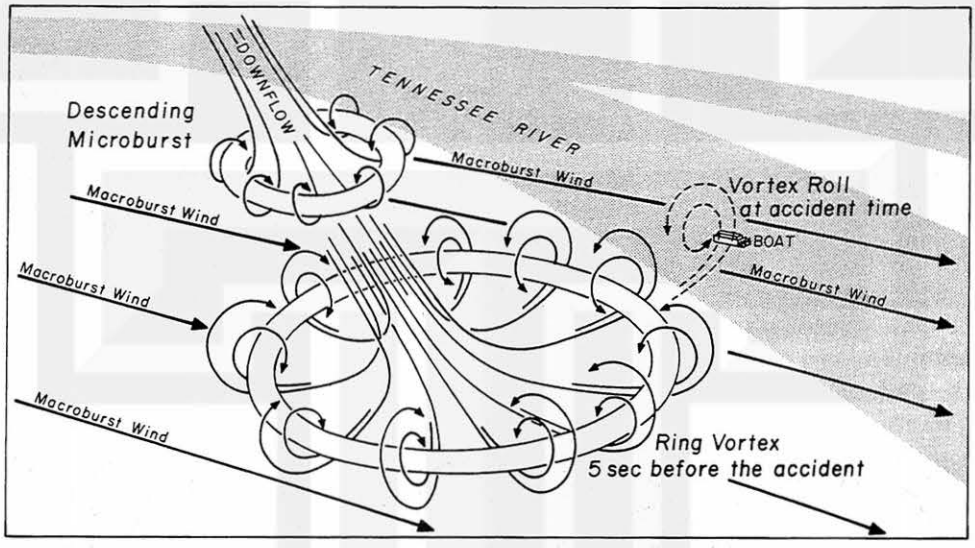

Fig. 6.49 A schematic view of the ring vortex which encircles the downflow of Microburst No.2. It is expected that the ring vortex expands rapidly after the touchdown. The sternwheeler boat was hit by south-southwesterly winds as the vortex roll passed over the boat.

Several years ago, Fernando Caracena of the Environmental Research Laboratories, NOAA proposed the initial concept of a ring vortex encircling the downflow region of a microburst. Since then, the existence of the ring vortex has been confirmed on various occasions. Refer to Figs. 1.5, 2.7, 2.9, 2.12, and 3.21.

The radar echo which gave rise to the formation of a microburst and four or more microbursts in the Huntsville area was relatively small. It was one of the line of echoes which moved over the Huntsville area between 1109 and 1135 CDT (Fig. 6.50).

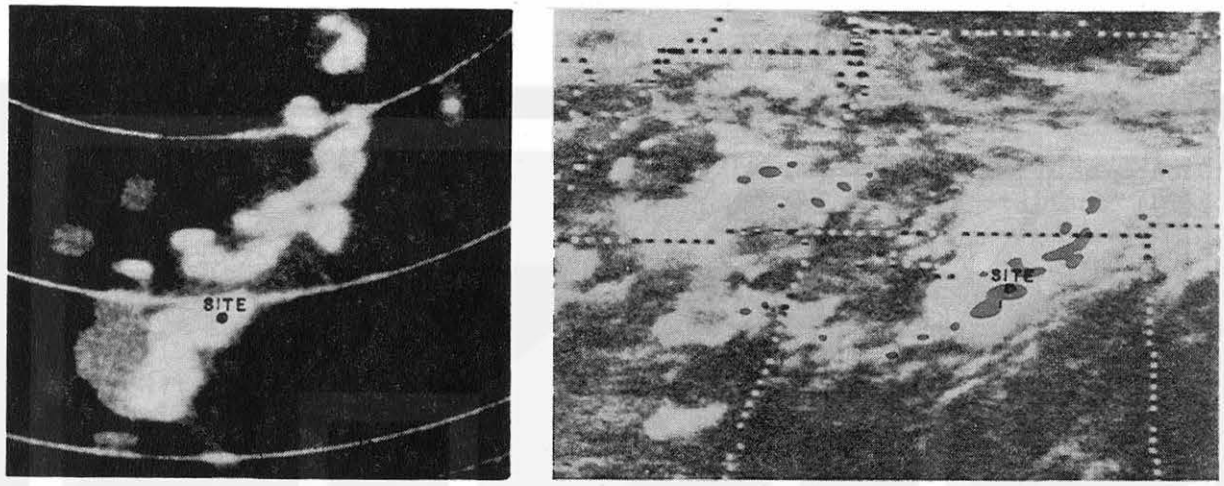

Fig. 6.50 A line of echoes at 1135 CDT (left) photographed by the National Weather Service, Nashville, Tennessee radar and a GOES East picture at 1135 CDT scan time (right) superimposed upon the radar echoes from Nashville and Centerville, Alabama. Analysis with Eric Peterson

The parent radar echo which induced the Huntsville boat microburst reached its peak intensity shortly before the accident. A satellite photograph taken 10 minutes after the accident shows an extensive anvil cloud covering the entire echo area. The coldest cloud-top temperature was -63°C (Fig. 6.50).

The area of cloud defined by that surrounded by a specific isotherm was computed as a function of cloud-top temperature. The result presented in Fig. 6.51 shows evidence that the first cloud began forming before 0700. Then, a rapid growth in area began at 0830, reaching the maximum between 1230 and 1400. The accident occurred at 1125, approximately one hour before the time of the coldest cloud-top temperature.

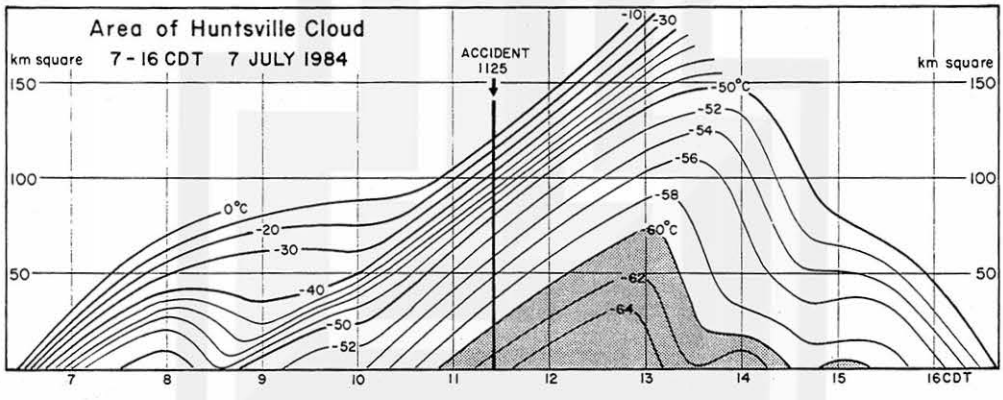

Fig. 6.51 Areas of the Huntsville cloud computed as a function of the cloud-top temperature ranging between 0°C and -64°C. Computation and analysis by Eric Peterson

6.12 Memphis Airport Microburst on 20 October 1984

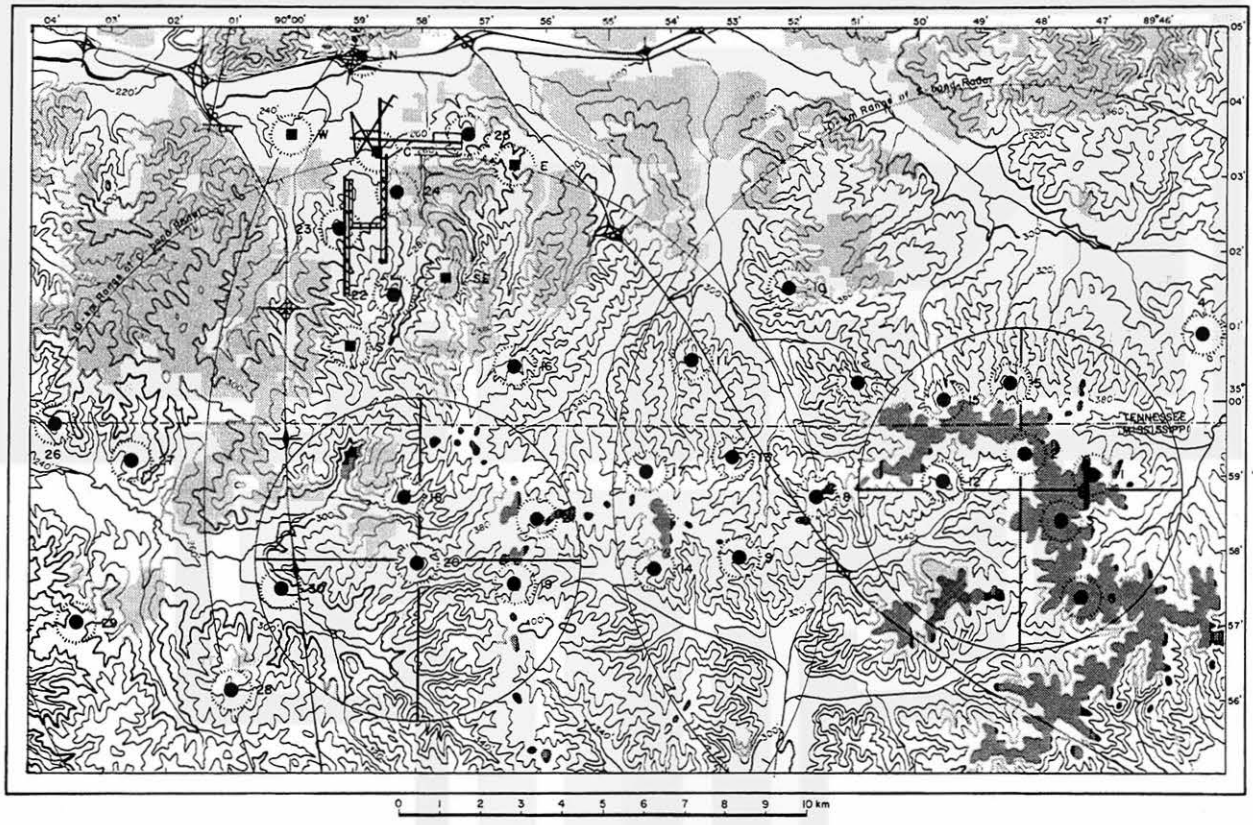

Fig. 6.52 FAA/Lincoln Laboratory wind-shear mesonet at Memphis, Tennessee established in 1984. An S-band Doppler radar is located in an open field to the west of Olive Branch Airport, Mississippi.

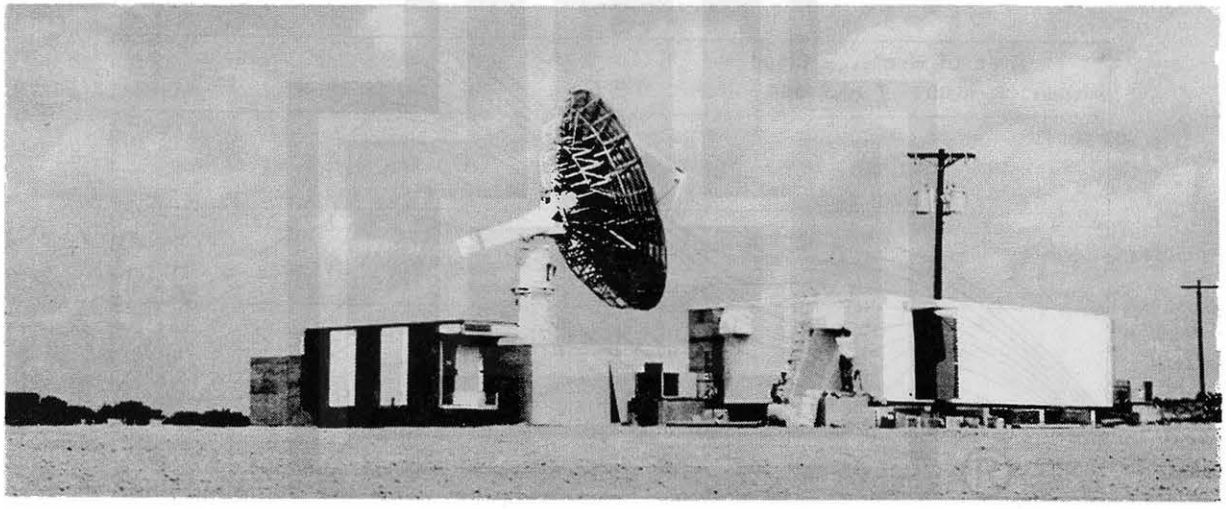

Fig. 6.53 The Lincoln Laboratory S-band Doppler radar without a radome. Photo by the MIT Lincoln Laboratory

In testing Doppler radars for operational uses in detecting low altitude wind shear, the Massachusetts Institute of Technology (MIT) Lincoln Laboratory, under the sponsorship of the Federal Aviation Administrtion (FAA), established in 1984 a mesometeorological network (mesonet) inside and in the southern sectors of the Memphis, Tennessee Airport. The mesonet consists of an S-band and a C-band radar and 30 mesonet stations (Figs. 6.52, 6.53, and 6.54).

In addition, the winds measured by six Low-Level Wind Shear Alert System (LLWAS) anemometers in and around the airport are also recorded and archived by the MIT Lincoln Laboratory.

Presented in this case study are the characteristics of a microburst which induced a 30.2 m/sec (68 mph) peak wind at mesonet station No. 25 at 1806 CST on 20 October 1984. Before the onset of the microburst, the environmental wind was 7 to 9 m/sec (16 to 20 mph) from a southerly direction. In two minutes the wind reached its peak, followed by a decrease to below 15 m/sec (34 mph) in the next two minutes. The duration of this microburst, defined as the period of one-half of the peak windspeed, was four minutes (Fig. 6.55).

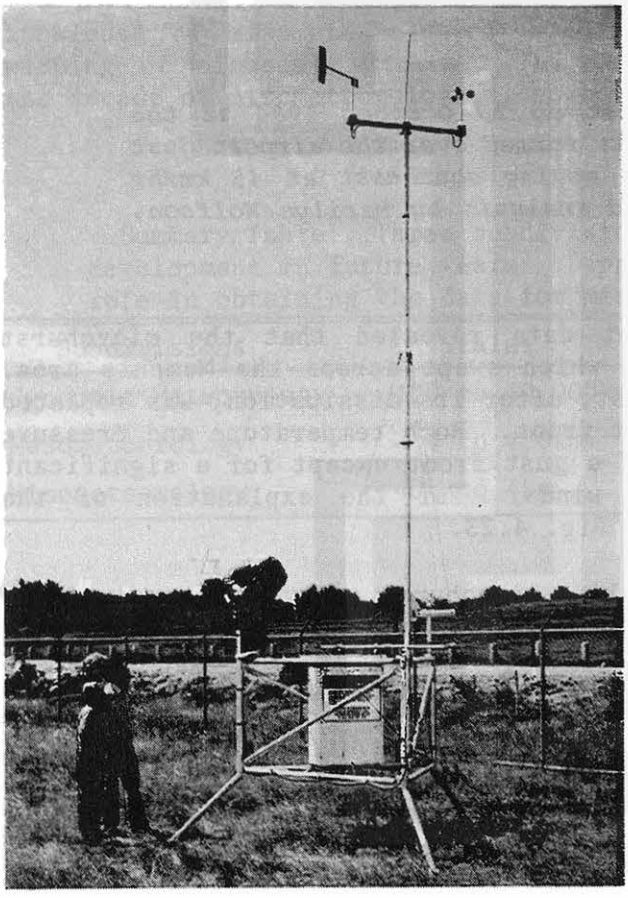

Fig. 6.54 A view of a modified PROBE station under construction. 30 stations, such as the one in this picture, are located in the Memphis Mesonet operated by the MIT Lincoln Laboratory. The average separation of mesomet stations is 1.5-3.0 km (1-2 miles).

The mesonet station is capable of measuring wind direction, mean windspeed, peak windspeed, air temperature, relative humidity, station pressure, and rainfall at one minute intervals. The measured parameters are transmitted via GOES satellite to a collection center and archived. Photo by the MIT Lincoln Laboratory

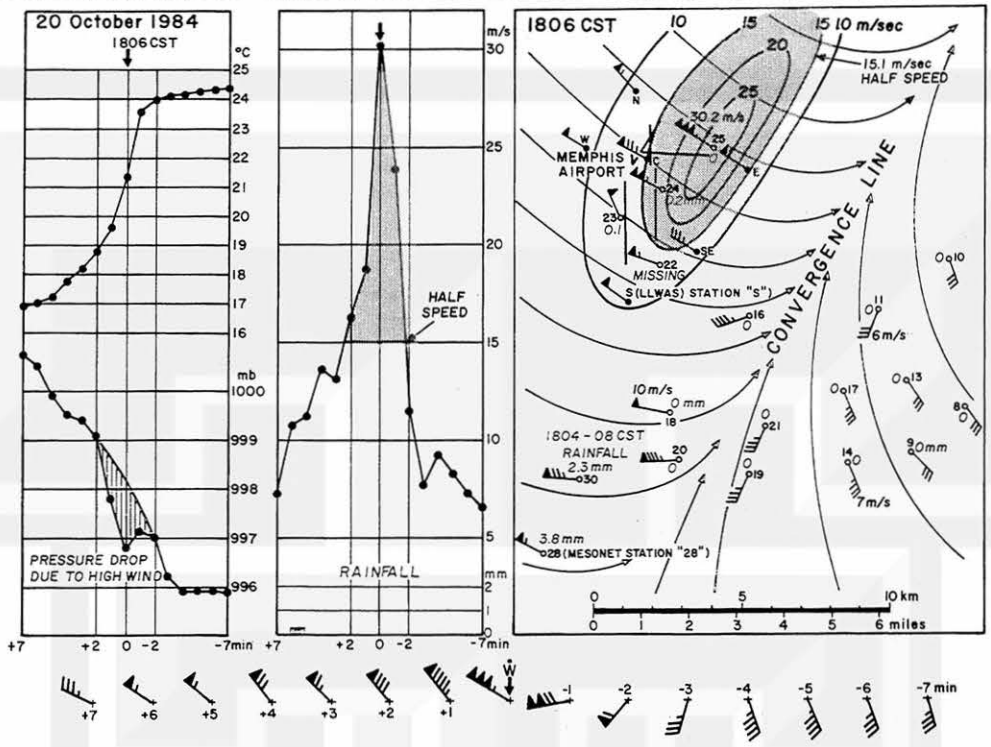

Fig. 6.53 A rotor microburst on 20 October 1984 at the Memphis Airport. The microburst formed over the airport just behind a gust front which was moving southeast at 45 km/hr (28 mph). Data collection and analysis by Marilyn Wolfson, MIT Lincoln Laboratory

A detailed analysis of the mesonet data revealed that the microburst was located just behind a gust front which swept across the Memphis area. Consequently, the area of the microburst, after its dissipation, was replaced by the cold air pushing behind the gust front. Both temperature and pressure changes were characterized by those of a gust front except for a significant pressure drop during the microburst winds. For the explanation of the pressure drop in microbursts, refer to Fig. 4.23.

Unlike the downflow microburst, this microburst was characterized by a group of parallel streamlines of strong winds which could induce a swath of wind damage, called a burst swath. As presented in the case study of the 30 June 1982 microburst in JAWS, this was also a "rotor microburst" accompanied by a roll vortex with its horizontal axis oriented southwest to northeast over the Memphis Airport.

This rotor microburst was accompanied by a very strong wind shear at low altitude. A hypothetical aircraft penetrating the storm from southeast to northwest would experience a 20 m/sec (39 kts) increase in headwind, followed by a 15 m/sec (29 kts) loss of headwind within approximately 3 km (10,000 ft) which is a typical length of runways at major airports.

Summary and Conclusions

So-called synoptic meteorology was developed by the Norwegian School back in the 1920s and 1930s, leading to the discovery of fronts accompanied by cyclones. The frontal model, thus established, greatly improved the daily weather forecast.

Since the 1950s, the demand for short-range forecasts in specific states, cities, etc., surfaced in various parts of the United States. This necessitated full understanding and modeling of mesoscale disturbances which had been treated as the noise of synoptic disturbances. Now, the 1980s are regarded as the decade of mesometeorological research, aiming at a significant improvement of mesoscale forecasting. If everything goes well, the time and location of the parent clouds of the specified type of storms can be predicted hours in advance.

The principle of uncertainty, nonetheless, will not permit us to pinpoint exact time and location of storms spawned by the predicted parent clouds. The best we can do is to develop fool-proof detection methods. The basic knowledge of misometeorology will improve significantly the detection and warning of misoscale storms. The author predicts that the 1990s will be the decade of misometeorological research.

Summary Table: Three subdivisions of meteorological research and development in future years. Doppler radars will play an important role in obtaining the data for misometeorological studies.

Subdivisions	Scales	Studies of	For improving
Synoptic Meteorology	400 to 40,000km	Highs and Lows	Daily Forecast
Mesometeorology	4 to 400km	Parent Clouds	Local Forecast
Misometeorology	40m to 4km	Storms	Storm Warning

Until several years ago, microbursts and tornadoes were regarded as being unrelated. This book presents an amazing similarity between these severe storms. A tornado is an intense misocyclone in which the swirling air rushes upward, while a microburst, at inflow and downflow levels, is surrounded by a misocyclone in which the swirling air rushes downward. A microburst may be regarded as an upside-down or inverted tornado.

REFERENCES

For Chapter 1, History of Downburst Identification

1976: Fujita, T.T. ■ Spearhead echo and downburst near the approach end of a John F. Kennedy Airport runway, New York City. SMRP Res. Paper 137, University of Chicago, 51 pages.

1977: Fujita, T.T. and H.R. Byers. ■ Spearhead echo and downbursts in the crash of an airliner. Mon. Wea. Rev., 105, 129-146.

For Chapter 2, Observations of Macrobursts and Microbursts

1978: Fujita, T.T. ■ Manual of downburst identification for Project NIMROD. SMRP Res. Paper 156, University of Chicago, 104 pages (out of print).

1981: Fujita, T.T. and R.M. Wakimoto ■ Five scales of airflow associated with a series of downbursts on 16 July 1980. Mon. Wea. Rev., 109, 1438-1456.

1981: Fujita, T.T. ■ Tornadoes and downbursts in the context of generalized planetary scales. J. Atmos. Sci., 38, 1512-1534.

1982: Wakimoto, R.M. ■ The life cycle of thunderstorm gust fronts as viewed with Doppler radar and rawinsonde data. Mon. Wea. Rev., 110, 1160-1082.

1983: Forbes, G.S. and R.M. Wakimoto ■ A concentrated outbreak of tornadoes, downbursts and microbursts, and implications regarding vortex classification. Mon. Wea. Rev., 111, 220-235.

1984: Wilson, J.W. et al. ■ Microburst wind structure and evaluation of Doppler radar for wind shear detection. J. Climate Appl. Meteor., 23, 898-915.

For Chapter 3, Microburst-related Aircraft Accidents

1977: Fujita, T.T. and F. Caracena ■ An analysis of three weather-related aircraft accidents. Bull. Amer. Meteor. Soc., 58, 1164-1181.

1981: Fujita, T.T. ■ Microburst as an aviation wind shear hazard. Preprints AIAA 19th Aerospace Sciences Meeting, St. Louis, AIAA-81-0386, 9 pages.

1983: Fujita, T.T. ■ Microburst wind shear at New Orleans International Airport, Kenner, Louisiana on July 9, 1982. SMRP Res. Paper 199, University of Chicago, 39 pages.

1983: National Academy of Sciences ■ Low-altitude wind shear and its hazard to aviation. National Academy Press, 112 pages.

1984: Bedard, A.J., Jr. et al. ■ Statistics from the operation of the low-level wind shear alert system during the JAWS project. DOT/FAA/PM-84-32. Federal Aviation Administration, 76 pages.

1984: McCarthy, J. ■ Recommendations for coping with microburst wind shear: An aviation hazard. J. Air Law and Commerce, 49, 337-359.

1984: McCarthy, J. and R.J. Serafin ■ The microburst hazard to aircraft. Weatherwise, 37, 120-127.

For Chapter 4, NIMROD and JAWS Networks

1979: Fujita, T.T. ■ Objectives, operation, and results of Project NIMROD. Preprints 11th Conf. on Severe Local Storms, Kansas City, Amer. Meteor. Soc., 259-266.

1983: Fujita, T.T. and R.M. Wakimoto ■ Microburts in JAWS depicted by Doppler radars, PAM, and aerial photographs. Preprints 21st Conf. on Radar Meteorology, Edmonton, Canada, Amer. Meteor. Soc., 638-645.

For Chapter 5, Types of Microbursts and Parent Clouds

1984: Roberts, R.D. and J.W. Wilson ■ Precipitation and kinematic structure of microburst producing storms. Preprints 22nd Conf. on Radar Meteorology, Zurich, Switzerland, Amer. Meteor. Soc., 71-76.

For Chapter 6, Specific Case Studies

1984: Fujita, T.T. ■ Andrews AFB microburst. SMRP Res. Paper 205, University of Chicago, 38 pages.

1984: Kessinger, C.J. et al. ■ The evolution of misososcale circulations in a downburst-producing storm and comparison to numerical results. Preprints 22nd Conf. on Radar Meteorology, Zurich, Switzerland, Amer. Meteor. Soc., 58-63.

SUBJECT INDEX

About the Author

Born at Kitakyushu City, Japan on October 23, 1920

1953 D.Sc., Tokyo University; 1953-55 Research Associate, University of Chicago; 1955-56 Returned to Japan for an immigrant visa; 1956-62 Director of Mesometeorology Project, University of Chicago; 1962 Associate Professor of Meteorology, Director of Satellite and Mesometeorology Research Project (SMRP), University of Chicago; 1965-present Professor of Meteorology, University of Chicago; 1968 Became a U.S. citizen

AWARDS - 1959 Okada Award (MSJ), 1960 Kamura Award (KIT), 1967 Meisinger Award (AMS), 1977 Admiral Luis de Flores Safety Award (FSF), 1977 Distinguished Service Award (FSF), 1978 First Annual Award (NWA), 1979 Distinguished Public Service Medal (NASA), 1982 Losey Atmospheric Service Award (AIAA).